University of Nevada, Reno

**Igneous Geology of the Carlin Trend, Nevada:
The Importance of Eocene Magmatism in Gold Mineralization**

A dissertation submitted in partial fulfillment of the
requirements for the degree of Doctor of Philosophy in
Geology

by

Michael Walter Ressel, Jr.

Dr. Christopher D. Henry/Dissertation Advisor

May, 2005

UMI Number: 3210296

UMI®

**UNIVERSITY
OF NEVADA
RENO**

THE GRADUATE SCHOOL

We recommend that the dissertation
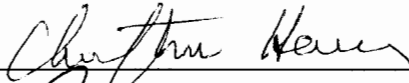prepared under our supervision by

MICHAEL WALTER RESSEL, JR.

entitled
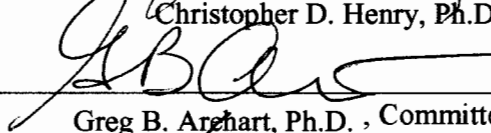
**Igneous Geology of the Carlin Trend, Nevada:
The Importance of Eocene Magmatism in Gold Mineralization**

be accepted in partial fulfillment of the
requirements for the degree of

DOCTOR OF PHILOSOPHY

_____
Christopher D. Henry, Ph.D. , Advisor

_____
Greg B. Arehart, Ph.D. , Committee Member

_____
Dhanesh Chandra, Ph.D. , Committee Member

_____
Alan R. Wallace, Ph.D. , Committee Member

_____
Kent M. Ervin, Ph.D. , Graduate School Representative

_____
Marsha H. Read, Ph. D., Associate Dean, Graduate School

May, 2005

ABSTRACT

Igneous rocks of five ages are present in the Carlin trend, Nevada, and include: 1) Paleozoic basalt of the Roberts Mountains al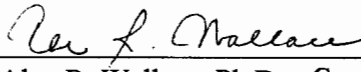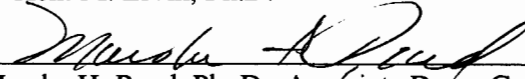lochthon, 2) the Jurassic (~158 Ma) Goldstrike intrusive complex, which includes the Goldstrike diorite laccolith and abundant dikes and sills, 3) a Cretaceous (112 Ma) granite stock, 4) lavas and intrusions of the Emigrant Pass volcanic field and widespread epizonal plugs and dikes of Eocene (~40-36 Ma) age that range from rhyolite through basalt, and 5) Miocene (15 Ma) rhyolite lava and tuff. Jurassic and Eocene igneous rocks are by far the most important volumetrically and are spatially associated with nearly all ore deposits of the Carlin trend.

This study focuses on the field relations, isotopic dating, and geochemistry of Eocene dikes that intrude sedimentary rocks in many deposits of the Carlin trend, because they are the youngest pre-mineral rocks and have simpler alteration histories than other host rocks. In the Beast, Genesis, Deep Star, Betze-Post, Rodeo-Goldbug, Meikle-Griffin, and Dee-Storm deposits, Eocene dikes are altered, commonly mineralized, and locally constitute ore. Gold-bearing dikes and sedimentary rocks have similar ore mineralogy, including arsenian pyrite, marcasite, and arsenopyrite, with late barite and stibnite. At Beast, as much as half the ore is hosted in a 37.3 Ma rhyolite dike. Post-gold alunite is ~18.6 Ma. At Meikle and Griffin, porphyritic dacite dikes yield concordant U/Pb zircon and ^{40}Ar/^{39}Ar biotite emplacement ages of ~39.2 Ma, and illite from the same QSP-altered dacite, with as much 9 ppm Au, yields similar, although imprecise ^{40}Ar/^{39}Ar ages. Thus, gold mineralization at these deposits closely followed emplacement of Eocene dikes.

Eocene dikes and volcanic rocks approximately coeval with ore deposition provide limits on the depth of formation of Carlin trend gold deposits and on the degree of tilting and extension since about 40 to 36 Ma. Altered and mineralized Eocene dikes at

the Beast, Genesis, Deep Star, Betze-Post, Rodeo-Goldbug, Meikle-Griffin, and Dee deposits were shallowly emplaced as indicated by their strongly porphyritic and commonly glassy, lithophysal, spherulitic, and felsitic textures. An estimated ≤2-km depth of dike emplacement is based on post-Paleozoic offset on faults between the northern Carlin trend and basal lavas of the Emigrant Pass volcanic field. This estimate is significantly less than the ~4-km or more from fluid inclusion studies. A shallow origin is consistent with steep dips of dikes and the subhorizontal volcanic rocks of the northern Emigrant Pass volcanic field, which suggest only modest tilting and extension since ~40 Ma.

A demonstrated spatial and temporal link between Eocene magmatism and gold mineralization is suggestive of a genetic link. Abundant Eocene silicic dikes of the northern Carlin trend are apophyses of much larger intrusions at depth. As many as six Eocene plutons are inferred for the Carlin trend based on the age, distribution, and composition of dike sets, and of associated aeromagnetic properties. Plutons are aligned approximately north to south, with generally older plutons and dikes to the north and younger ones to the south, similar to regional trends. Based on geologic relations and published fission-track data, Eocene plutons are also more deeply buried to the north.

Carlin-type gold deposits in northeastern Nevada have been variously interpreted as partly syngenetic with Paleozoic carbonate rocks, products of Mesozoic contraction and metamorphism with or without significant magmatism, and of Tertiary age and related or not to magmatism, metamorphism, and/or large-scale extension. A recently established Eocene age for major gold introduction narrows the possibilities, and two principal models have emerged: one involving Eocene magmatism as the heat source to drive shallow hydrothermal circulation and the other advocating deeply sourced metamorphic fluids released into the upper crust during regional extension. Critical to the

latter argument is the temporal association of extension to gold mineralization, which as yet, is not demonstrated. We argue that Eocene magmatism in the form of large underlying plutons, was the major recognized process that affected the Carlin trend during gold mineralization. These plutons supplied the heat that drove discrete hydrothermal systems.

ACKNOWLEDGEMENTS

Don Noble introduced me to igneous rocks and ore deposits of Nevada by, as he would say, "brute force". For his part, there is never a lack of curiosity, dedication, or enthusiasm for geology. I am thankful for the support I received from the Ralph J. Roberts Center for Research in Economic Geology (CREG) for most of my studies and for the discipline demanded by this program. CREG, under the direction of Tommy Thompson, has fueled interest in studies of Carlin-type deposits in Nevada and provided a much needed forum for collaboration and exchange of ideas. Barrick Goldstrike Mines, Newmont Mining Corporation, the U.S. Geological Survey and namely, Steve Peters and Alan Wallace, the Society of Economic Geologists, the Geological Society of America, and Lisa Shevenell of the Nevada Bureau of Mines and Geology (NBMG) provided additional funds during those many pinches.

The mines of the Carlin trend are fascinating and extremely hectic places. This work would not have been possible without the support of Barrick and Newmont and in particular, the many geologists from these companies who helped out at every stage, even when gold prices languished. They shared their knowledge without hesitation, were eager to hear of my progress, and rarely passed up a chance to "talk rock" at the outcrop. And like Ralph J. Roberts, these geologists shared with me their passion for gold. Dave Haney gave me a place to live during several field seasons, and what a place it is against the beautiful backdrop of the Ruby Mountains in Lamoille.

The Mackay School of Mines provided me with many of the tools I needed to learn: good and knowledgeable faculty and staff, excellent analytical facilities and library, and a bunch of fellow graduate students and friends in the same boat as me. I am fortunate to have collaborated with many from Mackay and elsewhere. I especially thank Chris Henry for his interest and commitment to our work in northeastern Nevada and his

PREFACE

This dissertation contains three stand-alone manuscripts presented in three chapters. Two of the manuscripts have been published in peer-reviewed publications; the third is in review as of April 2005. The papers are arranged in draft form, with text in front and figures, tables, and appendices following text for each paper. At the start of each paper is an introductory section that includes a detailed review of the pertinent literature on the geology of the Carlin trend and Carlin-type deposits. Appendices at the end of each paper describe the analytical methods used and contain supplemental data.

This research evolved from a regional synthesis of Eocene magmatism in the northern Great Basin to more focused study of the relationships of magmatism to ore deposition in the Carlin trend gold belt of northeastern Nevada. In the end, however, the detailed work on the trend led to new insights on the regional scale. Thus, this research has gone "full-circle" over the course of several years.

A recently controversial subject in the ore deposits arena has been the age of huge Carlin-type gold deposits in Nevada. The difficulty in dating mineralization has led to numerous conflicting theories on ore genesis. This debate has been particularly lively on the Carlin trend, where the largest deposits occur. Many studies, including the ones presented here, now demonstrate that the age of most, if not all, Carlin-type deposits in northern Nevada is Eocene. The approach used here to address the age issue on the Carlin trend was detailed characterization and dating of Eocene dikes, the youngest altered rocks in the trend. In chapter 1, evidence is presented on the age and nature of mineralization in the Beast deposit of the Carlin trend. Although typical of Carlin-type deposits in terms of alteration, ore mineralogy, and geochemistry, the Beast deposit is unique because it is hosted in large part by an Eocene rhyolite dike instead of the more usual sedimentary rocks. Later discussion focuses on the implications of Eocene intrusions on the depth of

formation of Carlin-type deposits, the amount of Tertiary tilting and extension in the region, and on Eocene magmatism as the fundamental process involved in the formation of Carlin trend deposits.

The concern of chapter 2 is on the character of altered and mineralized Eocene dikes of the Griffin deposit and the large and high-grade Meikle deposit, both in the Carlin trend. We first document the types of dikes that occur in the deposits, then identify and describe the nature of "Carlin-type" gold mineralization in Eocene dike rocks. This characterization leads to isotopic dating, which again provides strong evidence for both an Eocene age of mineralization and a link to Eocene magmatic activity.

The final chapter builds on the previous two topical chapters and discusses the age, composition, and distribution of the four major suites of igneous rocks of the Carlin trend of Mesozoic and Tertiary age. We focus on Eocene magmatism as the major process in forming Carlin-type deposits based on its close spatial and temporal association to gold mineralization. Key topics include: 1) the styles of mineralization associated with each pulse of magmatism, 2) the number, size, and depth of emplacement of Eocene plutons, 3) timing of Eocene plutons relative to formation of Carlin-type deposits, and 4) the depth of formation of Carlin-type deposits. The southward sweep of Eocene magmatism evident regionally, is also marked in the Carlin trend by a series of felsic dike swarms that range from ~40 to 36 Ma and young southward. We argue that each discrete swarm defined by its age, distribution, and composition, requires its own proximal magma chamber. Plutons are inferred to be more shallowly emplaced to the south. We argue that many closely spaced Eocene plutons were the source for heat to drive hydrothermal circulation that formed Carlin-type deposits on the Carlin trend.

Appendices 3-1 through 3-5 contain comprehensive geochemical and isotopic data on igneous rocks of the Carlin trend. These data do not bear directly on many of the

conclusions from Chapter 3, but are included as supporting information for the first three chapters and for the purpose of completeness.

TABLE OF CONTENTS

LIST OF FIGURES

Chapter 1

Chapter 2

Chapter 3

LIST OF TABLES

Chapter 1

LIST OF APPENDICES

Chapter 1

**Dike-Hosted Ores of the Beast Deposit and the Importance of Eocene Magmatism
in Gold Mineralization of the Carlin Trend, Nevada[†]**

Michael W. Ressel and Donald C. Noble

Department of Geological Sciences, MS 172, Mackay School of Mines,

University of Nevada, Reno, Reno, Nevada 89557

Christopher D. Henry

Nevada Bureau of Mines and Geology, MS 178

University of Nevada, Reno, Reno, Nevada 89557

and Wayne S. Trudel

Newmont Gold Company, P.O. Box 669, Carlin, Nevada 89822

Abstract

The Beast, low-grade (7.3 mt @ 0.7 g/t), disseminated Au deposit in the Carlin trend, Nevada is unique among Carlin-type Au deposits in having as much as 50 percent of the ore hosted by a 37.3 Ma porphyritic rhyolite dike. Nonetheless, the deposit has requisite characteristics of Carlin-type deposits, including 1) an ore mineral assemblage consisting mostly of fine-grained pyrite, arsenian pyrite and arsenopyrite, 2) association of Au with As, Sb, Hg, and Tl, and high Au/Ag ratios, 3) a paragenesis that includes early Fe-As sulfides and kaolinite, intermediate stibnite, and latest barite, and 4) moderate to strong silicification and/or kaolinitization of rocks in ore zones and decarbonatization of silty carbonate rocks peripheral to faults. The Beast deposit is <1 km from the Genesis deposit and 3 km from the huge Betze-Post deposit, and all deposits are located along the Post-Genesis fault system.

The rhyolite dike at Beast not only provides an important age constraint on Carlin-type mineralization in the Carlin trend, but also gives information on the nature of mineralization largely free from precursor diagenetic, thermal, or hydrothermal alteration experienced by Paleozoic and Mesozoic host rocks. Strong leaching and silicification of the rhyolite produced rock composed mostly of quartz and kaolinite. Gold is most concentrated in matrix- and clast-supported siliceous breccia developed in and near the faulted footwall of the rhyolite dike adjacent to Silurian-Devonian laminated silty carbonate rocks but also occurs as massive quartz-kaolinite in both rhyolite and limestone. Secondary oxidation of the bulk of the ores produced abundant hematite, jarosite, scorodite, and alunite. Supergene alunite yielded an $^{40}Ar/^{39}Ar$ age of 18.6 Ma that is within the range of alunite ages from deposits in the Carlin trend (30 to 8 Ma).

Eocene intrusive rocks dated between 40.1 and 37.3 Ma are common in the northern Carlin trend. The rocks are high-K calc-alkaline, and most range in composition from dacite to rhyolite. In addition to Beast, mineralized Eocene dikes are recognized in

the Betze-Post, Deep Star, Genesis, and Meikle-Griffin deposits, and indicate that major Au mineralization in the Carlin trend occurred after ~40 Ma, perhaps as a consequence of multiple Eocene intrusive events. Textures in dikes that are locally altered and mineralized as well as tilt data on dikes and nearby Eocene volcanic rocks are consistent with shallow emplacement and only modest extension since 40 Ma. This suggests that mineralization on the Carlin trend occurred at equally shallow depths without major extension.

Eocene dikes of the northern Carlin trend underlie or are immediately adjacent to a large (700-km^2) positive aeromagnetic anomaly. The anomaly also corresponds closely with exposures of contemporaneous volcanic and intrusive rocks of the nearby 200-km^2 Emigrant Pass volcanic field and smaller Welches Canyon center. It is likely that the anomaly represents a buried, mainly Eocene, plutonic complex. Growing evidence for a spatial and temporal association between Carlin-type Au mineralization and Eocene magmatism suggests a genetic relationship. Eocene magmatism is considered the major process that drove hydrothermal circulation that formed Carlin-type deposits of the Carlin trend. This relationship allows the possibility that magmas may also have contributed metals and other components. If Carlin-type deposits are pluton-related, as suggested here, then their association with other pluton-related Au deposits, including distal-disseminated Au-Ag and Au skarn, requires re-evaluation.

Introduction

Disseminated gold deposits hosted by originally carbonate-bearing sedimentary rocks, known as sedimentary rock-hosted or "Carlin-type" deposits, are the major source of gold in the United States. The deposits are found mainly within the Great Basin of the western United States, with the greatest number concentrated in belts or other discrete areas of north-central Nevada (Fig. 1-1). The 60-km long Carlin trend in north-central Nevada has production and reserves of gold in excess of 2,640 tonnes (Teal and Jackson,

1997), making it the world's richest known concentration of such deposits.

The origin of Carlin-type deposits is controversial, with their age and association or lack thereof with magmatism being two of the most important parts of the controversy (Seedorff, 1991; Arehart et al., 1993b; Christensen, 1996; Emsbo et al., 1996; Arehart, 1996; Ilchik and Barton, 1997; Henry and Boden, 1998b; Hofstra et al., 1999; Henry and Ressel, 2000). The age of deposits places strong constraints on origin, but age assignments have ranged widely. Based on dating of adularia or on crosscutting relations with dated dikes, a consensus has developed that most deposits are Eocene (Wells et al., 1969; Thorman and Christensen, 1991; Hofstra, 1994; Emsbo et al., 1996; Phinisey et al., 1996; Groff et al., 1997; Hall et al., 1997; Ressel et al., 1998, 1999, 2000; Hofstra et al., 1999). Unfortunately, most of these studies address deposits outside the Carlin trend. In the Carlin trend, Arehart et al. (1993b) initially interpreted a Cretaceous age for the giant Betze-Post deposit. In contrast, Emsbo et al. (1996) concluded that Betze-Post is Eocene or younger based on chemical and mineralogical characteristics of an altered Eocene dike in the deposit. Most deposits of the Carlin trend remain undated.

An Eocene age and association with magmatism is consistent with the abundance of Eocene igneous rocks in northern Nevada (Fig. 1-1; McKee, 1971; Brooks et al., 1995a, b; Thorman et al., 1995; Henry and Boden, 1997, 1998b; Henry and Ressel, 2000), including rocks present within important areas of base- and precious-metal mineralization such as the Battle Mountain and Tuscarora districts (Seedorff, 1991; Henry et al., 1998). Physical characteristics of Carlin-type deposits range widely, however (e.g., Bagby and Berger, 1985; Arehart, 1996; Christensen, 1996), so more than one period or process of gold deposition could be involved.

This report presents detailed geologic, geochemical, mineralogic, and isotopic age data on the largely Eocene-dike hosted Beast deposit of the northern Carlin trend. These data address both issues. The Beast deposit has the characteristics of the more common,

sedimentary rock-hosted, Carlin-type deposits. However, the young (syn- or shortly pre-mineral) dike has not undergone the multiple episodes of diagenesis and alteration that the Paleozoic sedimentary rocks have. Moreover, the primary composition of the dike is well understood, which allows quantitative assessment of the effects of mineralization. Therefore, the deposit provides unique constraints on the character and timing of the Carlin-type ore-forming process. Furthermore, the association of the Beast deposit and other deposits of the northern Carlin trend with Eocene magmatism provides strong evidence for a magmatic link.

Geology and Igneous Episodes of the Carlin Trend

Rocks of the Carlin trend consist of variably deformed Lower Paleozoic sedimentary rocks that are intruded or unconformably overlain by igneous rocks of four magmatic episodes: Jurassic, Cretaceous, Eocene, and Miocene (Fig. 1-2; Table 1-1). Most outcrops are Ordovician through Devonian sedimentary rocks of the lower and upper plates of the Roberts Mountains allochthon (Evans and Theodore, 1978; Evans, 1980; Christensen, 1996). Lower-plate rocks consist of calcareous siltstone, limestone, dolomite, and lesser mudstone and chert. These were deposited in relatively shallow water on the western edge of the North American craton and are the dominant ore hosts. Generally considered parautochthonous, they are moderately deformed (Saucier, 1997). Upper-plate rocks, which were tectonically emplaced over lower-plate rocks by the Roberts Mountains thrust, consist of fine-grained clastic sedimentary rocks and chert that were deposited in deeper water at a large, but uncertain, distance to the west. Upper-plate rocks are highly folded and imbricately thrust-faulted and host little ore. Emplacement of the Roberts Mountains allochthon and related deformation are attributed mainly to the mid-Paleozoic Antler orogeny, during which upper-plate rocks were thrust eastward over lower-plate strata. Later Paleozoic and Mesozoic deformation also affected the region (Silberling and Roberts, 1962; Roberts, 1964; Evans and Theodore, 1978; Ketner and

Smith, 1982; Christensen, 1996; Saucier, 1997).

Rocks produced during the four igneous episodes affecting the Carlin trend are distinctive in their distribution, relative volume, style of emplacement, and chemical and petrographic characteristics (Fig. 1-2; Table 1-1). Jurassic magmatism produced the Goldstrike diorite stock or laccolith (Evans, 1980; Arehart et al., 1993b), related dikes and sills, and lamprophyric dikes. The Goldstrike intrusion is exposed over about 2 km^2 in the north-central part of the trend; scattered outcrops a few kilometers to the southeast and an associated magnetic anomaly suggest that the overall body may underlie as much as 10 km^2. Lamprophyric dikes are widespread in the district but appear to be most abundant near the Goldstrike intrusion. The phlogopite- and hornblende-bearing lamprophyre dikes mostly occupy northwest-trending structures. $^{40}Ar/^{39}Ar$ ages on several phases of the Goldstrike intrusion and on lamprophyric dikes indicate that all were emplaced about 157 to 158 Ma (Arehart et al., 1993b; Emsbo et al., 1996; M.W. Ressel, unpublished data). Jurassic volcanic rocks are absent in the Carlin trend, but Jurassic felsic volcanic rocks crop out in the Cortez Mountains to the south (Fig. 1-2).

Based on outcrop, Cretaceous magmatism was volumetrically least significant. The Richmond granite crops out over 0.25 km^2 south of Richmond Mountain (Fig. 1-2) and has a biotite K-Ar age of 108 Ma (Evans, 1980). Its contact metamorphic halo suggests the intrusion underlies ~3 km^2. Evans (1974a) mapped several nearby dikes as Cretaceous, but petrographic and chemical characteristics of the dikes show that most are Eocene (Table 1-1). For example, the largest dike just north of the granite gives a sanidine $^{40}Ar/^{39}Ar$ age of 37.34±0.09 Ma (Table 1-2).

Eocene magmatism (~40-36 Ma) of high-K, calc-alkaline composition was by far the most voluminous around the Carlin trend and was intense throughout northern Nevada and Utah (Armstrong, 1970; McKee, 1971; Stewart, 1980; Brooks et al., 1995a, b; Henry and Boden, 1998a, b). This area encompasses all known Carlin-type deposits in

the northern Great Basin and many porphyry, skarn, and epithermal precious-metal deposits of Eocene age. Several large volcano-intrusive centers surround or adjoin the trend (Fig. 1-2), and Eocene dikes are abundant within it. The nearly 2,000 km^2 Tuscarora volcanic field north of the Carlin trend, and the 200 km^2 Emigrant Pass volcanic field on the southwest edge, are the largest centers. The Emigrant Pass field and shallow intrusions in Welches Canyon and Boulder Valley lie within a 700-km^2 magnetic anomaly (Fig. 1-3). Although Evans (1980) interpreted the anomaly to reflect the Cretaceous granite, the anomaly overwhelmingly coincides with Eocene intrusions and volcanic rocks and probably indicates a large, Eocene plutonic complex (Henry and Boden, 1998b). Other major centers are at Lone Mountain, Swales Mountain, and the Railroad district (Ketner and Smith, 1963; Evans and Ketner, 1971; Ketner, 1998). Smaller Eocene intrusions include the dacitic Hatter stock, 20 km north of the trend, and a small intrusion near Suzie Creek, 22 km east of the Gold Quarry mine (Fig. 1-2). Andesite to dacite lavas and compositionally equivalent, shallow intrusions are prominent in all Eocene centers (Evans and Ketner, 1971; Brooks et al., 1995a; 1995b; Henry and Boden, 1998a). More silicic rocks, including voluminous rhyolitic ash-flow tuffs, small intrusions, and some lavas, are also widespread (Henry and Boden, 1998a, b). All Eocene centers show prominent magnetic anomalies (Fig. 1-3).

Five types of Eocene dikes are recognized in the northern Carlin trend (Table 1-1), and similar dikes are found in nearly all of the Eocene igneous centers of the region. The types are classified primarily on the basis of phenocryst assemblage, which varies narrowly within each type and is distinctive between types. Porphyritic dacites contain plagioclase, biotite, and hornblende phenocrysts and are 39.3 Ma. Porphyritic rhyodacites contain plagioclase and biotite ± minor quartz. Crosscutting relations indicate rhyodacites are younger than the porphyritic dacites, but a single $^{40}Ar/^{39}Ar$ age on rhyodacite of 39.1 Ma is indistinguishable from the dacite ages. Aphyric rhyolites are imprecisely dated at

about 38 Ma. Basaltic andesite dikes dated at about 37.6 Ma occur in the Dee and Rossi-Storm deposits. A particularly distinctive suite of 37.3-Ma, porphyritic low-silica rhyolites and high-silica dacites containing coarse phenocrysts of plagioclase, quartz, biotite, hornblende ± sanidine are the focus of this study, both as an ore host at the Beast deposit and for what they imply about related plutons.

Middle Miocene (~14 to 15 Ma) rhyolitic lavas and tuffs are the youngest igneous rocks in the area and are exposed along the southwestern edge of the Carlin trend (Fig. 1-2) (Evans, 1980; Smith and Ketner, 1978; Henry and Faulds, 1999). Miocene lavas are sparsely porphyritic, fayalite-bearing, high-silica rhyolites lacking biotite and hornblende phenocrysts. Coeval tuffs and tuffaceous sediments of the Carlin Formation may be derived both from local and more distant sources (Fleck et al., 1998). $^{40}Ar/^{39}Ar$ ages on the tuffs and one lava range from 14.6 to 15.3 Ma (Fleck et al., 1998; Henry and Faulds, 1999). Although Miocene volcanism was regionally voluminous, for example in the northern Nevada rift (Wallace and John, 1998), Miocene volcanic rocks lie only along the flank of the Carlin trend, and Miocene intrusions are absent in the trend.

Implications of the Regional Distribution of Porphyritic Rhyolite Dikes

For reasons explained here, we interpret the porphyritic rhyolite dike of the Beast deposit and other Eocene dikes in the northern Carlin trend to be apophyses from much larger intrusions, that is, a major plutonic complex that fed the dikes. We infer that this complex underlies the 700-km^2 magnetic anomaly that encompasses the Emigrant Pass volcanic field and extends northward to approximately 5 km south of the Beast deposit. This interpretation is based on (1) the regional association of porphyritic rhyolite dikes with major Eocene igneous centers in northeastern Nevada, (2) the association of all centers with large magnetic anomalies that indicate underlying plutons, and (3) the location of the dike at Beast just north of the 700-km^2 anomaly (Fig. 1-3).

The porphyritic rhyolite dike of the Beast deposit is representative of the

distinctive coarsely porphyritic dikes of low-silica rhyolite to high-silica dacite that are present in nearly all major Eocene igneous centers near the Carlin trend (Table 1-1; Fig. 1-2). Large magma chambers are required to generate silicic melts by differentiation of basalt, by melting or assimilation of crust, or by a combination of processes (e.g., Barker, 1981; Anderson, 1990). Therefore, the porphyritic rhyolite and other Eocene dikes almost certainly were derived from such chambers. We first document the association of the porphyritic rhyolite dikes to major igneous centers, then discuss the setting of the dike at Beast relative to the magnetic anomaly and inferred plutonic complex.

Porphyritic rhyolite dikes have been recognized in the Tuscarora volcanic field (Henry and Boden, 1998a), at Lone Mountain and Swales Mountain (Evans and Ketner, 1971; Ketner, 1998; our investigation), in the Railroad mining district (Ketner and Smith, 1963; R.M. Tosdal, personal communication, 1998), and in the Emigrant Pass volcanic field (Henry and Faulds, 1999) extending northward into the northern Carlin trend (Evans, 1974a, b, 1980; this study). In the Tuscarora volcanic field, five major igneous centers were active during an intense period of magmatism between 39.9 and 39.3 Ma (Henry and Boden, 1998a). Porphyritic rhyolite dikes and other silicic to intermediate dikes were emplaced between 39.5 and 39.3 Ma in a northeast-striking swarm about 15 km long by 6 km wide centered on one of the centers (Fig. 1-2). The dikes coincide with an ~120 km^2 aeromagnetic anomaly that reflects a buried intrusion that probably fed volcanic rocks of the center (Fig. 1-3). Dikes extend no more than about 5 km from the edges of the magnetic anomaly and probably from the buried intrusion.

At Lone Mountain (Ketner, 1998) and Swales Mountain (Evans and Ketner, 1971), porphyritic rhyolite dikes were mapped as quartz porphyry or monzonite porphyry. They are closely associated with moderately large granodiorite to quartz monzonite plutons. Magnetic anomalies of ~50 km^2 at Lone Mountain and ~40 km^2 at Swales Mountain indicate that the dikes are probably apophyses from larger bodies at

depth (Fig. 1-3). Most porphyritic rhyolite dikes lie within about 3 km of exposed granodiorite or quartz monzonite. However, at Swales Mountain, the most distant of a chain of dikes crops out 8 km north-northeast of the larger intrusions and 7 km from the edge of the magnetic anomaly.

In the Railroad mining district (Ketner and Smith, 1963), a 1-km-diameter, equigranular granodiorite stock that is cored by a rhyolite porphyry intrusion is surrounded by numerous porphyritic rhyolite dikes. These dikes can be traced as much as 6 km from the outcrop of the central stock (R.M. Tosdal, oral commun., 1998). Magnetic data and the distribution of hornfelsed rock suggest a buried intrusion of about 80 km^2 (Fig. 1-3; R.M. Tosdal, personal communication, 1998). Dikes extend no more than 3 km from this larger intrusion.

The Emigrant Pass volcanic field is the southern, volcanic part of what we term the northern Carlin trend-Emigrant Pass igneous complex (NCEP). The Emigrant Pass field consists of numerous lava flows and shallow intrusions of andesite to low-silica rhyolite (Henry and Faulds, 1999). Small (≤ 1 km^2), shallow, porphyritic intrusions are also exposed to the north in Welches Canyon, where volcanic rocks are absent. Still farther north, in the northern Carlin trend, Eocene rocks consist only of dikes. Porphyritic rhyolite dikes are abundant in a north-striking swarm 25 km long and as much as 8 km wide extending from the central part of the Emigrant Pass field through Welches Canyon to the Beast deposit (Fig. 1-2; Evans, 1980; Henry and Faulds, 1999). In the Emigrant Pass field, dikes intrude Eocene volcanic rocks. In and north of Welches Canyon, dikes and other intrusions cut Paleozoic rocks.

The overall dimensions of the NCEP are best defined by the limits of the associated aeromagnetic anomaly (Fig. 1-3; Hildenbrand and Kucks, 1988), which coincides closely with all the Eocene igneous rocks. The anomaly contrasts with those associated with other Eocene centers in being much larger and consisting of numerous

discrete highs within an overall positive area. This complexity suggests the presence of numerous, separate but partly overlapping intrusions in the subsurface. Furthermore, the distribution of volcanic and intrusive rocks and their relation to the magnetic anomaly suggest that volcanic rocks of the Emigrant Pass field represent the highest, least eroded part of the complex. The shallow intrusions in Welches Canyon are a slightly deeper level from which volcanic rocks have been eroded. The larger, main intrusions that fed all volcanic rocks and dikes are at still deeper levels and underlie the anomaly. Nevertheless, all dikes are probably within a few kilometers of a source pluton.

^{40}Ar/^{39}Ar ages of intrusive and volcanic rocks indicate the NCEP was active from possibly 40 Ma to 36 Ma. Igneous rocks in the Emigrant Pass field range from approximately 36 to 38 Ma (Henry and Faulds, 1999). Two ages of andesitic and dioritic intrusions in Welches Canyon are identical at 38.34 Ma (WC-31, H97-21; Table 1-2). Porphyritic rhyolite dikes in Welches Canyon and northeast of the Cretaceous granite are 37.19±0.11 and 37.34±0.09 Ma (H97-22b, Rich-10, Table 1-2), indistinguishable in age from the dike of the Beast deposit. Other Eocene dikes in the northern Carlin trend, discussed here, are 38, 39.3, and possibly 40.1 Ma.

The porphyritic rhyolite dike at the Beast deposit is approximately 5 km north of the north edge of the magnetic anomaly (Fig. 1-3). This distance is similar to the distance that these dikes extend from other Eocene igneous centers. From its location and age, the dike at Beast is probably an apophysis from one of the intrusions of the magnetic anomaly. Aternatively, the dike could be an apophysis from an intrusion that is closer to or even directly beneath the Beast deposit. Such an intrusion would have to have almost no magnetic expression, unless the modest anomaly generally attributed to the Goldstrike diorite reflects both it and an Eocene body.

The Beast Deposit

District setting

The Beast deposit is in the northern Carlin trend about 0.7 km south of the Genesis deposit and 3 km south of the huge Betze-Post deposit (Fig. 1-4). Through 1997, Beast had produced 7.3 million tonnes of oxide ore at an average grade of 0.7 g/t gold (5,110 kg), about half of which was hosted by the porphyritic rhyolite dike. The remaining ore was hosted by laminated silty carbonate rock and calcareous mudstone of the lower part of the Siluro-Devonian Roberts Mountains Formation (Ressel et al., 1999). Both units are strongly silicified and brecciated in the center of the deposit, with argillic rock comprising peripheral areas.

Ore at Beast is dominantly structurally controlled, as are many sedimentary rock-hosted deposits of the Carlin trend (Christensen, 1996). The 800-m long and 50-m wide deposit follows the dike and Beast fault (Fig. 1-5), an east-dipping splay of the Genesis fault that the dike intruded, and is subparallel to the north-northwest-striking Tuscarora anticline. The Genesis fault is one of several major north-northwest-striking, high-angle faults with substantial dip-slip displacement that acted as first-order controls on mineralization in the Betze-Post, Genesis, Deep Star, and Meikle deposits (Teal and Jackson, 1997).

Beast dike

The principal structure of the Beast deposit is the north-striking porphyritic rhyolite dike, which is as much as 55 m wide in the mine (Figs. 1-5, 1-6a). The dike is altered to varying degrees along its 1-km strike length in the pit. The dike is covered to the north but probably extends at least 2 km to the south, because similar rhyolite has been intersected in drill holes and is present as float in colluvium. Only small parts of the dike cropped out before mining (Evans, 1974b).

The rhyolite dike contains about 30% phenocrysts consisting mostly of euhedral

plagioclase 0.3 to 0.5 cm in diameter, embayed quartz as much as 0.4 cm in diameter, minor euhedral sanidine as much as 2.5 cm long, and altered biotite and hornblende (Fig. 1-6b). Apatite, Fe-Ti oxides, and zircon occur in trace amounts. Based on phenocryst mineralogy and analyses of weakly altered samples (Table 1-3, BST-30, BST 130), the dike is low-Si rhyolite.

In most of the dike, plagioclase and hornblende are altered to quartz, kaolinite, carbonate, and hematite; biotite to kaolinite, barite, and carbonate; and sanidine to kaolinite and barite. Biotite and sanidine are unaltered in the least argillized, non-ore-bearing rock. Optically visible growth zoning in sanidine phenocrysts reflects varying barium content as qualitatively determined by SEM-EDS analysis. Barite in former sanidine may reflect high initial Ba contents. The rhyolite matrix is altered to quartz, kaolinite and/or montmorillonite, carbonate, and minor sericite but probably consisted of fine-grained, intergranular quartz, alkali feldspar, and biotite.

The dike has been sheared and brecciated along the Beast and associated faults (Figs. 1-5 and 1-6a). Breccia, which is generally silicified and mineralized, is best developed along the footwall of the dike. Away from brecciated zones, argillic alteration predominates. Fluids apparently preferentially followed the faulted contact between the dike and Paleozoic wallrock and were not able to readily penetrate unbrecciated parts of the dike. Structural thickening of the dike along the north-striking, east-dipping (65-70º) Beast normal fault is possible, because the dike is thickest in a highly sheared and altered zone in the core of the Beast deposit (Fig. 1-5). On the 6,075-foot elevation, a thin north-trending sliver of silicified and brecciated thin-bedded limestone is preserved between silicified and brecciated rhyolite on the west and mildly argillized rhyolite on the east, implying the presence of a fault having post-mineral movement; alternatively, a dike splay may be present. North and south of the mineralized zone, the dike thins

substantially, is characteristically argillized, and is generally much less fractured.

In the Beast pit, the porphyritic rhyolite dike truncates an altered 5- to 10-m wide dike of finely porphyritic rhyodacite (Fig. 1-5) of probable Jurassic age (M.W. Ressel, unpublished $^{40}Ar/^{39}Ar$ data). Intensely brecciated and silicified rocks in the center of the deposit at and near the intersection between the rhyolite dike and the vertical, N40ºE-striking Jurassic dike have higher Au grades (>1 g/t).

Alteration and mineralization of porphyritic rhyolite

The dike is moderately to strongly silicified, particularly near its footwall where it is brecciated. The breccia-dominated ores are extensively oxidized, but relict pods of sulfidic rock are common where silica flooding has prevented complete oxidation of sulfides. Silica flooding is expressed by pervasive replacement of rhyolite to jigsaw-textured quartz (0.2-0.4 mm dia.; Lovering, 1972) and lesser kaolinite after feldspar, infilling between breccia clasts by fine-grained jigsaw quartz (≤30 μm dia.), and by abundant quartz veinlets from 1 to 10 mm thick. Phenocrysts are largely converted to quartz and kaolinite. Veinlet quartz is clear and vitreous and commonly has comb-textured margins and cores of fine-grained jigsaw quartz, alunite, and kaolinite. Fe sulfides occur in both veinlets and silica-replaced rocks but are generally more abundant in silica-replaced rock.

Rhyolite just outside of the zone of brecciation is moderately silicified and fractured and contains sparse quartz-sulfide veinlets. Density of fracturing and degree of silicification progressively decrease away from the footwall of the dike, and the amount of clay, predominantly kaolinite grading outward to montmorillonite, increases both laterally across the dike nearer its hanging wall (Fig. 1-7) and along strike to the north and south. Argillized phenocrysts of sanidine and plagioclase are common, as are mafic phenocrysts altered to clay and iron oxides/hydroxides. Carbonate is common in more distal montmorillonite-altered rhyolite.

Silty carbonate rocks in the footwall of the Beast dike are silicified and brecciated in the ore zone. The degree of silicification and fracturing decreases over ~20 to 30 m from the Beast fault/dike to form a zone of decarbonatized rock that is locally bleached white (Fig. 1-7). The rocks appear fresh and are carbonate-bearing at distances >60 m from the Beast fault/dike.

Breccia types

Two, somewhat gradational, types of siliceous breccia, matrix-supported and crackle, are the dominant ore hosts (Figs. 1-6c, d). Both breccias are mostly along the footwall of the Beast fault/dike and are therefore collectively termed footwall breccias. They form a tabular body along the fault and dike that averages 10 m wide but is as much as 40 m wide in the center of the deposit**.** Matrix-supported breccia occurs at the contact of the dike and underlying Roberts Mountains Formation and is the most important ore host. Matrix-supported breccia (Fig. 1-6d) is mostly heterolithic and contains rounded, oblate, or subangular clasts of silicified rhyolite, limestone, and minor Jurassic rhyodacite, ranging from <0.1 to 3 cm diameter. Part of the breccia contains clasts that are roughly graded with respect to size. Breccia matrix is composed largely of fine-grained, jigsaw-textured quartz and lesser Fe sulfides, kaolinite, alunite, and solid carbon. Sulfides constitute <1 to 5 volume percent. Abundant vugs and veinlets occur in the breccia, the most common of which contain quartz, quartz, pyrite, and stibnite, or alunite and kaolinite.

Crackle breccia, a mostly clast-supported siliceous breccia (Fig. 1-6c), grades outward from matrix-supported breccia away from faults. Crackle breccia is monolithologic, either with clasts of rhyolite or limestone. The clasts are angular and widely variable in size from about 0.1 to 10 cm in diameter. Individual clasts commonly match with surrounding clasts in "jigsaw" manner. The breccia matrix is composed of fine-grained jigsaw and drusy quartz, with smaller amounts of Fe sulfides, kaolinite, and

alunite like that of matrix-supported breccia. Veinlets in crackle breccia are more quartz-rich and sulfide-poor than those in the matrix-supported breccia, and Au grades are generally lower. Crackle breccia grades outward to massive quartz-kaolinite rock.

Both footwall breccias likely formed from a combination of faulting, hydrothermal activity, and possibly collapse. Because breccia is concentrated along the fault, fault-related disruption is probably the most important process. The heterolithic, rounded clasts in matrix-supported breccia would appear to require a significant amount of transport and mixing. Silicified clasts in matrix-supported breccia locally have "fluidized" forms that define a crude foliation. Development of foliation is consistent with shearing associated with faulting before silicification of the clasts. Hydrothermal fluids channeled along the Beast fault subsequently silicified the tectonized rock. Crackle breccia appears to have formed from fault-induced fracturing but farther from faults.

Ore petrology

Matrix-supported breccia hosts as much as 80% of the ore. The black or dark gray matrix consists of extremely fine-grained quartz, Fe-As sulfides (pyrite, arsenopyrite and marcasite), and solid carbonaceous material (Fig. 1-6d). Veinlets with a similar sulfide assemblage crosscut rounded clasts of porphyritic rhyolite that are altered to a mixture of quartz, kaolinite, and Fe sulfides. Clasts of Jurassic rhyodacite are composed of quartz+sericite±pyrite that contrasts markedly with ore-stage quartz-kaolinite-pyrite alteration of the rhyolite. Veins containing Fe sulfides and clasts with disseminated sulfides are, in turn, cut by multiple generations of veinlets containing quartz and kaolinite, with remaining open-space filled by variable amounts of stibnite, sphalerite, alunite, and barite. In many places, clasts of brecciated rock cut by Fe sulfide-rich veins have been subsequently incorporated in later sulfide-poor breccia. Clearly, the footwall of the dike underwent multiple brecciation events.

Brecciation and mineralization must, in large part, postdate emplacement of the

Beast dike, as abundant clasts of mineralized porphyritic rhyolite are included within these footwall breccias. There is no apparent correlation between the presence of fine-grained Fe sulfide and the type of clasts. The highest Au grades (>2 ppm) are associated with fine-grained or "sooty" Fe sulfides. This may be related to the greater abundance of Fe sulfide in matrix-supported breccias rather than strict association of Au with fine sulfides. Rhyolite crackle breccia ores, for example, contain less abundant and coarser-grained Fe sulfides.

Early ore-stage sulfides in footwall breccias occur primarily within abundant sinuous veinlets and as disseminations of very fine grained (<1 to 10 μm), irregularly-shaped, porous pyrite and arsenic-rich pyrite, and euhedral arsenopyrite (Figs. 1-6e, f) accompanied by carbonaceous material. Sulfides comprise as much as several percent of the breccias. Arsenian pyrite commonly forms discrete bands around cores of arsenic-free pyrite (Fig. 1-6f), although some smaller grains appear to be composed wholly of arsenian pyrite. In addition, arsenopyrite commonly envelops and partly replaces arsenian pyrite, indicating late arsenopyrite precipitation (Fig. 1-6e). Less commonly, an absence of overgrowth or replacement textures between arsenian pyrite and arsenopyrite suggests coprecipitation. Marcasite is rare in the Beast deposit, although laths of porous, isotropic Fe sulfide having the habit of marcasite are abundant, suggesting that some pyrite may have inverted from precursor marcasite (Murowchick, 1992). Similar Au-stage Fe-sulfide parageneses are described for high-grade gold ores at Lone Tree (Kamali, 1996) and Betze-Post (Ferdock et al., 1997).

Crosscutting veinlets and open-space fillings that lack gold are composed of comb quartz, kaolinite, barite, alunite, sphalerite, stibnite, rutile, and Ni-Co sulfides and minor amounts of Fe-As sulfide minerals (Fig. 1-6g). Similar occurrences have been described in several other Carlin-type deposits (e.g., Joralemon, 1951; Ferdock et al., 1997). Fe-poor, mammillary sphalerite, commonly associated with alunite, partly replaces stibnite

in late-stage veinlets and vugs.

Inward from the footwall of the dike, a stockwork of veins forming both clast- and matrix-dominated ores consists mostly of quartz with lesser amounts of Fe-As sulfides and kaolinite. These quartz veins contain the same sulfide assemblage but in much lesser abundance than do veins nearer the footwall. The morphology of sulfide grains, however, is markedly different. Pyrite grains are characteristically euhedral and commonly have well-defined outer zones of arsenian pyrite that are, in turn, enveloped by arsenopyrite. Arsenopyrite appears to be intergrown with arsenian pyrite, suggesting coprecipitation. Barite, covellite, sphalerite, and chalcocite(?) partly replace the Fe-As sulfides (Fig. 1-6h). However, zinc and copper contents of the crackle breccia are low, $\leq$150 ppm and 10 to 30 ppm, respectively (Table 1-3). Kaolinite, in some cases as coarse grains, forms late-stage patches and veinlets associated with drusy quartz as well as earlier finer-grained replacements of feldspar phenocrysts. Multiple stages of late quartz±kaolinite±alunite veinlets, similar to that observed in the matrix-supported breccia, are present in crackle breccia ores. These veinlets truncate earlier quartz-Fe sulfide-kaolinite veinlets. In a few instances, alunite replaces igneous clasts together with quartz, kaolinite, and pyrite. More commonly, however, coarse alunite and kaolinite accompanied by rare sulfides form the cores of comb-quartz veinlets.

The morphological differences in vein sulfides between matrix-supported and crackle breccias may largely reflect sulfide content. Total sulfide contents, and corresponding gold grades, are highest in matrix-supported breccias, in which sulfides and carbonaceous material form fine-grained, "sooty" masses, whereas crackle breccias contain veins with greater amounts of quartz and lower concentrations of sulfides and carbonaceous material. An irregular and relatively narrow transition exists between the two types of breccia. Increased precipitation of Fe-As sulfides may have occurred at the contact between rhyolite and host carbonates as a result of its higher degree of

brecciation, permeability, and reactivity.

Multiple stages of precipitation of both kaolinite and quartz are indicated by mutually crosscutting relationships and morphological constraints. Hypogene kaolinite and Fe-As sulfides replace feldspar phenocrysts in the dike. Early kaolinite is in turn cut by later quartz+kaolinite± alunite±barite veinlets. Late veinlets are zoned from quartz margins to cores of alunite, kaolinite, and locally, barite.

Supergene oxidation of sulfides generated kaolinite, alunite, hematite, jarosite, goethite, scorodite, and dussertite (Ba-Fe arsenate). Late chalcedonic quartz veinlets predate oxidation. Oxidation does not appear to have redistributed gold significantly because unoxidized and oxidized parts of otherwise similar silicified dike breccias have similar Au concentrations

Paragenesis

Crosscutting relations in breccia, vein, and replacement ore indicate four paragenetic stages, each of which produced distinct assemblages of ore and gangue minerals (Fig. 1-8). The earliest episode (stage 1), resulting in quartz-kaolinite alteration of rhyolite, was the most important for gold deposition. Alteration is manifested in rhyolite by pervasive replacement of feldspar and other phenocrysts by kaolinite and Fe sulfides and replacement of groundmass by silica and fine-grained Fe sulfides. Abundant fine-grained arsenopyrite and pyrite (Figs. 1-6e, f) and lesser amounts of early-formed marcasite accompany quartz and kaolinite and both comprise the matrix of footwall breccias and occur in veins and within disseminated ores. Arsenopyrite was deposited late in stage 1 (Fig. 1-6e). Solid carbonaceous material, probably derived from the Roberts Mountains Formation, commonly is present with fine-grained Fe-As sulfides. In sulfide-poor crackle breccia, euhedral arsenian pyrite has overgrowths of arsenopyrite.

Early Fe sulfide and carbon-bearing mineralization is overprinted by stage 2 veinlets and vug fillings that contain quartz, stibnite, iron-poor sphalerite, alunite, barite,

and minor Ni-Co sulfide (Figs. 1-6g and 8). The sulfide and sulfate phases generally do not occur together, although locally alunite appears to be intergrown with sulfides (Fig. 1-6g). Also, some of the minerals may have precipitated at different times. For example, sphalerite consistently rims stibnite in stage 2 veinlets. Iron is notably absent from mineral phases that precipitated during stage 2.

Stage 3 veins and vug fillings composed of drusy quartz, kaolinite, and alunite with little or no sulfide succeed stage 2 veinlets. In some cases, mutually intersecting stage 3 veinlets (Fig. 1-8) contain small amounts of Fe sulfide and rutile(?) within their cores. In crackle breccia, stage 3 mineralization also includes barite, covellite, sphalerite, and chalcocite, which commonly envelope and partly replace earlier-formed euhedra of pyrite and arsenopyrite (Fig. 1-6h), similar to relations in the Lone Tree deposit (Kamali, 1996).

Abundant Fe-As oxides, including jarosite, scorodite, dussertite, hematite, and goethite (Fig. 1-8) were produced during supergene oxidation of sulfide-bearing rocks. Oxidized rocks comprise the bulk of the ores mined at Beast to date. Supergene alunite and kaolinite typically form veinlets, vug fillings and fracture coatings.

Alunite of two types is a common late mineral in rhyolite breccia-hosted ores of the Beast deposit. The first is closely associated with quartz, barite, kaolinite, stibnite, and sphalerite, predominantly in veinlets that clearly postdate major deposition of Fe-As sulfide and as fine-grained replacement of feldspar and groundmass minerals of igneous clasts in ore breccia also containing pyrite and kaolinite. Although alunite in Carlin-type deposits is interpreted to be entirely supergene (Arehart et al., 1992), the close textural ties between alunite and these minerals suggest a hypogene origin.

Supergene alunite is associated with jarosite, hematite, dussertite, scorodite, goethite, and other Fe-As oxide minerals formed at the expense of sulfides. This alunite is light pink and is commonly present as monomineralic vug fillings and veinlets similar

to occurrences described by Arehart et al. (1992) for several deposits of the Carlin trend.

Geochemistry

Multi-element geochemical data have been obtained on nineteen samples of ore and altered rock from the Beast deposit (Table 1-3) using X-ray fluorescence (XRF), instrumental neutron activation (INAA), and inductively coupled plasma-atomic emission spectrometry (ICP). Concentrations of gold range from about 1 ppb in argillically-altered rhyolite to as high as 5.9 ppm in siliceous, matrix-supported breccia. The mean Au content of 13 samples of siliceous ore breccia, including crackle breccia, is 1.5 ppm, whereas the mean of 7 samples of matrix-supported breccia is 2.4 ppm. Argillically-altered samples generally have very low concentrations of Au (1 to 73 ppb), the exception being one pervasively kaolinitized and sulfide-rich breccia from the orebody that contains 1.1 ppm. These data indicate that Au is strongly concentrated in silicified rocks, and particularly in matrix-supported breccia.

Ore and mineralized rock at Beast contain elevated concentrations of Ag (0.1 to 3.5 ppm), As (maximum = 11,000 ppm; mean = 3,000 ppm), Sb (4,600 ppm; 519 ppm), Hg ($\leq$15.8 ppm), and Tl ($\leq$30.8 ppm). Au does not correlate well with these or other ore elements (Fig. 1-9). Arsenic generally correlates well with Sb, but two distinct populations may reflect the introduction of Sb during both stages 1 and 2 paragenetic events and As mainly during stage 1 (Fig. 1-9). Arsenic also correlates well with Tl. The strong spatial association of Au with these elements, but its generally poor numerical correlation is typical of many Carlin-type deposits in Nevada (e.g., Harris and Radtke, 1976) and suggests complex parageneses.

Other elements were also introduced in smaller and more variable amounts during mineralization. Most notable are Ni (maximum = 459 ppm; mean = 96 ppm), Co (144 ppm; 35 ppm), Mo (78 ppm; 16 ppm), W (42 ppm; 19 ppm), Zn (maximum = 1,623 ppm)

and Se (maximum = 36 ppm). Ni and Co appear to be introduced as Ni-Co sulfide during stage 2. Zinc occurs sporadically in Fe-poor sphalerite of stage 2, commonly in association with stibnite. The phases that contain Mo, W, and Se are not known, but these elements are probably dispersed in late-stage minerals as well. At the Griffin deposit, late quartz veins contain Mo and Pb in Ag-Sb sulfosalts (Ressel et al., 2000).

Au/Ag ratios at Beast vary from 0.5 to 6, possibly reflecting the small number of analyses. Alternatively, differences in Au/Ag ratios may reflect mixing of two or more ore fluids or complex overlap of minerals of different paragenetic stages (e.g., stages 1 and 2).

Element mobility

The isocon method (Grant, 1986) helps evaluate relative gains and losses of elements and mass change between mildly altered and variably mineralized and brecciated samples of porphyritic rhyolite (Fig. 1-10). Samples BST-30 and BST-130 of mildly argillic rhyolite are least altered. Sample BST-111 is representative of matrix-supported breccia ore. Sample BST-122A is an argillically altered, mineralized rhyolite that has had little silica added. The results demonstrate the addition of components commonly associated with Carlin-type deposits in ore-grade porphyritic rhyolite, including As, Sb, Hg, and Tl. Also apparent is the addition of Ni, Co, W, ±Mo. Hofstra et al. (1999) showed similar W addition for mineralized dikes from deposits of the Jerritt Canyon district, Nevada. The high Cu content of altered sample BST-122A (169 ppm) is not representative of the deposit, as all other samples have Cu contents below 31 ppm.

In contrast, the alkali and alkaline earth elements (Mg, K, Ca, Ba) and Mn have been strongly leached from silicified rhyolite (Fig. 1-10). Nearly all Na and most Sr have been removed from both argillically-altered and silicified rhyolite. The removal of Na and Ca from all host rocks appears to be a fundamental process related to Carlin-type

mineralization (e.g., Phinisey et al., 1996) and differs markedly from Na and Ca metasomatism that commonly is associated with many "mesothermal" gold deposits.

The isocon method can also be used to evaluate mass change that results from hydrothermal alteration and mineralization. Mass change is shown by the variation in concentrations of elements determined as immobile. Figure 1-10 shows lower concentrations of immobile elements in mineralized rhyolite breccia relative to unmineralized rhyolite that indicates dilution through the addition of silica during hydrothermal alteration. The data suggest about 60% mass gain in a representative siliceous, matrix-supported rhyolite breccia ore relative to mildly clay-altered porphyritic rhyolite. Mass gain in siliceous ores at Beast, mainly through sililca addition, is analogous to the gains that accompany silicification of carbonate rocks to form jasperoid in Carlin-type deposits, including Carlin (Bakken and Einaudi, 1990).

Conclusions of the Beast deposit study

The alteration assemblage, paragenesis, and geochemistry of ores and its location within the Carlin trend provide compelling evidence for classification of the Beast deposit as Carlin-type. Beast is unique among such deposits only in having a large percentage of ore hosted in felsic igneous rock. Quartz-kaolinite alteration at Beast is a common feature of many other Carlin-type deposits. The dominance of siliceous ore at Beast is most similar to jasperoid ores at other Carlin-type deposits.

Gold deposition at Beast was associated with early Fe sulfides including arsenian pyrite, which was followed by stibnite, Fe-poor sphalerite, Ni sulfides, and barite. This paragenetic sequence is similar to those described for many Carlin-type gold deposits in Nevada (Joralemon, 1951; Radtke et al., 1980; Kuehn and Rose, 1992; Hofstra, 1994; Arehart, 1992; 1996; Ilchik, 1991; Kamali, 1996; Ferdock et al., 1997).

Mineralized and ore-grade rhyolite at Beast is similar geochemically to sediment-

hosted ores in the Carlin trend and elsewhere in Nevada. All have characteristically high contents of As, Sb, Hg, and Tl. In addition, elevated concentrations of other elements, including Ni, Co, Mo, W, Zn, and Se, have been reported for other Carlin-type gold deposits in Nevada (Bagby and Berger, 1985; Berger and Bagby, 1991; Lauha and Bettles, 1993; Leonardson and Rahn, 1996; Hofstra et al., 1999). Au/Ag ratios are consistent with most other Carlin-type deposits, although the lower ratios of some Beast ores overlap with the distal-disseminated Au-Ag deposits such as Lone Tree, Nevada.

Ages and Relation to Ore of Eocene Dikes of the Carlin Trend

Eocene dikes (Table 1-1) of the Carlin trend are variably altered and mineralized. Their ^{40}Ar/^{39}Ar ages (Figs. 1-4, 1-11, and 1-12; Table 1-2; Appendix 1-1) demonstrate that intrusion lasted ~3 Ma and that ore formation was broadly coeval with dike emplacement.

Porphyritic rhyolite that hosts ore at the Beast deposit

^{40}Ar/^{39}Ar ages of sanidine and biotite phenocrysts from the host porphyritic rhyolite dike and of supergene alunite bracket gold mineralization between 37.3 and 18.6 Ma. Biotite and, less commonly, sanidine phenocrysts are locally preserved in the altered and mineralized dike. Sanidine yielded a step-heating plateau age of 37.37±0.11 Ma (all ages quoted at 2σ) and weighted mean single-crystal age of 37.34±0.12 Ma (BST-114; Figs. 1-5 and 1-11; Table 1-2). These ages are identical within analytical uncertainty to the plateau age of 37.31±0.14 Ma obtained from biotite (BST-30). The concordance of all ages and the flat spectra of sanidine preclude Ar loss or excess Ar and demonstrate that the dike was emplaced at 37.3 Ma, which is a maximum age for mineralization. A sample of supergene alunite from a monomineralic vein in oxidized matrix-supported breccia ore yielded a ^{40}Ar/^{39}Ar laser fusion "plateau" age of 18.6±1.2 Ma (Fig. 1-11). The large uncertainty resulted from low ^{40}Ar yield (Appendix 1-1). This age lies within the 30 to 8

Ma range of supergene alunite of the Carlin trend (Arehart et al., 1992; Hofstra et al., 1999).

Porphyritic rhyodacite and dacite dikes of the Meikle - Betze-Post corridor

Dikes of porphyritic dacite and porphyritic rhyodacite intrude along the Post fault zone between the Meikle and Betze-Post deposits (Fig. 1-4). The dacite dikes form a continuous 4-km-long set of at least 4 parallel dikes, each 5 to 30 m thick and petrographically indistinguishable. All dacite dikes are altered to some degree. Alteration ranges from mild montmorillonite-carbonate, barren of ore, to ore-bearing, quartz-sericite-pyrite. The porphyritic rhyodacite dikes are restricted to the Betze-Post deposit where they parallel and, at the south end of the deposit, are in contact with porphyritic dacite dikes. At one contact, the rhyodacite has a glassy margin that demonstrably chilled against dacite. Therefore, at least at this location, the rhyodacite is younger.

Biotite $^{40}Ar/^{39}Ar$ ages have been determined on two samples of porphyritic dacite. A relatively unaltered part of a dike in the Griffin deposit gives a plateau age of 39.21±0.15 Ma (G11-005-4-492; Figs. 1-4 and 1-11; Table 1-2). A dike in the Betze-Post deposit gives an age of 39.3±0.8 Ma (Arehart et al., 1993b; their published age has been recalculated using the monitor age of 27.84 Ma on Fish Canyon Tuff sanidine used in this study). The similarity in petrographic character and in the two ages argues that all porphyritic dacites were emplaced at one time.

Biotite and plagioclase phenocrysts and matrix of glass and microlites from a single sample of porphyritic rhyodacite gave discordant ages (BP-2; Fig. 1-11; Table 1-2). Biotite yielded 39.07±0.21 Ma, which is the best estimate of emplacement age. Plagioclase gave a slightly u-shaped spectrum with a 3-step plateau age of 38.10±0.37 Ma. The matrix gave a highly disturbed spectrum that indicates excess Ar. The lowest-temperature step is 862 Ma; ages dropped to a low of 40 Ma in higher temperature steps. Combined with the field relations, the 39.07 Ma age indicates rhyodacite intruded shortly

after porphyritic dacite.

Porphyritic dacite dikes in the Rodeo, Griffin, and Meikle deposits (Fig. 1-4) are locally ore grade (≤8 g/t; Ressel et al., 2000). These mineralized dikes are strongly quartz-sericite-pyrite altered and have compositions that are similar to ores at Beast and other Carlin trend deposits. The 39.21-Ma dike at Griffin is ~160 m from, and, based on drillcore, probably continuous with an ore grade dike. Therefore, Au mineralization at Griffin occurred after 39.21 Ma.

Porphyritic dacite in the Betze-Post deposit is variably interpreted as having been emplaced post ore (Arehart et al., 1993b), during the latest stage of Au-related hydrothermal alteration (Leonardson and Rahn, 1996), or pre ore (Emsbo et al., 1996). The post-ore interpretation is based on the dike containing inclusions of ore but not being enriched in Au (≤100 ppb; Arehart et al., 1993b). However, Emsbo et al. (1996) showed that the dike is pervasively quartz-sericite-pyrite altered, argillically altered along margins and fractures, and contains As-rich pyrite as veinlets and overgrowths on pyrite; argillic alteration added Au, S, As, Sb, Hg, Tl, W, Ag, and Te. All features are characteristic of Carlin-type deposits. Combining these data, Leonardson and Rahn (1996) concluded the dike was emplaced near the end of mineralization. Late- or pre-mineral dike intrusion requires that gold mineralization be ≤39.3 Ma. This could be either the same event that generated the Beast deposit or a separate, older event.

The 39.07-Ma porphyritic rhyodacite dike in the Betze-Post pit appears unaltered, having unaltered plagioclase and biotite phenocrysts in a matrix of hydrated glass and microlites. However, matrix and phenocrysts at the margins of the dike are partly altered to clay. Interaction with meteoric water is suggested by low hydrogen isotopic compositions of the glassy matrix (M.W. Ressel, unpublished data). Glass retains excess Ar. These data suggest the dike was affected by hydrothermal solutions, and that mineralization at Betze-Post postdates the dike. Given that its age is indistinguishable

with the older dacite, this relation has similar implications for timing of mineralization.

A porphyritic rhyodacite dike in the Genesis deposit was dated at 40.1±0.3 Ma and interpreted to be post-mineral (Fig. 1-4; Farmer, 1996). However, the dike is quartz-sericite-pyrite and argillically altered and mineralized in the lower parts of the deposit where it intersects the Post-Genesis fault zone (M.W. Ressel, unpublished data). Alteration is typically argillic, although mineralized rock contains abundant sericite and pyrite.

Aphyric rhyolite dike, Deep Star deposit

The most silicic dikes in the northern Carlin trend are aphyric rhyolites that are found in the Deep Star and Genesis deposits (Fig. 1-4) as well as near Richmond Mountain and as a lava dome in Welches Canyon. At Deep Star, the dike is 7 m thick and has green, hydrated glass margins surrounding a core that is spherulitically devitrified to K feldspar and quartz. ^{40}Ar/^{39}Ar analysis of devitrified rock gave an irregular spectrum with an apparent age around 38 Ma (DS-13; Figs. 1-4 and 1-11; Table 1-2). The aphyric rhyolite at Deep Star mostly forms the footwall of the orebody but locally hosts ore, so is pre ore (Altamirano and Thompson, 1999). Montmorillonite alteration of formerly glassy rock next to the orebody is locally strong. Devitrified rock contains minor white mica, carbonate, pyrite, and arsenopyrite.

Summary of age relations

Our ^{40}Ar/^{39}Ar ages of dikes and their relations to ore demonstrate that Carlin-type mineralization occurred after 37.3 Ma at the Beast deposit. Mineralization occurred after ~39.2 Ma at Griffin and Betze-Post and after 38 Ma at Deep Star. However, these data allow either a single episode after 37.3 Ma or several episodes beginning as early as about 39.2 Ma. The area demonstrably underwent multiple igneous episodes between at least 40.1 Ma and 37.3 Ma (Fig. 1-12). As noted above, the silicic dikes are apophyses

from underlying plutons. Therefore, plutons spanning this age range lie nearby, presumably beneath the NCEP. Multiple igneous episodes allow multiple thermal episodes and, therefore, multiple hydrothermal events. Further examination of field relations between Eocene dikes and ore are needed to resolve the possibilities.

Depth of Mineralization and Amount of Tilting Since Late Eocene Time

The gentle tilts of Eocene volcanic rocks in the Emigrant Pass field and the steep dips of dikes in the northern Carlin trend (Fig. 1-4) show that the area of the trend has not undergone large-scale extension since volcanism. Eocene lavas of the Emigrant Pass field are tilted eastward from 5 to 30º, resulting from east-oriented extension dominantly after 25 Ma (Henry and Faulds, 1999). Dips decrease northward, toward the Carlin trend, and dips in the northernmost volcanic outcrops are ≤5°. The dominantly north-striking dikes in the trend dip steeply both to the west and east (Fig. 1-4), which suggests little post-Eocene tilting of the trend. Preliminary data suggest minor extension in the Eocene, approximately during inferred Au deposition (Henry and Faulds, 1999), but these induced little tilting in the trend.

Although Carlin-type deposits are considered to have formed at depths of 4 km (e.g., Kuehn and Rose, 1992; 1995), our data suggest shallower formation. Common glassy, spherulitic, lithophysal, felsitic, or granophyric textures in Eocene dikes suggest shallow, sub-volcanic emplacement. In addition, Eocene volcanic rocks retain well-preserved volcanic landforms in the nearby Emigrant Pass field and at Swales Mountain, Lone Mountain, and Tuscarora at comparable elevations to the Carlin trend; this suggests only modest erosion since late Eocene. Emigrant Pass and Welches Canyon are in the same fault block as the northern Carlin trend, so Basin and Range faulting has not altered their relative elevations. Because Eocene dikes are mineralized in the Carlin trend, it follows that some gold was deposited at shallow levels, less than ~2 km below the paleosurface. A relatively shallow origin is consistent with some of the lower pressures

determined by fluid-inclusion studies of ores from the Betze-Post and Meikle deposits (Lamb and Cline, 1997).

Relation of Mineralization to Eocene Magmatism in the Northern Great Basin

The large quantity of gold present as well as widespread hydrothermal alteration surrounding Carlin-type deposits in the northern Great Basin indicates the involvement of a regional process in their formation (e.g., Christensen, 1996; Arehart, 1996; Ilchik and Barton, 1997; Henry and Boden, 1998b). Suggested mechanisms range from the generation of gold-bearing fluids through metamorphism in the deep crust either during large-scale Eocene extension (Seedorff, 1991) or Cretaceous contraction (Arehart, 1996), by the elevation of regional geothermal gradients and large-scale hydrothermal circulation induced by amagmatic Basin and Range extension (Ilchik and Barton, 1997), or by the introduction of large volumes of Eocene magma into the upper crust (Thorman et al., 1995; Henry and Boden, 1998b).

The association of the Carlin trend with a major Eocene igneous center that appears to be contemporaneous with mineralization strongly argues that Eocene magmatism is the key factor. This conclusion is supported by regional data. Eocene, intermediate to silicic calc-alkaline rocks define a coherent, east-west belt in the northern Great Basin (Fig. 1-1; McKee, 1971; Christiansen and Yeats, 1992). This area encompasses the region of known Carlin-type deposits and many porphyry, skarn and epithermal precious-metal deposits of Eocene age. Many of the more important sedimentary rock-hosted gold deposits are situated near Eocene magmatic centers. Examples include several pluton-related deposits in the Battle Mountain and McCoy mining districts, Nevada, that are adjacent to 38 to 39 Ma porphyry Cu-Au and Au skarn systems (Theodore and Blake, 1975; Emmons and Eng, 1995; Theodore, 1998). In Utah, the Barney's Canyon and Melco deposits are located near the giant 38.5 Ma Bingham Canyon Cu-Au porphyry system, and other Eocene intrusions are spatially associated

with the Mercur deposit (Wilson and Parry, 1995; Presnell and Parry, 1996; Mako, 1997).

Other factors, such as major basement faults that controlled the distribution of Carlin-type deposits in Nevada (e.g., Wooden et al., 1998), were also important. In contrast, the Carlin trend has undergone only modest total extension, and only some of it occurred in the Eocene. Therefore, large-magnitude extension to generate metamorphism or high heat flow is unlikely to have been important, although faults and fractures certainly provided pathways for hydrothermal fluids. We conclude that, without Eocene magmatism, Carlin-type deposits probably would not have formed.

The association of Carlin-type deposits with Eocene magmatism in general and of the Carlin trend with a large Eocene plutonic complex indicates that Carlin-type deposits should be considered "pluton-related" (e.g., Sillitoe and Bonham, 1990). The distinction between Carlin-type and Carlin-like or distal-disseminated deposits (Seedorff, 1991; Cox, 1992; Mosier et al., 1992) probably should be reexamined.

Summary and Conclusions

The Beast deposit of the northern Carlin trend is hosted largely by a 37.3-Ma porphyritic rhyolite dike. The deposit has alteration and ore mineralogy, paragenesis, and geochemistry of typical Carlin-type deposits, but the dike has not undergone the multiple alteration episodes that Paleozoic sedimentary host rocks have. This allows better assessment of the characteristics of Carlin-type deposits. Based on 40 to 37 Ma ages of other mineralized dikes in the northern Carlin trend, the deposits may have formed in a single episode ≤37.3 or in multiple episodes between ~40 and 37 Ma. Glassy and other textures indicating shallow emplacement of dikes, as well as lack of tilting of dikes and nearby, coeval volcanic rocks, indicate shallow ore formation and negligible tilting and extension during or after mineralization.

Five types of Eocene dikes are recognized in the northern Carlin trend based on

petrographic and geochemical characteristics and age (Table 1-1): (1) coarsely and abundantly porphyritic low-silica rhyolite and high-silica dacite (37.3 Ma), (2) olivine-bearing basaltic andesite, (3) mostly aphyric rhyolite (~38 Ma), (4) porphyritic plagioclase-biotite±quartz rhyodacite (39.1 Ma), and (5) plagioclase-biotite-horblende dacite (39.3 Ma). Similar dikes are found in all Eocene igneous centers in the region. Based on association of the dikes with exposed plutons and major aeromagnetic anomalies that indicate buried plutons, the dikes of the northern Carlin trend emanated from a large plutonic complex that is marked by a 700 km^2 anomaly. The anomaly and inferred plutonic complex intersect the northern Carlin trend and come within 5 km of the Beast deposit.

The spatial and temporal association of Carlin-type deposits of the trend with Eocene dikes and the plutonic complex argues for a genetic link between mineralization and Eocene plutonism. Carlin-type deposits of the northern Carlin trend should be considered pluton-related, and the distinction between Carlin-type and Carlin-like or distal disseminated deposits should be reevaluated.

References

Altamirano, C., and Thompson, T.B., 1999, Structural geology and hydrothermal alteration associated with the Deep Star orebody, northern Carlin trend, Nevada, *in* Ralph J. Roberts Center for Research in Economic Geology Annual Research Meeting Program and Reports, January 7-8, 1999, University of Nevada, Reno, 19 p.

Anderson, J.L., 1990, The nature and origin of Cordilleran magmatism: Geological Society of America Memoir 174, 414 p.

Arehart, G.B., 1996, Characteristics and origin of sediment-hosted gold deposits: A review: Ore Geology Reviews, v. 11, p. 383-403.

Arehart, G.B., Kesler, S.E., O'Neil, J.R., and Foland, K.A., 1992, Evidence for the supergene origin of alunite in sediment-hosted micron gold deposits, Nevada: Economic Geology, v. 87, p. 263-270.

Arehart, G.B., Chryssoulis, S.L., and Kesler, S.E., 1993a, Gold and arsenic in iron sulfides from sediment-hosted disseminated gold deposits: Implications for depositional processes: Economic Geology, v. 88, p. 171-185.

Arehart, G.B., Foland, K.A., Naeser, C.W., and Kesler, S.E., 1993b, ^{40}Ar/^{39}Ar, K-Ar, and fission-track geochronology of sediment-hosted disseminated gold deposits at Post/Betze, Carlin Trend, northeastern Nevada: Economic Geology, v. 88, p. 622-646.

Armstrong, R.L., 1970, Geochronology of Tertiary igneous rocks, eastern Basin and Range province, western Utah, eastern Nevada, and vicinity, U.S.A.: Geochimica et Cosmochimica Acta, v. 34, p. 203-232.

Bagby, W.C., and Berger, B.R., 1985, Geological characteristics of sediment-hosted, disseminated precious-metal deposits in the western United States, *in* Berger, B.R., and Bethke, P.M., eds., Geology and Geochemistry of Epithermal Systems, vol. 2, Reviews in Economic Geology: Society of Economic Geologists, p. 169-202.

Bakken, B.M., Hochella, M.F., Jr., Marshall, A.F., and Turner, A.M., 1989, High-resolution microscopy of gold in unoxidized ore from the Carlin mine, Nevada: Economic Geology, v. 84, p. 171-179.

Bakken, B.M., and Einaudi, M.T., 1990, Volume-change and mass-transport during hydrothermal alteration and weathering of the Main orebody, Carlin mine, Nevada, *in* Gold mineralization, wall-rock alteration, and the geochemical evolution of the hdrothermal system in the Main orebody, Carlin mine, Nevada: unpublished Ph.D. dissertation, Stanford University, California, p. 75-146.

Barker, F., 1981, Introduction to special issue on granites and rhyolites: A commentary for the nonspecialist: Journal of Geophysical Research, v. 86, p. 10131-10135.

Berger, B.R., and Bagby, W.C., 1991, The geology and origin of Carlin-type gold deposits, *in* Foster, R.P., ed., Gold Metallogeny and Exploration: Blackie, Glasgow, p. 210-248.

Brooks, W.E., Thorman, C.H., and Snee, L.W., 1995a, The $^{40}Ar/^{39}Ar$ ages and
tectonic setting of the middle Eocene northeast Nevada volcanic field: Journal of
Geophysical Research, v. 100, B7, p. 10403-10416.

Brooks, W.E., Thorman, C.H., Snee, L.W., Nutt, C.J., Potter, C.J., and Dubiel, R.F.,
1995b, Summary of chemical analyses and $^{40}Ar/^{39}Ar$ age-spectra data for Eocene
volcanic rocks from the central part of the northeast Nevada volcanic field: U.S.
Geological Survey Bulletin 1988-K, p. K1-K33.

Christensen, O.D., 1996, Carlin trend geologic overview, *in* Peters, S.G., Williams, C.L.,
and Volk, J., eds., Field trip guidebook for Trip B - Structural Geology of the
Carlin trend, *in* Green, S.M., and Struhsacker, E., eds., Geology and Ore Deposits
of the American Cordillera: Geological Society of Nevada, Reno, Nevada, p. 147-
156.

Christiansen, R.L., and Yeats, R.S., 1992, Post-Laramide geology of the U. S. Cordilleran
region, *in* Burchfiel, B.C., Lipman, P.W., and Zoback, M.L., eds., The Geology of
North America, The Cordilleran Region: Geological Society of America Decade
in North American Geology Series, v. G-3, p. 261-406.

Cox, D.P., 1992, Descriptive model of distal-disseminated Ag-Au, *in* Bliss, J.D., ed.,
Developments in mineral deposits modeling: U. S. Geological Survey Bulletin
2004, p. 19.

Deino, A., and Potts, R., 1990, Single-crystal $^{40}Ar/^{39}Ar$ dating of the Olorgesailie
Formation, Southern Kenya Rift: Journal of Geophysical Research, v. 95, p.
8453-8470.

Emmons, D.L., and Eng, T.L., 1995, Geologic map of the McCoy mining district, Lander
County, Nevada: Nevada Bureau of Mines and Geology Map 103 with text, 12 p.,
scale, 1:24,000.

Emsbo, P., Hofstra, A.H., Park, D., Zimmerman, J.M., and Snee, L.W, 1996, A mid-
Tertiary age constraint on alteration and mineralization in igneous dikes on the
Goldstrike property, Carlin Trend, Nevada: Geological Society of America
Abstracts with Programs, v. 28 (7), p. A476.

Evans, J.G., 1974a, Geologic map of the Welches Canyon quadrangle, Eureka County,
Nevada: U.S. Geological Survey Geological Quadrangle Map GQ-1117, scale,
1:24,000.

Evans, J.G., 1974b, Geologic map of the Rodeo Creek Northeast quadrangle, Eureka
County, Nevada: U.S. Geological Survey Geological Quadrangle Map GQ-1116,
scale 1:24,000.

Evans, J.G., 1980, Geology of the Rodeo Creek northeast and Welches Canyon
quadrangles, Eureka County, Nevada: U. S. Geological Survey Bulletin 1473, 81
p.

Evans, J.G., and Ketner, K.B., 1971, Geologic map of the Swales Mountain quadrangle
and part of the Adobe Summit quadrangle, Elko County, Nevada: U.S. Geological
Survey Miscellaneous Geologic Investigations Map I-0667, scale, 1:24,000.

Evans, J.G., and Theodore, T.G., 1978, Deformation of the Roberts Mountains allochthon
in north-central Nevada: U.S. Geological Survey Professional Paper 1060, 18 p.

Farmer, M., 1996, An intrusive study of the Bluestar subdistrict: Internal report,
Newmont Gold Company, 33 p.

Ferdock, G.C., Castor, S.B., Leonardson, R.W., and Collins, T., 1997, Mineralogy and
paragenesis of ore stage mineralization in the Betze gold deposit, Goldstrike
mine, Eureka County, Nevada, *in* Vikre, P., Thompson, T.B., Bettles, K.,
Christensen, O., and Parratt, R., eds., Carlin-Type Gold Deposits Field
Conference: Society of Economic Geologists, Guidebook Series v. 28, p. 75-86.

Fleck, R.J., Sutter, J.F., and Elliott, D.H., 1977, Interpretation of discordant $^{40}Ar/^{39}Ar$ age-spectra of Mesozoic tholeiites from Antarctica: Geochimica et Cosmochimica Acta, v. 41, p. 15-32.

Fleck, R.J., Theodore, T.G., Sarna-Wojcicki, A., and Meyer, C.E., 1998, Age and possible source of air-fall tuffs of the Miocene Carlin Formation, northern Carlin trend, *in* Tosdal, R.M., ed., Contributions to the Gold Metallogeny of Northern Nevada: U. S. Geological Survey Open-File Report 98-338, p. 176-192.

Grant, J.A., 1986, The isocon diagram-a simple solution to Gresens' equation for metasomatic alteration: Economic Geology, v. 81, p. 1976-1982.

Groff, J.A., Heizler, M.T., McIntosh, W.C., and Norman, D.I., 1997, $^{40}Ar/^{39}Ar$ dating and mineral paragenesis for Carlin-type gold deposits along the Getchell Trend, Nevada: Evidence for Cretaceous and Tertiary gold mineralization: Economic Geology, v. 92, p. 601-622.

Hall, C.M., Simon, G., and Kesler, S.E., 1997, Age of mineralization at the Twin Creeks SHMG Deposit, Nevada, *in* Vikre, P., Thompson, T.B., Bettles, K., Christensen, O., and Parratt, R., eds., Carlin-type Gold Deposits Field Conference: Society of Economic Geologists Guidebook Series, v. 28, p. 151-154.

Harris, M., and Radtke, A.S., 1976, Statistical study of selected trace elements with reference to geology and genesis of the Carlin gold deposit, Nevada: U.S. Geological Survey Professional Paper 960, 21 p.

Henry, C.D., and Boden, D.R., 1997, Eocene magmatism of the Tuscarora volcanic field, Elko County, Nevada, and implications for Carlin-type mineralization, *in* Vikre, P., Thompson, T.B., Bettles, K., Christensen, O., and Parratt, R., eds., Carlin-Type Gold Deposits Field Conference: Society of Economic Geologists Guidebook Series, v. 28, p. 193-202.

Henry, C.D., and Boden, D.R., 1998a, Geologic map of the Mount Blitzen quadrangle, Elko County, Nevada: Nevada Bureau of Mines and Geology Map 110 with text, 20 p., scale, 1:24,000.

Henry, C.D., and Boden, D.R., 1998b, Eocene magmatism: The heat source for Carlin-type gold deposits of northern Nevada: Geology, v. 26, p. 1067-1070.

Henry, C.D., Boden, D.R., and Castor, S.B., 1998, Geology and mineralization of the Eocene Tuscarora volcanic field, Elko County, Nevada, *in* Tosdal, R. M., ed., Contributions to the Gold Metallogeny of Northern Nevada: U.S. Geological Survey Open-file Report 98-338, p. 279-290.

Henry, C.D., and Faulds, J.E., 1999, Geologic map of the Emigrant Pass Quadrangle, Nevada: Nevada Bureau of Mines and Geology, Open-File Report 99-9, scale, 1:24,000.

Henry, C.D., and Ressel, M.W., 2000, Eocene magmatism of northeastern Nevada: The smoking gun for Carlin-type deposits, *in* Geological Society of Nevada Symposium 2000.

Hildenbrand, T.G., and Kucks, R.P., 1988, Total intensity magnetic anomaly map of Nevada: Nevada Bureau of Mines and Geology Map 93A, scale, 1:750,000.

Hofstra, A.H., 1994, Geology and genesis of the Carlin-type gold deposits in the Jerritt Canyon district, Nevada: unpublished Ph.D. dissertation, University of Colorado, Boulder, 719 p.

Hofstra, A.H., Snee, L.W., Rye, R.O., Folger, H.W., Phinisey, J.D., Loranger, R.J., Dahl, A.R., Naeser, C.W., Stein, H.J., and Lewchuk, M., 1999, Age constraints on Jerritt Canyon and other Carlin-type gold deposits in the western United States-Relationship to mid-Tertiary extension and magmatism: Economic Geology, v. 94, p. 769-802.

Ilchik, R.P., 1991, Geology of the Vantage gold deposits, Alligator Ridge, Nevada, *in* Raines, G.L., Lisle, R.E., Schafer, R.N., and Wilkinson, W.H., eds., Geology and Ore Deposits of the Great Basin, symposium proceedings, Geological Society of Nevada, p. 645-663.

Ilchik, R.P., and Barton, M.D., 1997, An amagmatic origin of Carlin-type gold deposits: Economic Geology, v. 92, p. 269-288.

Joralemon, P., 1951, The occurrence of gold at the Getchell mine, Nevada: Economic Geology, v. 46, p. 267-310.

Kamali, C., 1996, $^{40}Ar/^{39}Ar$ dating of barite and characterization of ore fluids at the Lone Tree gold deposit, Humboldt County, Nevada: unpublished M.S. thesis, New Mexico Institute of Mining and Technology, Socorro, 137 p.

Ketner, K.B., 1998, Geologic map of the southern Independence Mountains, Elko County, Nevada: U.S. Geological Survey Miscellaneous Geologic Investigations Series Map I-2629, scale, 1:24,000.

Ketner, K.B., and Smith, J.F., Jr., 1963, Geology of the Railroad mining district, Elko County, Nevada: U.S. Geological Survey Bulletin 1162-B, p. B1-B27.

Ketner, K.B., and Smith, J.F., Jr., 1982, Mid-Paleozoic age of the Roberts thrust unsettled by new data from northern Nevada: Geology, v. 10, p. 298-303.

Kuehn, C.A., and Rose, A.W., 1992, Geology and geochemistry of wall-rock alteration at the Carlin gold deposit, Nevada: Economic Geology, v. 87, p. 1697-1721.

Kuehn, C.A., and Rose, A.W., 1995, Carlin gold deposits, Nevada: Origin in a deep zone of mixing between normally pressured and overpressured fluids: Economic Geology, v. 90, p. 17-36.

Lamb, J.B., and Cline, J., 1997, Depths of formation of the Meikle and Betze/Post
deposits, *in* Vikre, P., Thompson, T.B., Bettles, K., Christensen, O., and Parratt,
R., eds., Carlin-type Gold Deposits Field Conference: Society of Economic
Geologists Guidebook Series, v. 28, p. 101-107.

Lauha, E.A., and Bettles, K.H., 1993, A geologic comparison of the Post/Betze and
Purple Vein deposits of the Goldstrike and Meikle mines, Nevada: Society for
Mining, Metallurgy and Exploration Preprint 93-170, 20 p.

Leonardson, R.W., and Rahn, J.E., 1996, Geology of the Betze-Post gold deposits,
Eureka County, Nevada, *in* Coyner, A.R., and Fahey, P.L., eds., Geology and Ore
Deposits of the American Cordillera: Geological Society of Nevada Symposium
Proceedings, v. 1, Reno/Sparks, Nevada, April, 1995, p. 61-94.

Lovering, T.G., 1972, Jasperoid in the United States - Its characteristics, origin, and
economic significance: U.S. Geological Survey Professional Paper 710, 164 p.

Mako, D.A., 1997, Characterization and dating of argillic alteration in the Mercur gold
district, Utah - A discussion: Economic Geology, v. 92, p. 633-634.

McKee, E.H., 1971, Tertiary igneous chronology of the Great Basin of the western
United States: Implications for tectonic models: Geological Society of America
Bulletin, v. 82, p. 3497-3502.

McIntosh, W.C., and Chamberlin, R.M., 1994, ^{40}Ar/^{39}Ar geochronology of middle to
late Cenozoic ignimbrites, mafic lavas, and volcaniclastic rocks in the Quemado
Region, New Mexico: New Mexico Geological Society Guidebook, v. 45, p. 165-
185.

Mosier, D.L., Singer, D.A., Bagby, W.C., and Menzie, W.D., 1992, Grade and tonnage
model of sediment-hosted Au, *in* Bliss, J.D., ed., Developments in mineral
deposits modeling: U. S. Geological Survey Bulletin 2004, p. 26.

Murowchick, J.B., 1992, Marcasite inversion and the petrographic determination of pyrite ancestry: Economic Geology, v. 87, p. 1141-1152.

Phinisey, J.D., Hofstra, A.H., Snee, L.W., Roberts, T.T., Dahl, A.R., and Loranger, R.J., 1996, Evidence for multiple episodes of igneous and hydrothermal activity and constraints on the timing of gold mineralization, Jerritt Canyon district, Elko County, Nevada, *in* Coyner, A.R., and Fahey, P.L., eds., Geology and Ore Deposits of the American Cordillera: Geological Society of Nevada Symposium Proceedings, Reno/Sparks, Nevada, April, 1995, p. 15-39.

Presnell, R.D., and Parry, W.T., 1996, Geology and geochemistry of the Barneys Canyon gold deposit, Utah: Economic Geology, v. 91, p. 273-288.

Radtke, A.S., Rye, R.O., and Dickson, F.W., 1980, Geology and stable isotopes of the Carlin gold deposit: Nevada: Economic Geology, v. 75, p. 641-672.

Ressel, M.W., Noble, D.C., and Connors, K.A., 1998, Eocene dikes of the Carlin Trend, Nevada: Magmatic As, Sb, Cs, Tl, CO_2 & excess argon suggest a deep degassing model for gold mineralization: Geological Society of America Abstracts with Programs, v. 30, p. A118.

Ressel, M.W., Noble, D.C., Henry, C.D., and Trudel, W.S., 1999, Eocene magmatism and coeval gold mineralization in the northern part of the Carlin trend, Nevada: Geological Society of America Abstracts with Programs, v. 31 (6), p. A88.

Ressel, M.W., Noble, D.C., Volk, J.A., Lamb, J.B., Park, D.E., Conrad, J.E., Heizler, M.T., and Mortensen, J.K., 2000, Precious-metal mineralization in Eocene dikes at Griffin and Meikle: Bearing on the age and origin of gold deposits of the Carlin trend, Nevada, *in* Geological Society of Nevada Symposium 2000.

Roberts, R.J., 1964, Stratigraphy and structure of the Antler Peak quadrangle, Humboldt and Lander Counties, Nevada: U.S. Geological Survey Professional Paper 459-A, 93 p.

Samson, S.D., and, Alexander, E.C., Jr., 1987, Calibration of the interlaboratory $^{40}Ar/^{39}Ar$ dating standard, Mmhb-1: Chemical Geology, v. 66, p. 27-34.

Saucier, A.E., 1997, The Antler thrust system in northern Nevada, *in* Perry, A. J., and Abbott, E. W., eds., The Roberts Mountains thrust, Elko and Eureka Counties, Nevada: Nevada Petroleum Society Field Trip Guidebook, p. 1-16.

Seedorff, E., 1991, Magmatism, extension, and ore deposits of Eocene to Holocene age in the Great Basin: mutual effects and preliminary proposed genetic relationships, *in* Raines, G.L., Lisle, R.E., Schafer, R.W., and Wilkinson, W.H., eds., Geology and Ore Deposits of the Great Basin: Geologic Society of Nevada Symposium Proceedings, p. 133-178.

Silberling, N.J., and Roberts, R.J., 1962, Pre-Tertiary stratigraphy and structure of northwestern Nevada: Geological Society of America Special Paper, 58 p., map scale, 1:62,500.

Sillitoe, R.H., and Bonham, H.F., 1990, Sediment-hosted gold deposits: Distal products of magmatic-hydrothermal systems: Geology, v. 18, p. 157-161.

Smith, J.F., Jr., and Ketner, K.B., 1978, Geologic map of the Carlin-Piñon Range area, Elko and Eureka Counties, Nevada: U.S. Geological Survey Miscellaneous Investigations Map I-1028.

Steiger, R.H., and Jäger, E., 1977, Subcommission on geochronology: Convention on the use of decay constants in geo- and cosmochronology: Earth and Planetary Science Letters, v. 36, p. 359-362.

Stewart, J.H., 1980, Geology of Nevada: Nevada Bureau of Mines and Geology Special Publication no. 4, 136 p.

Stewart, J.H., and Carlson, J.E., 1978, Geologic map of Nevada: U.S. Geological Survey in collaboration with Nevada Bureau of Mines and Geology, scale, 1:500,000.

Teal, L., and Jackson, M., 1997, Geologic overview of the Carlin trend gold deposits and descriptions of recent deep discoveries: SEG Newsletter, no. 31, p. 1, 13-25, also *in* Vikre, P., Thompson, T.B., Bettles, K., Christensen, O., and Parratt, R., eds., Carlin-Type Gold Deposits Field Conference: Society of Economic Geologists Guidebook Series, v. 28, p. 3-38.

Theodore, T.G., 1998, Pluton-related Au in the Battle Mountain mining district   An overview, *in* Tosdal, R.M., ed., Contributions to the Gold Metallogeny of Northern Nevada: U.S. Geological Survey Open-File Report 98-338, p. 251-252.

Theodore, T.G., and Blake, D.W., 1975, Geology and geochemistry of the Copper Canyon porphyry copper deposit and surrounding area, Lander County, Nevada: U. S. Geological Survey Professional Paper 798-B, 86 p.

Thorman, C.H., Brooks, W. E., Snee, L.W., Hofstra, A.H., Christensen, O.D., and Wilton, D.T., 1995, Eocene-Oligocene model for Carlin-type deposits in northern Nevada: Geological Society of Nevada Symposium Abstracts, April, 1995, Reno/Sparks, Nevada, p. 75.

Thorman, C.H., and Christensen, O.D., 1991, Geologic settings of gold deposits in the Great Basin, western United States, *in* Ladeira, E.A., ed., Brazil Gold '91: Rotterdam, Balkema, p. 65-75.

Wallace, A.R., and John, D.A., 1998, New studies on Tertiary volcanic rocks and mineral deposits, northern Nevada rift, *in* Tosdal, R.M., ed., Contributions to the Gold Metallogeny of Northern Nevada: U.S. Geological Survey Open-File Report 98-338, p. 264-278.

Wells, J.D., Stoiser, L.R., and Elliot, J.E., 1969, Geology and geochemistry of the Cortez gold deposit: Economic Geology, v. 64, p. 526-537.

Wilson, P.N., and Parry, W.T., 1995, Characterization and dating of argillic alteration in the Mercur gold district, Utah: Economic Geology, v. 90, p. 1197-1216.

Wooden, J.L., Kistler, R.W., and Tosdal, R.M., 1998, Pb isotopic mapping of crustal structure in the northern Great Basin and relationships to Au deposit trends, *in* Tosdal, R.M., ed., Contributions to the Gold Metallogeny of Northern Nevada: U.S. Geological Survey Open-File Report 98-338, p. 20-33.
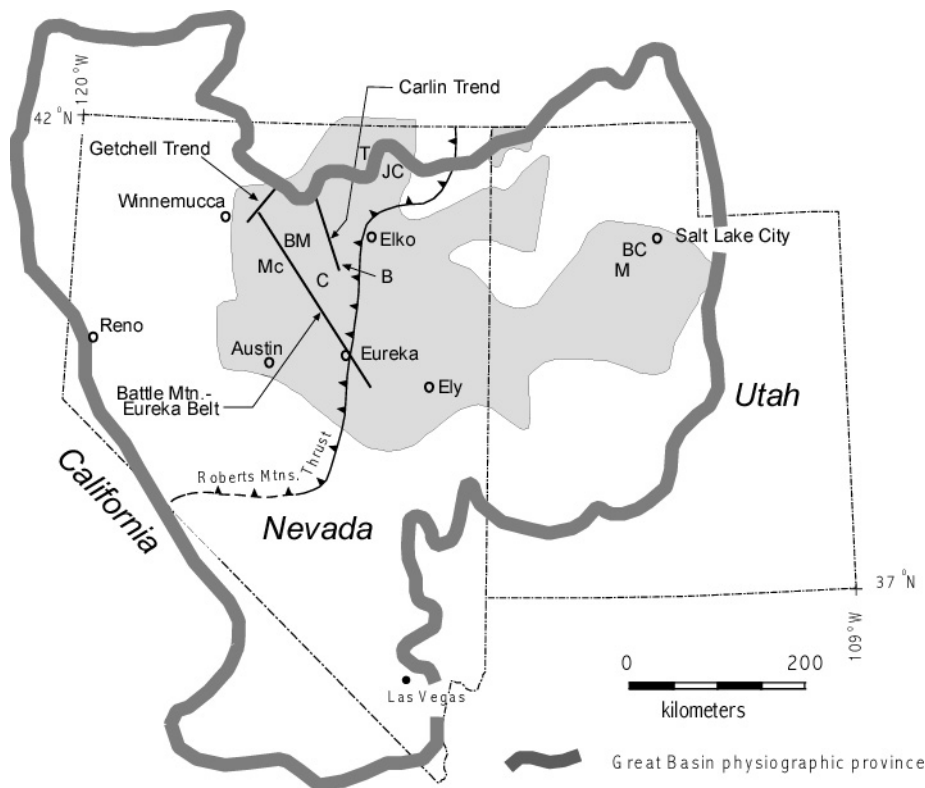
Figure 1-1. Location of prominent gold belts and selected sedimentary rock-hosted gold deposits of the Great Basin, Nevada and Utah. The distribution of rocks comprising the late Eocene igneous province of the northern Great Basin is shown by shading. Abbreviations: B = Bullion, BC = Bingham Canyon, BM = Battle Mountain, C = Cortez, JC = Jerritt Canyon, M = Mercur, Mc = McCoy-Cove, T = Tuscarora.

116

JC = Jerritt Canyon
TVF = Tuscarora volcanic field
H = Hatter stock
LM = Lone Mountain
G = Goldstrike intrusion
B = Beast deposit and dike
RM = Richmond Mountain
SM = Swales Mountain
SC = Suzie Creek intrusion
Q = Gold Quarry mine
WC = Welches Canyon
BV = Boulder Valley
EP-WC = Emigrant Pass volcanic field
R = Railroad district

Mount Blitzen
Volcanic Center

JC

Ei
LM

Ev

TVF
Ei

H
Ei

CARLIN TREND

G
Ji
B

RM
Ki

WC
Ei

SM
Ei

SC Ei

Q

Ei BV

EP-
WC
Ei?

R
Ei

41

Nevada

Interstate 80

QT Quaternary—late Tertiary deposits
Tv Miocene—Oligocene volcanic rocks
Ev Eocene volcanic rocks
     Eocene porphyritic rhyolite dikes
     (Beast—type dikes)
Ei Eocene intrusion
Ki Cretaceous intrusion
Jv Jurassic volcanic rocks
Ji Jurassic intrusion
P   Paleozoic rocks undivided

N

0   10 miles
0   10 kilometers

Figure 1-2. Simplified geologic map of the region of Eocene igneous centers surrounding the Carlin trend in northeastern Nevada. Igneous centers generally consist of both intrusive and volcanic rocks. Porphyritic rhyolite dikes similar to the host rock at the Beast deposit are abundant in most centers, but have been mapped in detail only in the Tuscarora volcanic field, Emigrant Pass volcanic field, Welches Canyon, and Carlin trend. Map modified from Stewart and Carlson (1978).

Aeromagnetic contours
in nanoteslas;
from Hildebrand and Kucks (1988)

0 contour labeled
40 nanoteslas interval
x200 contour = heavy lines

N

0 _____ 10 miles

0 _____ 10 kilometers
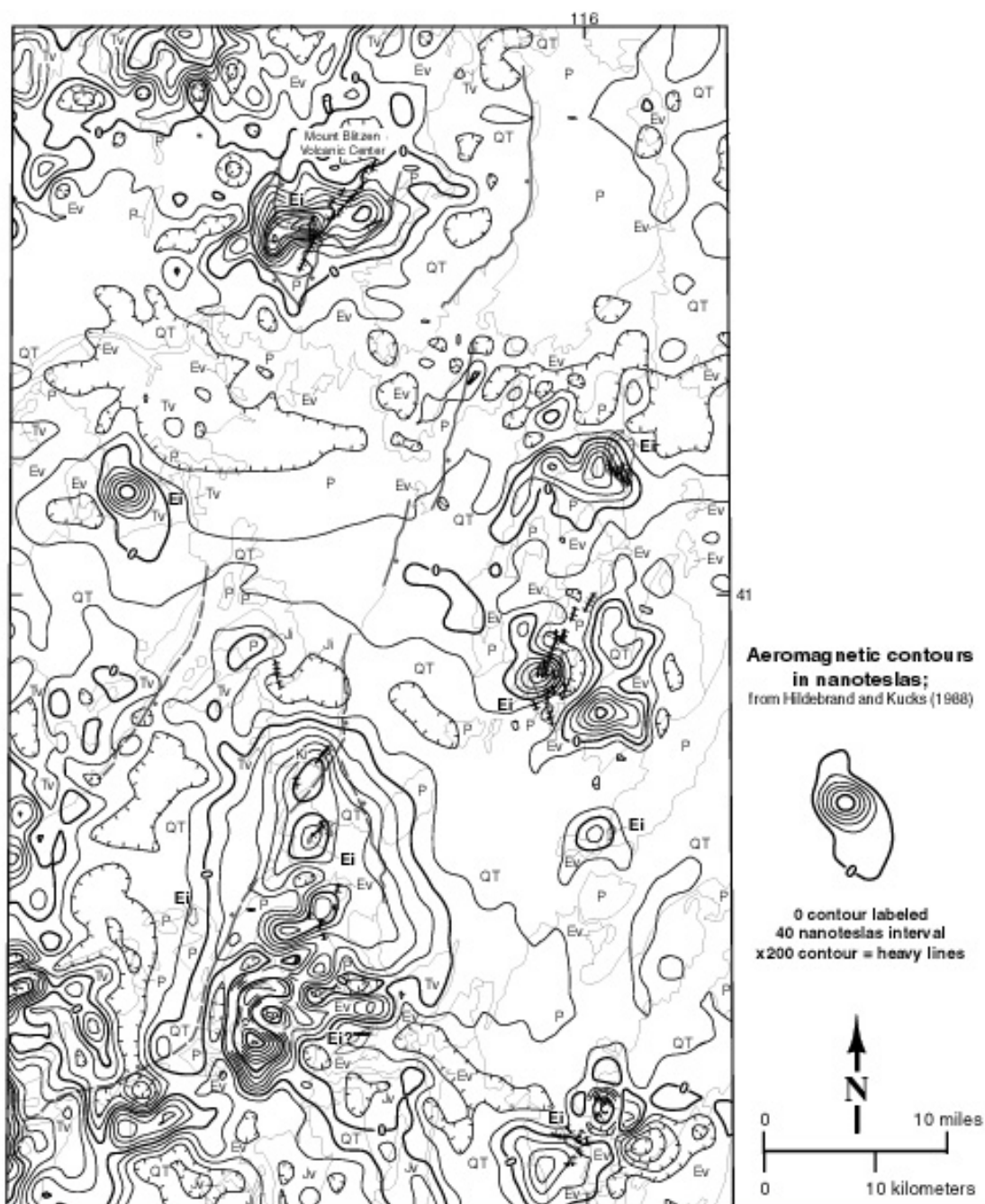
Figure 1-3. Aeromagnetic map (from Hildenbrand and Kucks, 1988) overlain on Figure 1-2; see Figure 1-2 for explanation of geologic units. All Eocene igneous centers are marked by prominent magnetic highs, which commonly extend well beyond the limits of exposed Eocene rocks, showing that Eocene intrusive rocks are more extensive in the subsurface. The magnetic anomaly associated with the Northern Carlin-Emigrant Pass center extends from the Emigrant Pass volcanic field northward into the northern Carlin trend to about 5 km south of the Beast deposit, an area marked by numerous shallow intrusions and dikes. This anomaly probably reflects a composite Eocene intrusion emplaced between about 40 and 36 Ma and, to a lesser extent, the Cretaceous Richmond intrusion.
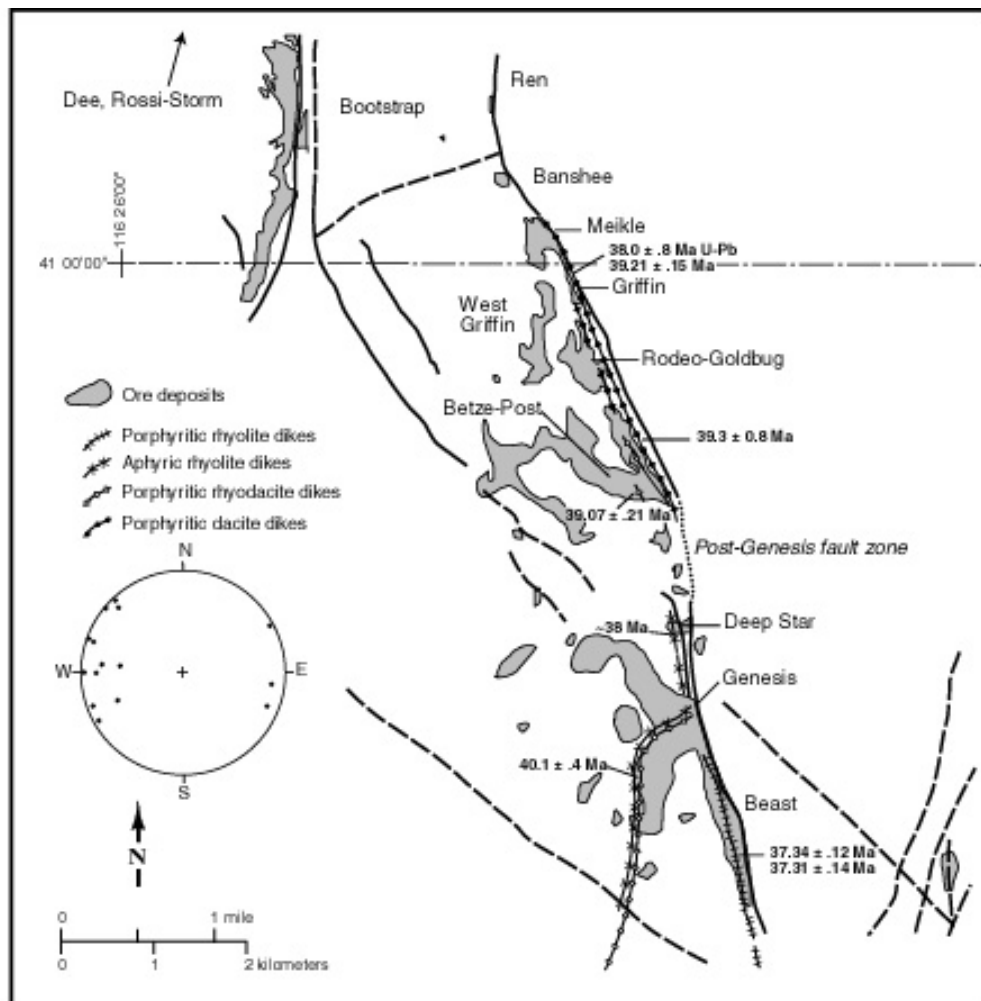
Figure 1-4. Generalized map of the northern Carlin trend, Nevada showing locations and ages of Eocene dikes discussed in text and mineralized rocks projected to surface (from Teal and Jackson, 1997). $^{40}Ar/^{39}Ar$ ages are from this study, Arehart et al. (1993b), and Farmer (1996). Lower hemisphere equal-area stereographic plot shows poles to Eocene dikes of the northern Carlin trend.
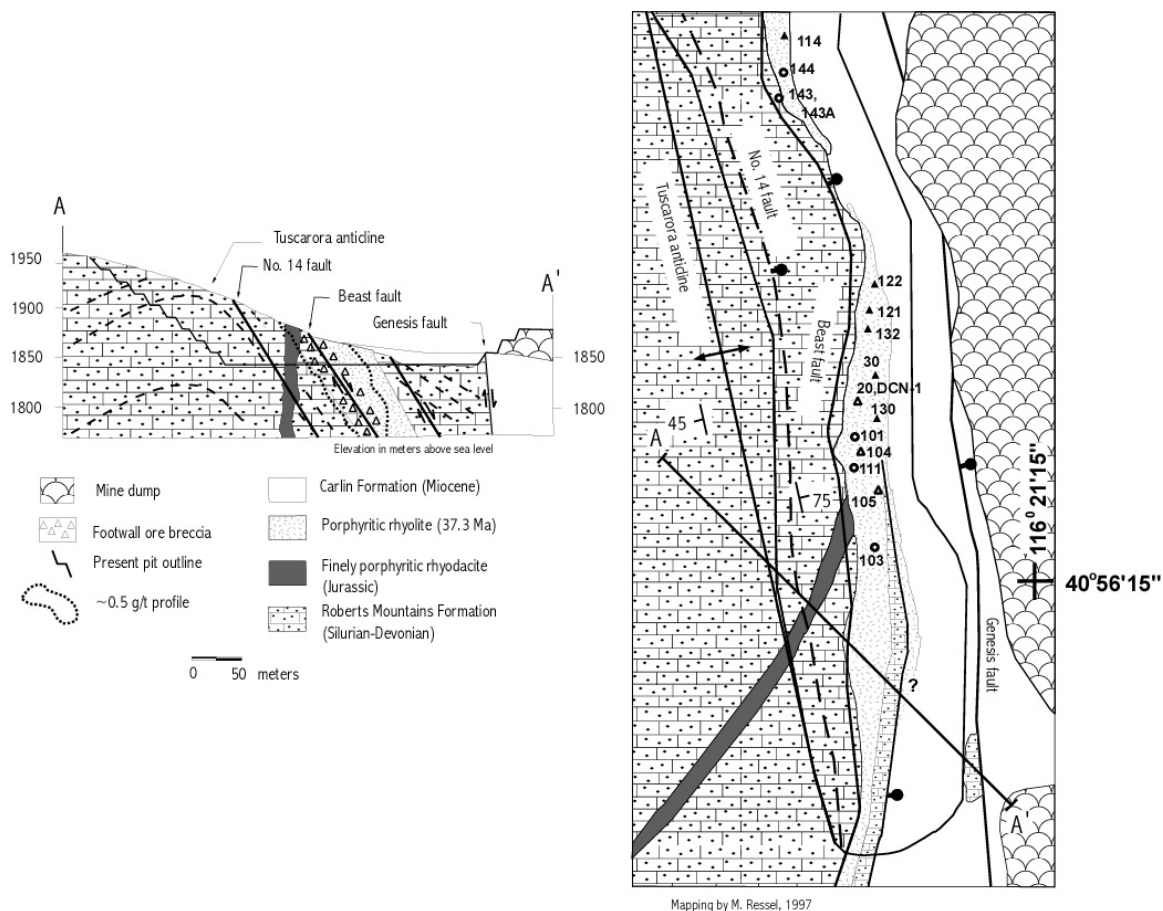
Figure 1-5. Simplified geologic map and cross section of the Beast mine area. Pit outline is of the 6075-ft. level and approximates ore zone. Numbers refer to analyzed samples presented in Tables 1-2 and 1-3. Symbols: open triangles = rhyolite crackle breccia; open circles = matrix-supported breccia; solid triangles = argillic rock; + = silicified limestone crackle breccia.
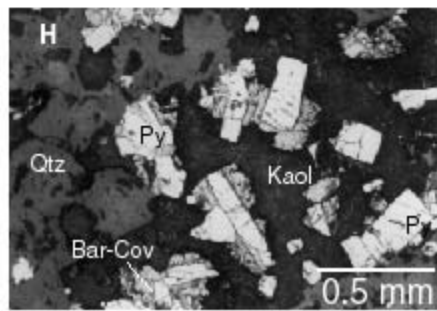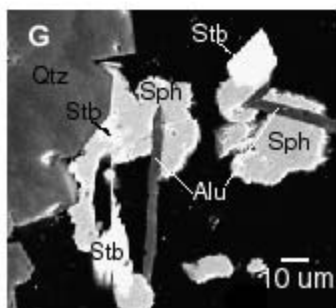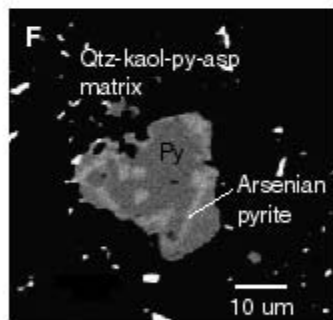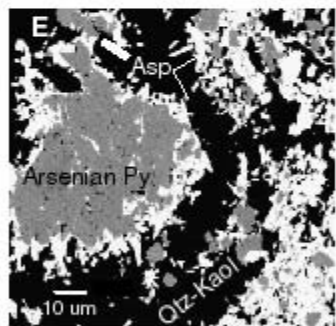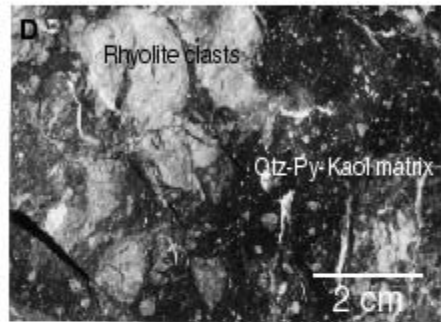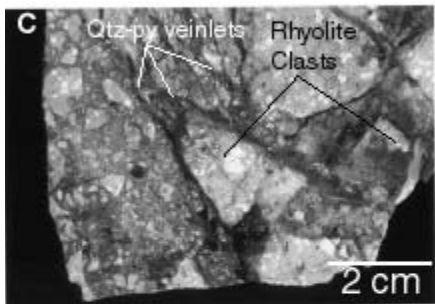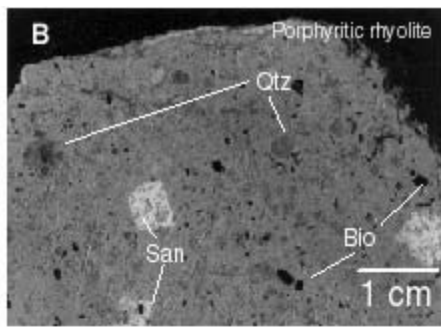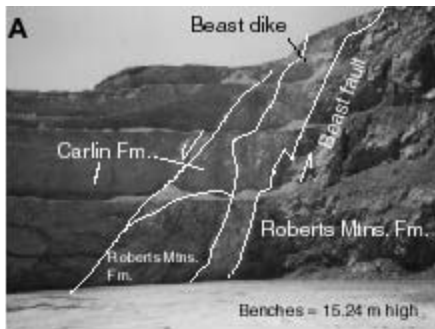
Figure 1-6. A. View of the south highwall of the Beast mine. The Beast porphyritic

rhyolite dike is the prominent east-dipping unit exposed in the highwall in the

center of the photograph. The footwall is comprised of intact folded laminated

silty limestone of the Roberts Mountains Formation. The hanging wall consists of

highly disrupted silty limestone overlain by nearly flat-lying volcaniclastic rocks

of the Miocene Carlin Formation. B. Argillically-altered, coarsely porphyritic

Beast rhyolite containing phenocrysts of abundant rounded quartz, sparse large

kaolinitized sanidine, and fresh biotite (labelled); abundant

kaolinitized/hematized plagioclase and rare altered hornblende are not resolved.

C. Crackle breccia developed in Beast rhyolite [No. 3, Table 1-2]. Veinlets are

composed of quartz and quartz+iron sulfide. Note kaolinitized feldspar (white) in

clasts. D. Footwall breccia ore with matrix containing "sooty" sulfide and carbon

[No. 6, Table 1-2]. Whitish clasts are from rhyodacite dike of Mesozoic age. E.

SEM-BS image of porous irregular pyrite and arsenian pyrite rimmed by

arsenopyrite (white) [No. 9, Table 1-2]. F. SEM-BS image of pyrite grain

showing irregular arsenian pyrite outer zones (light gray band) and small amounts

of late arsenopyrite (white) (No. 8, Table 1-2). G. SEM-BS image of minerals

residing in late-stage drusy quartz vug in heterolithic breccia. Stibnite (abbrev.

Stb, brightest) is intergrown with sphalerite (abbrev. Sph, intermediate) and

alunite (abbrev. Alu, elongate laths) on the edge of terminated quartz crystals

(left). H. Photomicrograph (crossed polars) of rhyolite crackle breccia ore

showing typical euhedral pyrite with arsenopyrite surrounded by late-stage barite,

chalcocite and covellite.
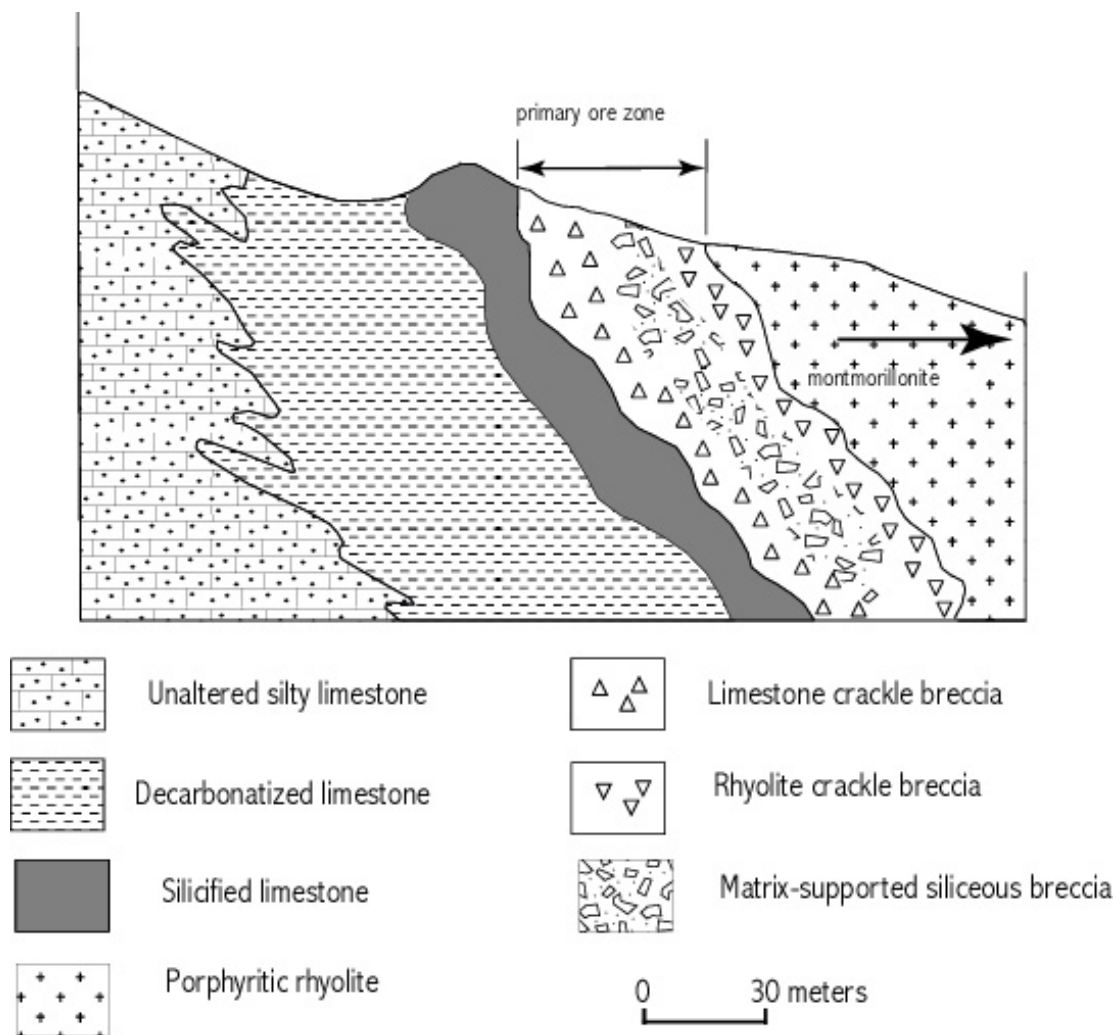
Figure 1-7. Schematic cross-section showing alteration zonation across the Beast deposit. Argillic alteration of silty limestone involves both argillization and bleaching of fine-grained silicates and decarbonitization of calcite.

Stages	Pre-Ore	Stage 1	Stage 2	Stage 3	Supergene
Mineral					
Quartz	————————————————————				
Kaolinite		·········———————	———————	———————	———————
Montmorillonite		—————	? ———		———
Sericite	··············				
Arsenopyrite		———			
Arsenian pyrite		———			
Pyrite	················	———————	———————		
Marcasite	··············				
Mobilized Carbon	········	—————————			
Stibnite			———————		
Sphalerite (Fe-deficient)			———	············	
Covellite				············	
Chalcocite				············	
Gold		····——————····			
Barite				········———————	
Alunite			——————··············		———————
Rutile			———————		
Chalcedony				——	
Fe-As oxides*					———————————

Figure 1-8. Paragenetic sequence for rhyolite-hosted ores of the Beast deposit. A presumption is made that gold is related to arsenian pyrite and/or arsenopyrite (Bakken et al., 1989; Arehart et al., 1993a); no free gold or electrum has been observed. * dussertite, goethite, hematite, jarosite, and scorodite.
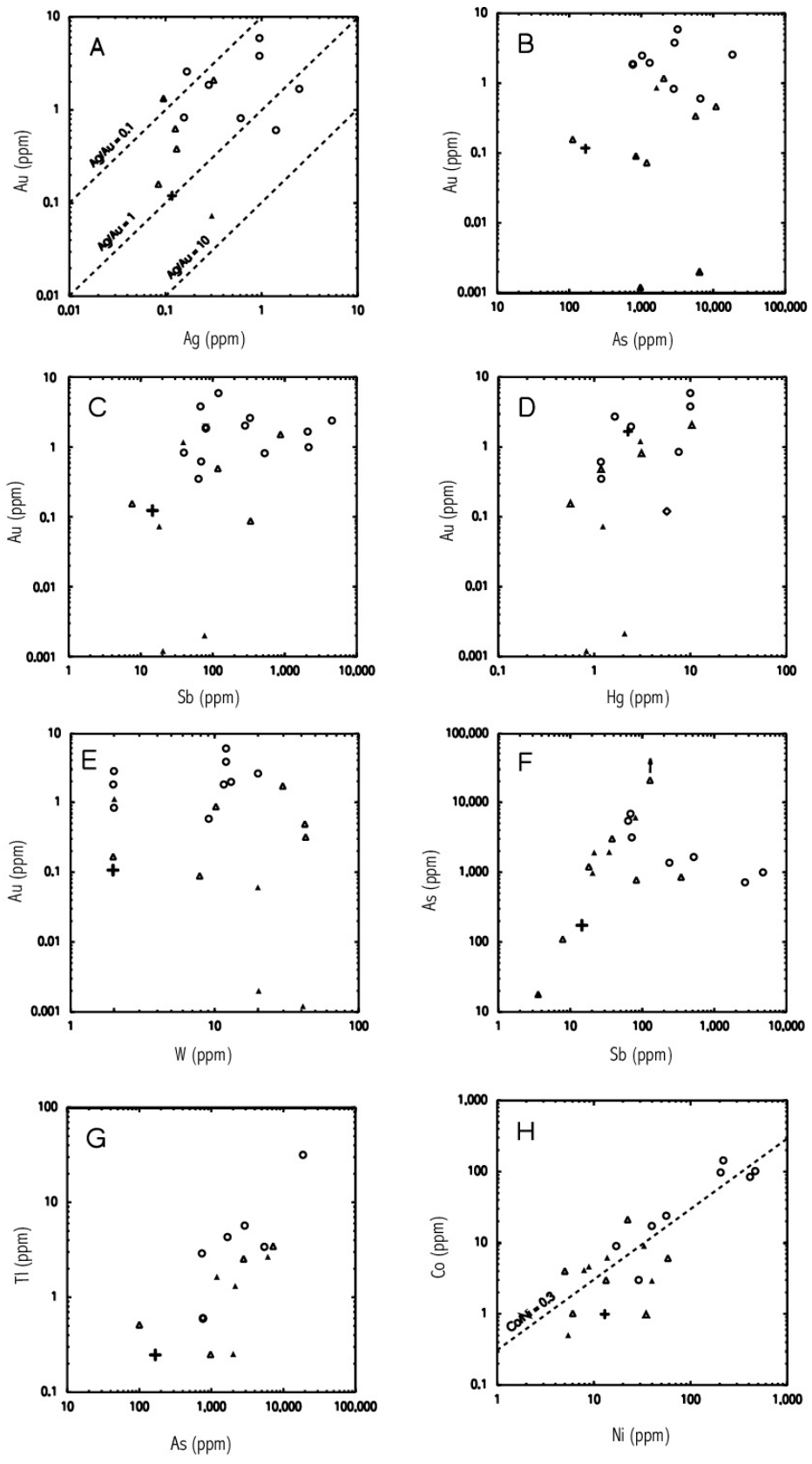
Figure 1-9. Variation diagrams of selected minor elements for rocks and ores of the Beast deposit. Symbols: circles, rhyolite crackle breccia; diamonds, heterolithic breccia; triangles, argillic rock; squares, rhyolite matrix-supported breccia; +, silicified limestone crackle breccia.
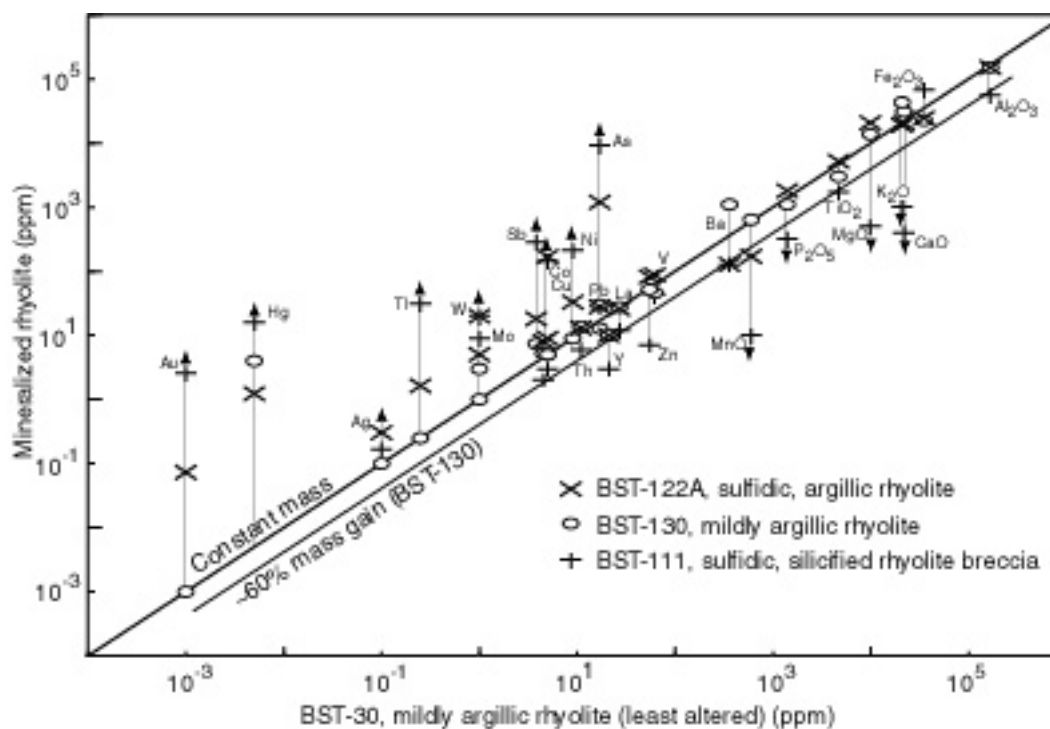
Figure 1-10. Isocon diagram (Grant, 1986) for selected non-mineralized and mineralized rhyolite and rhyolite breccia samples from the Beast deposit. Shown are the marked addition of As, Sb, Hg, Tl ± Ag, ±Ni, ±Co, ±W, ±Mo in mineralized rocks and large-scale removal of Ca, K, Mg, Mn and P. Sodium was nearly completely removed in both weakly altered and mineralized rocks and is therefore not depicted in the plot. Based on a nearly constant Al_2O_3/TiO_2 ratio of about 36, the most highly mineralized sample (BST-111) has experienced about 60% mass increase mainly through the addition of silica.

A

% Radiogenic

K/Ca

BST 114, Porphyritic rhyolite, Sanidine

37.37 ± 0.11 Ma

1000   1200   1300   1400   1600

Integrated Age = 37.39 ± 0.17 Ma

Cumulative %39Ar Released

B

% Radiogenic

K/Ca

BST-30, Porphyritic rhyolite, Biotite

37.31 ± 0.14 Ma

850   1000   1110   1180   1210   1250

Integrated Age = 37.42 ± 0.10 Ma

Cumulative %39Ar Released

C

% Radiogenic

K/Ca

18.6 ± 1.2 Ma

BST-144, Alunite

Integrated Age = 17.9 ± 2.5 Ma

Cumulative %39Ar Released

D

% Radiogenic

K/Ca

39.07 ± 0.21 Ma

850   1000   1110   1180   1210   1250

BP-2, Porphyritic rhyodacite, Biotite

Integrated Age = 39.1 ± 0.4 Ma

Cumulative %39Ar Released

E

% Radiogenic

K/Ca

38.10 ± 0.37 Ma

875   975   1075   1250   1350   1650

BP-2, Porphyritic rhyodacite, Plagioclase

Integrated Age = 43.7 ± 15.3 Ma

Cumulative %39Ar Released

F

% Radiogenic

K/Ca

BP-2, Porphyritic rhyodacite, Matrix

700   800   875   975   1170   1650

Integrated Age = 110 ± 30 Ma

Cumulative %39Ar Released

G

% Radiogenic

K/Ca

39.21 ± 0.15 Ma

920   1000   1110   1180   1210

G11-005-4-492, Porphyritic dacite, Biotite

Integrated Age = 39.29 ± 0.22 Ma

Cumulative %39Ar Released

H

% Radiogenic

K/Ca

DS-13, Aphyric rhyolite, Whole Rock

800   900   1000   1100   1400

700

Integrated Age = 37.70 ± 0.07 Ma

Cumulative %39Ar Released

Figure 1-11. Incremental heating ^{40}Ar/^{39}Ar age spectra for Eocene dikes of the northern Carlin trend. Uncertainties are 2 sigma. Numbers below age spectra are incremental-heating temperatures. Plateau ages were calculated using the criteria of Fleck et al. (1977). Best estimate of true age of BP-2 rhyodacite dike is 39.07 Ma from biotite spectrum; spectrum for BP-2 matrix indicates presence of excess Ar. Disturbed spectrum for aphyric rhyolite indicates partial loss of Ar from fine-grained devitrification products; age of rock is about 38 Ma.
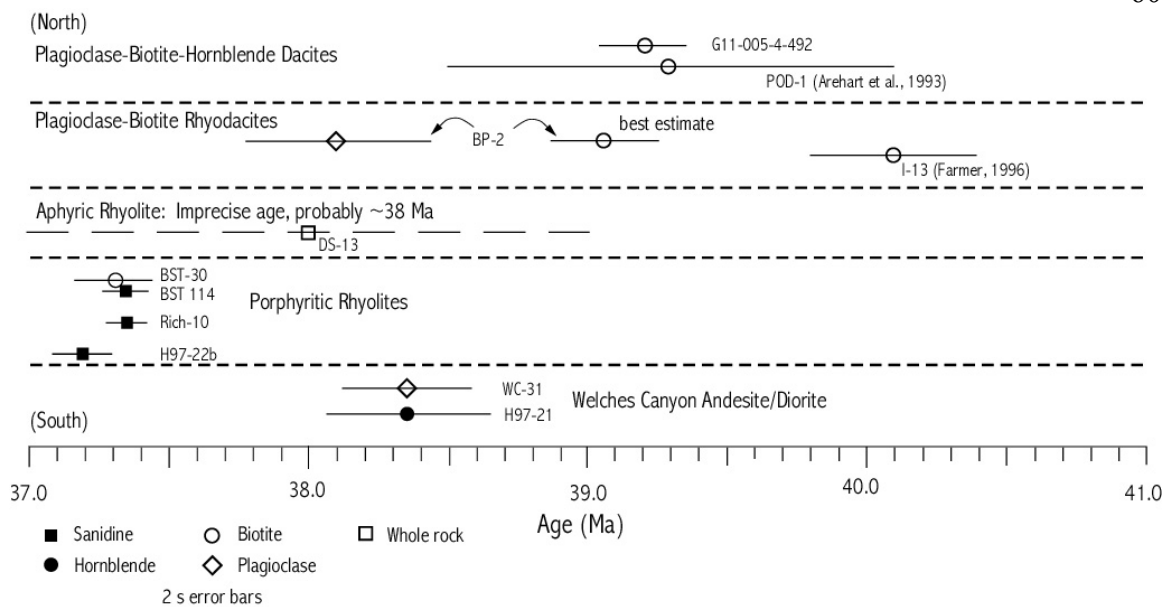
Figure 1-12. Plot showing ranges in ^{40}Ar/^{39}Ar ages of Eocene dikes of the Carlin trend. Ages decrease southward similar to regional patterns.

Table 1-1. Magmatic Episodes and Generalized Igneous Rock Types of the Carlin Trend, Nevada

Event	Age (Ma)	Rock Type	Texture/Mineralogy	Occurrence
Miocene	14.5-15.3 Ma[1,6]	Ferrorhyolite	~5% fine phenocrysts: san, fay, opx, qtz	Lavas and non-welded tuff in western and southern parts of district
Eocene	37.3 Ma[3] (N. Carlin Trend)	Porphyritic rhyolite	30-35% coarse phenocrysts: plag, bio, qtz, hbl, san	Beast-Lantern deposits, Richmond Mountain, Welches Canyon-Emigrant Pass centers
	~38 Ma[3]	Aphyric rhyolite	Aphyric or very sparse (<1 %) phenocrysts: bio, qtz; locally vitric	Deep Star, Genesis, Bluestar deposits; Richmond Mountain, Welches Canyon
	39.1-40.1 Ma[3,7]	Porphyritic rhyodacite	10-15% fine phenocrysts: plag, bio, qtz ; locally vitric	Betze-Post, Genesis, Bluestar deposits; similar rocks in Welches Canyon center
	39.2-39.3 Ma[2,3]	Porphyritic dacite	20-25% coarse phenocrysts: plag, bio, hbl, minor qtz	Meikle, Griffin, Rodeo-Goldbug, Betze-Post deposits; similar rocks in Welches Canyon center
Cretaceous	108-112 Ma[1]	Granite	Porphyritic phaneritic; ksp phenocrysts, plag, qtz, bio	Richmond Mountain stock
Jurassic	157-159 Ma[2,5]	Diorite (also minor granodiorite and gabbro)	Equigranular phaneritic; plag, hbl, bio, cpx, ksp, qtz;	Goldstrike intrusion and nearby satellite stocks and dikes, Betze-Post and Genesis deposits
	157-159 Ma[4,7]	Lamprophyre	Porphyritic, commonly foliated; phlog and/or hbl phenocrysts, ksp, plag, carb, apt	Thin dikes and sills abundant within 5 km of Goldstrike intrusion

Abbreviations: hbl = hornblende; bio = biotite; phlog = phlogopite; cpx = clinopyroxene; opx = orthopyroxene; fay = fayalite; plag = plagioclase; ksp = potassium feldspar; san = sanidine, qtz = quartz; apt = apatite; carb = carbonate

[1]Evans, 1974a, b
[2]Arehart et al., 1993
[3]this study
[4]Emsbo et al., 1996
[5] M.W. Ressel, unpublished data
[6] Fleck et al., 1998
[7] Matthew Farmer, 1996

Table 1-2. $^{40}Ar/^{39}Ar$ ages, Eocene dikes of the Carlin Trend, Nevada

Sample	Location	N. Lat.	W. Long.	Material	Age Method		n* or %^{39}Ar	Age (Ma)	±2σ
Plagioclase-biotite-hornblende dacite (Betze dacite)									
G11-005-4-492	Griffin deposit	40° 59.8'	116° 22.4'	Biotite	step heating	plateau	76.9	39.21	0.15
Plagioclase-biotite rhyodacite (K dikes)									
BP-2	Goldstrike pit	40° 58.6'	116° 21.9'	Biotite	step heating	plateau	98.5	39.07	0.21
"	"	"	"	plagioclase	step heating	plateau	55.1	38.10	0.37
"	"	"	"	Matrix	step heating	no plateau		excess Ar	
Aphyric rhyolite (Deep Star rhyolite)									
DS-13	Deep Star	40° 57.8'	116° 21.7'	whole rock	step heating	no plateau		~~38	
Porphyritic Rhyolite (Beast-type dikes)									
BST 114	Beast pit	40° 56.4'	116° 21.3'	sanidine	single crystal	mean	14	37.34	0.12
"	"	"	"	sanidine	step heating	plateau	72.6	37.37	0.11
BST-30	Beast pit	40° 56.5'	116° 21.3'	Biotite	step heating	plateau	60.5	37.31	0.14
Rich-10	Richmond Mtn	40° 51.8'	116° 18.2'	sanidine	single crystal	mean	15	37.34	0.09
H97-22b	Welches Canyon	40° 48.0'	116° 18.4'	sanidine	single crystal	mean	14	37.19	0.11
Welches Canyon andesite/diorite									
H97-21	Welches Canyon	40° 47.4'	116° 19.2'	hornblende	step heating	plateau	88.3	38.34	0.33
WC-31	Welches Canyon	40° 47.7'	116° 17.9'	plagioclase	step heating	plateau	61.7	38.34	0.23
Other									
BST-144	Beast pit	40° 56.5'	116° 21.3'	Alunite	laser "step"	plateau	89.5	18.6	1.2

All analyses at New Mexico Geochronology Research Laboratory, New Mexico Institute of Mining and Technology

* = number of single grains analyzed; %^{39}Ar = percent ^{39}Ar used in plateau

Monitor age = 27.84 Ma, Fish Canyon sanidine

$\lambda_\beta = 4.963 \times 10^{-10}$ yr^{-1}; $\lambda_{\varepsilon+\varepsilon'} = 0.581 \times 10^{-10}$ yr^{-1}; $^{40}K/K = 1.167 \times 10^{-4}$

Table 1-3. Major- and Minor-Elemental Composition of Rocks and Ores of the Beast Deposit

Sample No.	1	2	3	4	5	6	7	8	9	10	11	12	13	14	15	16	17	18	19
Major Elements (complete analyses recalculated to 100% volatile-free)																			
SiO2	73.87	70.74	86.7			83.82	86.94	88.66					92.9		93.7				
TiO2	0.47	0.36	0.27	0.15	0.1	0.38	0.23	0.36	0.17	0.17		0.23	0.18	0.05	0.19	0.4	0.08	0.52	0.27
Al2O3	16.7	15.83	10.1	6.3	5.2	14.71	10.5	6.26	3.2	5.6		7.5	3.35	1.15	4.15	13.2	1.93	15.2	10.8
Fe2O3 *	3.5	2.7	2.57	1.57	0.5	0.44	1.01	3.07	1.77	6.8		4.68	2.6	0.74	1.42	2.66	1.37	2.43	2.1
MnO	0.06	0.03	0	0.002	0.002	<0.001	<0.001	0.001	0.008	<0.001		0.03	0.008	0.002	0.007	0.011	0.057	0.017	0.13
MgO	0.99	1.44	0.03	0.02	0.02	<0.14	<0.06	0.12	0.15	0.05		0.03	0	0.05	0.1	0.48	6.5	2.07	1.77
CaO	2.18	4.08	0.09	0.03	0.03	0.14	0.18	0.04	0.08	0.04		0.08	0.14	0.13	0.09	1.41	15.5	2.06	11.2
Na2O	0	0.27	0.03	0.01	0.01	0.03	0.13	0.01	0.01	0.01		0.01	0.01	0.01	0.01	0.01	0.01	0.03	0.01
K2O	2.09	4.39	0.09	0.06	0.06	0.33	1.01	1.42	0.65	0.1		0.02	0.78	0.17	0.29	0.36	0.43	1.9	0.22
P2O5	0.14	0.16	0.11	0.037	0.023	0.13	0.07	0.057	0.05	0.032		0.092	0.05	0.039	0.04	0.13	0.071	0.18	0.096
LOI	6.66	7.13	5.13			4.97	3.92	4.48				4.31	5.14		2.61				
Minor Elements, in ppm																			
Ni	9	9	17	22	13	60	6	56	459	211	410	29	39	13	212	13	38	33	5
Co	5	5	9	20	3	6	<2	23	97	144	79	3	17	<2	100	6	3	9	4
Sc	4.5	5.2	2.3	2	1	3.8	3	3.4	3	2	3	3	3	1	2	5	4	8	4
V	62	46		29	25		62	114	84	43		74	193	85	56	55	180	87	36
Cu	5	5	5.7	5.03	3.89		2.5	21.1	26.3	2.39		6.02	8.2	21.5	30.8	17.9	12.6	169	1.08
Pb	17	30	11.4	26	15		33	14	14	28		24	14	6	10	33	5	28	17.1
Zn	55	52	11.2	2.47	<1	146	4.8	3.2	1,103	5.91	1,270	79.3	<1	8.97	1,623	44.3	4.91	94.4	31.9
Bi		<5	0.29	<0.25	<0.25		<0.25	<0.25	<0.25	<0.25		<0.25	<0.25	<0.25	<0.25	1	<0.25	0.65	<0.25
Cd		1	37.2	<0.1	<0.1		<0.1	<0.1	0.6	0.27		0.97	<0.1	0.34	1.69	<0.1	<0.1	0.44	<0.1
Sn	<200	<100	<400	<2	<2	<200	<2	<2	2	2	<1,000	2	<2	<2	<2	7	2	5	3
W	<1	3	42	10	<4	8	12	12	<4	20	<4	13	9	<4	<4	20	<4	20	41
Mo	<1	<1	1.5	10.1	7.64	78	3	4.4	5.56	7.71	60	62.2	4.14	14.8	2.51	2.24	5.07	4.73	0.58
As	17	12.8	11,000	2,823	107	800	765	3,200	738	>9,170	1,000	1,310	6,460	170	1,612	6,442	1,966	1,195	1,974
Sb	3.8	7.4	120	39.8	7.66	340	80.1	120	2219	284	4,600	248	67.7	15.1	541	71.9	35.5	18.1	20.4
Ag	<5	<0.4	0.13	0.16	0.09	<5	0.3	0.95	2.53	0.17	<5	0.29	1.45	0.12	0.61	0.06	0.1	0.3	0.03
Au	<2	<0.002	0.48	0.83	0.15	0.085	1.86	5.9	1.66	2.54	2.48	1.96	0.61	0.12	0.83	0	1.12	0.07	0
Hg	<1	4	1.18	3.1	0.57	<1	9.2	10	2.24	15.8	<4	2.41	1.18	5.69	7.6	2.13	3.14	1.23	0.83
Rb	80	149	<15			<15		38			<15								
Cs	18	27	<1			1		3			<1								
Ba	360	1,100	540	226	271	200	752	580	231	126	<200	2,350	202	315	200	78	116	128	51
Sr	28	58	55	38	29	<500	39	47	31	19	<500	36	21	17	36	16	111	38	35
Tl			3.4	2.54	0.51		0.6	5.7	2.93	30.8		<0.5	3.2	<0.5	4.45	2.74	1.29	1.64	<0.5
Ta	1	1	4.3			<0.5		<0.5			<0.5								
Nb	12			5	3		8	7	3	4		7	3	<2	5	6	<2	9	7

Sample No.	1	2	3	4	5	6	7	8	9	10	11	12	13	14	15	16	17	18	19
Hf	4	4	3			3		3			6								
Zr	*109*			*2*	*<2*		*39*	*111*	*29*	*22*		*36*	*32*	*13*	*23*	*47*	*17*	*62*	*33*
Y	*21*	*10*	*7*	*4*	*3*		*6*	*11*	*7*	*3*		*8*	*4*	*2*	*3*	*7*	*13*	*10*	*18*
Th	11	13.8	7.3	*6*	*5*	10	*9*	6.2	*3*	*6*	<0.5	*8*	*2*	*<2*	*4*	*11*	*2*	*13*	*7*
U	5.4	5.7	6.1	*<10*	*<10*	5.6	*18*	5.9	*<10*	*<10*	<3.8	*<10*	*<10*	*<10*	*<10*	*<10*	*<10*	*<10*	*<10*
La	27	27.6	20	*12*	*8*	20	*21*	19	*17*	*12*	17	*20*	*6*	*3*	*10*	*25*	*7*	*26*	*21*
Ce	45	51	34			34		30			<6								
Nd	18	18	<5			11		10			<10								
Sm	3	3.5	2.9			2.6		1.4			1.2								
Eu	0.8	1	<0.2			0.5		<0.2			<0.2								
Tb	<0.5	<0.5	<0.5			<0.5		<0.5			<0.5								
Yb	0.9	1.1	1.7			0.9		1.3			<0.8								
Lu	0.16	0.17	0.3			0.18		0.21			<0.12								
Se	<3	<3	**<1**			<3	**1.09**	**2.71**	**26.2**	**3.41**	**<5**	**<1**	**<1**	**<1**	**36.6**	**<1**	**<1**	**<1**	**<1**
Te			**<0.5**				**<0.5**	**<0.5**	**<0.5**	**<0.5**		**<0.5**	**<0.5**	**<0.5**	**<0.5**	**<0.5**	**<0.5**	**<0.5**	**<0.5**

Major elements by XRF or ICP total digestion

Minor elements by XRF (iltalics), ICP-total digestion (bold italics), INAA (regular font), ICP-aqua regia (bold regular)

1. Field number BST-30. Moderate argillically altered rhyolite of Beast Dike; Ar-Ar (biotite) sample.
2. Field number BST-130. Moderate argillically altered rhyolite of Beast Dike.
3. Field number BST-20. Silicified and pyritized crackle breccia of Beast Dike.
4. Field number N1-SULF. "Sooty" sulfide-rich Beast rhyolite crackle breccia.
5. Field number N1-SILC. Sulfide-poor Beast rhyolite crackle breccia from same hand specimen as previous sample.
6. Field number BST-104. Oxidized silicic crackle breccia of Beast Dike.
7. Field number BST-105. Oxidized silicic crackle breccia of Beast Dike.
8. Field number BST-103. Silicified and pyritized heterolithic breccia.
9. Field number BST-103A "Sooty" sulfide-bearing, silicified heterolithic breccia with stibnite.
10. Field number BST-111. "Sooty" sulfide-bearing monolithic, matrix-supported breccia containing clasts of Beast rhyolite.
11. Field number BST-101. "Sooty" sulfide-bearing, silicified and pyritized heterolithic footwall breccia with stibnite.
12. Field number BST-141. Silicified Beast rhyolite crackle breccia
13. Field number BST-143. Silicified and pyritized heterolithic footwall breccia.
14. Field number BST-143A. Silicified limestone crackle breccia
15. Field number BST-144. Silicified and pyritized heterolithic footwall breccia with alunite veins; Ar-Ar (alunite) sample
16. Field number BST-121. Argillically altered Beast rhyolite containing abundant scorodite and other Fe-oxide staining.
17. Field number BST-122. Partially oxidized argillically altered breccia.
18. Field number BST-122A. Pervasively argillically altered Beast rhyolite containing unoxidized sulfide minerals.
19. Field number BST-132. Argillically altered Beast rhyolite containing unoxidized sulfide minerals.

Appendix 1-1: ^{40}Ar /^{39}Ar Dating Methods and Table of Analytical Data

Dating Methods

^{40}Ar/^{39}Ar analyses were done on sanidine, biotite, hornblende, or plagioclase phenocrysts; whole-rock samples; and alunite. Phenocrysts were concentrated to >99 percent purity using magnetic and density separation and hand picking. Feldspars were treated with dilute HF. Samples were irradiated at Texas A&M University for 7 hours and analyzed at the New Mexico Geochronology Research Laboratory using procedures described in McIntosh and Chamberlin (1994). Neutron flux was monitored using interlaboratory standard Fish Canyon Tuff sanidine FC-1 with an assigned age of 27.84 Ma (Deino and Potts, 1990), relative to Mmhb-1 at 520.4 Ma (Samson and Alexander, 1987). Individual sanidine grains were fused using a CO_2 laser operating at 1.6 watts for 5 seconds. Variance-weighted mean ages reported in Table1- 2 were calculated by the method of Samson and Alexander (1987) using decay constants of Steiger and Jäger (1977). Other phenocryst phases and whole-rock samples were heated incrementally in a low-blank resistance furnace. Plateau ages were calculated using the definition of Fleck et al. (1977). Alunite was degassed using a CO_2 laser at progressively increasing power levels. This procedure is somewhat similar to incremental heating in a furnace but does not have precise temperature control. Age results and data are presented in Table 1-2 and Figs. 1-6 and 1-13.

ID	Temp (°C)	40Ar/ 39Ar	37Ar/ 39Ar	36Ar/39Ar (x 10-3)	39ArK (x 10-15 mol)	K/Ca	40Ar* (%)	39Ar (%)	Age (Ma)	±2s (Ma)
G11-005-4-4492, C4:101, 4.29mg bi, J=0.000763599±0.10%, D=1.00361±0.00157, NM-101, Lab#=9959-02										
A	*650*	*136.9*	*0.3304*	*407.3*	*0.076*	*1.5*	*12.1*	*0.4*	*22.7*	*5.0*
B	*750*	*61.78*	*0.0868*	*119.7*	*0.221*	*5.9*	*42.8*	*1.5*	*36.0*	*1.3*
C	*850*	*31.50*	*0.0092*	*9.949*	*1.14*	*55.5*	*90.7*	*7.1*	*38.92*	*0.26*
D	*920*	*29.67*	*0.0056*	*2.511*	*1.91*	*91.6*	*97.5*	*16.5*	*39.42*	*0.19*
E	1000	29.33	0.0097	1.663	1.78	52.5	98.3	25.2	39.30	0.18
F	1075	29.14	0.0146	1.079	2.84	34.9	98.9	39.2	39.27	0.18
G	1110	29.12	0.0197	1.171	1.86	25.9	98.8	48.3	39.22	0.18
H	1180	29.03	0.0580	1.384	2.88	8.8	98.6	62.5	39.01	0.18
I	1210	29.09	0.0722	1.020	6.29	7.1	99.0	93.4	39.23	0.17
J	*1250*	*29.50*	*0.0468*	*1.566*	*1.13*	*10.9*	*98.4*	*99.0*	*39.57*	*0.21*
K	*1300*	*31.44*	*0.1292*	*3.473*	*0.166*	*3.9*	*96.8*	*99.8*	*41.43*	*0.62*
L	*1650*	*112.6*	*6.254*	*119.8*	*0.044*	*0.082*	*69.0*	*100.0*	*104.4*	*4.4*
total gas age		n=12			20.3	27.7			39.29	0.22
plateau		n=5	steps E-I		15.6	19.8		76.9	39.21	0.15
BP-2, h5#4:81, biotite, 7.76 mg, J=0.000807327±0.09%, D=1.0052±0.00069, NM-81, Lab#=8662-01										
A	*650*	*1685.8*	*0.0742*	*5538.3*	*0.223*	*6.9*	*2.9*	*0.2*	*70.4*	*116.7*
B	*750*	*87.75*	*0.0245*	*205.8*	*1.17*	*20.8*	*30.7*	*1.2*	*38.8*	*1.9*
C	850	39.90	0.0040	42.90	7.97	127.2	68.2	7.8	39.23	0.28
D	920	30.12	0.0051	9.199	8.66	100.8	91.0	15.1	39.48	0.19
E	1000	28.82	0.0040	5.691	10.0	127.9	94.2	23.5	39.10	0.18
F	1075	28.83	0.0039	4.972	8.43	130.7	94.9	30.5	39.42	0.15
G	1110	28.44	0.0047	4.431	12.1	108.0	95.4	40.7	39.10	0.16
H	1180	28.31	0.0125	4.938	24.1	40.9	94.8	60.8	38.70	0.13
I	1210	28.27	0.0121	4.818	22.8	42.2	95.0	80.0	38.68	0.18
J	1250	28.66	0.0265	5.384	18.7	19.3	94.5	95.6	39.00	0.12
K	1300	28.81	0.0193	5.205	4.85	26.4	94.7	99.7	39.29	0.17
L	*1650*	*48.06*	*0.0000*	*38.10*	*0.385*	*-*	*76.6*	*100.0*	*52.8*	*1.2*
total gas age		n=12			119.3	67.3			39.09	0.40
plateau		n=9	steps C-K		117.6	68.1		98.5	39.07	0.21
BP-2, h6#6:81, plag, 31.13 mg, J=0.000807418±0.09%, D=1.0052±0.00069, NM-81, Lab#=8663-01										
A	*625*	*15131.8*	*0.0367*	*49778.6*	*0.308*	*13.9*	*2.8*	*1.0*	*529.2*	*1465.8*
B	*700*	*114.8*	*1.174*	*297.0*	*0.797*	*0.43*	*23.6*	*3.6*	*39.2*	*2.9*
C	*750*	*57.54*	*1.957*	*87.04*	*0.054*	*0.26*	*55.6*	*3.8*	*46.0*	*9.1*
D	*800*	*44.50*	*2.623*	*51.91*	*1.35*	*0.19*	*66.0*	*8.3*	*42.35*	*0.80*
E	*875*	*31.78*	*4.149*	*15.37*	*1.75*	*0.12*	*86.7*	*14.1*	*39.82*	*0.43*
F	*975*	*29.58*	*5.975*	*10.52*	*3.94*	*0.085*	*91.0*	*27.1*	*38.97*	*0.24*
G	1075	29.78	7.658	13.00	2.36	0.067	89.1	34.9	38.44	0.34
H	1250	30.91	6.965	17.81	9.70	0.073	84.7	66.9	37.92	0.17
I	1350	36.56	6.617	35.81	4.63	0.077	72.4	82.2	38.35	0.40
J	*1650*	*33.29*	*8.598*	*24.07*	*5.40*	*0.059*	*80.6*	*100.0*	*38.91*	*0.25*
total gas age		n=10			30.3	0.23			43.7	15.3
plateau		n=3	step G-I		16.7	0.07		55.1	38.10	0.37

ID	Temp (°C)	40Ar/39Ar	37Ar/39Ar	36Ar/39Ar (x 10-3)	39ArK (x 10-15 mol)	K/Ca	40Ar* (%)	39Ar (%)	Age (Ma)	±2s (Ma)
BP-2, h3:81, wr, 6.70 mg, J=0.000807202±0.09%, D=1.0052±0.00069, NM-81, Lab#=8660-01										
A	625	11919.6	0.0822	37770.1	2.22	6.2	6.4	7.5	861.7	685.3
B	0	62.76	0.0737	96.30	5.83	6.9	54.7	27.3	49.29	0.22
BB	700	52.32	0.0825	61.94	0.496	6.2	65.0	29.0	48.9	1.2
C	750	40.55	0.0983	22.93	1.28	5.2	83.3	33.3	48.54	0.60
D	800	34.14	0.1093	9.710	2.39	4.7	91.6	41.4	44.99	0.32
E	875	31.07	0.1282	4.893	4.43	4.0	95.4	56.4	42.65	0.19
F	975	29.24	0.1967	3.213	4.49	2.6	96.8	71.6	40.76	0.18
G	1075	29.21	0.3487	4.837	2.03	1.5	95.2	78.5	40.05	0.31
H	1170	30.70	0.4452	10.37	3.24	1.1	90.1	89.5	39.87	0.23
I	1250	43.30	0.6506	51.74	1.53	0.78	64.8	94.6	40.42	0.61
J	1650	63.35	1.474	115.1	1.58	0.35	46.5	100.0	42.45	0.96
total gas age		n=11			29.5	3.8			105.3	51.9
plateau		n=11	steps A-J		29.5	3.8		100.0	42.9	2.1
DS-13 Whole rock B:3, Rhyolite WR, 12.70 mg, J=0.000786178±0.10%, D=1.00362±0.00105, nm-93										
A	600	532.0	0.3611	1743.9	0.429	1.4	3.1	1.2	23.6	9.1
B	700	76.64	0.5754	177.8	3.17	0.89	31.5	10.0	33.94	0.84
C	750	41.27	1.089	48.65	3.21	0.47	65.4	18.9	37.90	0.36
D	800	32.71	1.033	15.37	2.57	0.49	86.4	26.1	39.65	0.24
E	850	30.26	0.1826	7.008	3.81	2.8	93.2	36.7	39.57	0.21
F	900	29.61	0.0535	5.596	3.45	9.5	94.4	46.3	39.23	0.19
G	950	34.79	0.0323	25.24	3.17	15.8	78.6	55.1	38.37	0.27
H	1000	29.51	0.0268	6.751	1.78	19.0	93.2	60.0	38.61	0.21
I	1050	29.50	0.0308	8.376	2.65	16.5	91.6	67.4	37.93	0.20
J	1100	30.27	0.0213	10.49	2.11	24.0	89.8	73.3	38.13	0.23
K	1150	31.00	0.0230	13.65	2.59	22.2	87.0	80.5	37.86	0.23
L	1250	33.41	0.0416	22.55	3.03	12.3	80.1	88.9	37.55	0.21
M	1400	35.20	0.0412	30.87	3.76	12.4	74.1	99.4	36.62	0.29
N	1650	97.25	0.0229	250.3	0.232	22.3	23.9	100.0	32.7	2.7
total gas age		n=14			35.9	10.4			37.70	0.42
plateau		n=14	steps A-N		35.9	10.4		100.0	38.38	0.53
BST-114 B:2, Sanidine, 10.06 mg, J=0.000785599±0.10%, D=1.00362±0.00105, NM-93, Lab#=9468										
A	*700*	*328.3*	*0.1264*	*1052.8*	*0.094*	*4.0*	*5.2*	*0.1*	*24.2*	*11.1*
B	*800*	*47.20*	*0.0165*	*72.91*	*0.525*	*30.9*	*54.4*	*0.8*	*35.99*	*0.78*
C	900	28.53	0.0073	6.473	1.52	69.7	93.3	2.8	37.33	0.18
D	1000	27.62	0.0057	3.143	3.54	90.0	96.6	7.4	37.44	0.16
E	1100	26.93	0.0048	1.011	5.85	105.4	98.9	15.0	37.35	0.13
F	1200	26.96	0.0057	0.7852	7.60	89.2	99.1	25.0	37.49	0.15
G	1250	27.24	0.0048	2.067	5.92	106.3	97.8	32.7	37.35	0.13
H	1300	27.10	0.0044	1.858	13.9	115.7	98.0	50.8	37.24	0.15
I	1350	27.75	0.0047	3.995	12.0	108.1	95.7	66.5	37.28	0.15
J	1400	27.44	0.0055	2.273	5.30	93.5	97.6	73.4	37.54	0.16
K	*1500*	*27.55*	*0.0070*	*2.648*	*6.17*	*72.8*	*97.2*	*81.5*	*37.54*	*0.12*
L	*1600*	*27.64*	*0.0054*	*2.741*	*8.77*	*93.7*	*97.1*	*92.9*	*37.63*	*0.15*
M	*1800*	*31.22*	*0.0088*	*14.80*	*5.19*	*57.7*	*86.0*	*99.7*	*37.65*	*0.18*
N	*1800*	*79.44*	*0.0661*	*181.4*	*0.224*	*7.7*	*32.5*	*100.0*	*36.3*	*1.8*
total gas age		n=14			76.7	95.8			37.39	0.17

68

ID	Temp (°C)	40Ar/39Ar	37Ar/39Ar	36Ar/39Ar (x 10-3)	39ArK (x 10-15 mol)	K/Ca	40Ar* (%)	39Ar (%)	Age (Ma)	±2s (Ma)
plateau		n=8	step C-J	55.7	103.4			72.6	37.37	0.11

BST-30, h4#2:81, biotite, 6.82 mg, J=0.00080722±0.09%, D=1.0052±0.00069, NM-81, Lab#=8661-01

ID	Temp (°C)	40Ar/39Ar	37Ar/39Ar	36Ar/39Ar (x 10-3)	39ArK (x 10-15 mol)	K/Ca	40Ar* (%)	39Ar (%)	Age (Ma)	±2s (Ma)
A	650	97.40	0.4520	249.7	1.24	1.1	24.3	1.2	34.1	1.5
B	750	66.75	0.1481	138.1	3.65	3.4	38.9	4.7	37.42	0.70
C	850	30.89	0.0070	16.52	7.87	72.8	84.2	12.2	37.48	0.19
D	920	28.30	0.0062	6.933	8.10	82.4	92.8	20.0	37.82	0.16
E	1000	27.90	0.0065	5.977	7.00	78.0	93.7	26.7	37.66	0.17
F	1075	28.05	0.0069	6.343	12.9	74.1	93.3	39.0	37.72	0.13
G	1110	27.36	0.0056	4.984	12.7	90.4	94.6	51.2	37.32	0.17
H	1180	27.39	0.0082	5.011	20.6	62.0	94.6	70.9	37.35	0.15
I	1210	27.44	0.0149	5.503	21.2	34.2	94.1	91.2	37.21	0.13
J	1250	28.08	0.0511	7.203	8.70	10.0	92.4	99.6	37.41	0.18
K	1300	28.36	0.1044	3.069	0.386	4.9	96.8	99.9	39.55	1.00
L	1650	91.30	0.0612	185.3	0.079	8.3	40.0	100.0	52.5	8.9
total gas age		n=12			104.5	57.4			37.42	0.20
plateau		n=4	steps G-J	63.2	51.2			60.5	37.31	0.14

H97-21, c4:81, hornblende, 4.97 mg, J=0.000811158±0.09%, D=1.0052±0.00069, NM-81, Lab#=8646-01

ID	Temp (°C)	40Ar/39Ar	37Ar/39Ar	36Ar/39Ar (x 10-3)	39ArK (x 10-15 mol)	K/Ca	40Ar* (%)	39Ar (%)	Age (Ma)	±2s (Ma)
A	800	473.8	2.162	1531.7	0.133	0.24	4.5	2.1	31.0	25.3
B	850	49.51	0.8808	81.19	0.119	0.58	51.7	4.1	37.1	3.7
C	950	31.33	0.6296	28.34	0.176	0.81	73.4	6.9	33.4	2.2
D	1020	28.99	0.7209	13.95	0.159	0.71	86.0	9.5	36.1	2.4
E	1080	28.45	2.040	17.63	0.123	0.25	82.2	11.5	34.0	3.0
F	1120	30.00	5.571	11.82	0.261	0.092	89.8	15.7	39.1	1.6
G	1160	29.30	7.608	12.40	1.95	0.067	89.5	47.2	38.18	0.31
H	1200	27.65	6.708	5.842	2.42	0.076	95.6	86.2	38.46	0.27
I	1300	28.99	8.009	11.29	0.819	0.064	90.6	99.5	38.25	0.57
J	1400	99.91	8.724	199.0	0.017	0.058	41.8	99.7	60.5	25.4
K	1650	281.6	2.637	617.2	0.016	0.19	35.3	100.0	140.1	64.7
total gas age		n=11			6.19	0.13			38.2	1.4
plateau		n=5	steps F-J	5.47	0.07			88.3	38.34	0.33

WC-31, D2:101, 26.23mg plag, J=0.000762051±0.10%, D=1.00361±0.00157, NM-101, Lab#=9950-01

ID	Temp (°C)	40Ar/39Ar	37Ar/39Ar	36Ar/39Ar (x 10-3)	39ArK (x 10-15 mol)	K/Ca	40Ar* (%)	39Ar (%)	Age (Ma)	±2s (Ma)
A	650	436.3	1.789	1303.7	0.125	0.29	11.7	0.5	69.2	10.8
B	750	44.93	0.7808	57.19	2.02	0.65	62.5	8.3	38.23	0.43
C	825	32.79	0.7404	12.84	1.69	0.69	88.6	14.8	39.53	0.24
D	900	31.84	0.6741	12.28	2.25	0.76	88.8	23.4	38.46	0.21
E	1000	31.77	0.4594	12.10	2.70	1.1	88.9	33.8	38.41	0.21
F	1100	33.86	0.3200	19.19	3.42	1.6	83.3	47.0	38.39	0.26
G	1250	32.59	0.3001	15.75	7.65	1.7	85.8	76.4	38.05	0.23
H	1450	34.11	2.845	17.44	5.79	0.18	85.5	98.7	39.75	0.22
I	1650	45.55	3.487	35.16	0.330	0.15	77.8	100.0	48.18	0.64
total gas age		n=9			26.0	1.0			38.93	0.30
plateau		n=4	steps D-G	16.0	1.4			61.7	38.34	0.23

BST-144, C6:101, 9.45mg alunite, J=0.000763799±0.10%, D=1.00361±0.00157, NM-101, Lab#=9961-02

ID	Temp (°C)	40Ar/ 39Ar	37Ar/ 39Ar	36Ar/39Ar (x 10-3)	39ArK (x 10-15 mol)	K/Ca	40Ar* (%)	39Ar (%)	Age (Ma)	±2s (Ma)
A	1	127.0	0.0000	361.5	0.012	-	15.9	0.9	27.5	16.9
B	1	174.7	0.0000	480.2	0.009	-	18.8	1.6	44.7	26.5
C	2	65.97	0.0000	159.5	0.007	-	28.5	2.1	25.7	15.4
D	2	271.3	0.0638	892.0	0.104	8.0	2.8	10.3	10.6	9.5
E	2	55.43	0.0857	139.5	0.086	6.0	25.7	17.0	19.5	2.3
F	3	39.77	0.0690	89.37	0.150	7.4	33.6	28.8	18.3	1.3
G	3	99.57	0.0000	260.1	0.004	-	22.8	29.2	31.0	26.6
H	3	33.41	0.0484	77.36	0.012	10.5	31.6	30.1	14.5	8.0
I	4	57.14	0.0684	149.0	0.653	7.5	23.0	81.3	18.0	1.1
J	4	29.62	0.0808	51.19	0.104	6.3	48.9	89.5	19.9	1.7
K	*4*	*21.95*	*0.0883*	*33.24*	*0.134*	*5.8*	*55.3*	*100.0*	*16.6*	*1.1*
total gas age			n=11		1.28	7.1			17.9	2.5
plateau			n=10	steps A-J	1.14	7.3		89.5	18.6	1.2

Isotopic ratios corrected for blank, radioactive decay, and mass discrimination,
not corrected for interfering reactions.
Individual analyses show analytical error only; mean age errors also include error in J and irradiation parameters.
Analyses in italics are excluded excluded from mean age
calculations.
Correction factors:

$(^{39}Ar/^{37}Ar)_{Ca}$ = 0.00070±0.00005

$(^{36}Ar/^{37}Ar)_{Ca}$ = 0.00026±0.00002

$(^{38}Ar/^{39}Ar)_K$ = 0.0119

$(^{40}Ar/^{39}Ar)_K$ = 0.0002±0.0003

Chapter 2

**Gold Mineralization in Eocene Dikes at Griffin and Meikle:
Bearing on the Age and Origin of Deposits of the Carlin Trend, Nevada**[1]

Michael W. Ressel and Donald C. Noble
Department of Geological Sciences /172,
Mackay School of Mines,
University of Nevada, Reno,Reno, Nevada 89557
e-mail: mressel@unr.edu

Jeffrey A. Volk, Jan B. Lamb, David Park
Barrick Goldstrike Mines, Inc.,
P.O. Box 29, Elko, Nevada 89803

James E. Conrad
U.S. Geological Survey
345 Middlefield Road, Menlo Park, California 94025

Matthew T. Heizler,
Geochronology Laboratory, New Mexico Bureau of Mines and Mineral Resources,
801 Leroy Place, Socorro, New Mexico 87801

James K. Mortensen
Department of Earth and Ocean Sciences,
University of British Columbia,
6339 Stores Road, Vancouver, B.C., V6T 1Z4

Abstract

Field relations, isotopic dating and petrographic and chemical analysis of dacite dikes suggest that Carlin-type Au mineralization at the Griffin and Meikle deposits is of Eocene age and closely linked to igneous activity. An $^{40}Ar/^{39}Ar$ age of 39.21 ± 0.12 Ma on biotite phenocrysts from mildly argillized dacite and U/Pb zircon age of 38.1 ± 0.8 Ma from mineralized dacite from the Griffin deposit confirm the Eocene emplacement age of several correlative dikes of porphyritic dacite that intrude the Post fault zone from north of Meikle to the Betze-Post deposit. The dacite dikes are variably altered and locally mineralized in both Meikle and Griffin deposits. Sericite (1M and 2M illite) associated with fine-grained pyrite and arsenopyrite was formed during the earliest and most Au-rich paragenetic stage recognized in dacite. Illite-quartz mixtures from dacite that contains 3 to 9 ppm Au and 3 to 55 ppm Ag yielded $^{40}Ar/^{39}Ar$ total gas ages of between 40.0 and 45.7 Ma, older than the ca. 39.2 Ma age of the dikes. Older apparent sericite ages resulted in part from ^{39}Ar recoil loss from fine-grained illite on irradiation. Nonetheless, the corre-spondence between illite ages and their similarity to biotite and zircon ages suggest that Au-related sericitic alteration closely followed intrusion at the Meikle and Griffin deposits.

Late hydrothermal activity at Griffin produced comb quartz veinlets containing Ag-Sb sulfosalts and native Ag and still later barite veinlets and vug fillings. Paragenetic and geochemical relationships of ore-grade dacite from Griffin and Meikle indicate that Au was deposited with fine-grained, As-bearing Fe sulfides similar to other deposits of the Carlin trend and that a later stage resulted in the precipitation of minerals containing more Ag, Sb, Se, Mo and probably, W but with lower amounts of S and only minor Fe.

Dacite marginal to mineralized dike or carbonate rock has been converted to a mixture of smectite, kaolinite, quartz, and carbonate with little or no pyrite, but commonly contains relict biotite phenocrysts. Moderately altered dacite contains

abundant mixed-layer illite-smectite, pyrite and carbonate. More intensely altered dacite, which commonly retains phenocrystic textures, contains mostly quartz, sericite, pyrite, and arsenopyrite, with lesser amounts of kaolinite, carbonaceous material, and carbonate. Multi-element analyses show progressive gains in pathfinder elements, including Au, Ag, S, As, Hg, Sb, and Tl, with greater intensity of sericitic alteration. Other elements that were added during quartz-sericite-pyrite alteration include Se, Mo, W, and Ni. In contrast, Na, Ba, Ca, Sr, Mg and Mn were removed; K was leached to a lesser degree. Variation in the Fe/Ti and Si/Ti of mineralized dacite indicate that Fe and Si were mobile. Some Fe and Si were added during mineralization.

Mineralized rocks of the various deposits of the Carlin trend have many common paragenetic and geochemical features that support common ore-forming processes and which argue against multiple, unrelated periods of Au deposition. The spatial and temporal link between 40 to 36 Ma intrusive activity and mineralization at the Meikle, Griffin, Betze-Post, Genesis, Deep Star and Beast deposits suggests that Eocene magmatism was critical in the formation of Au deposits of the Carlin trend.

Introduction

Carlin-type deposits (CTDs) are the leading producers of Au in the United States and are an important global source of gold. The largest deposits are concentrated in four mining provinces in northern Nevada, including the Carlin trend, Getchell trend, Battle Mountain-Eureka belt, and Jerritt Canyon district (Fig. 2-1), but numerous smaller deposits occur elsewhere in northern Nevada. Production and reserves of Au from CTDs of the 60-km long Carlin trend are more than 2,640 tonnes (~85 million ounces) or more than half of the total Au from CTDs in Nevada (Teal and Jackson, 1997). CTDs occur mainly in moderately folded Paleozoic carbonate rocks in or adjacent to structural

windows developed in allochthonous Paleozoic siliciclastic rocks (Roberts, 1960). Orebodies are localized in favorable silty carbonate rocks in or adjacent to high-angle faults, which commonly bound ranges. The deposits are characterized by an abundance of fine-grained, disseminated Fe sulfides, including pyrite, arsenian pyrite, arsenopyrite and marcasite, enrichment in the elements As, Sb, Hg, and Tl, and, Au/Ag ratios greater than 1 (Christensen, 1996; Arehart, 1996; Hofstra et al., 1999). Base metal contents in ores are characteristically low, and there has been very little base metal production from CTDs in Nevada. The high Au/Ag ratios and lack of base metals have been used to differentiate CTDs from other sedimentary rock-hosted deposits in northern Nevada such as Lone Tree, Nevada, which are classified as pluton-related or distal-disseminated Ag-Au (e.g., Cox, 1992; Mosier et al., 1992; Doebrich and Theodore, 1996). Decarbonitization, silicification, and argillization are the main types of alteration affecting carbonate host rocks of CTDs. In deposits such as Carlin, Betze-Post, and Beast, alteration is zoned from siliceous cores in faults outward to kaolinitic halos, to more distal zones of decarbonitized rock (Bakken and Einaudi, 1986; Rota and Hausen, 1991; Arehart, 1996; Ferdock et al., 1997; Ressel et al., 2000). Intrusive rocks near ore are sericitically altered or silicified.

The fine-grained replacement style of mineralization and the difficulty in isolating dateable hydrothermal minerals clearly related to Au deposition has made determination of the age of CTDs of the Carlin trend as well as in other parts of northern Nevada problematic. In part for this reason, certain genetic aspects of mineralization remain equivocal. The results of isotopic dating of fine-grained, K-bearing phyllosilicates (e.g., illite) occurring in ores have been controversial (Arehart et al., 1993a; Ilchik, 1995; Folger et al., 1996, 1998; Hall et al., 1997; Hofstra et al., 1999) because of multiple illite-forming hydrothermal and/or magmatic events that have affected the host sedimentary

rocks. Illite from mineralized host rocks of the Jerritt Canyon district was shown by Folger et al. (1996; 1998) to be of mixed diagenetic and hydrothermal origins, indicating insignificant thermal resetting of old illite. Aside from being difficult to separate from pre-existing illite, poorly developed ore-stage illite is prone to ^{39}Ar recoil loss on irradiation resulting in complex ^{40}Ar/^{39}Ar spectra and older apparent ages.

Adularia related to late-stage Au mineralization has been dated at about 42 Ma at the Twin Creeks CTD (Groff et al., 1997; Hall et al., 1997). However, adularia is apparently absent in the majority of the deposits, including those of the Carlin trend. In contrast, post-Au alunite is common in many CTDs. Arehart et al. (1993b) and Hofstra et al. (1999) interpret alunite from several deposits in the Carlin trend as supergene based on sulfur isotopic compositions, although others (Heitt, 1992; Rota and Hausen, 1991; Ilchik, 1996; Ressel et al., 2000) suggest hydrothermal origins of some alunite based on textural evidence. Regardless of origin, alunite provides minimum mineralization ages of between about 30 and 8 Ma for several deposits of the Carlin trend. Recent Rb/Sr dating of Au-related galkhaite, a Cs-Hg sulfosalt found in ores from the Getchell underground mine, yielded an Eocene age (Arehart et al., 2000). Many important age constraints have been determined by the ^{40}Ar/^{39}Ar dating of intrusive rocks that are in places, hydrothermally altered and locally mineralized or which appear to postdate ore (e.g., Silberman et al., 1974; Arehart et al., 1993a; Emsbo et al., 1996; Phinisey et al., 1996; Groff et al., 1997).

Recent age studies on the Carlin trend are few, and their results are conflicting (Arehart et al., 1993a; Drews-Armitage et al., 1996; Emsbo et al., 1996; Ressel et al., 1999; 2000). Arehart et al. concluded that mineralization at the Betze-Post deposit postdated the 158 Ma Goldstrike intrusion but predated a 39 Ma porphyritic dacite dike, which contains inclusions of ore. They interpreted the age of Au mineralization as

Cretaceous (~117 Ma) based on 14 imprecise ^{40}Ar/^{39}Ar and K-Ar sericite ages that range from about 65 to 194 Ma. Emsbo et al. (1996) interpreted that a compositionally similar porphyritic dacite dike at Betze-Post is pre-mineral because it is altered to quartz, sericite, and pyrite as are sedimentary ores, contains arsenian pyrite, and has enrichments in pathfinder elements. Leondardson and Rahn (1996) suggested that the same Eocene dacite dikes at Betze-Post were emplaced during the late stages of hydrothermal activity, thus providing an explanation for the presence of ore fragments in the dikes, their generally less intense alteration, and their lack of gold.

We focus on altered and mineralized Eocene dikes of the Meikle and Griffin deposits in the northern Carlin trend using a combination of geologic relations, petrographic and paragenetic studies, geochemistry, and isotopic dating of igneous and alteration minerals. Eocene rocks are the youngest Au-mineralized rocks in the Carlin trend and not only provide reasonable constraints on the timing of mineralization, but also yield information on the character of Carlin-type mineralization free from earlier thermal or hydrothermal alteration that affects Paleozoic sedimentary and Mesozoic intrusive rocks. The results have implications for the origin of CTDs and for precious-metal exploration in the Great Basin.

Geologic Setting

Gold deposits of the Carlin trend from the Gold Quarry deposit north to the Dee-Storm deposits are hosted mainly in silty carbonate rocks and to a lesser degree siltstone and mudstone of Siluro-Devonian age or breccias derived from them. The carbonate rocks underlie the Roberts Mountains thrust (e.g., Christensen, 1996; Teal and Jackson, 1997), a regional fault along which Lower Paleozoic eugeoclinal siliciclastic rocks, including mudstone and chert, were placed over the parautothonous miogeoclinal strata (e.g., Evans, 1980; Saucier, 1997). Ore is also present in highly deformed allochthonous

siliciclastic rocks and in intrusions of late Jurassic and Eocene age, which are spatially associated with all of the deposits of the trend. Post-mineral tuffaceous and alluvial deposits of the Miocene Carlin Formation and locally, Miocene rhyolite lavas, unconformably overlie Paleozoic sedimentary rocks and Jurassic and Eocene intrusive rocks. The orebodies are concentrated in folded carbonate rocks in the footwalls of range-bounding north-northwest-striking high-angle normal faults with large vertical displacements ($\geq$100 m) (e.g., Lauha and Bettles, 1993; Christensen, 1996; Volk et al., 1996; Teal and Jackson, 1997). These faults cut the Carlin Formation, demonstrating some post- Miocene (~15 Ma) movement. Deposits vary greatly in size and in degree of structural and stratigraphic control (Christensen, 1996; Teal and Jackson, 1997), but all contain pyrite as the principal ore mineral and have a geochemical signature marked by As, Sb, Hg, Tl ± Ba (e.g., Arehart, 1996). Alteration is dominated by decarbonatization, argillization and silicification of carbonate host rocks; veining is relatively minor.

Meikle and Griffin Deposits

The Meikle and Griffin deposits are located in the northern part of the Carlin trend (Figs. 2-1 and 2-2) and form the northernmost part of a nearly continuous structurally-controlled zone of Au-mineralized rock that also includes the Betze-Post and Goldbug-Rodeo deposits to the south and the Banshee and Ren deposits to the north. The deposits within this 6-km long corridor contained at least 1,400 tonnes (45 million ounces) of Au prior to mining (Teal and Jackson, 1997). All of the deposits lie in the footwall of the Post fault zone, which consists of a series of major north-northwest-striking, steeply east-dipping, high-angle normal faults (Lauha and Bettles, 1993; Volk et al., 1996). The Griffin deposit is hosted mainly in argillaceous siltstone and carbonate of the Rodeo Creek unit (Fig. 2-3), that overlie Devonian and Silurian carbonate rocks of the Roberts Mountains and Popovich Formations and siliceous breccias derived from those carbonate

rocks. The Meikle deposit is hosted in large part by complex siliceous breccia bodies (Volk et al., 1996). Host rocks are overlain by Lower Paleozoic chert and mudstone of the Roberts Mountains allochthon and by late Tertiary rocks of the Carlin Formation. Reserves and production of Au from the Griffin and Meikle deposits total about 218 tonnes (~7 million ounces) through 1999.

Intrusive Rocks

Numerous dikes intrude Paleozoic sedimentary rocks in the Post fault zone from the Betze-Post deposit north-northwest to the Meikle deposit; the largest dikes are shown on Figure. 2-3. The dikes, of late Jurassic (157-158 Ma) and Eocene (39.2 Ma) age, can be distinguished by textural and geochemical features (Tables 1 and 2) as well as isotopic composition (M.W. Ressel, unpublished data). In the vicinity of orebodies, dikes of both ages are altered and locally mineralized. Alteration is broadly similar in all dike types and is characterized by quartz, sericite, and pyrite (QSP) near or within orebodies that grades outward to argillically-altered rock. Phenocrysts, except for quartz, are pervasively altered in QSP-altered rocks, but porphyritic textures are generally preserved.

Jurassic dikes

Two types of Jurassic dikes are present in the Meikle-Rodeo corridor. The first consists of finely porphyritic plagioclase-biotite-quartz rhyodacite (Meikle rhyodacite). The second is composed of phlogopite- and hornblende-phyric lamprophyre (minette and vogesite). Lamprophyre dikes cut the 158 Ma Goldstrike intrusion at Betze-Post and other nearby CTDs (e.g., Orobona, 1996). Close to the Goldstrike intrusion, equigranular to porphyritic diorite dikes also are present.

Structural relations between the north striking Meikle rhyodacite and dominantly northwest-striking lamprophyre dikes at the Meikle mine are equivocal; indirect evidence from drilling suggests that some lamprophyre dikes cut the Meikle rhyodacite dikes (A.

Bourget, personal communication). However, near the Genesis mine to the south, north-northeast-striking dikes mineralogically and texturally similar to the Meikle rhyodacite cut northwest-striking lamprophyre and diorite dikes. Biotite from one of the rhyodacite dikes west of the Genesis deposit yielded an $^{40}Ar/^{39}Ar$ age of 157.4 ± 0.4 Ma (M.W. Ressel, unpublished data) that is consistent with or slightly younger than other Jurassic intrusions, including the Goldstrike intrusion. Evidence obtained to date indicates that the Goldstrike intrusion, as well as lamprophyre and rhyodacite dikes, were emplaced over a relatively short period from about 157 to158 Ma (Arehart et al., 1993a; Emsbo et al., 1996; Mortensen et al., 2000; M.W. Ressel, unpublished data).

Eocene dikes

Porphyritic dacite dikes intrude the Post fault zone north of the Betze-Post deposit, and several other distinct Eocene dike types are recognized from the Dee-Storm deposits to the Carlin deposit (Arehart et al., 1993a; Ressel et al., 1998, 1999, 2000; Henry and Ressel, 2000). These shallowly-emplaced felsic dikes were formed from magmas that were locally sourced. An inferred buried plutonic complex defined by a 700 km^2 positive aeromagnetic anomaly, probably represents the source for Eocene dikes and small intrusions in the Carlin trend as well as coeval lavas and intrusive rocks of the nearby Emigrant Pass volcanic field (Henry and Ressel, 2000; Ressel et al., 2000). The Eocene dacite of the Betze-Post-Meikle corridor, called Betze dacite (also termed biotite-feldspar porphyry by Arehart et al., 1993a), is composed of abundant phenocrysts of plagioclase, biotite, and hornblende with small amounts of quartz (Table 3-1). The dacite dikes are well exposed in the Betze-Post pit (Figs. 2-2 and 2-3)and extend under cover continuously for more than 5 km to the north. At Betze-Post, the dikes become more abundant and wider with depth (J. Rahn, personal communication, 1999).

Chemical features of felsic dikes

Eocene and Jurassic dikes of felsic composition are chemically distinct. Pervasively altered Betze dacite contains higher concentrations of relatively immobile major and minor elements than Meikle rhyodacite. (Figs. 2-4A,B; Table 2-2). Alumina contents show greater variation (±2 wt.%) among individual dike types as a result of the degree of clay alteration and removal of Na, Ca and K. Even with this variation, differences in alumina contents between the Meikle rhyodacite and Betze dacite are large.TiO_2 contents remain nearly constant for variably altered and non-veined rocks of each type, strongly suggesting Ti is immobile. Similarly, P, REE, Y, Hf and Zr can be used to distinguish the two rock types (Fig. 2-4B; Table 2-2). In all cases, the older Meikle rhyodacite has considerably lower concentrations of these elements than Betze dacite.

Isotopic Dating

Eocene dacite dikes in the Meikle-Rodeo/Goldbug corridor are variably altered and mineralized. $^{40}Ar/^{39}Ar$ ages (Table 2-3; Figs. 2-5A-E; Appendix 2-1) on Au-related sericite from mineralized dikes correspond closely with $^{40}Ar/^{39}Ar$ and U/Pb emplacement ages suggesting that Carlin-type mineralization at these deposits is temporally linked to Eocene magmatism.

Age of Betze dacite

Arehart et al. (1993a) reported an $^{40}Ar/^{39}Ar$ age on biotite (corehole PNC-213-1780'; POD-1) of 38.8 ± 0.8 Ma (2σ), which was normalized to 39.3 Ma using an age of 27.84 Ma for Fish Canyon Tuff sanidine. This recalculated age agrees well with a $^{40}Ar/^{39}Ar$ age of 39.21 ± 0.12 Ma obtained on fresh phenocrystic biotite from mildly argillized Betze dacite at the Griffin deposit (sample G11-5-4-492'). Although the flat $^{40}Ar/^{39}Ar$ spectrum (Fig. 2-5A) does not preclude argon loss, the plateau age is interpreted as the emplacement age of the dike.

U/Pb dating of two zircon fractions from mineralized Betze dacite from Griffin (sample G11-12-1-550/560'; Au = 2 to 6 ppm) yielded concordant lower intercept ages of 38.1 ± 0.8 Ma (Mortensen et al., 2000), consistent with the ^{40}Ar/^{39}Ar data. Two other fractions had considerable inherited components. Because of the higher precision of the ^{40}Ar/^{39}Ar determination, we prefer 39.21 ± 0.12 Ma as the emplacement age of the Betze dacite.

Clay mineralogy

Ore-bearing Betze dacite has been largely converted to a mixture of quartz, white mica and Fe sulfides, with smaller amounts of kaolinite. Two types of white mica can be distinguished: optically-continuous white mica (mostly 2M illite) that replaces biotite phenocrysts and groundmass biotite, and contains granules of rutile; and nearly pure aggregates of very fine-grained («1 μm) white mica (mostly 1M illite) that replace both phenocrystic and groundmass feldspar. Randomly-oriented powder mounts of quartz-illite samples were run on a Philips 1800 X-ray diffractometer with CuKα radiation set at 35 kV, 25 mA, and 2 sec/0.02° scan rate. Composite illite samples produce broad, poor-intensity 001/002 peaks that have crystallinity indices of about 0.8°. The crystallinity index is taken as the width of the 001/002 reflection at half height in °2θ. This poorly ordered illite has <5% interstratified smectite based on the relatively large 2θ spacing of 8.8° between the 001/002 and 002/003 peaks of glycolated samples (Moore and Reynolds, 1997). Illite that replaces plagioclase has grain sizes ranging from <0.1 to 0.3-μm thickness and 0.5 to 3-μm diameter as determined by SEM methods. These data indicate that illite from hydrothermally altered and mineralized dacite is poorly crystallized and therefore, is prone to ^{39}Ar recoil upon irradiation (e.g., Folger et al., 1998).

Age of mineralization

Three illite-quartz samples from mineralized Betze dacite were analyzed using $^{40}Ar/^{39}Ar$ incremental heating (Table 2-3; Figs. 2-5B-E, Appendix 2-1). Two of the samples are from Griffin corehole G11-12-1 (footages 550 and 569) and a third sample is from corehole M12-3525-2 (footage 103), which intersected the upper main zone of the Meikle orebody. The Griffin bulk dacite samples contained between 3 and 9 ppm Au, and the Meikle sample contained more than 6 ppm Au. The dacites are altered to mixtures containing mostly quartz and illite, with smaller amounts of kaolinite, arsenian pyrite and arsenopyrite.

The illite-quartz samples yield complex results (Figs. 2-5B-E). The $^{40}Ar/^{39}Ar$ spectra for all three samples are similar; all plots show low-temperature steps with relatively older ages, intermediate-temperature steps, where the majority of gas was released, that are relatively flat and give intermediate ages, and highest-temperature steps that give low ages. The total gas ages of the three samples are between 40.03 ± 0.05 and 45.68 ± 0.68 Ma, somewhat older than the ca. 39.2 Ma age of the Betze dacite as determined by U/Pb zircon and $^{40}Ar/^{39}Ar$ biotite ages on the same and on a nearby less altered dike. We interpret the step-heating data to reflect varying degrees of ^{39}Ar recoil, a possibility supported by XRD and SEM analyses of the sericite. If recoil is a significant factor, then two possibilities arise in terms of the fate of recoiled ^{39}Ar. First, some ^{39}Ar may have been removed from the samples upon irradiation, thus producing larger integrated $^{40}Ar/^{39}Ar$ ratios and older total gas ages. Second, some ^{39}Ar may have been adsorbed into quartz or some other refractory phase. Consistently younger apparent ages for the highest temperature steps and older ages for lower temperature steps of all three samples conceivably could result from recoil processes (e.g., Dickin, 1995). Thus, total gas ages are maxima, and the true ages of sericite are less than 40 Ma.

An isochron plot of one sample (Fig. 2-5E, sample G11-12-1-569) shows two discrete arrays, both of which yield overlapping ages of 39.3 + /-1.8 and 38.3 +/- 2.1 Ma. One array (steps b-i) has an initial $^{40}Ar/^{36}Ar$ ratio of about 800 that suggests the presence of excess argon trapped during crystallization. Such trapped argon would also produce relatively older ages. However, the isochron ages are indistinguishable from the 39.21 ± 0.12 Ma age of the dike. It is unclear what influence ^{39}Ar recoil may have had on the $^{40}Ar/^{39}Ar$ ratio, and thus the distribution of points on the isochron plot. Possibly, the effect was relatively minor so as to yield meaningful isochron ages.

We interpret the $^{40}Ar/^{39}Ar$ data to reflect an Eocene age of formation for illite in mineralized Betze dacite. The total gas ages of illite are similar but slightly older than the age of the Betze dacite and probably reflect some ^{39}Ar loss through recoil during irradiation. A small amount of excess argon may also have contributed to older calculated ages but is not well constrained. The ages are consistent with Au-related sericitic alteration occurring shortly after dike emplacement. On-going $^{40}Ar/^{39}Ar$ experiments on sealed illite samples may contribute further to the age interpretations presented here.

Possibility of Jurassic mineralization

Two fractions of zircon from the Meikle rhyodacite (sample EX-24c-1600/1650') yielded a weighted Pb/Pb age of 159.3 ± 4.2 Ma, which is the best estimate for the crystallization age of the rock. The two zircon fractions appeared to be free of inherited components but show evidence for slight Pb loss. Four other zircon fractions contained large amounts of inherited components. The U/Pb data are reported in Mortensen et al. (2000). The age of the Meikle rhyodacite overlaps the ages determined for the Goldstrike intrusion and associated dikes (Arehart et al., 1993a; Mortensen et al., 2000; M.W. Ressel, unpub. data).

Sericite from altered and mineralized Meikle rhyodacite was dated using $^{40}Ar/^{39}Ar$ incremental heating methods (Appendix) and yielded a plateau age of 154.6 ± 1.4 Ma (Table 2-3; Fig. 2-6). An 18-foot composite of core from drillhole EX-24c (1600-1618') contained 6.4 g/t Au, mainly in quartz-pyrite veinlets. Although the age could be interpreted to reflect the age of Au mineralization, two aspects of the sample suggest that Au postdates the sericitic alteration. First, the rhyodacite is highly fractured and pervasively altered to quartz, sericite ± euhedral pyrite; unveined clasts contain ≤5 ppb Au. This alteration is characteristic of Jurassic felsic dikes throughout the northern part of the Carlin trend, even where unfractured, and reflects alteration that took place shortly after emplacement (Brake et al., 1998). Later, relatively low-temperature (< 250°C) and sericite-stable Au-bearing fluids would not reset the white mica (Folger et al., 1996; 1998; Hofstra et al., 1999). Similarly, no large intrusive body younger than the Jurassic Goldstrike stock, which may have disturbed pre-existing K-bearing minerals, has been recognized in the immediate area of the Meikle and Griffin deposits. Second, in contrast to the Betze dacite, which locally contains abundant disseminated Fe sulfides and Au, mineralization of the Meikle rhyodacite appears limited to places where the rock has been broken and subsequently veined (Lauha and Bettles, 1993; Volk et al., 1996). Gold-bearing Fe sulfides are found within quartz-pyrite veinlets and immediately adjacent wallrock. These relationships suggest that sericite in the Meikle rhyodacite was formed before Au mineralization and that previously formed sericite was not reset, nor was a significant amount of new sericite formed, during Au mineralization.

Mineralized Dacite

Alteration and mineralization

Several hundred meters of Betze dacite core from the Meikle, Griffin, and Rodeo deposits was logged to determine the lateral continuity of the dacite dikes and the

variation in alteration that affects them. More detailed work was done at Griffin, where mineralized dacite was first recognized. Although the dacite is variably altered in the Meikle-Rodeo corridor (Fig. 2-7A), the original coarsely porphyritic texture is typically preserved. Zones of intensely argillized dacite in which the porphyritic texture is not recognizable can be traced continuously into less altered rock. Mineralized dacite is characterized by sericitic alteration wherein white feldspar phenocrysts are pseudomorphed by illite that is readily distinguished from the gray sulfidic groundmass (Fig. 2-7A, right specimen). Sites of mafic phenocrysts are less obvious, but even these can generally be identified in hand specimen as cream-colored pseudomorphs comprised of illite, with lesser amounts of other clay minerals and carbonate. Mafic phenocrysts were also important sites for sulfide nucleation, although fine-grained Fe sulfides more commonly replace the groundmass.

Mineralized Betze dacite containing from about 1 to 9 ppm Au consists mostly of quartz, 10-30% illite, <10% kaolinite, and 1-5% Fe sulfide, which includes pyrite, arsenian pyrite, and arsenopyrite, with smaller amounts of marcasite (Fig. 2-7B). Pyrite is commonly fine-grained and chemically and petrographically zoned, with discrete bands or broader areas of As enrichment that correspond to framboidal rims or zones containing porous pyrite with irregular habit (Fig. 2-7C). Arsenic contents of pyrite are highly variable even within individual grains. Variable amounts of solid carbon are also present with fine-grained Fe sulfides at and near contacts with sedimentary wallrock. Minor secondary minerals include carbonate, rutile, and clay minerals. Magmatic apatite and zircon are preserved, even where the dacite is strongly altered and mineralized.

In general, dacite with more than 5 ppm Au appears to contain greater amounts of quartz and Fe sulfide than dacite with 1 to 4 ppm Au, which has greater amounts of illite. This reflects the presence of more abundant quartz-pyrite and late-stage comb quartz

veinlets in more mineralized dacite. In some core, weakly mineralized (0.1-1 ppm Au) QSP-altered dacite grades into non-mineralized (<5 ppb), argillically-altered (illite-smectite) dacite containing only small amounts of disseminated pyrite. Other clay-rich rocks are mainly composed of smectite with smaller amounts of kaolinite, chlorite and carbonate (Fig. 2-7A, left specimen). Relict biotite phenocrysts are locally well preserved in smectite-altered dacite, and in many cases, show no petrographic evidence of alteration to chlorite, vermiculite or other phases.

A distinctive characteristic of less-altered Betze dacite is the preservation of thin rims of biotite that envelop hornblende phenocrysts pseudomorphed by smectite and carbonate. The composition of biotite in rims is equivalent to groundmass and phenocrystic biotite. In addition, the low-temperature smectite-carbonate alteration ($\leq$ 200° C; Essene and Peacor, 1995) of hornblende and groundmass is incompatible with formation of hydrothermal biotite. Therefore, biotite rims are of magmatic origin and may have formed by reaction with the melt on magma decompression. The biotite rims were later altered to illite, with the interface between rims and phenocrysts commonly serving as a nucleation site for Fe sulfides in QSP-altered dacite.

Vein petrology

Veinlets are common in QSP-altered dacite. Veinlets are also present in argillically-altered dacite but are less abundant and of different composition. There are three types of veinlets in ore-bearing, QSP-altered dacite: type 1 veinlets composed of granular quartz-pyrite $\pm$ sericite containing Au (Fig. 2-7D); type 2 veinlets consisting of comb quartz-Ag sulfosalts $\pm$ native Ag (Fig. 2-7E) with rare arsenopyrite, arsenian pyrite and chalcopyrite; and less abundant type 3 veinlets and vug fillings that mostly contain euhedral pyrite, barite, and calcite.

Type 1 veinlets are black or bronze, anastomosing and commonly web-like (Fig. 2-7D). They are composed of fine-grained Fe-sulfides, quartz, and solid carbonaceous material and trace sericite. The proportion of sulfides to quartz is variable, although total sulfide content is high, probably greater than 20%. Veinlets of this type separate angular dacite clasts in crackle breccia of the footwall of some mineralized dikes. Irregular vugs associated with these veinlets have very fine-grained linings of pyrite and drusy quartz encrusted with later coarse barite. Type 1 veinlets are also common in the Meikle rhyodacite, and rock containing abundant Type 1 veinlets can constitute ore. Type 1 veinlets as well as rock subject to quartz-iron sulfide-illite-carbon alteration are cut by type 2 quartz veinlets (Fig. 2-7B). These relations suggest that type 1 veinlets are fracture-fill equivalents to the disseminated quartz-Fe sulfide rock typical of Au-bearing dacite, and therefore are related to the main stage of Au deposition. The trace sericite in type 1 veinlets compared to pervasively QSP-altered dacite reflects the formation of sericite from alteration of K-bearing rock and not net K addition.

Type 2 veinlets are clear to slightly milky and clearly cut earlier disseminated fine-grained pyrite and arsenopyrite (Fig. 2-7F). The cores of type 2 quartz veinlets contain Ag-Sb sulfosalts, including pyrargyrite (Fig. 2-7G), miargyrite, and discrasite, of hypogene origin. Native silver occurs locally in association with sulfosalts. Lauha and Bettles (1993) and Volk et al. (1996) report Ag-bearing minerals, including Ag sulfosalts and tetrahedrite in ores of the Meikle deposit. Comb quartz comprises most of type 2 veinlets, but fine-grained granular quartz is also common, particularly in the cores of veinlets. Comb quartz is commonly plumose. Granular quartz veinlets both truncate and are truncated by comb quartz veinlets, suggesting that the two types of quartz were deposited alternately. Type 2 veinlets contain small amounts of Fe sulfides (arsenian pyrite, chalcopyrite), mainly at veinlet margins; some Fe and S may have been scavenged

from pyrite in QSP-altered dacite in the walls of the veinlets. Chalcopyrite is rare as inclusions in Ag-Sb sulfosalts.

Type 3 veinlets and vug fillings in Au-bearing dacites at Griffin and Meikle consist of euhedral, clear to light yellow barite and some pyrite. Occurrences of late barite, in some cases very coarse grained, have long been recognized in ores from the Meikle and other mines of the Carlin trend. The barite that is present in dacite precipitated in open spaces upon earlier-formed euhedral pyrite. Vug and fracture fillings of stage 3 pyrite cut stage 2 quartz veinlets in Au-bearing dacite from Griffin.

Two types of veinlets in argillically-altered dacite are anastomosing pyrite-arsenopyrite vein-lets and carbonate veinlets. The Fe sulfide veinlets are composed of larger, euhedral grains of "brassy" pyrite and arsenopyrite (Fig. 2-7A, center dacite) distinct from the Fe sulfides of type 1 veinlets. In addition, these sulfide veinlets lack the quartz that is ubiquitous to the type 1 veinlets in QSP-altered dacite Calcite veinlets are generally-planar.

Paragenetic relations

Field and petrographic relations of mineralized dacite from the Griffin, Meikle and Rodeo deposits document three main stages of mineralization in Au-bearing dacite that correspond, in part, with type 1, 2 and 3 veinlets, respectively: stage 1 Fe sulfide (pyrite, arsenopyrite, ±marcasite), quartz, sericite, and carbon; stage 2 Ag-Sb sulfosalts, native Ag, quartz, and minor Fe sulfides; and stage 3 late barite and minor pyrite. Stage 1 mineralization is associated with most or all of the Au, although some may have been deposited during the formation of stage 2 quartz veinlets. Stage 1 mineralization was accompanied by QSP-alteration and the formation of anastomosing type 1 quartz-pyrite veinlets (Fig. 2-8). The Fe sulfides of stage 1 have a well-developed order of crystallization. Darker yellow, typically porous, arsenian pyrite forms distinct

overgrowths on non-porous, As-poor pyrite (Figs. 2-7C and 2-8). Similar relationships in sedimentary ores commonly have been interpreted as overgrowths on diagenetic pyrite (e.g., Arehart et al., 1993b; Ilchik and Barton, 1997; Simon et al., 1999), but the presence of compositionally zoned pyrite in the Tertiary dikes is unequivocally the result of hydrothermal alteration. Both forms of pyrite are commonly rimmed by euhedral arsenopyrite, although arsenopyrite also appears intergrown with arsenian pyrite.

Stage 2 is mineralogically simple, being composed almost exclusively of comb and fine-grained, granular quartz veinlets (type 2) that also contain intergrowths of Ag-Sb sulfosalts and smaller amounts of native Ag. Minor pyrite is reverse-zoned from As-rich cores to rims containing less As.

The temporal increase in the As content of stage 1 sulfides may reflect progressive lowering in the amount of reactive Fe available to hydrothermal fluids. Similar paragenetic relationships are described for ores from the Meikle (Volk et al., 1996), Betze-Post (Ferdock et al., 1997), Carlin (Radtke et al., 1980), Deep Star (Fleet and Mumin, 1997), and Beast (Ressel et al., 1999; 2000) deposits. Likewise, late Sb-rich assemblages are common if not ubiquitous in deposits of the Carlin trend as well as other CTDs in northern Nevada (Radtke et al., 1980; Arehart et al., 1993b; Hofstra, 1994; Ferdock et al., 1997; Groff et al., 1997; Ressel et al., 2000). Similar paragenetic relations among CTDs in Nevada suggest that similar conditions and processes were involved in their formation.

As with other stages described above, late-formed barite of stage 3 is a common feature of CTDs in Nevada (e.g., Arehart et al., 1996). The euhedral, "brassy" pyrite that coats many cavities in mineralized dacite is similar to that described for ores of Betze-Post described by Ferdock et al. (1997) and differs from the finer-grained, "sooty" Fe sulfides that typically are associated with Au.

Geochemistry of altered and mineralized dacite

Chemical analyses were made on 22 variably altered and mineralized dacite samples from the Meikle, Griffin, and Rodeo deposits (Table 2-4; Fig. 2-9; Appendix 2-1). The data show higher concentrations of Au (mean = 2.8 ppm, maximum = 8.7 ppm), Ag (weighted mean = 3 ppm not including highest value, maximum = 54.5 ppm), As, Hg, Sb, Tl, and S in QSP-altered dacite. This element suite is characteristic of CTDs (e.g., Christensen, 1996) and suggests that the dacite was affected by the same fluids responsible for forming sedimentary rock-hosted ores. Mo, W, Se and some Ni were also added, particularly in samples containing abundant stage 2 quartz veinlets. Base metal concentrations in mineralized dacite are comparable to least-altered dacite except in some veined dacites, which can have slightly higher Pb (as much as 87 ppm) and Zn (as much as 387 ppm). Cu contents are uniformly low ($\leq$ 30 ppm) but increase slightly in more mineralized rocks. Au/Ag in mineralized dacite containing more than 200 ppb Au ranges from about 0.4 to 4.5, with a mean of about 1.4. The mean Au/Ag in dacite is somewhat lower than the overall ratio of about three for Meikle ores (Lauha and Bettles, 1993).

Concentrations of Au generally increase with higher amounts of Ag, As, Sb, Hg, Mo, W, Ni and S (Figs. 2-9 and 2-10). However, Au correlates only moderately (R = 0.68 to 0.41) with Cu, Sb, and S, and poorly with other elements. In contrast, Ag correlates very well with Sb, Hg, and Mo (R $\geq$ 0.95) and moderately well with Pb (R = 0.55). In addition, Ni, V, and Zn inter-correlate (R > 0.85).

The strong correlation between Ag, Mo, Sb, Hg $\pm$ Pb almost certainly reflects the presence of these elements in sulfosalts of stage 2 quartz veinlets and suggests that these elements were largely deposited after stage 1 (main Au stage). It is likely that this elemental association and paragenetic stage are analogous to the late stibnite stage found in many deposits of the Carlin trend (e.g., Radtke et al., 1980; Lamb, 1995; Ferdock et

al., 1997; Ressel et al., 2000). Similar post-Au elemental associations (Ag, As, Sb, Hg, Cu, Pb and Zn) are described for deposits at Carlin (Harris and Radtke, 1976), Betze-Post (Ferdock et al., 1997), and Beast (Ressel et al., 2000). Where Ni, V, and Zn fit paragenetically in mineralized dacite is not established, and no discrete sulfide minerals have been identified. However, at Betze-Post (Ferdock et al., 1997) and Beast (Ressel et al., 2000), Ni and Zn occur in sulfides, including sphalerite and siegenite, that post-date Au deposition. Small amounts of these elements may also be associated with pyrite.

Element mobility

Isocon diagrams (Grant, 1986) were made to illustrate the relative gains and losses of elements on alteration and mineralization of unveined dacite. Data from three variably altered dacites are shown on a representative isocon diagram (Fig. 2-10). The dacites range in degree of alteration from mildly argillic and unmineralized (G11-24-1-739', Au = 4 ppb), with unaltered biotite phenocrysts, to intensely quartz-sericite-pyrite altered (G11-12-1-569', Au = 2.76 ppm). Concentrations of the rare earths, Ti and Al, vary little (Table 3-4) as do ratios of Al_2O_3/TiO_2 (~36 for unveined dacites). Therefore, these elements were essentially immobile, and their concentrations define the constant mass line of Fig. 2-10, indicating little net mass gain or loss during mineralization. Concentrations of Au, Ag, As, Sb, Mo, W, Se, and S, however, vary from one to several orders of magnitude. Dacite with more intense QSP alteration is correspondingly more enriched in these elements, suggesting that Au accompanied sericitic alteration. In contrast, large depletions in Ba, Ca, Na, Sr, Mg, and Mn are evident. Even the least altered dacite, found peripheral to mineralized rock, shows large-scale removal of Na, Ca, Sr, and Ba. Phinisey et al. (1996) noted similar net losses of Ba from dike-hosted ores at Jerritt Canyon. Loss of Ba is surprising because barite is common and formed in open spaces of mineralized dacite during the latest stages of mineralization. The concentrations

of Ba in mineralized dacite (G11-12-1-552'; 569') may be low due to analytical procedures. For example, barite may not have been fully dissolved in four-acid digestions because of very low solubility. Manganese concentrations are consistently lower in mineralized dacite, including samples with high Ag contents, suggesting that Mn was removed during stage 2 Ag mineralization (Fig. 2-10).

Although not apparent on Figure 2-10, Fe and Si have been added in variable amounts to mineralized dacite. This is shown by plots of Fe and SiO_2 versus relatively immobile Ti (Figs. 2-11A and B). Fe/Ti ratios of altered and mineralized Eocene dacite of the Griffin and Meikle deposits vary between about 5 and 40, much larger than the analytical uncertainty of these elements. Several veined rocks have Fe/Ti more than four times that of the specimens with the lowest Fe/Ti. Moreover, most samples contain from 2.5 to almost 6 weight percent Fe, values that are higher than the original composition of the dacite estimated at about 2 weight percent from contemporaneous unaltered dacite in the nearby Emigrant Pass volcanic field (Henry and Faulds, 1999). The higher concentrations of Fe in the majority of specimens are strongly suggestive of net addition. The lower concentrations of Fe and Ti in some dacite (Fig. 2-11A) suggest Fe dilution, probably through silica addition.

Contents of Fe and S in sulfide-bearing dacite vary uniformly, with Fe/S (by weight) of about one, suggesting most Fe and S are in pyrite (Fig. 2-11C). Three argillically-altered rocks have moderate to high Fe and very low S contents. In these rocks, part of the Fe is contained in Fe-bearing carbonate, reflecting addition of significant amounts of CO_2 into certain of the dike rocks.

The addition of silica can be demonstrated in a manner similar to that used for Fe. The ratio SiO_2/Ti varies by about 50 percent (Fig. 2-11B), which can only in part be explained by analytical uncertainty. Note particularly that the QSP-altered rocks, as a

group, have higher SiO_2/Ti ratios than do the argillically altered rocks, and that the specimen with quartz veins has the highest SiO_2/Ti ratio. The introduction of Si is also reflected by the low concentrations of Ti in vein-bearing rocks (Fig. 2-11A).

These data suggest that Fe, S, and Si were added in varying amounts to altered and mineralized dacite. Fe addition contradicts some aspects of the sulfidation model invoked for some CTDs, wherein Fe present in Fe sulfides was derived mainly from host rocks (Hofstra, 1994, 1997; Gammons, 1997; Fortuna and Kesler, 1998).

Age of Carlin-Type Deposits in Northern Nevada

Geologic and isotopic data reported in this study suggest that the Griffin and Meikle deposits are of Eocene age (Table 2-3). Ressel et al. (2000) have recently shown that the relatively small Beast deposit (Fig. 2-2), which is in large part hosted by the 37.3 Ma Beast dike, is of late Eocene or younger age. Likewise, the formation of the Deep Star deposit postdated or was contemporaneous with emplacement of the Deep Star rhyolite dike (Altamirano and Thompson, 1999) dated at about 38 Ma (Ressel et al., 1999; 2000). A rhyodacite dike, dated at 40.1 Ma (Farmer, 1996), is altered and locally contains abundant Fe sulfides in the lower reaches of the Genesis open pit. The world-class Betze-Post deposit, which is structurally linked with the Meikle, Griffin, and Rodeo/Goldbug deposits on its eastern side by the Post fault zone (Fig. 2-2), may also be of late Eocene age (Emsbo et al., 1996; Leonardson and Rahn, 1996; Ressel et al., 2000, John Jory, personal communication, 1999).

Studies in other districts containing CTDs in Nevada and Utah also indicate or suggest an Eocene or younger age for Au mineralization. Examples include deposits at Jerritt Canyon ($\leq$ 40.8 Ma; Hofstra, 1994; Phinisey et al., 1996; Hofstra et al., 1999), Getchell (~38 Ma; Arehart et al., 2000), Twin Creeks (42 Ma; Groff et al., 1997; Hall et al., 1997), Tonkin Springs ($\leq$34 Ma; Maher et al., 1993), Mercur ($\leq$33 Ma; Mako, 1997),

and Barneys Canyon/Melco (≤39 Ma; Babcock et al., 1995; Gunter and Austin, 1997). Other sedimentary rock-hosted Au deposits, known as "Carlin-like", pluton-related or distal-disseminated Au-Ag deposits (Seedorff, 1991; Cox, 1992; Mosier et al., 1992), that are similar in many respects to the CTDs listed above but with an Eocene igneous association, include Cove (42-38 Ma; Emmons and Eng, 1995; Johnston, 2000) and Lone Tree (~38 Ma; Bloomstein et al., 1993).

In contrast, Mesozoic ages for CTDs inferred from isotopic ages on sericite lack the consistency of the Eocene ages, having yielded highly variable results, even within individual orebodies or districts (e.g., Kuehn and Rose, 1992; Arehart et al., 1993a; Hofstra, 1994; Drews-Armitage et al., 1996). Mesozoic plutons are spatially associated with some CTDs, including Betze-Post and Getchell. However, the Mesozoic plutons are of differing ages ranging from Jurassic through Cretaceous, and are located near deposits having well-documented Eocene age constraints. Folger et al. (1996; 1998) have demonstrated that sericite in ores at Jerritt Canyon formed in multiple episodes (Paleozoic, Mesozoic, and Cenozoic), were not reset during ore formation, and suffer from ^{39}Ar loss by recoil in very fine-grained samples. Therefore, sericite "ages" determined from Paleozoic sedimentary rocks do not indicate the time of ore formation.

CTDs of Eocene age in the northern Great Basin appear to have formed during a relatively short period from about 42 and 36 Ma, contemporaneous with calc-alkaline magmatism (Fig. 2-12). Henry and Ressel (2000) argue that most or all CTDs in northern Nevada are Eocene and are "pluton-related" inasmuch as they are spatially and temporally related to Eocene plutons. In the case of CTDs, such a causal link between Eocene magmatism and ore deposition allows the possibility that metals were sourced in magmas. Thus, the range in Eocene "pluton-related" deposit types in north-central

Nevada, including Carlin-type, distal disseminated Au-Ag, Au skarn, and Cu-Au porphyry, may reflect the distinct metallogene character of Eocene magmatism.

Conclusions

Eocene dikes intrude the Post fault zone and parallel structures along the Meikle-Rodeo/Goldbug corridor. These dikes are composed of porphyritic dacite dated at 39.21 ± 0.12 Ma and are correlative to dacite dikes of the Betze-Post deposit. Eocene dacite differs mineralogically and chemically from Jurassic finely porphyritic rhyodacite also present in the Post structural zone. Both dike types are extensively altered and locally mineralized in the Meikle, Griffin, and Rodeo deposits.

Samples with as much as 9 ppm Au have been obtained on mineralized Eocene dacite, and higher concentrations probably exist in the Meikle and Griffin deposits. Au is closely associated with QSP alteration and correlates positively with intensity of QSP alteration and sulfide content. Illite from ore-bearing dacite from Griffin and Meikle yield ^{40}Ar/^{39}Ar apparent ages that approximate but are slightly older than the emplacement age of the Betze dacite. Older illite ages probably result from ^{39}Ar loss through recoil on irradiation. Although too old, illite yields Eocene ages that are consistent with the age of magmatic activity. The age of mineralization at Meikle and Griffin is similar to many other CTDs in the Great Basin and strongly suggests a link to magmatic activity.

Three stages of mineralization affect Eocene dacite at the Meikle and Griffin deposits. Au in dacite is mostly associated with early-formed quartz, sericite and Fe sulfides. Late quartz veinlets that cut QSP vein and replacement mineralization contain appreciable quantities of Ag-Sb sulfosalts and native Ag. Contents of Ag in quartz stockwork dacite are as much as 55 ppm. These relations suggest that Au and Ag were in part decoupled and that some Ag was deposited with little or no Au during late stage(s)

of mineralization. Barite and pyrite vug fillings and veinlets comprise the latest stage of dacite-hosted mineralization at Meikle and Griffin.

Although the Eocene dikes were probably less permeable and reactive to ore fluids, Au, Ag, S, As, Sb, Hg, Tl, Fe, and Si and other elements were added by ore fluids. Alteration resulted in the loss of Na, Ca, Ba, Mn and some K. Ti, Al, P, and the REE, were largely immobile.

Acknowledgements

References

Altamirano, C., and Thompson, T.B., 1999, Structural geology and hydrothermal alteration associated with the Deep Star orebody, northern Carlin trend, Nevada, *in* Ralph J. Roberts Center for Research in Economic Geology Annual Research Meeting Program and Reports, January 7-8, 1999, University of Nevada, Reno, 19 p.

Arehart, G.B., 1996, Characteristics and origin of sediment-hosted gold deposits: A review: Ore Geology Reviews, v. 11, p. 383-403.

Arehart, G.B., Foland, K.A., Naeser, C.W., and Kesler, S.E., 1993a, $^{40}Ar/^{39}Ar$, K/Ar, and fission-track geochronology of sediment-hosted disseminated gold deposits at Post/Betze, Carlin Trend, northeastern Nevada: Economic Geology, v. 88, p. 622-646.

Arehart, G.B., Eldridge, C.S., Chryssoulis, S.L., and Kesler, S.E., 1993b, Ion microprobe determination of sulfur isotope variations in iron sulfides from the Post/Betze sediment-hosted disseminated gold deposit, Nevada, USA: Geochimica et Cosmochimica Acta, v. 57, p. 1505-1519.

Arehart, G.B., Tretbar, D., Chakurian, A., 2000, Review of the age of Carlin-type deposits in Nevada and implications for their formation *in* Cluer, K., Price, J., and Morris, C., eds., Geology and Ore Deposits 2000: The Great Basin and Beyond: Geological Society of Nevada, Symposium Proceedings, May 15-18, 2000.

Bakken, B.M., and Einaudi, M.T., 1986, Spatial and temporal relations between wall-rock alteration and gold mineralization, Main pit, Carlin gold mine, Nevada, *in* Macdonald, A.J., ed., Proceedings of Gold '86, an International Symposium on the Geology of Gold: Toronto, p. 388-403.

Babcock, R.C., Jr., Ballantyne, G.H., and Phillips, C.H., 1995, Summary of the geology of the Bingham district, Utah, *in* Pierce, F.W., and Bolm, J.G., eds., Porphyry Copper Deposits of the American Cordillera: Arizona Geological Society Digest, v. 20, p. 316-335.

Bloomstein, E., Braginton, B., Owen, R., Parratt, R., Raabe, K., and Thompson, W., 1993, Geology and geochemistry of the Lone Tree gold deposit, Humboldt County, Nevada: Society for Mining, Metallurgy and Exploration, Inc., Preprint 93-205, 23 p.

Brake, S.S., Ressel, M.W., Connors, K.A., Noble, D.C., and Weiss, S.I., 1998, Auto-alteration of dikes of the Matalla-Santa Rosa center, Peru, the Carlin trend and Bare Mountain, Nevada, by closed-system crystallization of CO_2- and S-bearing magmas: Geological Society of America Abstracts with Programs, v. 30, p. A377.

Chapman, F.W., Marvin, G.G., and Tyreem, S.Y., 1949, Volatilization of elements from perchloric and hydrofluoric acid solutions: Analytical Chemistry, v. 21, p. 700-701.

Christensen, O.D., 1996, Carlin trend geologic overview, *in* Peters, S.G., Williams, C.L., and Volk, J., eds., Field trip guidebook for Trip B – Structural Geology of the Carlin trend, *in* Green, S.M., and Struhsacker, E., eds., Geology and Ore Deposits of the American Cordillera: Geological Society of Nevada, Reno, Nevada, p. 147-156.

Christiansen, R.L., and Yeats, R.S., 1992, Post-Laramide geology of the U. S. Cordilleran region, *in* Burchfiel, B.C., Lipman, P.W., and Zoback, M.L., eds., The Geology of North America, The Cordilleran Region: Geological Society of America Decade in North American Geology Series, v. G-3, p. 261-406.

Cox, D.P., 1992, Descriptive model of distal disseminated Ag-Au, *in* Bliss, J.D., ed., Developments in Mineral Deposit Modeling: U.S. Geological Survey Bulletin 2004, p. 19.

Cox, D.P., and Singer, D.A., 1988, Distribution of gold in porphyry copper deposits: U.S. Geological Survey Open-File Rpt. 88-46, 23 p.

Deino, A., and Potts, R., 1990, Single-crystal ^{40}Ar/^{39}Ar dating of the Olorgesailie Formation, Southern Kenya Rift: Journal of Geophysical Research, v. 95, p. 8453-8470.

Doebrich, J.L., and Theodore, T.G., 1996, Geologic history of the Battle Mountain mining district, Nevada, and regional controls on the distribution of mineral systems, *in* Coyner, A.L., and Fahey, P.L., eds., Geology and ore deposits of the American Cordillera: Geological Society of Nevada Symposium Proceedings, Reno/Sparks, Nevada, April, 1955, v. 1, p. 453-483.

Drews-Armitage, S.P., Romberger, S.B., and Whitney, C.G., 1996, Clay alteration and gold deposition in the Genesis and Blue Star deposits, Eureka County, Nevada: Economic Geology, v. 91, p. 1383-1393.

Emmons, D.L., and Eng, T.L., 1995, Geologic map of the McCoy mining district, Lander County, Nevada: Nevada Bureau of Mines and Geology Map 103 with text, 12 p., 1:24,000-scale.

Emsbo, P., Hofstra, A.H., Park, D., Zimmerman, J.M., and Snee, L.W, 1996, A mid-Tertiary age constraint on alteration and mineralization in igneous dikes on the Goldstrike property, Carlin Trend, Nevada: Geological Society of America Abstracts with Programs, v. 28 (7), p. A476.

Essene, E.J., and Peacor, D.R., 1995, Clay mineral thermometry – a critical perspective: Clays and Clay Minerals, v. 43, p. 540-553.

Evans, J.G., 1980, Geology of the Rodeo Creek northeast and Welches Canyon quadrangles, Eureka County, Nevada: U. S. Geological Survey Bulletin 1473, 81 p.

Farmer, M., 1996, An intrusive study of the Bluestar subdistrict: Newmont Gold Company, unpublished report, 33 p.

Ferdock, G. C., Castor, S.B., Leonardson, R.W., and Collins, T., 1997, Mineralogy and paragenesis of ore stage mineralization in the Betze gold deposit, Goldstrike mine, Eureka County, Nevada, *in* Vikre, P., Thompson, T.B., Bettles, K., Christensen, O., and Parratt, R., eds., Carlin-Type Gold Deposits Field Conference: Society of Economic Geologists, Guidebook Series, v. 28, p. 75-86.

Fleck, R.J., Sutter, J.F., and Elliott, D.H., 1977, Interpretation of discordant ^{40}Ar/^{39}Ar age-spectra of Mesozoic tholeiites from Antarctica: Geochimica et Cosmochimica Acta, v. 41, p. 15-32.

Folger, H.W., Snee, L.W., Mehnert, H.H., Hofstra, A.H., and Dahl, A.R., 1996, Significance of K-Ar and ^{40}Ar/^{39}Ar dates from mica in Carlin-type gold deposits: Evidence from the Jerritt Canyon district, Nevada, *in* Coyner, A.R., and Fahey, P.L., eds., Geology and Ore Deposits of the American Cordillera: Geological Society of Nevada Symposium Proceedings, Reno/Sparks, Nevada, April 1995, p. 41-60.

Folger, H.W., Hofstra, A.H., Eberl, D.D., and Snee, L.W., 1998, Importance of clay characterization to interpretation of ^{40}Ar/^{39}Ar dates on illite from Carlin-type gold deposits: Insights from Jerritt Canyon, Nevada, *in* Tosdal, R.M., ed., Contributions to the Gold Metallogeny of Northern Nevada: U. S. Geological Survey Open-File Report 98-338, p. 193-201.

Fleet, M.E., and Mumin, A.H., 1997, Gold-bearing arsenian pyrite and marcasite and arsenopyrite from Carlin Trend gold deposits and laboratory synthesis: American Mineralogist, v. 82, p. 182-193.

Fortuna, J.H., and Kesler, S.E., 1998, Role of igneous rocks in sulfidation, Twin Creeks Carlin-type gold deposit, Nevada: Geological Society of America Abstracts with Programs, v. 30, no. 7, p. 372.

Gammons, C.H., 1997, Thermochemical sulfate reduction: A key step in the origin of sediment-hosted disseminated gold deposits *in* Vikre, P., Thompson, T.B., Bettles, K., Christensen, O., and Parratt, R., eds., Carlin-Type Gold Deposits Field Conference: Society of Economic Geologists Guidebook Series, v. 28, p. 141-146.

Grant, J.A., 1986, The isocon diagram – A simple solution to Gresen's equation for metasomatic alteration: Economic Geology, v. 81, p. 1976-1982.

Groff, J.A., Heizler, M.T., McIntosh, W.C., and Norman, D.I., 1997, $^{40}Ar/^{39}Ar$ dating and mineral paragenesis for Carlin-type gold deposits along the Getchell Trend, Nevada: Evidence for Cretaceous and Tertiary gold mineralization: Economic Geology, v. 92, p. 601-622.

Gunter, W.L., and Austin, G.W., 1997, Geology of the Melco gold deposit, Oquirrh Mountains, Utah: Society of Economic Geologists Guidebook 29, p. 227-240.

Hall, C.M., Simon, G., and Kesler, S.E., 1997, Age of mineralization at the Twin Creeks SHMG Deposit, Nevada, *in* Vikre, P., Thompson, T.B., Bettles, K., Christensen, O., and Parratt, R., eds., Carlin-type Gold Deposits Field Conference: Society of Economic Geologists Guidebook Series, v. 28, p. 151-154.

Harris, M., and Radtke, A.S., 1976, Statistical study of selected trace elements with reference to geology and genesis of the Carlin gold deposit, Nevada: U.S. Geological Survey Professional Paper 960, 21 p.

Heitt, D.G., 1992, Characterization and genesis of alunite from the Gold Quarry mine, Eureka County, Nevada: Unpublished M.S., thesis, Cheney, Washington, Eastern Washington University, 98 p.

Henry, C.D., and Boden, D.R., 1998, Eocene magmatism: The heat source for Carlin-type gold deposits of northern Nevada: Geology, v. 26, p. 1067-1070.

Henry, C.D., and Faulds, J.E., 1999, Geologic map of the Emigrant Pass Quadrangle, Nevada: Nevada Bureau of Mines and Geology, Open-File Report 99-9, scale: 1:24,000.

Henry, C.D., and Ressel, M.W., 2000, Eocene magmatism of northeastern Nevada: The smoking gun for Carlin-type gold deposits *in* Cluer, K., Price, J., and Morris, C., eds., Geology and Ore Deposits 2000: The Great Basin and Beyond: Geological Society of Nevada, Symposium Proceedings, May 15-18, 2000.

Hitchborn, A.D., Arbones, D.G., Peters, S.G., Connors, K.A., Noble, D.C., Larson, L.T., Beebe, J.S., and McKee, E.H., 1996, Geology and gold deposits of the Bald Mountain mining district, White Pine County, Nevada, *in* Coyner, A. R., and Fahey, P. L., eds., Geology and Ore Deposits of the American Cordillera: Geological Society of Nevada Symposium Proceedings, Reno/Sparks, Nevada, April, 1995, p. 505-546.

Hofstra, A.H., 1994, Geology and genesis of the Carlin-type gold deposits in the Jerritt Canyon district, Nevada: unpublished Ph.D. dissertation, University of Colorado, Boulder, 719 p.

Hofstra, A.H., 1997, Isotopic composition of sulfur in Carlin-type gold deposits: Implications for genetic models *in* Vikre, P., Thompson, T.B., Bettles, K., Christensen, O., and Parratt, R., eds., Carlin-Type Gold Deposits Field Conference: Society of Economic Geologists Guidebook Series, v. 28, p. 119-130.

Hofstra, A.H., Snee, L.W., Rye, R.O., Folger, H.W., Phinisey, J.D., Loranger, R.J., Dahl, A.R., Naeser, C.W., Stein, H.J., and Lewchuk, M., 1999, Age constraints on Jerritt Canyon and other Carlin-type gold deposits in the western United States-Relationship to mid-Tertiary extension and magmatism: Economic Geology, v. 94, p. 769-802.

Ilchik, R.P., 1995, ^{40}Ar/^{39}Ar, K/Ar, and fission-track geochronology of sediment-hosted disseminated gold deposits at Post-Betze, Carlin trend, northeastern Nevada – A discussion: Economic Geology, v. 90, p. 208-210.

Ilchik, R.P., Geology and geochemistry of the Vantage gold deposits, Alligator Ridge-Bald Mountain mining district, Nevada: Economic Geology, v. 85, p. 50-75.

Ilchik, R.P., and Barton, M.D., 1997, An amagmatic origin of Carlin-type gold deposits: Economic Geology, v. 92, p. 269-288.

Johnston, M.K., 2000, Geology of the Cove gold-silver mine, Lander County, Nevada, with emphasis on alteration and ore mineralogies, distributions, relations, and controls *in* Cluer, K., Price, J., and Morris, C., eds., Geology and Ore Deposits 2000: The Great Basin and Beyond: Geological Society of Nevada, Symposium Proceedings, May 15-18, 2000.

Kuehn, C.A., and Rose, A.W., 1992, Geology and geochemistry of wall-rock alteration at the Carlin gold deposit, Nevada: Economic Geology, v. 87, p. 1697-1721.

Lamb, J.B., 1995, A petrographic and fluid inclusion study of the Purple Vein and Post/Betze orebodies, Carlin, Nevada, unpublished M.S. thesis: University of Nevada, Las Vegas.

Lauha, E.A., and Bettles, K.H., 1993, A geologic comparison of the Post/Betze and Purple Vein deposits of the Goldstrike and Meikle mines, Nevada: Society for Mining, Metallurgy, and Exploration, Inc., Preprint 93-170, 20 p.

Leonardson, R.W., and Rahn, J.E., 1996, Geology of the Betze-Post gold deposits, Eureka County, Nevada, *in* Coyner, A.R., and Fahey, P.L., eds., Geology and Ore Deposits of the American Cordillera: Geological Society of Nevada Symposium Proceedings, v. 1, Reno/Sparks, Nevada, April, 1995, p. 61-94.

Maher, B.J., Browne, Q.J., and McKee, E.H., 1993, Constraints on the age of gold mineralization and metallogenesis in the Battle Mountain-Eureka mineral belt, Nevada: Economic Geology, v. 88, p. 469-478.

Mahon, K.I., 1996, The new "York" regression: Application of an improved statistical method to geochemistry: International Geology Review, v. 38, p. 293-303.

Mako, D.A., 1997, Characterization and dating of argillic alteration in the Mercur gold district, Utah – A discussion: Economic Geology, v. 92, p. 633-634.

McIntosh, W.C., and Chamberlin, R.M., 1994, $^{40}Ar/^{39}Ar$ geochronology of middle to late Cenozoic ignimbrites, mafic lavas, and volcaniclastic rocks in the Quemado Region, New Mexico: New Mexico Geological Society Guidebook, v. 45, p. 165-185.

McKee, E.H., 1971, Tertiary igneous chronology of the Great Basin of the western United States: Implications for tectonic models: Geological Society of America Bulletin, v. 82, p. 3497-3502.

Moore, D.M., and Reynolds, R.C., 1997, X-Ray Diffraction and the Identification and Analysis of Clay Minerals, 2nd ed.: New York, Oxford University Press, 378 p.

Mortensen, J.K., Thompson, J.F.H., and Tosdal, R.M., U-Pb geochronology of intrusive rocks in north-central Nevada: Implications for the timing of gold and base-metal deposits in the northern Great Basin *in* Cluer, K., Price, J., and Morris, C., eds., Geology and Ore Deposits 2000: The Great Basin and Beyond: Geological Society of Nevada, Symposium Proceedings, May 15-18, 2000.

Mosier, D.L., Singer, D.A., Bagby, W.C., and Menzie, W.D., 1992, Grade and tonnage model of sediment-hosted Au in Bliss, J.D., Developments in Mineral Deposit Modeling: U.S. Geological Survey Bulletin 2004, p. 26-28.

Noble, D.C., 1972, Some observations on the Cenozoic volcano-tectonic evolution of the Great Basin, western United States: Earth and Planetary Sciences Letters, v. 17, p. 142-150.

Orobona, M.J.T., 1996, Structural setting of the Bluestar subdistrict: Implications for the origin of the Carlin trend, Eureka County, Nevada: unpublished M.S. thesis, Queens University, Kingston, Ontario, Canada, 207 p.

Panhorst, T.L., 1996, Structural control and mineralization at the Lone Tree mine, Humboldt County, Nevada with implications on sampling protocol: unpublished Ph.D. dissertation, University of Nevada, Reno, 263 p.

Phinisey, J.D., Hofstra, A.H., Snee, L.W., Roberts, T.T., Dahl, A.R., and Loranger, R.J., 1996, Evidence for multiple episodes of igneous and hydrothermal activity and constraints on the timing of gold mineralization, Jerritt Canyon district, Elko County, Nevada, in Coyner, A.R., and Fahey, P.L., eds., Geology and Ore Deposits of the American Cordillera: Geological Society of Nevada Symposium Proceedings, Reno/Sparks, Nevada, April, 1995, p. 15-39.

Radtke, A.S., Rye, R.O., and Dickson, F.W., 1980, Geology and stable isotopes of the Carlin gold deposit, Nevada: Economic Geology, v. 75, p. 641-672.

Ressel, M.W., Noble, D.C., and Connors, K.A., 1998, Eocene dikes of the Carlin Trend, Nevada: Magmatic As, Sb, Cs, Tl, CO_2 & excess argon suggest a deep degassing model for gold mineralization: Geological Society of America Abstracts with Programs, v. 30, p. A118.

Ressel, M.W., Noble, D.C., Henry, C.D., and Trudel, W.S., 1999, Eocene magmatism and coeval episodic gold mineralization in the northern part of the Carlin trend, Nevada: Geological Society of America Abstracts with Programs, v. 31, no. 6, p. A-88.

Ressel, M.W., Noble, D.C., Henry, C.D., and Trudel, W.S., 2000, Dike-hosted ores of the Beast deposit and the importance of Eocene magmatism in gold mineralization of the Carlin trend, Nevada: Economic Geology, v. 95, p.1417-1444.

Roberts, R.J., 1960, Alignment of mining districts in north-central Nevada: U.S. Geological Survey Professional Paper 400-B, p. B17-B19.

Rota, J.C., and Hausen, D.M., 1991, Geology of the Gold Quarry mine: Ore Geology Reviews, v. 6, p. 83-105.

Seedorff, E., 1991, Magmatism, extension, and ore deposits of Eocene to Holocene age in the Great Basin – mutual effects and preliminary proposed genetic relationships, *in* Raines, G.L., Lisle, R.E., Schafer, R.W., and Wilkinson, W.H., eds., Geology and Ore Deposits of the Great Basin: Geologic Society of Nevada Symposium Proceedings, p. 133-178.

Samson, S.D., and, Alexander, E.C., Jr., 1987, Calibration of the interlaboratory $^{40}Ar/^{39}Ar$ dating standard, Mmhb-1: Chemical Geology, v. 66, p. 27-34.

Saucier, A.E., 1997, The Antler thrust system in northern Nevada, *in* Perry, A. J., and Abbott, E. W., eds., The Roberts Mountains thrust, Elko and Eureka Counties, Nevada: Nevada Petroleum Society Field Trip Guidebook, p. 1-16.

Sillitoe, R.H., and Bonham, H.F., Jr., 1990, Sediment-hosted gold deposits: Distal products of magmatic-hydrothermal systems: Geology, v. 18, p. 157-161.

Silberman, M.L., Berger, B.R., and Koski, R.A., 1974, K-Ar age relations of granodiorite emplacement and W and Au mineralization near the Getchell mine, Humboldt County, Nevada: Economic Geology, v. 69, p. 646-656.

Simon, G., Kesler, S.E., and Chryssoulis, S., 1999, Geochemistry and textures of gold-bearing arsenian pyrite, Twin Creeks, Nevada: Implications for deposition of gold in Carlin-type deposits: Economic Geology, v. 94, p. 405-422.

Snee, L.W., Sutter, J.F., and Kelly, W.C., 1988, Thermochronology of economic mineral deposits – dating the stages of mineralization at Panasqueira, Portugal by high-precision $^{40}Ar/^{39}Ar$ age spectrum techniques on muscovite: Economic Geology, v. 83, p. 335-354.

Steiger, R.H., and Jäger, E., 1977, Subcommission on geochronology: Convention on the use of decay constants in geo- and cosmochronology: Earth and Planetary Science Letters, v. 36, p. 359-362.

Teal, L., and Jackson, M., 1997, Geologic overview of the Carlin trend gold deposits and descriptions of recent deep discoveries: SEG Newsletter, no. 31, p. 1, 13-25, also *in* Vikre, P., Thompson, T.B., Bettles, K., Christensen, O., and Parratt, R., eds., Carlin-Type Gold Deposits Field Conference: Society of Economic Geologists Guidebook Series, v. 28, p. 3-38.

Volk, J.A., Lauha, E., Leonardson, R.W., and Rahn, J.E., 1996, Structural geology of the Betze-Post and Meikle deposits, Elko and Eureka Counties, Nevada *in* Green, S.M., and Struhsacker, E., eds., Road log for Trip B; Structural Geology of the Carlin Trend; Geology and Ore Deposits of the American Cordillera field trip guidebook compendium: Geological Society of Nevada, p. 180-194.

York, D., 1969, Least squares fitting of a straight line with correlated errors: Earth and Planetary Sciences Letters, v. 5, p. 320-324.
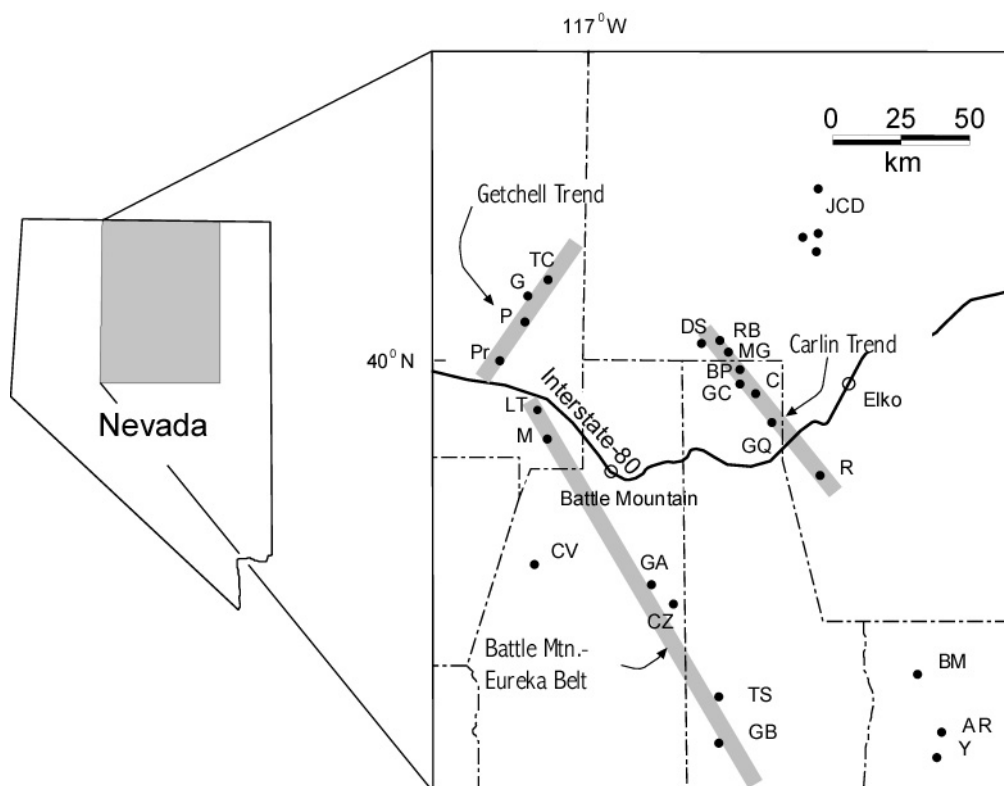
Fig. 2-1. Map of north-central Nevada showing selected Carlin-type deposits. Prominent mineral belts are shown with stippled pattern. Abbreviations: AR-Alligator Ridge; BP-Betze-Post; C-Carlin; CZ-Cortez; DS-Dee-Storm; G-Getchell-Turquoise Ridge; GA-Gold Acres-Pipeline; GB-Gold Bar; GC-Genesis-Beast-Deep Star; GQ-Gold Quarry; JCD-Jerritt Canyon deposits; MG-Meikle-Griffin-Rodeo; P-Pinson; Pr-Preble; R-Rain; RB-Ren-Banshee; TC-Twin Creeks; TS-Tonkin Springs; Y-Yankee. Also shown are the Bald Mountain (BM), Lone Tree (LT), Marigold (M), and Cove (CV) pluton-related disseminated Au-Ag deposits.
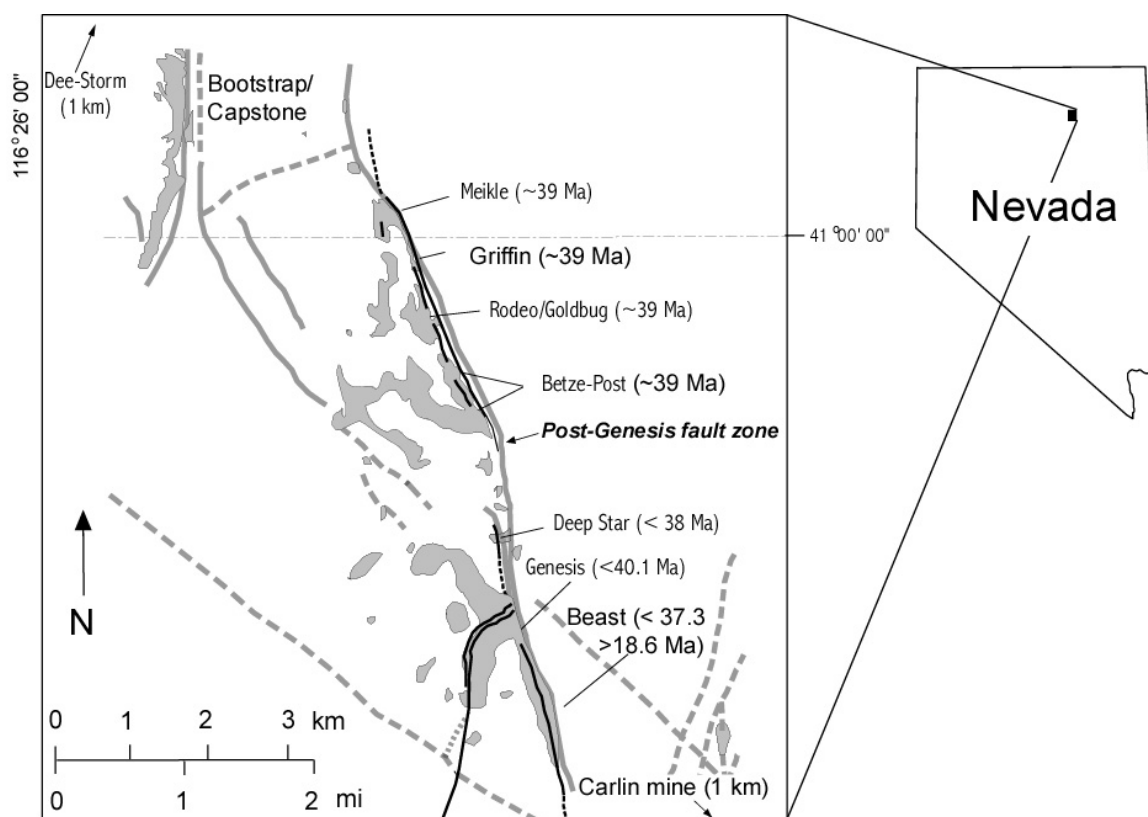
Fig. 2-2. Map of the northern part of the Carlin trend, Nevada, showing CTDs projected to the surface. Faults are shown by stippled lines and prominent Eocene dikes are shown with black lines. Eocene isotopic age constraints are indicated for many deposits. Map modified from Teal and Jackson (1997).
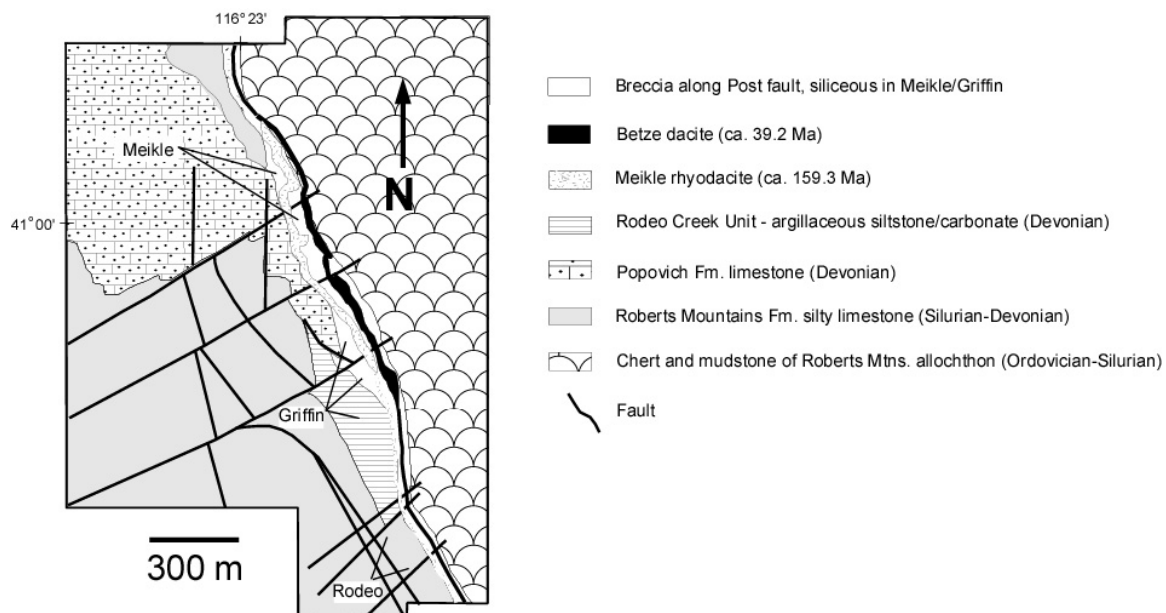
Fig. 2-3. Generalized geologic map of the 4150-ft. level, Meikle-Rodeo/Goldbug corridor.
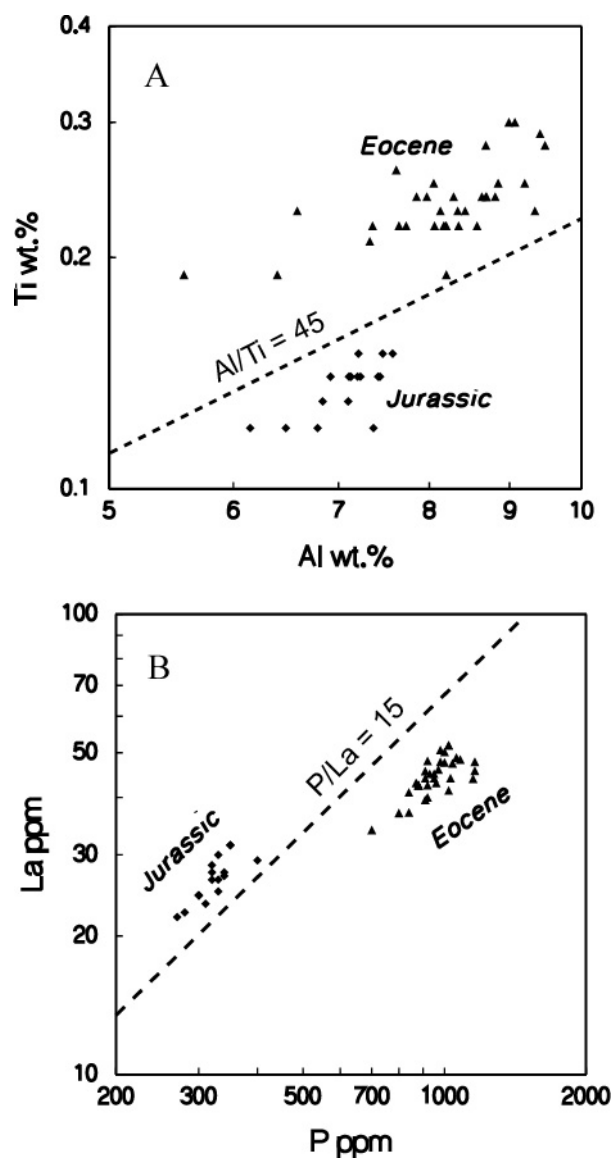
Fig. 2-4. Variation diagrams showing compositional differences between Jurassic Meikle
rhyodacite (solid diamonds) and Eocene Betze dacite (solid triangles). A. Plot of Ti
versus Al and B. La versus P. Data in part from S. Yesilyurt, unpublished Barrick
internal report, 1999).
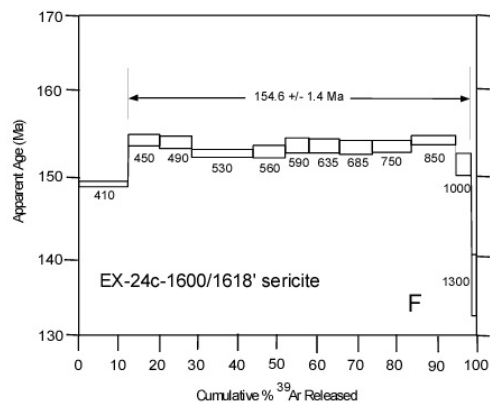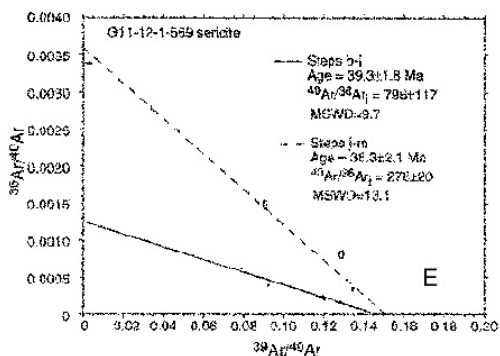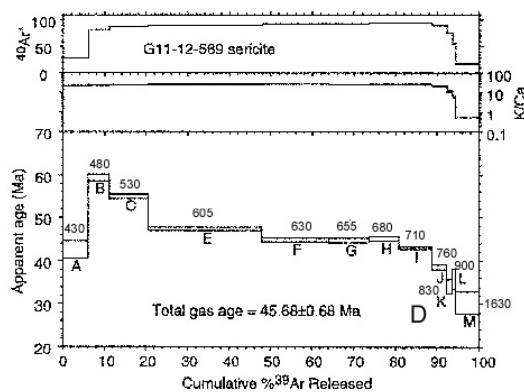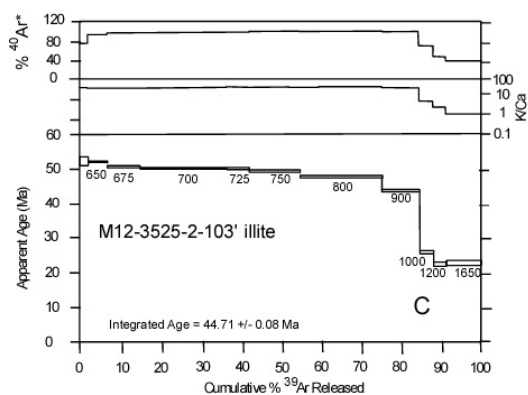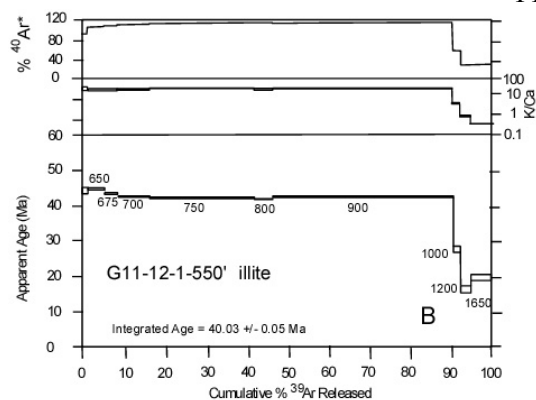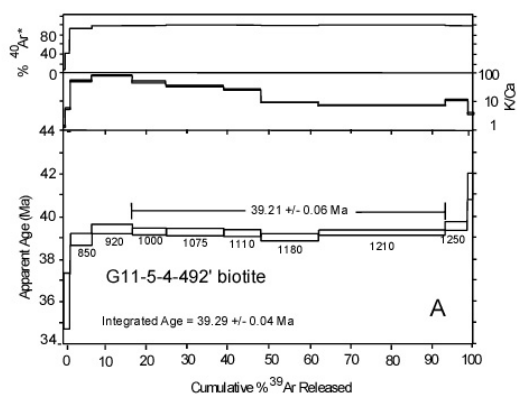
Fig. 2-5. ^{40}Ar/^{39}Ar step-heating spectra (A) through (D); (F) and isochron plot (E) for: A. phenocrystic biotite from Betze dacite of the Griffin deposit (sample G11-5-4-492'); B. illite-quartz from mineralized Betze dacite of Griffin corehole G11-12-1-550'; C. illite-quartz from mineralized Betze dacite of Meikle corehole M12-3525-2-103'; D and E. illite-quartz from mineralized Betze dacite of Griffin corehole G11-12-1-569'; F. sericite from mineralized Meikle rhyodacite of Meikle corehole EX-24c-1600/1618'.

A

SCK

QIK

QSP

2 cm

Distal   Proximal

Relative distance from ore

B

Type 2 veinlet

0.1 mm

C

2 cm

Type 1 veinlets

G11-12-1-562'

D

G11-12-1-552'

Type 2 veinlet

2 cm

E

Type 2 veinlet

1 mm

F

Py

As-py

Asp

100 μm

G

Py

Cpy

Pyarg

100 μm

114
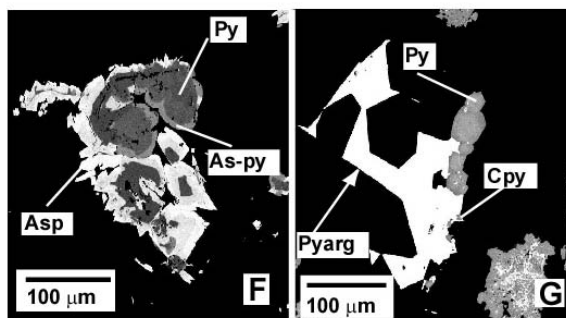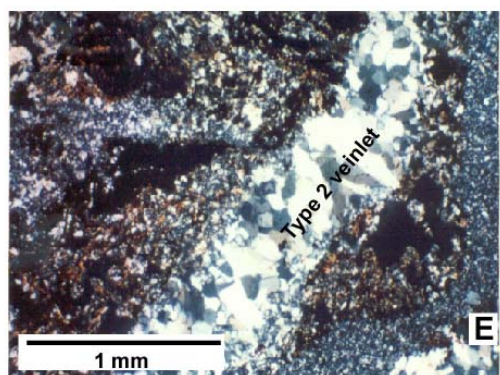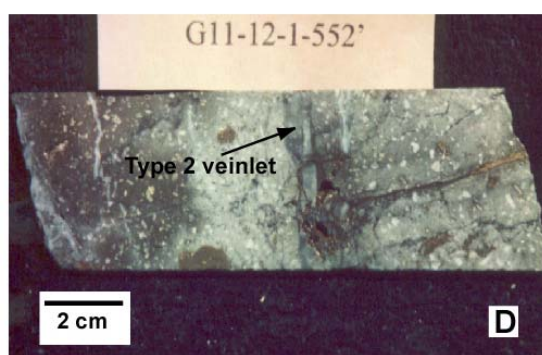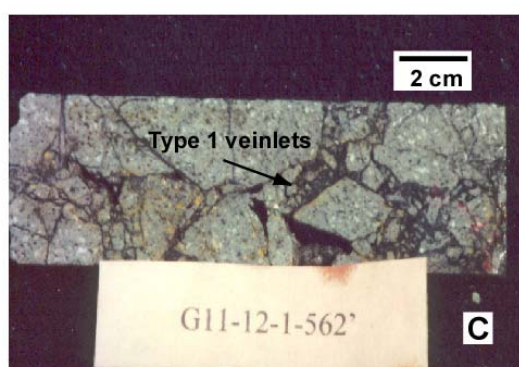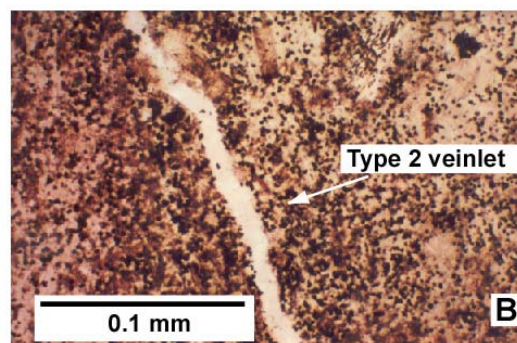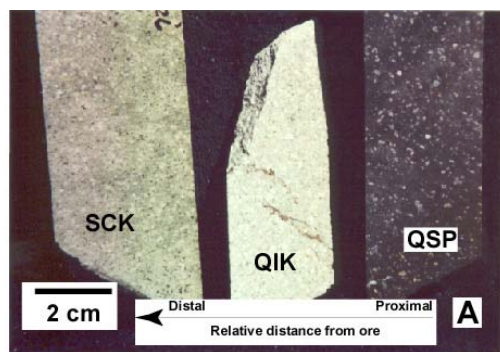
Fig. 2-6. A. Variation in alteration of porphyritic dacite dike from the Meikle-Rodeo/Goldbug corridor. Dacite on the left (SCK) is altered to smectite with lesser amounts of carbonate and kaolinite, and contains fresh biotite phenocrysts. Au content = 4 ppb; center dacite (QIK) is altered to quartz-illite-kaolinite with irregular veinlets of arsenopyrite and brassy pyrite. Au content = 0.3 ppm; dacite on right (QSP) is altered to quartz-illite-pyrite with dark color resulting from very fine-grained pyrite and arsenopyrite that replaced the groundmass. Au content = 8.66 ppm. B. Photomicrograph of QSP-altered porphyritic dacite from the Griffin deposit (corehole G11-12-1-525'). Photomicrograph of quartz-sericite-pyrite replacement of dacite groundmass. Black grains are very fine-grained pyrite with smaller amounts of arsenopyrite, which occur in close association with abundant sericite and quartz (cloudy and clear minerals). Type 2 quartz veinlet cuts QSP altered dacite. Transmitted light, uncrossed polars. C. Sample of Betze dacite crackle breccia from the Griffin deposit (corehole G11-12-1). Clasts are moderately QSP-altered; web-like veinlets (type 1) are composed of fine-grained quartz, Fe sulfide (arsenian pyrite and arsenopyrite), and carbonaceous material. Vugs contain late barite. Gold content of bulk rock is 3.2 ppm. D. Strongly QSP-altered dacite with crosscutting type 2 comb-quartz veinlets. Type 2 veinlets commonly have pyrite-bearing selveges. Cores of type 2 veinlets contain Ag-Sb sulfosalts, including pyrargyrite and miargyrite, and native silver. Gold content of whole-rock = 4.1 to 8.7 ppm; Ag = 7.2 to 8.6 ppm. E. Type 2 comb-quartz veinlets crosscutting dacite clast altered during type 1 QSP alteration (sample G11-12-1-525'). Dark areas are mainly composed of Fe sulfides. Whole-rock analyses yielded as much as 4.4 ppm Au and 55 ppm Ag. Transmitted light, crossed polars. F. Scanning electron microscope-backscattered electron image (SEM-BSE) image of zoned early Fe sulfides from Griffin (corehole G11-5-4-394'). Arsenic

contents of sulfides are indicated by relative brightness. Interior pyrite is arsenic-poor or arsenic-free (Py); light gray rims represent arsenian pyrite (As-py), and white areas are of arsenopyrite (Asp). G. SEM-BSE image of pyrargyrite (Pyarg) in type 2 quartz veinlet from mineralized Betze dacite at Griffin (G11-12-1-536'). Pyrargyrite contains small inclusions of pyrite (Py) and chalcopyrite (Cpy). Pyrite is reverse-zoned, with As-rich cores and As-poor rims. Dark areas are euhedral quartz.

Mineral	Stage 1 (Type 1 veinlets and replacements)	Stage 2 (Type 2 comb quartz veinlets)	Stage 3 (Type 3 veinlets and vug fillings)
Pyrite	———— "sooty"	—	·········· brassy
Arsenian pyrite	————————		—
Arsenopyrite	—————		
White mica	————		
Rutile	————		
Replacement quartz	————————		
Comb quartz	————————————		
Calcite	··························		————
Ag-Sb sulfosalts		————	
Native silver		·············	
Chalcopyrite		··············	
Barite			————

Fig. 2-7. Paragenetic sequence for mineralized Betze dacite from the Griffin, Meikle and Rodeo deposits.

117
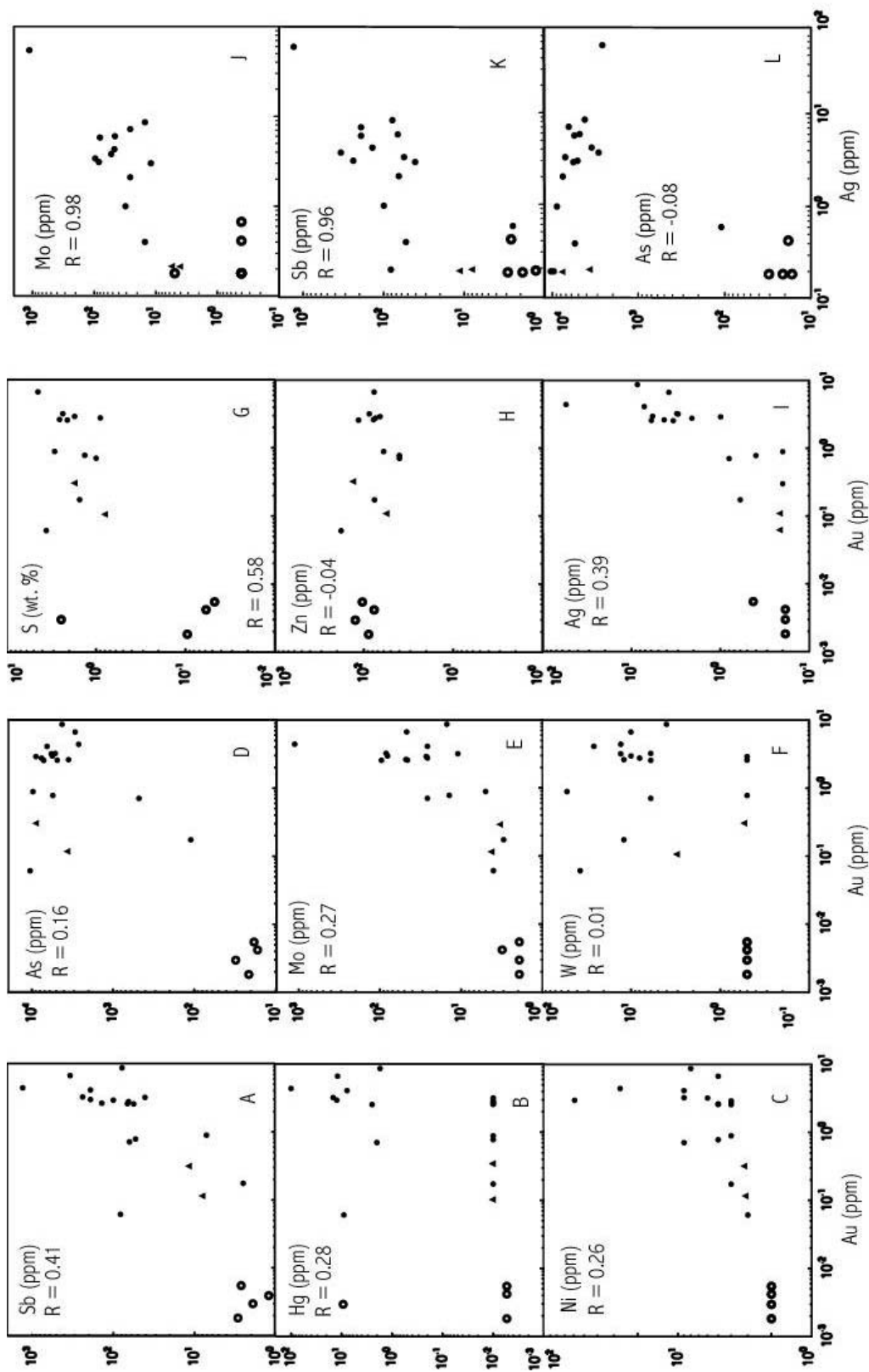
Fig. 2-8. Geochemical variation diagrams for altered and mineralized Eocene dacite from the Meikle, Griffin and Rodeo deposits. Argillically-altered dacite: open circles; mixed illite-kaolinite-altered dacite: solid triangles; quartz-sericite-pyrite-altered dacite: solid circles. Values less than detection limit are plotted at one half the detection limit.
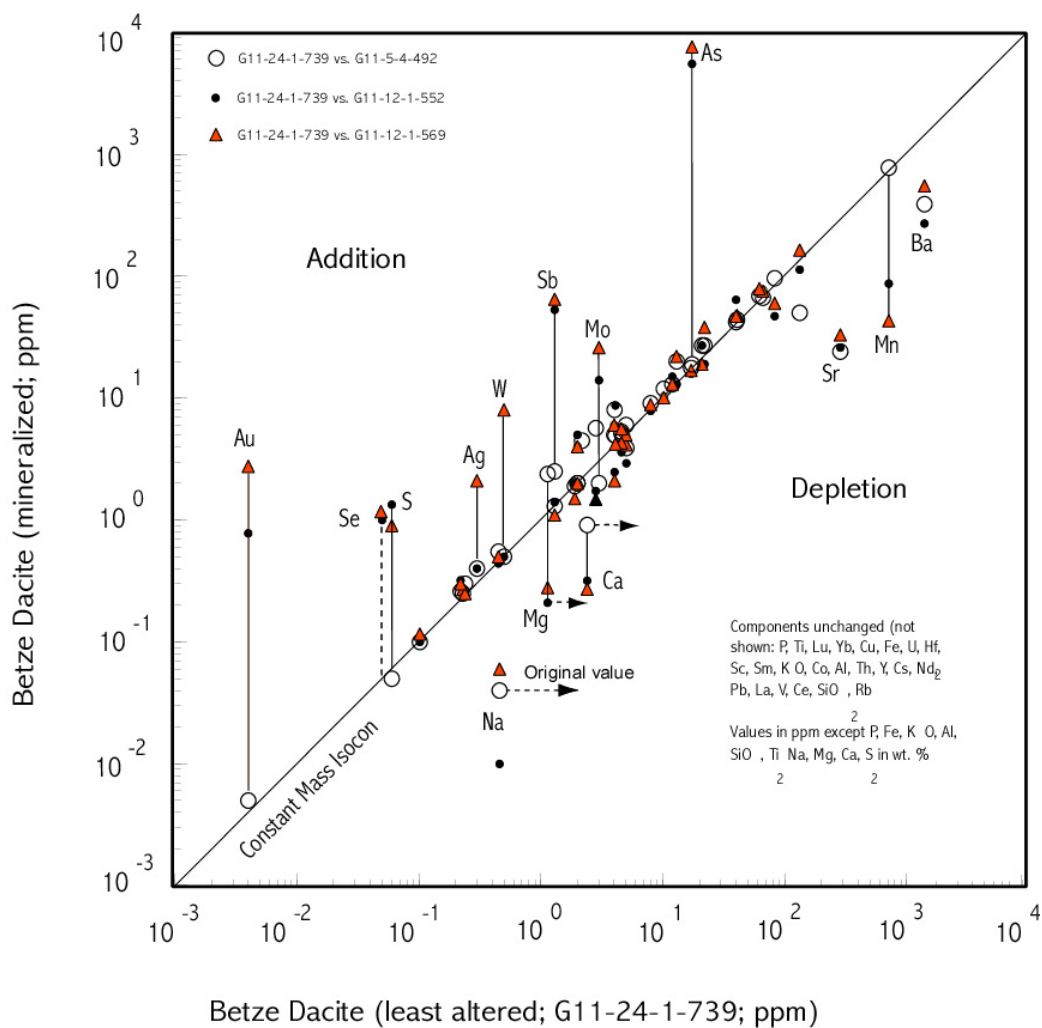
Fig. 2-9. Isocon diagram for mineralized dacite from the Griffin deposit showing relative gains and losses of components. Sample description: G11-24-1-739' and G11-5-4-492' are argillized dacite containing fresh biotite phenocrysts but altered plagiolcase and hornblende; Au content is <5 ppb; G11-12-1-552' is moderately QSP-altered dacite containing 0.8 ppm Au; and G11-12-1-569' is strongly QSP-altered dacite, with 2.8 ppm Au. Data from Table 3-4.
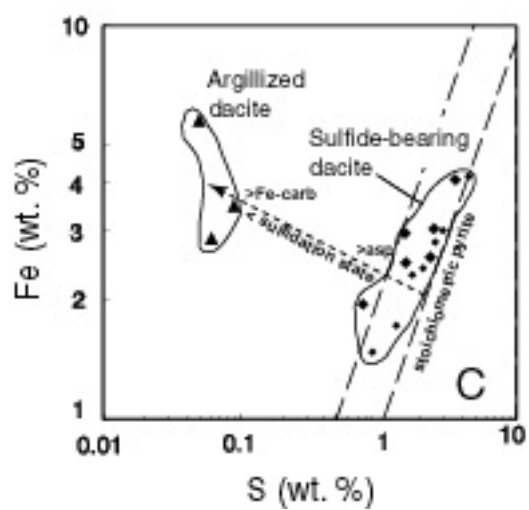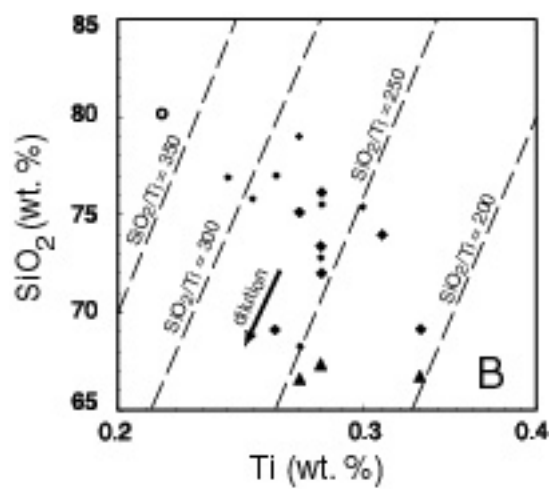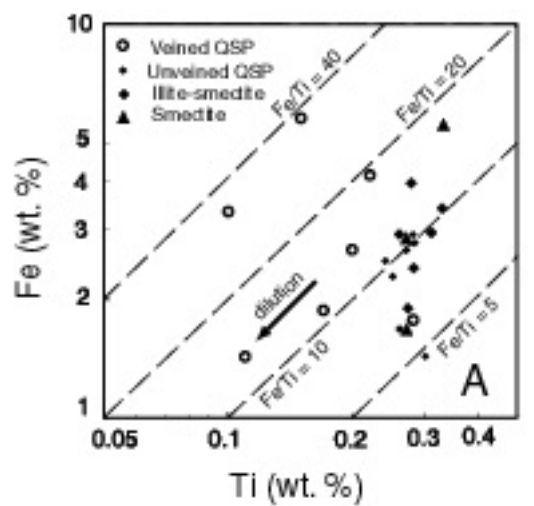
Fig. 2-10. Geochemical variation plots for Eocene dacite from the Griffin and Meikle deposits. A. Plot of Fe versus Ti; B. SiO_2 versus Ti; and C. Fe versus S. Abbreviations: asp = arsenopyrite; Fe-carb = iron-rich carbonated
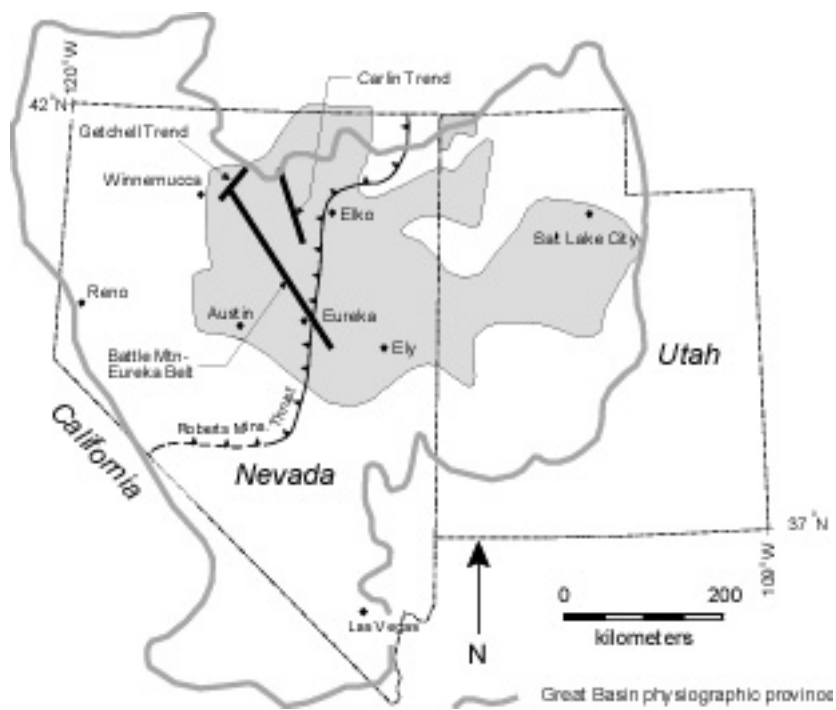
Fig. 2-11. Map of Nevada and Utah. The Eocene igneous belt of the northern Great

Basin is represented by the shaded region.

Table 2-1. Petrographic Characteristics of Felsic Dikes of the Meikle-Rodeo Corridor

Rock Type	Age	Phenocrysts[†]	Phenocryst Size	Phenocryst Abundance
Rhyodacite (Meikle rhyodacite)	Jurassic (~157 Ma)	Plagioclase,biotite, quartz	Feldspar ≤ 1 mm; biotite, quartz ≤ 2 mm	≤ 5-10 %
Porphyritic dacite (Betze dacite or "biotite-feldspar porphyry")	Eocene (39.2 Ma)	Plagioclase, biotite, hornblende, +/- quartz	Feldspar and biotite 2-5 mm; hornblende 2-8 mm	20-25%

[†]in order of abundance

Table 2-2. Average Concentrations of Some Elements in Felsic Dikes of the Meikle-Rodeo Corridor

	Meikle Rhyodacite (Jurassic)	Betze Dacite (Eocene)
Al_2O_3	13.4	16.1
TiO_2	0.22	0.44
P_2O_5	0.08	0.25
La	32	43
Ce	47	77
Sm	2.5	5.5
Y	9	14
Hf	4	5.5
Zr	145	195

Major elements in weight percent oxide; trace elements in parts per million. Major elements and Zr determined by XRF, other trace elements by INAA and/or ICP

Table 2-3. Summary of New Isotopic Ages for Felsic Dikes of the Meikle and Griffin Deposits

Sample	Deposit	N lat.	W long.	Mineral	Age Method		Age Type	Age (Ma)	±2σ
Betze Dacite G11-5-4-492'	Griffin	40°59' 53"	116°22' 38"	Bio	$^{40}Ar/^{39}Ar$ step heating	plateau	Emplacement	39.21	0.12
G11-12-1-550'	Griffin	40°59' 50"	116°22' 35"	Zir	U/Pb	2 concordant fractions	Emplacement	38.1[†]	0.8
"	Griffin	40°59' 50"	116°22' 35"	Ill	$^{40}Ar/^{39}Ar$ step heating	total gas	Alteration	40.03*	0.05
G11-12-1-569'	Griffin	40°59' 50"	116°22' 35"	Ill	$^{40}Ar/^{39}Ar$ step heating	total gas	Alteration	45.68*	0.68
"	Griffin	40°59' 50"	116°22' 35"	Ill	$^{40}Ar/^{39}Ar$ step-heating	isochron	Alteration	39.3	1.8
"	Griffin	40°59' 50"	116°22' 35"	Ill	$^{40}Ar/^{39}Ar$ step-heating	isochron	Alteration	38.3	2.1
M12-3525-2-103'	Meikle	41°00' 12"	116°22' 50"	Ill	$^{40}Ar/^{39}Ar$ step heating	total gas	Alteration	44.71*	0.08
Mekle Rhyodacite EX-24c-1600-1618'	Meikle	41°00' 14"	116°22' 52"	Ser	$^{40}Ar/^{39}Ar$ step heating	plateau	Alteration	154.6	1.4
EX-24c-1600-1618'	Meikle	41°00' 14"	116°22' 52"	Zir	Pb/Pb	weighted	Emplacement	159.3[†]	4.2

Mineral abbreviations: Bio=biotite, Zir=zircon, Ill=illite, Ser=sericite

$^{40}Ar/^{39}Ar$ monitor age = 27.84 Ma, Fish Canyon sanidine (Deino and Potts, 1990)

λ_β = 4.93 x 10^{-10} yr^{-1}; $\lambda\epsilon+\epsilon$' = 0.581 x 10^{-10} yr^{-1}; $^{40}K/K$ = 1.167 x 10^{-4} (Steiger and Jäger, 1977)

*Determined age too old, in large part from ^{39}Ar recoil loss

[†]Data reported in Mortensen et al., 2000

Table 2-4. Chemical Analyses of Altered and Mineralized Eocene Porphyritic Dacite from the Meikle-Rodeo Corridor

Sample	1	2	3	4	5	6	7	8	9	10	11	12	13	14	15	16	17	18	19	20	21	22

Analyses by X-ray fluorescence methods, M.W. Ressel, analyst. All analyses recalculated to 100 percent minus LOI. All values in weight percent.

	1	2	3	4	5	6	7	8	9	10	11	12	13	14	15	16	17	18	19	20	21	22
SiO_2	72.8	73.6	75.4	66.6	69.1	73.9	79.9	77.2	69.1	66.5	72.0	79.3	--	--	77.3	76.1	75.4	--	68.3	75.9	76.3	67.2
TiO_2	0.47	0.47	0.45	0.55	0.55	0.52	0.36	0.40	0.44	0.45	0.46	0.45	--	--	0.44	0.42	0.50	--	0.45	0.46	0.47	0.46
Al_2O_3	16.6	16.8	16.7	17.6	19.2	17.2	10.2	14.6	16.4	17.1	16.7	13.8	--	--	15.8	15.7	16.8	--	16.8	16.8	17.3	17.2
Fe_2O_3	4.66	3.62	2.35	8.01	5.11	4.43	6.15	3.77	4.30	4.03	5.62	3.76	--	--	2.47	3.06	2.10	--	2.39	2.11	3.00	5.31
MnO	0.01	0.01	0.01	0.11	0.13	0.08	0.01	0.01	0.14	0.09	0.01	0.01	--	--	0.01	0.01	0.01	--	0.09	0.01	0.01	0.11
MgO	0.34	0.48	0.40	4.47	2.52	1.36	0.41	0.41	1.53	2.18	0.25	0.14	--	--	0.38	0.10	<0.04	--	0.82	0.24	0.63	1.63
CaO	0.47	0.50	0.48	1.39	2.20	2.08	0.38	0.48	4.01	3.55	0.54	0.45	--	--	0.45	0.49	0.48	--	7.59	0.72	0.48	2.75
Na_2O	0.14	0.09	0.14	0.14	0.16	0.19	<0.01	0.01	0.15	0.79	0.18	0.21	--	--	0.02	0.13	0.34	--	0.14	0.07	0.01	1.33
K_2O	4.27	4.11	3.90	0.80	0.71	0.03	2.45	3.03	3.69	5.03	4.00	1.64	--	--	2.92	3.77	4.14	--	3.19	3.49	1.58	3.68
P_2O_5	0.23	0.28	0.25	0.34	0.32	0.27	0.20	0.15	0.23	0.23	0.26	0.22	--	--	0.24	0.19	0.27	--	0.26	0.24	0.27	0.28
LOI	6.06	5.30	4.31	8.10	8.51	8.95	5.12	5.22	8.16	7.11	6.48	5.93	--	--	4.99	3.97	3.88	--	9.68	4.24	6.77	7.71

Instrumental neutron activation analyses on vein-poor sample portions, Activation Laboratories Ltd. All values in ppm except as indicated.

All samples have Br<0.5 ppm, Ir<5 ppm, and Se <3 ppm.

	1	2	3	4	5	6	7	8	9	10	11	12	13	14	15	16	17	18	19	20	21	22
Na	0.02	0.03	0.03	0.04	0.03	0.01	0.02	0.02	0.05	0.46	0.04	0.02	0.01	--	0.01	0.02	0.06	--	--	--	--	--
Rb	146	158	154	50	22	50	104	101	77	133	69	84	62	--	113	114	164	--	--	--	--	--
Cs	12	15	18	20	17	2	11	10	11	13	18	10	12	--	13	13	22	--	--	--	--	--
Ba	220	440	2200	390	480	90	340	300	1300	1400	600	650	340	--	270	540	550	--	--	--	--	--
Fe%	3.02	2.48	1.96	5.67	3.52	3.05	4.14	2.59	2.98	2.83	4.09	2.82	2.42	--	1.73	2.36	1.48	--	--	--	--	--
Co	5	4	5	5	5	5	4	6	4	4	8	4	5	--	6	4	6	--	--	--	--	--
Sc	4.2	4.3	4.5	5.1	5.4	5.0	3.0	4.1	4.6	4.6	4.7	6.9	5.6	--	3.6	4.2	4.3	--	--	--	--	--
Mo	<1	4	<1	<1	<1	<1	53	12	<1	4	5	47	46	--	15	31	26	--	--	--	--	--
Zn	60	129	52	103	90	120	77	87	76	80	180	78	115	--	<50	66	74	--	--	--	--	--
W	52	<1	3	<1	<1	<1	10	13	12	<1	37	12	<1	--	<1	<1	8	--	--	--	--	--
Au	0.889	0.299	0.107	0.005	0.002	0.003	6.67	3.19	0.174	0.004	0.061	2.62	2.57	--	0.778	2.90	2.76	--	--	--	--	--
Ag	<5	<5	<5	<5	<5	<5	<5	<5	<5	<5	<5	<5	6	--	<5	<5	<5	--	--	--	--	--
As	9690	8170	3420	18.9	21.4	29.2	2920	5740	110	17.4	10500	3530	4850	--	5500	8900	7600	--	--	--	--	--
Sb	7.1	11.4	7.4	2.5	2.7	1.9	340	40.7	2.5	1.3	81.5	138	66.9	--	53.0	99.7	64.8	--	--	--	--	--
Hg	<1	<1	<1	<1	<1	5	12	<1	<1	<1	9	<1	<1	--	<1	<1	<1	--	--	--	--	--
Hf	4	6	5	6	6	6	4	5	6	5	5	5	4	--	5	4	5	--	--	--	--	--
Ta	2.2	1.5	<0.5	2.3	1.7	<0.5	<0.5	1.1	1.5	<0.5	<0.5	<0.5	1.8	--	<0.5	<0.5	1.6	--	--	--	--	--
Th	10.6	10.5	11.6	11.9	11.2	11.1	7.0	9.7	9.5	10.2	10.0	10.4	10.4	--	10.3	9.5	10.1	--	--	--	--	--
U	<0.5	<0.5	4.2	4.6	5.1	<0.5	6.0	4.4	4.1	1.0	19.5	26.7	--	8.7	6.3	4.2	--	--	--	--	--	
La	50.7	48.3	45.7	44.0	47.4	43.9	37.1	45.6	41.4	40.7	48.8	51.9	50.2	--	47.6	47.8	47.8	--	--	--	--	--
Ce	84	77	72	69	73	67	60	78	63	62	75	77	85	--	73	77	79	--	--	--	--	--
Nd	24	44	28	27	27	25	30	28	25	22	31	25	32	--	19	32	38	--	--	--	--	--
Sm	4.4	5.4	5.2	5.3	5.3	5.1	4.2	4.8	4.6	4.6	5.3	5.6	5.5	--	5.2	4.9	5.6	--	--	--	--	--
Eu	1.3	1.5	1.2	1.3	1.3	1.3	0.9	1.1	1.3	1.2	1.4	1.5	1.4	--	1.4	1.4	1.1	--	--	--	--	--
Tb	<0.5	<0.5	0.9	0.6	<0.5	<0.5	<0.5	<0.5	<0.5	<0.5	<0.5	<0.5	0.9	--	<0.5	<0.5	<0.5	--	--	--	--	--
Yb	1.5	2.0	1.7	1.9	2.0	1.8	1.3	1.7	1.7	1.9	2.4	4.3	5.4	--	2.0	1.9	1.5	--	--	--	--	--
Lu	0.21	0.38	0.33	0.26	0.26	0.25	0.24	0.25	0.22	0.22	0.40	0.51	0.69	--	0.32	<0.05	0.30	--	--	--	--	--
Se	<5	<3	<3	<3	<3	<3	<3	<3	<3	<3	<3	<3	<3	--	<3	<3	<3	--	--	--	--	--

Four-acid dissolution followed by inductively-coupled plasma-emission spectrographic analyses on vein-poor sample portions, Activation Laboratories Ltd.

All data in ppm, except as indicated

	1	2	3	4	5	6	7	8	9	10	11	12	13	14	15	16	17	18	19	20	21	22
K%	3.60	3.58	3.58	0.62	0.58	0.06	2.21	2.39	2.75	4.32	3.36	1.26	0.66	--	2.26	3.16	--	--	--	--	--	--
Mg%	0.29	0.32	0.32	2.39	1.49	0.57	0.28	0.23	0.93	1.14	0.16	0.22	0.12	--	0.21	0.27	0.28	--	--	--	--	--
Ca%	0.33	0.35	0.37	0.91	1.48	1.53	0.27	0.32	2.71	2.40	0.38	0.27	0.26	--	0.30	0.35	0.32	--	--	--	--	--
Sr	33	27	34	24	29	43	18	18	143	286	42	17	14	--	26	33	33	--	--	--	--	--
Al%	8.99	9.20	9.34	9.07	9.41	9.48	5.58	7.36	7.73	7.97	8.69	6.59	7.62	--	7.85	8.05	8.85	--	--	--	--	--
Ti%	0.30	0.25	0.23	0.30	0.29	0.28	0.19	0.22	0.22	0.24	0.28	0.23	0.26	--	0.24	0.25	0.25	--	--	--	--	--
Ni	4	3	3	2	2	2	5	6	4	2	3	5	5	--	5	4	4	--	--	--	--	--

Sample	1	2	3	4	5	6	7	8	9	10	11	12	13	14	15	16	17	18	19	20	21	22
V	44	36	40	42	44	41	84	46	36	38	40	152	106	--	64	81	47	--	--	--	--	--
Mn	61	94	103	776	851	627	72	93	1060	714	59	23	33	--	87	88	43	--	--	--	--	--
P%	0.098	0.108	0.116	0.103	0.104	0.115	0.084	0.091	0.102	0.102	0.106	0.102	0.097	--	0.100	0.098	0.116	--	--	--	--	--
Cu	3	2	2	2	2	2	4	6	6	2	2	3	5	--	4	2	2	--	--	--	--	--
Mo	5	3	4	2	2	2	47	11	3	3	4	48	46	--	14	27	26	--	--	--	--	--
Pb	34	28	28	27	16	29	20	26	37	21	36	29	30	--	27	20	19	--	--	--	--	--
Bi	<5	<5	<5	<5	<5	<5	<5	<5	<5	<5	<5	<5	<5	--	<5	<5	<5	--	--	--	--	--
Zn	55	101	65	96	82	117	44	44	78	83	142	68	66	--	47	65	60	--	--	--	--	--
Cd	<0.5	<0.5	<0.5	<0.5	0.9	0.6	<0.5	<0.5	0.6	0.7	1.1	0.6	<0.5	--	<0.5	<0.5	<0.5	--	--	--	--	--
Ag	<0.4	<0.4	<0.4	0.4	<0.4	<0.4	3.8	3	0.6	<0.4	<0.4	4.3	6	--	0.4	1.0	2.1	--	--	--	--	--
Y	13	15	14	13	13	14	13	13	11	12	12	31	61	--	15	13	13	--	--	--	--	--
Be	2	2	2	2	2	<2	2	2	2	2	2	2	<2	--	2	2	2	--	--	--	--	--
S%	2.92	1.62	0.78	0.05	0.09	2.46	4.49	2.36	1.53	0.06	3.62	2.57	2.1	--	1.34	1.74	0.90	--	--	--	--	--

Inductively-coupled plasma spectrographic analyses on vein-rich samples, U.S. Mineral Laboratories (hot HCl digestion, italics) and Acme Laboratories (4-acid "total" digestion, with HF, regular font). All data in ppm unless otherwise indicated.

Sample	1	2	3	4	5	6	7	8	9	10	11	12	13	14	15	16	17	18	19	20	21	22
Na%	--	--	--	--	--	--	--	--	--	--	--	0.01	--	0.01	0.01	0.01	0.04	0.01	--	--	--	--
Mg%	--	--	--	--	--	--	--	--	--	--	--	0.19	--	0.16	0.23	0.21	0.28	0.11	--	--	--	--
Na%	--	--	--	--	--	--	--	--	--	--	--	0.18	--	0.15	0.25	0.24	0.35	0.15	--	--	--	--
Sr	--	--	--	--	--	--	--	--	--	--	--	20	--	17	19	19	29	17	--	--	--	--
Ba	--	--	--	--	--	--	--	--	--	--	--	270	--	174	193	201	387	702	--	--	--	--
Be	--	--	--	--	--	--	--	--	--	--	--	1	--	2	2	3	3	1	--	--	--	--
Ti%	--	--	--	--	--	--	--	--	--	--	--	0.15	--	0.10	0.20	0.17	0.28	0.11	--	--	--	--
Fe%	--	--	--	--	--	--	--	--	--	--	--	5.78	--	3.33	2.68	1.87	1.77	1.43	--	--	--	--
Ni	--	--	--	--	--	--	--	--	--	--	--	27	--	8	9	9	4	59	--	--	--	--
Co	--	--	--	--	--	--	--	--	--	--	--	4	--	<2	3	3	6	4	--	--	--	--
V	--	--	--	--	--	--	--	--	--	--	--	198	--	72	69	73	50	448	--	--	--	--
Sc	--	--	--	--	--	--	--	--	--	--	--	4	--	3	3	3	4	3	--	--	--	--
Mn	--	--	--	--	--	--	--	--	--	--	--	29	--	33	51	49	37	30	--	--	--	--
P%	--	--	--	--	--	--	--	--	--	--	--	0.057	--	0.041	0.073	0.068	0.11	0.049	--	--	--	--
Cu	--	--	--	--	--	--	--	--	--	--	--	31	--	30	9	6	6	17	--	--	--	--
Cu	--	--	--	--	--	--	--	--	--	--	--	*25.9*	--	*28.6*	*7.83*	*4.67*	*3.35*	*16.3*	--	--	--	--
Mo	--	--	--	--	--	--	--	--	--	--	--	987	--	15	23	69	85	72	--	--	--	--
Mo	--	--	--	--	--	--	--	--	--	--	--	*1128*	--	*15.0*	*25.9*	*84.1*	*96.1*	*80.8*	--	--	--	--
Pb	--	--	--	--	--	--	--	--	--	--	--	87	--	22	23	22	29	16	--	--	--	--
Pb	--	--	--	--	--	--	--	--	--	--	--	*74.7*	--	*20.1*	*20.6*	*20.6*	*24.9*	*12.6*	--	--	--	--
Bi	--	--	--	--	--	--	--	--	--	--	--	<5	--	<5	<5	<5	<5	<5	--	--	--	--
Bi	--	--	--	--	--	--	--	--	--	--	--	*<0.25*	--	*<0.25*	*<0.25*	*<0.25*	*<0.25*	*<0.25*	--	--	--	--
Zn	--	--	--	--	--	--	--	--	--	--	--	146	--	47	36	51	102	387	--	--	--	--
Zn	--	--	--	--	--	--	--	--	--	--	--	*202*	--	*49.6*	*38.9*	*54.6*	*102*	*393*	--	--	--	--
Cd	--	--	--	--	--	--	--	--	--	--	--	1.1	--	<0.4	<0.4	<0.4	<0.4	5.8	--	--	--	--
Cd	--	--	--	--	--	--	--	--	--	--	--	*1.46*	--	*<0.1*	*<0.1*	*0.129*	*0.14*	*4.74*	--	--	--	--
W	--	--	--	--	--	--	--	--	--	--	--	13	--	4	26	6	6	10	--	--	--	--
Sn	--	--	--	--	--	--	--	--	--	--	--	2	--	<2	2	<2	4	<2	--	--	--	--
Ag	--	--	--	--	--	--	--	--	--	--	--	54.5	--	8.6	7.2	3.1	3.4	5.8	--	--	--	--
Ag	--	--	--	--	--	--	--	--	--	--	--	*48.0*	--	*8.12*	*6.61*	*2.77*	*3.35*	*4.92*	--	--	--	--
Au	--	--	--	--	--	--	--	--	--	--	--	4	--	8	<4	<4	<4	<4	--	--	--	--
Au	--	--	--	--	--	--	--	--	--	--	--	*4.40*	--	*8.66*	*4.11*	*3.23*	*2.55*	*2.96*	--	--	--	--
As	--	--	--	--	--	--	--	--	--	--	--	205	--	240	484	427	638	442	--	--	--	--
As	--	--	--	--	--	--	--	--	--	--	--	*2646*	--	*4236*	*6494*	*5142*	*7129*	*5585*	--	--	--	--
Sb	--	--	--	--	--	--	--	--	--	--	--	1306	--	78	191	239	56	191	--	--	--	--
Sb	--	--	--	--	--	--	--	--	--	--	--	*1195*	--	*63.1*	*174*	*224*	*53.0*	*161*	--	--	--	--
Hg	--	--	--	--	--	--	--	--	--	--	--	*100*	--	*1.73*	*7.79*	*14.7*	*2.49*	*12.4*	--	--	--	--
Tl	--	--	--	--	--	--	--	--	--	--	--	*70.6*	--	*2.01*	*15.6*	*16.0*	*6.34*	*12.6*	--	--	--	--
Th	--	--	--	--	--	--	--	--	--	--	--	6	--	4	6	7	9	3	--	--	--	--
Nb	--	--	--	--	--	--	--	--	--	--	--	7	--	7	11	10	14	5	--	--	--	--

Sample	1	2	3	4	5	6	7	8	9	10	11	12	13	14	15	16	17	18	19	20	21	22
Zr	--	--	--	--	--	--	--	--	--	--	--	74	--	54	75	88	66	43	--	--	--	--
La	--	--	--	--	--	--	--	--	--	--	--	24	--	18	31	28	40	16	--	--	--	--
Y	--	--	--	--	--	--	--	--	--	--	--	17	--	7	11	10	13	11	--	--	--	--
Se	--	--	--	--	--	--	--	--	--	--	--	68.9	--	11.4	4.22	6.2	4.61	9.12	--	--	--	--
Te	--	--	--	--	--	--	--	--	--	--	--	5.37	--	<0.5	<0.5	0.555	<0.5	0.711	--	--	--	--

Sample Descriptions:

1 Specimen G11-5-4-394, Griffin deposit. Eocene Betze dacite, strongly QSP-altered, unveined, containing sooty sulfide minerals and no carbonate phases.
2 Specimen G11-5-4-403, Griffin deposit. Betze dacite, moderately QSP-altered, unveined, containing substantial amounts of clay and very minor amounts of carbonate.
3 Specimen G11-5-4-4-405, Griffin deposit. Betze dacite, weakly QSP-altered, unveined, containing moderate amounts of clay. and very minor amounts of carbonate
4 Specimen G11-5-4-492, Griffin deposit. Betze dacite, moderately argillically (smectite) altered with very abundant carbonate, containing phenocrysts of relict biotite with an Ar-Ar age of 39.2±0.1 Ma.
5 Specimen G11-5-4-503, Griffin deposit. Betze dacite argillically and sericitically altered with abundant carbonate and containing grains of bronze pyrite.
6 Specimen G11-5-4-520, Griffin deposit. Betze dacite; strong argillically altered and containing disseminated grains of euhedral pyrite and very abundant carbonate.
7 Specimen M12-3525-2-103, Meikle mine. Betze dacite, moderately veined and QSP-altered with no carbonate. $^{40}Ar/^{39}Ar$ total gas sericite age: 44.7 Ma.
8 Specimen M15-0022-3-54, Meikle mine. Betze dacite, medium gray, unveined and moderately to strongly QSP altered with a moderate amount of carbonate.
9 Specimen R11-152M-4-361. Rodeo mine. Betze dacite, unveined and weakly QSP-altered with abundant carbonate and minor amounts of pyrite(?).
10 Specimen G11-0024-1-739. Griffin deposit. Betze dacite, weakly argillically (smectite) altered with very abundant carbonate and containing phenocrysts of fresh (relict) biotite.
11 Specimen M5-3750-12-600, Meikle mine. Betze dacite, unveined and moderately QSP-altered with a very minor amount of carbonate.
12 Specimen G11-12-1-525, Griffin deposit. Betze dacite, moderately veined, medium gray, and strongly QSP-altered, containing sooty sulfide minerals and a moderate amount of carbonate.
13 Specimen G11-12-1-527VNS. Griffin deposit. Betze dacite, veined, strong QSP-altered, containing sooty sulfide minerals and no carbonate.
14 Specimen G11-12-1-550, Griffin deposit. Betze dacite, strongly QSP-altered with very minor carbonate and a few stage 2 quartz veinlets. Total gas Ar-Ar sericite age: 40.0 Ma; zircon age: 38.1±0.8 Ma.
15 Specimen G11-12-1-552, Griffin deposit. Betze dacite, unveined, medium gray, strongly QSP-altered, containing sooty sulfide minerals and a minor amount of carbonate..
16 Specimen G11-12-1-561, Griffin deposit. Betze dacite, dacite clasts from QSP-altered crackle breccia containing minor amounts of carbonate. Veins are composed of black mixture of quartz and pyrite.
17 Specimen G11-12-1-569, Griffin deposit. Betze dacite, intensely QSP-altered with small amounts of disseminated pyrite and very minor amounts of carbonate. $^{40}Ar/^{39}Ar$ total gas sericite age: 45.7 Ma.
18 Specimen G11-12-1-570, Griffin deposit. Betze dacite breccia, strong QSP-altered with no carbonate and abundant stage 2 quartz veinlets.
19 Specimen M13-20-2-385, Meikle mine. Betze dacite, oxidized, argillically altered, with clear porphyritic texture containing some relict biotite phenocrysts, rare calcite-filled fractures.
20 Specimen M12-3575-2-130, Meikle mine. Betze dacite, slightly argillically altered and moderately silicified, containing sparse disseminated pyrite, very abundant disseminated and veinlet carbonate.
21 Specimen G11-14-3-514, Griffin deposit. Betze dacite, unveined, slightly QSP-altered with no carbonate.
22 Specimen R11-152M-4-378, Rodeo mine. Betze dacite, slightly argillically-altered (smectite) with very abundant carbonate, containing fresh biotite phenocrysts.

Appendix2-1: Analytical Methods

Isotopic Dating

$^{40}Ar/^{39}Ar$ analyses were done on biotite phenocrysts and sericite. Biotite was concentrated to >99 percent purity using magnetic and density separation and hand picking. Fine-grained white mica from Meikle and Griffin was intergrown with at least 5-10% quartz and very small amounts of pyrite (<1%). Samples except for EX-24c-1600/1618' were irradiated at the Ford reactor at the University of Michigan for 24 hours and analyzed at the New Mexico Geochronology Research Laboratory using procedures described in McIntosh and Chamberlin (1994). Sericite sample EX-24c-1600/1618' was irradiated at the U.S. Geological Survey Triga reactor in Denver, and the age determination was made in the Geochronology Laboratory of the U.S. Geological Survey in Menlo Park. Neutron flux of all samples was monitored using interlaboratory standard Fish Canyon Tuff sanidine FC-1 with an assigned age of 27.84 Ma (Deino and Potts, 1990), relative to Mmhb-1 at 520.4 Ma (Samson and Alexander, 1987). Biotite and sericite were heated incrementally in a low-blank resistance furnace. The plateau age of biotite was calculated using the definition of Fleck et al. (1977). Isochron age, $^{40}Ar/^{36}Ar_i$, and MSWD values were calculated from regression results obtained by the methods of York (1969). The MSWD for three illite-quartz samples was outside the 95% confidence level (cf. Mahon, 1996); therefore the error was determined by multiplying by the square root of the MSWD. Decay constants and isotopic abundances are those reported by Steiger and Jäger (1977).

Geochemistry

Twenty-two samples of pervasively altered and mostly unveined dacite were analyzed for major elements by X-ray fluorescence analysis (XRF) on fused disks. Most

samples were also analyzed for trace elements by inductively coupled plasma-emission spectrometry (ICP) following hot, four-acid ($HCl-HNO_3-HF-HClO_4$) dissolutions and by instrumental neutron activation (INA) (Table 3-4). In addition, solutions from six vein-rich splits were analyzed by ICP following a combination of hot, four-acid and aqua regia dissolutions. Concentrations of ore elements determined by the two different extractions agree closely suggesting that the partial digestion liberated all of the elements of interest. An exception is As, of which there were much lower concentrations ($\geq 40\%$) in samples that underwent 4-acid digestion (Table 3-4) than aqua regia dissolution. The demonstration that As and similar elements such as Sb and Se, can be lost during $HClO_4$ dissolution was shown by Chapman et al. (1949).

Chapter 3

Igneous Geology of the Carlin Trend, Nevada: Evolution of the Eocene Plutonic Complex and Significance for Carlin-type Gold Deposits

Michael W. Ressel*, Mike.Ressel@Newmont.com, Department of Geological Sciences,

University of Nevada, Reno, Nevada 89557-0088

Christopher D. Henry, chenry@unr.edu, Nevada Bureau of Mines and Geology,

University of Nevada, Reno, Nevada 89557-0088

Abstract

The Carlin trend contains the largest concentration of Carlin-type Au deposits in the world. Two major controversies about these giant Au deposits have been their age, which is now firmly established as Eocene, and the source of heat, fluids, and metals, which remains debated. We present data that demonstrate an intense period of Eocene magmatism was the heat source. Geologic studies over the last 40 years have emphasized the stratigraphy and structure of Paleozoic sedimentary rocks, which are the major ore hosts. However, four igneous episodes affected the Carlin trend, in the Jurassic, Cretaceous, Eocene, and Miocene. A Jurassic laccolith – dike complex was emplaced about 158 Ma in the northern Carlin trend. A Cretaceous pluton intruded the north-central part of the trend at 112 Ma. Abundant Eocene dikes intruded along most of the trend and were accompanied by lavas in a large volcanic field along the southwest edge of the trend between ~40 and 36 Ma. Miocene rhyolite lavas erupted just west of and across the southern part of the trend at ~15 Ma.

In addition to age, the different igneous suites of the Carlin trend are distinguished by composition, volume, distribution, and, most importantly, relation to gold mineralization. Jurassic rocks range from lamprophyre dikes through a diorite-granodiorite laccolith to rhyolite dikes. They are generally altered and locally host ore. Cretaceous and Miocene rocks are granite and rhyolite, respectively. Minor Cu mineralization accompanied Cretaceous intrusion. Miocene rocks are least altered, largely because they postdate Carlin-type mineralization.

Exposed Eocene rocks are dikes, lavas, and epizonal intrusions, predominantly silicic to intermediate, but ranging from rhyolite to basaltic andesite. Eocene dikes are present in most deposits, are generally altered, but, with a few exceptions, were poor ore hosts. The significance of the Eocene rocks is that they demonstrate that a major Eocene

plutonic complex underlies the Carlin trend. Distinct Eocene igneous suites, which are restricted to specific areas of the trend, are from north to south: (1) 40.3-39.0 Ma rhyolite to dacite dikes in the northern Carlin trend, centered approximately on the Betze-Post deposit and the richest part of the trend, (2) 37.6 Ma porphyritic rhyolite dikes including those that host ore at the Beast deposit, (3) 38.6 Ma intermediate to silicic intrusions of Welches Canyon, (4) 38.1-37.4 Ma andesite to dacite lavas and shallow intrusions of the Emigrant Pass volcanic field, (5) 36.2 Ma rhyolite dikes in the Emigrant Pass field that are indistinguishable from the 37.6 Ma suite except for age and location, and (6) ~37.5 Ma rhyolite to dacite intrusions and lavas of the southern Carlin trend (Rain subdistrict). Additionally, a few basaltic andesite dikes were emplaced at 37.8 Ma near Dee in the northernmost part of the trend and at 38.2 Ma near Rain.

The petrography, distribution, and age of these Eocene suites require that each be underlain by a major, silicic pluton, which is substantiated by aeromagnetic data. The longer duration suites require either multiple plutons or long-lived magma chambers. All Eocene dikes cannot have come from any single magma chamber, e.g., from a chamber beneath the Welches Canyon intrusions as proposed by some. This interpretation would require that (1) individual age and petrographic suites only be emplaced some 12 to 15 km north of the northern edge of the source pluton, (2) they not be emplaced above it or symmetrically around it, and (3) they be distinct in age from the proposed source pluton. These possibilities are physically unrealistic.

The combined data for the Eocene igneous rocks require a plutonic complex about 50 km long north-south, essentially coincident with the northern and central Carlin trend, and between 12 and 23 km across, or underlying an area of ~1000 km^2. This complex was emplaced over a 4 Ma span that coincided with the time of formation of the Carlin-type deposits of the Carlin trend. Although many factors probably had to converge to

generate these deposits and the Carlin trend, magmatic heat was abundant in the right place and at the right time to generate the deposits. The Carlin trend is probably the largest concentration of Carlin-type deposits because the Eocene igneous episode there was the largest and longest of the Great Basin.

Introduction

The 60-km long Carlin trend is the most important of several major gold producing areas of north-central Nevada and by far the greatest concentration of Carlin-type gold deposits (CTDs) in the world. Gold production, reserves, and resources from about 40 sedimentary rock-hosted or CTDs of the Carlin trend are estimated to exceed 3,100 t, or more than 60 percent of past production and reserves from all CTDs in the Great Basin, USA (Teal and Jackson, 1997; Hofstra and Cline, 2000). The deposits of the trend are hosted mainly in Paleozoic sedimentary rocks, particularly Devonian and Silurian carbonate rocks. Other host rocks include calc-silicate hornfels derived from Devonian and Silurian carbonate rocks; Silurian and Ordovician chert and argillite; and Jurassic and Eocene intrusive rocks. Eocene dikes are the youngest ore-bearing rocks of the trend (Ressel et al., 2000a, b).

The Carlin trend and CTDs have been intensely studied for about 40 years (Hausen and Kerr, 1968; Radtke et al., 1980; Bakken, 1990; Kuehn and Rose, 1992; Hofstra, 1994; Arehart et al., 1993). Two major controversies have surrounded the origin of CTDs. The first was the age of formation, which was variously interpreted as Mesozoic (~117 Ma; Arehart et al., 1993), Eocene (~40 Ma; McKee et al., 1995; Thorman et al., 1995; Emsbo et al., 1996; Henry and Boden, 1998; Henry and Ressel, 2000a; Ressel et al., 2000a), or Miocene (~15 Ma; Radtke et al., 1980). Abundant data in the last 10 years unequivocally demonstrate an Eocene age (Emsbo et al., 1996; Leonardson and Rahn, 1996; Phinisey et al., 1996; Groff et al., 1997; Hall et al., 1997, 2000; Hofstra et al.,

1999; Hofstra and Cline, 2000; Johnston, 2000; Ressel et al., 2000a, b; Tretbar et al., 2000; Arehart et al., 2003; Chakurian et al., 2003).

The second controversy, which remains unresolved, is the source of heat, fluids, and metals for the deposits. Models for the generation of CTDs in the Great Basin include (1) an entirely amagmatic origin (Ilchik and Barton, 1997; Seedorff, 1991; Hofstra and Cline, 2000; Seedorff and Barton, 2004) involving deep circulation of meteoric water under high geothermal gradients driven by extension and large-scale (10^2-10^3 km^3) leaching of rocks in the middle and upper crust, (2) mixing of deep, Au-bearing metamorphic fluids with meteoric fluids (Seedorf, 1991; Arehart, 1996; Hofstra and Cline, 2000), possibly along crustal-scale faults, (3) a partly magmatic origin in which Eocene magmatism was the heat source but not necessarily the source of metals (Henry and Boden, 1998; Henry and Ressel, 2000a; Ressel et al., 2000a, b), (4) strictly magmatic origin (Sillitoe and Bonham, 1990; Johnston, 2003; Johnston and Ressel, 2004) for ore components and heat, and (5) leaching of Au from Paleozoic sedimentary exhalative Pb-Zn-Ag-Au deposits in carbonate host rocks (Emsbo et al., 1999; Emsbo et al., 2003).

Stable isotope and other geochemical compositions of hydrothermal fluids indicate the dominance of meteoric fluids in some CTDs and magmatic or deep metamorphic fluids in others (Hofstra and Cline, 2000; Cline et al., 2003)). Hydrogen and oxygen isotope compositions of ore-related kaolinite from the Deep Star deposit of the northern Carlin trend indicate that a gold-bearing, magmatic or deep metamorphic fluid mixed with meteoric water (Heitt et al., 2003). Sulfur isotope compositions of ore-related pyrite in part of the giant Betze-Post (Goldstrike) deposit indicate a probable magmatic source (Kesler et al., 2003).

Some of the controversy about origin arises because early studies focused on the Paleozoic host rocks (Evans and Mullens, 1976; Radtke et al., 1980; Radtke, 1985,

Bakken, 1990; Kuehn and Rose, 1992), and the highly altered and weathered igneous rocks in the upper parts of deposits were difficult to recognize. Although such focus was reasonable, it may have given the impression that igneous rocks were insignificant or even absent. In fact, intrusive rocks, particularly Eocene and Jurassic dikes, are ubiquitous features of deposits of the Carlin trend, and four significant episodes of magmatism have affected the rocks of the trend. These episodes are: (1) Jurassic intrusion of diorite, rhyolite, and lamprophyre, (2) Cretaceous granitic intrusion, (3) Eocene silicic to intermediate intrusion and volcanism, and (4) Miocene rhyolitic volcanism. A fifth, Paleozoic basaltic volcanism, was limited to the allochthon of the Roberts Mountains thrust and is excluded from this discussion because the basalts are not rooted in the Carlin trend and generally distant from ore deposits. Intrusive rocks played important roles in nearly all deposits by localizing ore due to their contrasting physical and hydrologic properties with sedimentary hosts and their association with high-angle faults. The intrusive rocks provide key age constraints on magmatism and mineralization, provide information on the structural history of the district, and yield information on the depths at which the deposits formed.

This paper characterizes and contrasts Jurassic, Cretaceous, Eocene, and Miocene igneous rocks on the basis of their age, emplacement style, extent, volume, mineralogy, descriptive geochemistry, and alteration. Of particular importance are Jurassic and Eocene intrusions, which are spatially associated with all of the more than 40 gold deposits of the Carlin trend (Teal and Jackson, 1997). Dikes of these suites intrude structures that also controlled ore fluids. No Cretaceous or Miocene intrusions are recognized in any deposit. Although we discuss all igneous rocks, we emphasize the Eocene magmatic pulse because of its close spatial and temporal association with gold deposition.

Regional Geologic Setting

The Carlin trend is located in the northern Great Basin, which is part of the Basin and Range province (Fig. 3-1). The trend lies near the Proterozoic rifted margin of the North American craton (DePaolo and Farmer, 1984; Wooden et al., 1998; Tosdal et al., 2000). The plate margin underwent multiple episodes of contraction beginning in the late Devonian-early Mississippian and extending into the early Mesozoic. During the earliest episode, deep-water marine rocks deposited farther west of the plate edge were thrust over autocthonous or parautocthonous shelf- and slope-facies marine rocks along the regional Roberts Mountains thrust (e.g., Roberts, 1964). Subsequent contraction in the Paleozoic produced a series of accretionary wedges that stacked sequentially westward, although thrusting continued far inland as well.

Mesozoic, particularly Cretaceous, granitic rocks are abundant in western Nevada, part of the great chain of Cordilleran batholiths of western North America that are broadly contemporaneous with subduction. Plutons diminish in abundance eastward and crop out only in scattered ranges in northeastern Nevada (Barton, 1996). Additional plutons may underlie Cenozoic cover. The largest Jurassic igneous center in eastern Nevada is in the Cortez Mountains (Fig. 3-1), where both intrusions and associated volcanic rocks are present. Other Jurassic plutons include those of the northern Fish Creek Mountains (Emmons and Eng, 1995), Ruby Mountains (Howard et al., 1979), Buffalo Mountain (Erickson et al., 1978), and the Goldstrike intrusion in the Carlin trend (Arehart et al., 1993). U-Pb and ^{40}Ar/^{39}Ar ages are narrowly focused around 158-159 Ma (Mortensen et al., 2000; Table 3-1). The oldest biotite K-Ar ages, which are presumed to be most reliable given the likelihood of Ar loss, are indistinguishable within their large uncertainties from the U-Pb and ^{40}Ar/^{39}Ar ages. Cretaceous intrusions are less common than Jurassic in northeast Nevada (Fig. 3-1) but have a much wider age range from ~86

Ma to 112 Ma. The largest Cretaceous pluton is in the Osgood Mountains (Groff et al., 1997), and other plutons are present in the Edna Mountains (Erickson et al., 1978), at Battle Mountain (Theodore et al., 1973; Theodore, 2000), and in the Carlin trend (Evans, 1980; Mortensen et al., 2000). Deeply emplaced Cretaceous granites are common in the Ruby Mountains but are not shown on Figure 3-1 because they are sills that are complexly interleaved with Paleozoic rocks (Snoke et al., 1997; Howard, 2000).

Magmatism resumed in the Eocene in the northern Great Basin with widespread eruption of high-K, calc-alkaline volcanic rocks and emplacement of shallow intrusions. This activity was part of much more extensive Eocene magmatism that swept southward from southern British Columbia beginning about 54 Ma and reaching Nevada about 43 Ma (Christiansen and Yeats, 1992; Henry and Ressel, 2000a). Eocene magmatism was contemporaneous with subduction and broadly with the onset of crustal extension.

Eocene igneous rocks are abundant throughout northeastern Nevada (Fig. 3-1; Brooks et al., 1995a, b; Henry and Boden, 1998; Henry and Ressel, 2000a; Castor et al., 2003). Most centers in northeastern Nevada are dominated by andesite to dacite lavas, with lesser rhyolite lava and ash-flow tuff, and subvolcanic intrusions. The largest, most diverse volcanic center is the Tuscarora volcanic field, which was active between 40.1 and 39.5 Ma (Henry and Boden, 1998a; Castor et al., 2003). Other major Eocene intrusive and volcanic areas of northeastern Nevada include the Emigrant Pass volcanic field adjacent to the Carlin trend (Henry and Faulds, 1999), the Robinson volcanic field south of the Carlin trend (Smith and Ketner, 1978), the numerous Au-Cu related porphyries at Battle Mountain (Theodore, 2000), hypabyssal intrusions and related volcanic rocks in the southern Independence Mountains (Ketner, 1998; Henry and Ressel, 2000b), and volcanic and intrusive rocks of the Jerritt Canyon gold district in the Independence Mountains (Phinisey et al., 1996; Hofstra et al., 1999).

Middle Miocene volcanism was focused in the northern Nevada rift (Fig. 3-1), a 500-km long, north-northwest-striking magnetic anomaly that lies west of the Carlin trend. The rift is characterized by numerous rhyolitic and basaltic eruptive centers, most of which were active between 16 and 14 Ma (Zoback et al., 1994; John et al., 2000; Wallace, 2003a). Miocene rocks of the rift host numerous epithermal Au-Ag deposits (John and Wallace, 2000; John, 2001; John et al., 2003; Wallace, 2003b). Miocene rhyolite lavas and tuffaceous sedimentary rocks are widespread in northern Nevada, including within and adjacent to the Carlin trend.

Episodic Cenozoic extension in northeastern Nevada was, in part, contemporaneous with Eocene and Miocene magmatism (John et al., 2000; Henry et al., 2001). Earliest extension probably generated the Elko basin and other Eocene basins at about 46 Ma (Haynes et al., 2002, 2003, Henry et al., 2001) and therefore predates major Eocene magmatism. Near the Carlin trend, the extensional history and geometry are best known in the Emigrant Pass volcanic field (Henry and Faulds, 1999; Henry et al., 2001). Episodes of extension are recognized (1) in the Eocene to generate the Elko basin, (2) following deposition of Elko basin deposits and preceding 38 to 36 Ma volcanism, (3) between 25 and 15 Ma, and (4) at about 15 Ma, contemporaneous with development of the northern Nevada rift (John et al., 2000). The episode between 25 and 15 Ma may correlate with the 23-Ma period of most rapid cooling and inferred uplift of the Ruby Mountains core complex (McGrew and Snee, 1994). Eocene and late Oligocene (25 Ma) volcanic rocks are tilted as much as 30° by numerous N- to NNE-striking normal faults in the Emigrant Pass field (Figs. 3-1 and 3-2). However, these faults and tilts die out northward into the northern Carlin trend. Paleozoic to Cenozoic structural and stratigraphic features are negligibly tilted in the trend, indicating only minor total extension there.

General Geochronology

Modern ^{40}Ar/^{39}Ar and U-Pb dating demonstrates that magmatism in the Carlin trend occurred in four distinct pulses at ~158, 112, 40-36, and ~15 Ma (Figs. 3-3 and 3-4; Table 3-1; this study; Ressel et al., 2000a, b; Mortensen et al., 2000). Early K-Ar dates of Mesozoic igneous rocks in the Carlin trend scatter widely (Fig. 3-3) and appear to indicate protracted magmatism. This scatter resulted from: (1) reheating of older intrusions, mostly the Jurassic Goldstrike intrusion, by younger igneous activity, and (2) hydrothermal alteration, which produced intergrowths of secondary minerals such as chlorite. Reheating induced partial Ar loss from biotite, the most commonly dated phase. K-Ar dates on the Goldstrike intrusion range from 149 Ma (Hausen et al., 1983), only slightly younger than the true age of 158 Ma (Mortensen et al., 2000), to as young as 78 Ma (Morton et al., 1977). In contrast, most early K-Ar dates of Eocene and Miocene volcanic rocks closely match the more recent work, probably because reheating by younger igneous activity was negligible.

Many of the modern ^{40}Ar/^{39}Ar dates in the Carlin trend are on biotite (Fig. 3-4), in part because it commonly survived alteration in rocks where other phenocrysts, e.g., feldspar, were destroyed. However, many biotite spectra are disturbed, which suggests that minor alteration, not always observable in hand specimen or thin section, has affected Ar retention and release. This interpretation is consistent with experimental studies that show that biotite with submicroscopic chlorite layers gives hump-shaped spectra with meaningless old and young ages (DiVicenzo et al., 2003). In some cases, total gas ages of these disturbed biotites approximate emplacement age. We consider flat spectra of biotite to reliably indicate age, but the emplacement age of samples that give hump-shaped or otherwise disturbed spectra cannot be determined as precisely.

Jurassic Intrusions (~158 Ma)

Goldstrike Complex

Jurassic intrusions vary widely in composition and emplacement style, from the mainly equigranular quartz diorite Goldstrike laccolith-sill complex to mostly northwest-striking lamprophyre and rhyolite dikes (Figs. 3-2, 3-5, 3-6, and 3-7; Tables 3-2 and 3-3). These intrusions appear to have been emplaced during a short interval at ~158 Ma (Table 3-1). Outcrop, drill, and mine data demonstrate that the tabular, gently southwest-dipping Goldstrike body was emplaced along and below the Roberts Mountains thrust and other low-angle structures. The Goldstrike intrusion extends at least 2.5 km from its southwestern limit, where it is more than 600 m thick, to the Post fault, where it is ~300-350 m thick (Fig. 3-2; Leonardson and Rahn, 1995; Bettles, 2002). The buried Little Boulder Basin intrusion is a probable continuation east of the Post fault; the top of the intrusion is in upper plate rocks there. A series of quartz diorite sills (Vivian sills) crop out still farther southeast in the main fault block of the Tuscarora Mountains (Fig. 3-2), where they intrude allocthonous rocks well above the Roberts Mountains thrust (Mohling, 2002). Intrusions in all three areas are of similar rock, dominantly equigranular quartz diorite. They likely formed a single contiguous body that cut up section to the east but has been displaced by the right-normal Post fault zone (Dunbar, 2001; Chakurian et al., 2003). If so, this intrusion underlies ~ 7 km^2; with an average thickness of 400 m, total volume is about 3 km^3. The Goldstrike laccolith was likely fed from a deeper magma chamber, whose depth and size are unknown.

Although dominantly quartz diorite, the composite intrusion varies from gabbro to granodiorite (Fig. 3-7). The Goldstrike body is crudely zoned, from mostly granodiorite along the southern or upper margin to a main mass of diorite and quartz diorite, with irregular segregations of gabbro most abundant along the northern or lower margin.

Numerous porphyritic diorite to monzonite sills and other apophyses are present,

especially along the northeast margin of the Goldstrike body in the Betze-Post deposit (Bettles, 2002). Another gently northward-dipping tabular intrusion, predominantly of equigranular biotite-hornblende quartz diorite, intrudes siliciclastic rocks of the Vinini Formation approximately 2 km north of the Dee Mine (M.Visher, personal communication, 2000).

The composite Goldstrike intrusion has a relatively weak magnetic anomaly and an extensive diopside hornfels and marble halo (Hildenbrand and Kucks, 1988; Bettles, 2002). The weak anomaly probably reflects the tabular form of the relatively magnetite-rich rocks and is strongest near its western, thickest end, which probably marks a feeder. The metamorphic halo is widest, $\geq$1 km, above the southern or upper margin near the Genesis Mine (Fig. 3-2).

Lamprophyre Dikes

Porphyritic mafic dikes (lamprophyres) are particularly abundant in the Carlin trend as a northwest-trending, 3- to 4-km wide swarm extending nearly 25 km from south of the Carlin mine to north of the Dee mine. These dikes are concentrated near the Goldstrike intrusion. Individual dikes are 0.1 to 2 m wide, northwest-striking, and generally high angle; some can be traced along strike for more than 1 km. The dike rocks are defined as lamprophyres on the basis of being highly porphyritic mafic rocks lacking feldspar phenocrysts and containing at least one hydrous mafic phenocryst (Fig. 3-7); this definition has no genetic implication. Generally, dikes contain abundant phenocrysts of either magnesian amphibole or phlogopite. Phlogopitic lamprophyres contain alkali feldspar in their groundmass whereas amphibole-bearing lamprophyres contain plagioclase as the groundmass feldspar. Aligned phlogopite makes a distinct foliation in many lamprophyres. The great extent of dikes probably reflects the low viscosity of the mafic magmas.

Porphyritic (plagioclase-biotite±quartz) Rhyolite Dikes

Abundant, finely porphyritic rhyolite dikes form a northwest-striking swarm centered on and within ~5 km of the Goldstrike intrusion. Individual dikes are as much as 15 m wide and can be traced for more than 2 km.

Geochronology of Jurassic Intrusions

U-Pb and ^{40}Ar/^{39}Ar dates on Jurassic intrusions suggest emplacement during a narrow time span around 158 Ma (Table 3-1; Figs. 3-2, 3-3, 3-4, and 3-5). The best U-Pb date is a lower intercept age of 157.7±0.4 from five zircon fractions from a monzonite sill related to the Goldstrike intrusion in the Betze-Post mine (Mortensen et al., 2000). Less precise U-Pb dates on the Goldstrike diorite and a rhyolite dike are 159.1±4.4 (range of three concordant ^{206}Pb/^{238}U titanite ages) and 159.3±4.2 (mean of two ^{207}Pb/^{206}Pb ages of zircon). Most ^{40}Ar/^{39}Ar ages range from 157.4±0.3 to 160.8±2.1 Ma and overlap with the U-Pb ages within analytical uncertainty. One phlogopite sample with a flat spectrum gives a significantly older age of 164.6±1.1 Ma. Although all samples were recalculated to the same monitor age (Table 3-1), it is possible that this sample has not been correctly recalculated. Support for this possibility comes from the fact that biotite analyzed at the same laboratory gives the oldest apparent age among Eocene igneous rocks (see below and comment in Eocene Dikes of the Northern Carlin Trend). Relative ages among the Jurassic rocks are sparse, but porphyritic rhyolite cuts diorite and lamprophyre dikes at Meikle, Beast, and nearby deposits (Bettles, 2002). Among K-Ar ages, those of lamprophyres most closely match the modern U-Pb and ^{40}Ar/^{39}Ar ages, which indicate they cooled rapidly following emplacement and have not been significantly reheated (Fig. 3-3).

Geochemistry

Almost all igneous rocks of the northern Carlin trend are altered to some degree,

with argillization leading to loss of some alkalis being particularly common (Drews-Armitage et al., 1996; Leonardson and Rahn, 1996; Ressel et al., 2000a, b). Nevertheless, total alkali/SiO_2 and K_2O/SiO_2 variations are routinely used for rock classification (LeBas et al., 1986), so we use them to characterize and compare the different suites (Fig. 3-6). However, we also use rare-earth elements (REE), which are relatively immobile during hydrothermal alteration (Fig. 3-8). A thorough petrogenetic study of Carlin trend igneous rocks is beyond the scope of this report and will be difficult, at best, because of the alteration. However, comprehensive geochemical and isotopic data on igneous rocks of the Carlin trend are presented in Appendices 3-1 through 3-5.

Jurassic intrusive rocks contain from ~51 to 77 percent SiO_2 (Fig. 3-6; Table 3-3). SiO_2 concentrations fall into three groups that match the three rock types. The least altered samples of lamprophyre contain 51 to 55 percent SiO_2, the Goldstrike diorite mostly 57 to 59 percent with the related but volumetrically less significant granodiorites about 66 percent, and rhyolite dikes 71 to 77 percent SiO_2. As with most Mesozoic and younger igneous rocks in the interior of the Great Basin, Jurassic rocks are moderately alkalic. They plot near the trachy- fields in total alkalis vs SiO_2 and in the high-K field of K_2O vs SiO_2 (Fig. 3-6).

All Jurassic rocks show steep, concave-upward REE patterns (Fig. 3-8). The lamprophyres have the highest concentrations, especially of LREE, despite being the most mafic of the Jurassic rock types, and the greatest variation in concentrations despite negligible variation in, or relation to, SiO_2. REE concentrations of Goldstrike rocks largely overlap with those of the lamprophyres and generally increase with increasing SiO_2, which makes a simple genetic tie between the two unlikely. Rhyolites have the lowest REE concentrations, which generally decrease with SiO_2. The Goldstrike rocks and rhyolites have small Eu anomalies.

Cretaceous "Richmond" Granite and Aplite-Pegmatite (112 Ma)

The only Cretaceous rock in the Carlin trend is a coarse-grained granite that intruded and thermally metamorphosed Paleozoic quartzite and limestone on the south flank of Richmond Mountain (Fig. 3-2). Outcrop area is small, ~0.4 km^2, but geophysical and other data indicate a larger body in the subsurface. The rock is true granite, with 75 percent SiO_2 (Fig. 3-6; Table 3-3) and characterized by phenocrysts of perthite up to 2 cm across (Fig. 3-7). Aplite is common as a border phase and as dikes cutting the main body; pegmatite pods are also common. Concordant $^{206}Pb/^{238}U$ ages of two zircon fractions demonstrate intrusion at 112.4±0.6 Ma (Table 3-1; Fig. 3-2; Mortensen et al., 2000). A biotite K-Ar age of 108±3 Ma (Evans, 1974b) suggests relatively rapid cooling after emplacement at no more than moderate depth and negligible reheating.

Aeromagnetic data, the coarseness of the intrusion, a broad zone of thermally metamorphosed rock around it, and K-Ar ages of hornfels minerals at the Mike composite Cu-Au deposit indicate the Richmond granite may underlie an area of as much as 20 km^2 (Fig. 3-2). A magnetic high extends southeastward from the granite to within 1.8 km of the deposit, and a separate high at the deposit is interpreted to indicate a cylindrical intrusion at a depth of 1800 m (Norby and Orobona, 2002). K-Ar ages of replacement K-feldspar of 107±2 and 111±2 Ma from, respectively, an altered lamprophyre dike and Paleozoic siltstone in the deposit (Branham and Arkell, 1995; Norby and Orobona, 2002) indicate that hornfels developed contemporaneously with the Richmond intrusion. Implication of these data for extent of the Richmond intrusion is complicated because Paleozoic rocks surrounding the Eocene Welches Canyon intrusions are also thermally altered (Evans, 1974b), and the magnetic high at the Mike deposit is most like the magnetic high associated with the Eocene intrusions (Norby and Orobona, 2002). Also, Evans (1974b) mapped several dikes around the Richmond intrusion as

Cretaceous, but our $^{40}Ar/^{39}Ar$ dates and petrographic comparison demonstrate that all of these are Eocene.

Eocene Igneous Rocks of the Carlin Trend (40-36 Ma)

The most abundant igneous rocks in and around the Carlin trend are Eocene dikes, small stocks, and lavas (Figs. 3-2 and 3-5; Tables 3-1 and 3-4). Eocene rocks include (1) abundant, mostly rhyolite dikes in the northern Carlin trend (i.e., from the Carlin deposit north to the Dee deposit), (2) small andesite to rhyolite stocks and dikes in Welches Canyon, (3) abundant andesite to dacite lavas and rhyolite dikes of the Emigrant Pass volcanic field, and (4) basaltic andesite to rhyolite dikes in the southern Carlin trend near the Rain mine. Isotopic ages indicate nearly continuous magmatism that generally migrated southward between 40 and 36 Ma (Table 3-1; Fig. 3-2). Dikes in the northern Carlin trend and at Rain were emplaced in several discrete pulses between about 40 and 36 Ma, which is coincident with the timing of mineralization (Ressel et al., 2000a,b; Tretbar et al., 2000; Arehart et al., 2003; Heitt et al., 2003). Dikes in the northern Carlin trend are commonly altered but only locally host ore (Leonardson and Rahn, 1996; Emsbo et al., 1996; Ressel et al., 2000a, b; Heitt et al., 2003).

Eocene Dikes of the Northern Carlin Trend (40.3-37.6 Ma)

Eocene dikes range from high-SiO_2 rhyolite to dacite, with minor basaltic andesite at the Dee deposit. These dikes intrude several major ore-controlling structures, including the Post fault zone and the Dee fault. Commonly, the north-northwest striking, steeply dipping dikes and faults are the immediate hanging wall to ore, but Eocene dikes locally host ore at the Meikle-Griffin, Betze-Post, and Beast deposits (Ressel et al., 2000a, b).

Five types of dikes are recognized based on phenocryst assemblage and age (Tables 3-1 and 3-4): (1) finely porphyritic (plagioclase-biotite±quartz) rhyolite (~40.3-39.3 Ma); (2) porphyritic (plagioclase-biotite-hornblende) dacite (~40.1-39.0 Ma); (3) aphyric,

high-silica rhyolite (~39.1 Ma); (4) olivine-phyric basaltic andesite (~37.8 Ma); and (5) coarsely porphyritic (plagioclase-biotite-hornblende-quartz±sanidine) rhyolite (~37.6 Ma).

Porphyritic (plagioclase-biotite±quartz) Rhyolite (40.3 to 39.3 Ma)

Finely porphyritic rhyolite dikes are exposed over a nearly 9-km length from Betze-Post to south of Genesis (Figs. 3-2, 3-5, and 3-7). Most dikes are concentrated along the north-northwest striking and major ore-controlling Post fault zone, but one, nearly 6-km-long dike diverges from the fault zone at Genesis to a south-southwest strike. Dikes range in width from 1 to 8 m. Concentration of the dikes along the Post fault zone and merging of the long dike with the fault zone suggest that intrusion and fault movement were coeval. Composite dikes in which porphyritic rhyolite adjoins porphyritic dacite or aphyric rhyolite are common.

Porphyritic rhyolite dikes are among the oldest Eocene dikes of the Carlin trend. $^{40}Ar/^{39}Ar$ ages of biotite from four samples range from 40.3±0.2 Ma at Genesis to 39.32±0.11 Ma at Betze-Post (Table 3-1). The oldest and youngest samples also have the flattest, and what we consider to be the most reliable, spectra and are supported by similar isochron ages. Two other samples have disturbed, decreasing spectra whose true age, other than ~39-40 Ma, are difficult to interpret (Fig. 3-4). Weighted mean, isochron, and total gas ages agree relatively well at about 39.9 Ma for sample DSU-190-906. The three age calculations do not agree as well for sample H00-50. Its total gas age of 39.7±0.2 Ma differs from the 40.3±0.2 Ma age on what appears to be the same dike. However, this oldest Eocene age is from the same data set as the oldest Jurassic age, and we may have under-normalized both for their monitor ages (see discussion in Geochronology of Jurassic Intrusions). Nevertheless, emplacement of similar rhyolite dikes may have continued for ~0.5 to 1 Ma.

Porphyritic (plagioclase-biotite-hornblende) Dacite (40.1 to 39.0 Ma)

Porphyritic dacite dikes are abundant in a 5-km-long belt between Meikle and Betze-Post deposits where they parallel and intrude the Post fault zone. Two similar dikes are also present on the west side of the Genesis deposit. Dacite dikes are present mostly north of the porphyritic rhyolite dikes, but the two types occur together, commonly as composite dikes, in the Betze-Post deposit. The presence of coarse, abundant, euhedral hornblende phenocrysts is a distinguishing feature. In all but one exposure, hornblende is altered to rims of biotite and cores of calcite and smectite but is recognizable by its shape (Fig. 3-7).

$^{40}Ar/^{39}Ar$ biotite ages range from 39.21±0.08 Ma in the Griffin deposit to 39.87±0.21 in Betze-Post. In contrast, hornblende from the one location where it was unaltered gives a younger plateau age of 38.95±0.22, which is supported by an isochron age of 39.03±0.23 Ma. Relatively imprecise U-Pb zircon ages of 37.8±2.1 Ma from Betze-Post and 38.1±0.8 Ma from Griffin (Mortensen et al., 2000) overlap with the hornblende age. Emplacement of these dikes probably spanned from ~40.1 to 39.0 Ma.

Aphyric Rhyolite (39.1 Ma)

Aphyric, glassy to devitrified, high-SiO_2 rhyolite dikes are widely distributed in the Deep Star and Genesis mines, the western and southern flanks of Richmond Mountain, and in Welches Canyon. A larger (~1 km^2), probably extrusive body of aphyric rhyolite is present in Welches Canyon. A swarm of aphyric rhyolite dikes intrudes along the Post and parallel faults in the Deep Star mine. From crosscutting relations, Dunbar (2001) and Heitt et al. (2003) suggest that two stages of aphyric rhyolite were emplaced closely in time and bracket the age of high-grade (>30 g/t) Au mineralization at Deep Star.

The dikes are distinguished by their lack of phenocrysts, prominent flow-bands, green to red-brown glassy margins, and white felsic cores (Fig. 3-7). Dikes range in

width from 0.5 to 12 m. Thin dikes are entirely glassy. Cores of thick dikes are spherulitically and granophyrically devitrified to a mix of sanidine and quartz.

The lack of phenocrysts has made obtaining a precise age of the aphyric rhyolites difficult (Ressel et al., 2000a; Heitt et al., 2003). The extremely fine-grained, devitrified matrix gives disturbed spectra that probably reflect poor Ar retention and recoil. Best estimates of the emplacement age are 39.15±0.26 Ma (sample DSU-150-106, Table 3-1; Fig. 3-4), which provided the flattest spectra of the three analyzed samples and is supported by an indistinguishable isochron age (39.07±0.33 Ma), and an isochron age of 38.98±0.05 on sample DS-13.

Petrographically similar, aphyric rhyolites around Richmond Mt and in Welches Canyon are included in this group in Figure 3-2 but are undated and need not be the same age as, or related to, the dated dikes in the Carlin trend. The large rhyolite in Welches Canyon is constrained to be between 38.6 and 37.6 Ma on the basis of crosscutting relations (see below).

Basaltic Andesite (37.8 Ma)

The only mafic Eocene dikes in the northern Carlin trend are basaltic andesites exposed at the Dee mine and covered by Miocene rocks about 2 km west of the Betze-Post mine. The dikes at Dee intruded along the north-striking, west-dipping Dee fault, the major ore-controlling structure. These dikes are strongly oxidized and leached through near-suface weathering, but the former presence of olivine phenocrysts is readily apparent in thin section. Relatively fresh rock containing sparse phenocrysts of calcic plagioclase, olivine, and clinopyroxene (Fig. 3-7) also occurs as an irregular pod-like body in the immediate footwall of the Dee fault (Dobak et al., 2002), where it intrudes massive limestone. Matrix from a sample of this body yielded good plateau and isochron ages of 37.80±0.21 and 37.73±0.17 Ma (Table 3-1; Fig. 3-2), indicating mineralization at

Dee probably postdates ~37.8 Ma.

Porphyritic (plagioclase-biotite-hornblende-quartz±sanidine) Rhyolite and Dacite (37.6 Ma)

Dikes of coarsely porphyritic, low-SiO$_2$ rhyolite and high-SiO$_2$ dacite form a discontinuous, 16-km-long belt from the Beast deposit, where they host ore southward to Welches Canyon (Figs. 3-2, 3-5, and 3-6: Ressel et al., 2000a). Coarse phenocrysts, e.g., biotite up to 1 cm and sanidine to 2 cm, are particularly distinctive (Fig. 3-7). Petrographically similar dikes are found in almost all Eocene igneous centers in Nevada (Ressel et al., 2000a; Castor et al., 2003).

In the northern Carlin trend, these dikes were emplaced along and parallel to the north-northwest-striking Gen, Beast and other faults that make up the Post fault zone in that area. The dike at the Beast mine is one of the largest, at least 3 km long and as much as 55 m wide, and contained about half the ore mined there (Ressel et al., 2000a). Coarsely porphyritic dikes give nearly indistinguishable ^{40}Ar/^{39}Ar dates of 37.58±0.06 Ma at the Beast mine, 37.58±0.05 Ma at Richmond Mt, and 37.43±0.06 Ma in Welches Canyon (Table 3-1; Figs. 3-2 and 3-5). The dike at Richmond Mt was one of those mapped as Cretaceous by Evans (1974b).

Geochemistry

Almost all dikes of the Carlin trend are rhyolite or dacite with 66 to 77 percent SiO$_2$; the few basaltic andesites have ~55 percent (Fig. 3-6; Tables 3-3 and 3-4). All dikes are moderately alkalic, similar to Jurassic rocks. This is well illustrated by the K$_2$O/SiO$_2$ plot, but Na$_2$O loss from alteration of plagioclase has distorted total alkali/SiO$_2$ trends. The relatively unaltered rocks of the Emigrant Pass volcanic field are probably the best indicators of pre-alteration alkali contents of the dikes.

Major oxide and REE concentrations of the different dike suites support our field-

petrographic-age subdivision (Figs. 3-6 and 3-8). With the exception of the pl-bi±qtz and pl-bi-hbl-qtz±sa rhyolites, the different dikes have distinct SiO_2 contents, which are consistent with their petrographic characteristics. Apparent variations in SiO_2 may be in part real and in part related to alteration. For example, analyzed SiO_2 contents in six dacites range from 66 to 70.5 percent, but REE concentrations are almost indistinguishable, with steep slopes and small Eu anomalies (Fig. 3-8). The dacites and basaltic andesite have the highest REE concentrations, although the difference is mostly in LREE. Progressively more silicic rocks have progressively lower LREE concentrations and generally larger Eu anomalies. The pl-bi±qtz and pl-bi-hbl-qtz±sa rhyolites again overlap. Eocene rocks have distinctly lower REE, especially LREE, concentrations than do Jurassic Goldstrike intrusions or lamprophyres. Appendices 3-1 through 3-5 contain comprehensive geochemical and isotopic data on igneous rocks of the Carlin trend.

Igneous Rocks of Welches Canyon

Eocene intrusions of Welches Canyon are distinguished as a separate group because they (1) include the northernmost occurrence of larger, stock-like intrusions (Fig. 3-2) and (2) range from rhyolite through andesite, a wider compositional range than dikes of the northern Carlin trend (Fig. 3-6; Table 3-3). In this discussion, we divide the Eocene rocks into three categories, aphyric rhyolite, porphyritic andesite and dacite, and fine-grained diorite-granodiorite. Aphyric rhyolites in Welches Canyon are similar to the dikes in the northern Carlin trend but are discussed separately because they are 10 km south of the northern cluster, include one much larger intrusion or volcanic dome, and are probably a different age.

Aphyric Rhyolite (38 Ma)

Aphyric rhyolite dikes are common in a 10 km belt from north of the Cretaceous

Richmond granite to south of the larger body in Welches Canyon (Fig. 3-2). Most dikes are single bodies a few meters wide, but the northernmost dike is composite with the 37.6-Ma porphyritic rhyolite. The large (~1 km^2) body in Welches Canyon has steep flanks, contains a carapace breccia on its eastern flank, and has widespread curvilinear joints or "ramp" structures; these features suggest it may be a volcanic dome. If so, it is the northernmost Eocene volcanic rock near the Carlin trend and thus could mark the closest recognized Eocene paleosurface. If it is intrusive, it must have underlain the surface by no more than ~200 m, based on the elevation of the Eocene paleosurface marked by Emigrant Pass volcanic rocks just to the south. This body must be younger than 38.6 Ma, the age of the fine-grained diorite it cuts, and older than 37.4 Ma, the age of the porphyritic rhyolite dike that cuts it.

Fine-grained Diorite-granodiorite (38.6 Ma)

A small intrusion consisting mostly of fine-grained diorite, with lesser granodiorite, underlies an area of about 0.9 km^2 in Welches Canyon immediately adjacent to the body of aphyric rhyolite (Fig. 3-2). This unit is the same as the granodiorite mapped by Evans (1974a). Plagioclase from granodiorite yielded an ^{40}Ar/^{39}Ar age of 38.59±0.12 Ma (Table 3-1). Most of the diorite has undergone a higher degree of hydrothermal alteration than the adjacent rhyolite, which suggests that the diorite is older. If the aphyric rhyolite did erupt, then some erosion must have occurred between the 38.6 Ma intrusion of the diorite and eruption of the rhyolite no later than about 37.4 Ma.

Porphyritic (plagioclase-biotite-hornblende) Andesite and Dacite (38.6 Ma)

One thick (200 m) and numerous thinner dikes of porphyritic andesite and dacite cut upper plate Paleozoic rocks around Welches Canyon. The dikes are similar mineralogically to fine-grained diorite, but are strongly porphyritic and locally glassy. Hornblende from the largest porphyritic andesite dike in Welches Canyon yielded an

$^{40}Ar/^{39}Ar$ age of 38.59±0.17 Ma, which is identical to the age of the diorite-granodiorite. Both rocks are slightly older than the oldest units of the Emigrant Pass field (~38.1 Ma) just 4 km to the south and fall within the 39.1 - 37.6 Ma hiatus in magmatism of the northern Carlin trend.

Geochemistry

Most Welches Canyon intrusions have between 61 and 65 percent SiO_2 and are distinctly less silicic than dikes of the Carlin trend (Fig. 3-6). The aphyric rhyolite in Welches Canyon is probably compositionally similar to the aphyric rhyolites of the Carlin trend but was not analyzed. Most Welches Canyon intrusions are less altered than are the Carlin dikes, which is apparent on the total alkali/SiO_2 plot. REE concentrations of Welches Canyon rocks vary only slightly, but appear to increase with increasing SiO_2, and are similar to those of the Carlin trend dacites, which they resemble in composition and mineralogy (Fig. 3-8).

Emigrant Pass Volcanic Field (38.1–37.4, 36.2 Ma)

In sharp contrast to the dikes and small intrusions of the northern Carlin trend and Welches Canyon, lavas, their eruptive vents, and a few shallow intrusions and dikes dominate the Emigrant Pass field (Fig. 3-2). Also in contrast to the Carlin trend dikes, Emigrant Pass rocks are dominantly andesite to dacite, with lesser rhyolite (Fig. 3-6). The rocks are divided into four sequences on the basis of stratigraphy, age, petrography, and composition (Tables 3-1, 3-3, and 3-4; Henry and Faulds, 1999). From oldest to youngest, these are the Primeaux lavas (andesite; 38.1-37.9 Ma), Mack Creek lavas (dacite; 37.9-37.6 Ma), Bob Creek lava (andesite lava; 37.4 Ma), and late porphyritic rhyolite and dacite dikes (36.2 Ma). The Primeaux and Mack Creek lavas, which constitute by far the greatest volume, are composite units made up of numerous individual lavas.

Primeaux lavas are dominantly finely and abundantly porphyritic andesite with lesser dacite (60 to 65% SiO_2, with most ≤63%). The lavas continue ~6 km south of the area shown on Fig. 3-2. They average about 300 to 400 m thick in the mapped area and have an estimated volume of at least 30 km^3. Thick, massive bodies with concentric vertical flow foliations and concentric flow bands in surrounding lavas mark at least 6 vents that fed the lavas. Hornblende $^{40}Ar/^{39}Ar$ plateau and isochron ages on the oldest and youngest parts based on field relations are 38.1 to 37.9 Ma (Table 3-1). These ages allow Primeaux lavas to have erupted over a brief, less than 0.1 Ma, or more extended, as much as 0.5 Ma, period on the basis of analytical uncertainties.

The Mack Creek lavas, the younger of the two major sequences, are abundantly and more coarsely porphyritic dacite with lesser andesite (60 to 67% SiO_2, with only one analyzed sample <63% SiO_2). The more silicic magmas generated relatively short, thick lava domes, which are restricted to the western parts of the volcanic field. Vents are recognized within the outcrop of two of the domes, and the thick, northeast-striking dike in the western part probably fed lava nearby to the east. The Boulder Valley intrusion (Fig. 3-2) may have also fed now eroded lavas. Total volume of preserved eruptive rocks is ~5 km^3. $^{40}Ar/^{39}Ar$ dates on two lava domes and the two western intrusions range from ~38.1 to 37.6 Ma (Table 3-1).

The 37.4-Ma Bob Creek lava is a single, extensive andesite lava characterized by ~10-12 percent hornblende phenocrysts and almost no plagioclase phenocrysts. At ~57 percent SiO_2 bordering on basaltic andesite, it is the most mafic igneous rock in the Emigrant Pass field. It erupted from a vent in the western part of the volcanic field, extended over an area of approximately 30 km^2, and is as much as 120 m thick.

The late, porphyritic rhyolite to dacite dikes form two, discontinuous, north-northeast-striking belts through the central and northeastern part of the volcanic field.

The western belt consists mostly of coarsely porphyritic rhyolite, whereas the eastern belt is mostly dacite. The western belt dikes are petrographically and compositionally indistinguishable from the 37.6 Ma rhyolite dikes of the northern Carlin trend but, at ~36.2 Ma, are distinctly younger.

Our $^{40}Ar/^{39}Ar$ dating indicates that the Primeaux, Mack Creek, and Bob Creek lavas and associated intrusions were emplaced nearly continuously over about 0.7 Ma. The distribution of identified vents and shallow intrusions suggests an underlying pluton of at least 20 by 12 km.

The two pulses in the Emigrant Pass volcanic field are compositionally distinct, with SiO_2 concentrations ranging from 57 to 67 percent in the older Primeaux, Mack Creek, and Bob Creek lavas and from 69 to 75 percent in the late, porphyritic rhyolite–dacite dikes (Fig. 3-6; Tables 3-3 and 3-4). Emigrant Pass rocks are unaltered, which is demonstrated by the narrow belts they make on the total alkali/SiO_2 and K_2O/SiO_2 plots (Fig. 3-6). Despite the wide SiO_2 range, Emigrant Pass rocks vary little in REE concentrations (Fig. 3-8). For example, SiO_2 in the Primeaux lavas varies almost 6 percent but La varies only from 38 to 46 ppm and does not correlate with SiO_2. The late, porphyritic rhyolite–dacite dikes, which are similar in field and petrographic characteristics to the pl-bi-hbl-qtz±sa rhyolite dikes of the Carlin trend, are also indistinguishable in major oxides and REE (Table 3-3; Fig. 3-8).

Intrusions of the Rain-Railroad Area (39.1, 38.2, 37.5 Ma)

The Rain subdistrict, including the Rain mine and Emigrant deposit, constitutes the southern Carlin trend, which is ~24 km from the Gold Quarry mine, the southernmost mine of the central Carlin trend (Figs. 3-1 and 3-9). The Rain and Emigrant deposits are in breccias in and near the unconformable contact between Mississippian and Devonian sedimentary rocks. Breccias and orebodies were controlled by, and spread along, the

west-northwest-striking Rain fault for about 8 km, especially near intersections with northeast-striking faults (Williams et al., 2000; Mathewson, 2001; Longo et al., 2002). The Emigrant deposit is along the north-striking Emigrant fault. The Railroad mining district, which lies about 10 km south of Rain and Emigrant (Fig. 3-9) and is not part of the Carlin trend, produced Cu, Pb, and Ag from mantos and veins in Paleozoic rocks adjacent to the Eocene Bullion stock (Ketner and Smith, 1963). Jasperoid-hosted Au deposits are more distant from the stock (Rayias, 1999; Gillerman, 1982).

Eocene igneous rocks of the Rain-Railroad area have been mapped in detail in the Railroad district (Ketner and Smith, 1963; Smith and Ketner, 1978) and in less detail around the Rain and Emigrant deposits (Longo et al., 2002). We divide the rocks into several packages based on petrography and age (Fig. 3-9). From oldest to youngest they are: basaltic andesite to porphyritic diorite dikes that mostly intruded along the Rain fault; a granitic stock in the Railroad district; porphyritic rhyolite to dacite dikes and small stocks that are most abundant around the Railroad district but also intrude along the Emigrant fault; and porphyritic rhyolite to dacite lavas and tuffs that make a thick pile that extends from south of Emigrant to more than 30 km south of the Railroad district and are in part extrusive equivalents of the porphyritic rhyolite dikes. Many dikes around Rain are too altered to be categorized with any confidence and are shown as undivided on Figure 3-9.

Mafic dikes along the Rain fault are variably altered and locally host ore (Shallow, 1999; Longo et al., 2002). Less altered dikes are identifiable as basaltic andesite and porphyritic diorite, with altered to partly preserved phenocrysts of olivine, pyroxene and/or hornblende, and biotite. The least altered rocks are weakly propylitized but more typically are altered to clay and iron oxides at and near the surface and to clay and iron sulfides at depth. These dikes were initially interpreted as probably Jurassic

lamprophyres because of their mafic phenocrysts (Longo et al., 2002), but our dating indicates they are Eocene.

Two less altered dikes intersected in core from the Saddle deposit along the Rain fault were dated (Table 3-1; Figs.3- 4 and 3-9). Biotite from a porphyritic diorite that contains fresh biotite and partly altered pyroxene and hornblende phenocrysts gives a slightly disturbed spectrum with a weighted mean age of 39.06± 0.20 Ma. This is supported by an isochron age of 39.13±0.18 Ma, so reasonably indicates the time of emplacement.

The second dike, a porphyritic basaltic andesite, contains altered pyroxene and olivine phenocrysts in a groundmass of relatively fresh plagioclase. The dike has been propylitically altered with abundant carbonate and about 0.5 percent pyrite. A matrix separate with altered phenocrysts, pyrite, and carbonate removed yielded a disturbed, dropping spectrum with ages ranging from ~41 to 37.8 Ma that probably indicates recoil. A weighted mean of the flattest, low-temperature part of the spectrum gives an apparent age of 38.21± 0.20 Ma (Table 3-1); an isochron of all steps gives 37.8±1.2 Ma. These data most likely indicate emplacement but possibly alteration at ~38 Ma.

The Bullion stock of the Railroad district consists of granite that is cut by an inner stock and numerous dikes of porphyritic rhyolite to dacite. The porphyritic dikes are petrographically similar to the coarsely porphyritic rhyolites of the northern Carlin trend. They contain large phenocrysts of plagioclase, biotite, hornblende, quartz, ± sanidine. These intrusions are near the northern end of the Robinson Mountain volcanic field (Fig. 3-1). An ~10 km diameter, aeromagnetic anomaly that is centered about 1 to 2 km southwest of the small stock is interpreted to indicate a buried pluton (Grauch, 1996). K-Ar ages of 36.3±1.1 and 37.8±1.0 Ma on rhyolite (Smith and Ketner, 1976) are confirmed by our sanidine date of 37.38±0.08 Ma (Table 3-1); another hypabyssal intrusion or lava

dome farther south in the Robinson field gives 37.51±0.19 Ma (Fig. 3-1; Table 3-1). Numerous porphyritic rhyolite dikes are centered around the stock and extend as much as 4 km away from it.

Porphyritic rhyolite dikes, termed monzonite porphyry in Longo et al. (2001), are also present in the Emigrant deposit. Longo et al. (2001) report a zircon U/Pb SHRIMP age of 37.5±0.8 Ma on one dike, indistinguishable from our dates (Fig. 3-9; Table 3-1). Although the deposit and dike are ~10 km north of the Bullion stock, they are only ~8 km north of the edge of the aeromagnetic anomaly. We interpret the dikes around the deposit to be distal apophyses from a large pluton beneath the stock and aeromagnetic anomaly. The area between the two has not been mapped in detail, and additional dikes may be present.

The Robinson Mountain volcanic field (Figs. 3-1 and 3-9) consists of numerous lavas and some ash-flow tuffs of coarsely porphyritic rhyolite to dacite, petrographically similar to the dikes at Railroad and Emigrant. One of the tuffs gives a $^{40}Ar/^{39}Ar$ date of 37.70±0.19 Ma (Table 3-1). This age and the petrographic similarity are consistent with the volcanic rocks being the extrusive equivalent of the intrusive rocks.

Mineralization at Rain postdates ~38.0 Ma, the date on the younger of the two dikes. That dike contains pyrite, and As and Sb have been added to both dikes. From similar data, Longo et al. (2002) concluded that mineralization at the Emigrant deposit postdates the 37.5 Ma porphyritic rhyolite.

Miocene Rhyolite (15 Ma)

Middle Miocene, sparsely porphyritic, rhyolite lavas are present along the west edge of the northern Carlin trend and between the Emigrant Pass volcanic field and the Rain subdistrict (Fig. 3-2). The lavas disappear beneath middle Miocene tuffaceous sedimentary rocks and Quaternary deposits in both areas, westward into Boulder Valley

from the northern Carlin trend and eastward beneath the Carlin basin in the south.
The northern sequence of flows thickens from only a few meters on the east nearest the
trend to hundreds of meters to the west under Boulder Valley. The southern flows thicken
eastward beneath Carlin basin and southeastward to the southeastern corner of Figure 3-
2. Rhyolitic, pyroclastic-fall tuffs are common in the lower parts of the Miocene
stratigraphic sequence throughout the Carlin trend. Some tuffs are related to the rhyolite
lavas, although Fleck et al. (1997) suggest that others erupted from sources in
southwestern Idaho.

No sources are recognized for these lavas within the Carlin trend. The source of the
northern flows could be buried beneath Boulder Valley. The source of the southern flows
is probably beneath their thickest pile in the southeast. One of the southern flows east of
the Emigrant Pass volcanic field gives a $^{40}Ar/^{39}Ar$ age on sanidine of 15.32±0.08 Ma
(Table 3-1). The northern flows have a K-Ar sanidine date of 14.6±0.3 Ma (Evans,
1974b).

Both northern and southern rhyolite lavas have 74 to 76 percent SiO_2, but they are
petrographically and compositionally distinct (Fig. 3-6; Table 3-3). The northern lavas
have sparse phenocrysts of olivine and Fe-rich pyroxene accompanying sanidine and
quartz. They also have high Fe, Zr, Nb, and REE. LREE are as high as in the Jurassic
lamprophyres, but the Miocene rocks have higher HREE and large Eu anomalies (Fig. 3-
8). A pyroclastic-fall tuff within Miocene sedimentary rocks at the southwestern edge of
the Emigrant Pass volcanic field has the same chemical signature and probably is related
to the lavas. Southern lavas are more typical rhyolites with phenocrysts of biotite
accompanying sanidine and quartz and having lower concentrations of Fe, Zr, Nb, and
REE. Both compositional types are present near Ivanhoe, but only the Fe-rich rhyolites
are present in the northern Nevada rift near Midas (Wallace, 1993, 2003a; John et al.,

2000). Miocene mafic to intermediate lavas, although abundant in the northern Nevada rift just 20 km to the west (John, 2001; John et al., 2000, 2003), are absent within the Carlin trend.

Association of Mineralization and Igneous Activity

Hydrothermal mineralization is associated with all four magmatic episodes of the Carlin trend. However, the style of mineralization represented by each episode is distinct. Mesozoic intrusion-related mineralization occurred at both higher temperature and pressure than other periods. Eocene mineralization was associated with epizonal intrusions emplaced at < 2 km depth and involved fluids of moderate temperature (~150°-250°C). Rare Miocene mineralization with temperatures less than ~200°C occurred at or very near the surface.

Jurassic Goldstrike Intrusion-related Mineralization

Mineralization related to more deeply seated Mesozoic intrusions is spatially restricted to relatively narrow thermal aureoles around intrusions, which commonly contain diopsidic and biotitic hornfels, rare marble, and quartz-sericite-pyrite alteration in felsic Jurassic dikes and sills. In the case of the Goldstrike intrusion, uneconomic base metal, Ag, and Au deposits occur mainly in sparse milky quartz veinlets and irregular sulfide-bearing pods that contain chalcopyrite, sphalerite, galena, freibergite, bismuthinite, and native Au (Arehart et al., 1993; Leonardson and Rahn, 1996; Ferdock et al., 1997; Emsbo et al., 2000). Relatively coarse-grained, preore sericite, which gives Jurassic ages in some dikes, is indicative of this early mineralization (Table 3-1; Ressel et al., 2000b; Emsbo et al., 2000). Sericite is commonly accompanied by coarse, euhedral pyrite, ankerite, and albite in altered Jurassic rhyolite dikes. Turquoise mined from historic workings approximately 1 km southwest of the Genesis mine may have been derived from oxidation of chalcopyrite deposited at the edge of the metamorphic aureole.

Jurassic mineralization was probably important in producing abundant iron sulfide in subjacent sedimentary rocks, which contributed to an abundance of nucleation sites upon which later Au-bearing arsenian pyrite was deposited (Arehart et al., 1993).

Cretaceous Richmond Stock-related Mineralization

The 112 Ma Richmond granite stock is also associated with hornfels and marble (Evans, 1974; 1980; Radtke, 1980) that locally contain small quantitities of base metals, W, and Bi. The edges of the metamorphic aureole at the Mike gold deposit contain particularly abundant secondary Cu and Zn, with grades of each locally exceeding 3 wt. percent (Norby and Orobona, 2002; Bawden, 2002). Sphalerite and lesser chalcopyrite, galena, molybdenite, and bismuthinite are present in veins and in disseminated replacement bodies in the unoxidized lower part of the deposit (Norby and Orobona, 2002). K-Ar ages of potassium feldspar from hornfels and from an altered dike are 107 ± 2 Ma and 111 ± 2 Ma, respectively (Branham and Arkell, 1995), similar to the age of the Richmond stock, suggesting that metamorphism was contemporaneous with intrusion of the stock. Norby and Orobona (2002) interpret economic gold mineralization, which is associated with crosscutting lower temperature clay and pyrite alteration, to be unrelated to metamorphism and base metal deposition.

Eocene Carlin-type Mineralization

Ore mined from the Carlin trend is almost exclusively from Carlin-type deposits (CTDs), which are hosted in a wide variety of rock types including silty limestone, siltstone, micrite, chert, argillite, calc-silicate hornfels, and felsic intrusions. Ores are characterized by (1) a consistent paragenesis that includes early fine-grained, replacement arsenian pyrite, with lesser marcasite and arsenopyrite followed by late stibnite, (2) a geochemical signature consisting of high concentrations of As, Sb, Hg, $\pm$ Tl, (3) low Ag/Au ($\leq$1), (4) argillization of feldspathic rocks to kaolinite or illite, (5)

decalcification or decarbonatization of carbonate host rocks, and (6) local silicification (e.g., Arehart, 1996; Hofstra and Cline, 2000). The deposits formed at depths of ~1-2 km (Ressel et al., 2000a; Henry and Ressel, 2000a; Tosdal et al., 2003), contemporaneously with porphyritic dikes, which locally contain ore (Ressel et al., 2000a, b; Arehart et al., 2003). The close spatial and temporal relations between Eocene magmatism and ore deposition suggest that the two are related, and that magmatism was at least the heat source for hydrothermal circulation and may have contributed some metals (Sillitoe and Bonham, 1990; Henry and Boden, 1998; Henry and Ressel, 2000a; Johnston and Ressel, 2004).

In addition, thermal aureoles of biotite hornfels in Paleozoic siliciclastic rocks surround Eocene intrusions in the Welches Canyon area (Evans, 1974b). The hornfels contain abundant pyrrhotite and lesser pyrite and rare arsenopyrite and chalcopyrite. This sulfide assemblage is similar to that found in distal-disseminated Au-Ag deposits elsewhere in northern Nevada such as Lone Tree and Cove that have clear ties to Eocene epizonal intrusions (Theodore, 2000; Johnston, 2003).

Three main types of alteration affect Eocene dikes of the Carlin trend: (1) smectite-carbonate, (2) quartz-illite±smectite-pyrite, and (3) quartz-kaolinite-pyrite/marcasite. All three types of alteration are restricted to areas in and near CTDs, indicating that they are products of Au-related hydrothermal activity, and all types are feldspar-destructive, with variable alkali mobility that includes nearly complete loss of Na (Fig. 3-6). The smectite-carbonate assemblage grades to quartz-illite-pyrite, which in turn produced quartz-kaolinite-pyrite with increasing intensity of alteration (Ressel et al., 2000a,b; Heitt et al., 2003). The latter two are associated with Au (to 10 ppm) as well as abundant As, Sb, ±Hg and locally host ore (Ressel et al., 2000a,b). Smectite-carbonate alteration is unique to Eocene dikes in the Carlin trend and results from alteration of glass, which is abundant

in Eocene rocks and absent in older intrusive rocks. The swelling character of smectite, which is particularly common in the originally glassy border zones of Eocene dikes, made the dikes much less permeable to hydrothermal flow, thereby offering an explanation for their generally weak mineralization compared to Jurassic intrusions. The less permeable character of all dikes relative to host carbonate rocks, however, certainly contributed to the footwall style of gold mineralization that characterizes CTDs of the Carlin trend.

Miocene Epithermal Mineralization

Chalcedonic silica, opal, montmorillonite, zeolite, and small amounts of pyrite and marcasite are locally present in Miocene silicic tuff of the Carlin trend (Ferdock et al., 1997). Lauha and Bettles (1993) describe a small Hg occurrence in Paleozoic rocks above the Meikle gold deposit, which they attribute to this younger stage of mineralization. This style of mineralization, which includes siliceous sinter elsewhere in north-central Nevada, is typical of the upper parts of low-sulfidation epithermal Au-Ag deposits of the 16 to 14 Ma northern Nevada rift (John, 2001; Wallace, 2003b; Fig. 3-1) and affects both mid-Miocene volcanic rocks and Paleozoic sedimentary rocks. Mineralization of the rift is characterized by: (1) bimodal basalt-rhyolite, with many deposits both spatially and temporally associated with silicic centers (John, 2001; Wallace, 2003a, b), (2) a geochemical signature that includes Hg, As, Sb, and Se, (3) high Ag/Au (>10), (4) very low total sulfide, and (5) abundant high-level Hg deposits. The Ivanhoe district (Fig. 3-1), which has both disseminated Au-Ag deposits and bonanza Au-Ag banded silica veins (Bartlett et al., 1991; Wallace, 2003b), is the closest concentration of Miocene deposits to the Carlin trend and lies 22 km NW of the Betze-Post deposit. Although considered to be in the Carlin trend (Bartlett et al., 1991), deposits in the district are ~15 Ma old, associated with similar age rhyolites (Wallace, 2003a, b),

and distinctly unlike CTDs.

Discussion

Number, Size, and Depth of Emplacement of Underlying Eocene Plutons

We have noted that the abundant, Eocene, porphyritic, silicic dikes require the presence of an underlying plutonic complex (Henry and Ressel, 2000a). The large aeromagnetic anomaly centered on the Emigrant Pass volcanic field (Hildenbrand and Kucks, 1988) is one major indicator of that plutonic complex (Grauch, 1996; Ressel et al., 2000a, 2001), and magnetic data presented here strengthen that conclusion (Fig. 3-10). The fundamental point is that silicic magmas as represented by the dikes require large magma chambers to develop, either by differentiation of mantle-derived, basaltic magmas, by crustal melting or, more commonly, by a combination of differentiation and crustal melting-assimilation (Barker, 1981; Hildreth, 1981; Barnes et al., 2001). The exposed dikes are only minor apophyses from the underlying plutonic complex. Critical observations are that individual age and petrographic suites of dikes are areally restricted (Fig. 3-2). All Eocene dikes cannot have come from any single chamber or only from the complex indicated by the southern magnetic anomaly; the dikes in the Betze-Post area did not emanate from Welches Canyon. The latter scenario would require that individual age and petrographic suites only be emplaced some 12 to 15 km north of the northern edge of the source pluton, that they not be emplaced above it or symmetrically around it, and that they be a different age than the source pluton. These possibilities are physically unrealistic.

The age and distribution of Eocene dikes and volcanic rocks require a minimum of five plutons that mostly young southward (Fig. 3-10). The oldest pluton is based on the distribution of the three oldest dike suites of the northern Carlin trend: 40.3-39.3 Ma pl-

bi±qtz rhyolites, 40.1-39.0 pl-bi-hbl dacites, and the ~39.1 Ma aphyric rhyolites. The nearly continuous span of ages allows for either a long-lived (≥1 Ma) magma chamber or multiple magma chambers, and we show two possible plutons on Figure 3-10. Because even large crustal magma chambers cool relatively rapidly, a long-lived system would require periodic replenishment by basaltic magma to remain molten (Cathles et al., 1997). A better understanding of the geochemical-isotopic characteristics and petrogenesis of the three dike suites, whether or not genetically related, would help evaluate the single vs multiple pluton alternatives. Although the southward younging, even in these temporally close rocks, could indicate multiple plutons, a conservative interpretation is a single pluton centered beneath the three dike suites, i.e., approximately beneath the Betze-Post deposit and the richest part of the Carlin trend. The pluton would have a diameter of about 10 km if the dikes rose vertically from it. Obviously, either a larger or smaller body is possible.

Magnetic data upward continued to 2000 m to remove near-surface effects are consistent with two or three plutons beneath the northern Carlin trend (Fig. 3-10). Anomaly A underlies the Goldstrike intrusion and is discussed below. Anomaly B (the barbell-shaped body in Fig. 3-10) is itself composite and lies along the margin and just north of a pluton inferred from dike distributions only. The close proximity of the dike-inferred body to the magnetic high suggests that the latter marks a pluton or plutons that fed the dikes. That anomaly B is composite is consistent with the possibility of a composite or long-lived source. The low magnitude of anomaly B suggests that the pluton or plutons are relatively deep.

The 37.6 Ma, pl-bi-hbl-qtz±sa rhyolites require a second major pluton (Fig. 3-10). These dikes extend over a distinctly elongate distance of about 18 km along the northern Carlin trend, which is the greatest distribution of any of the silicic dikes of the trend. That

distribution is comparable to the distribution of petrographically similar dikes around several Eocene igneous centers where a central stock is exposed (e.g., Tuscarora or Swales Mountain; Evans and Ketner, 1971; Henry and Ressel, 2000b; Ressel et al., 2001a; Castor et al., 2003). However, the central stock in these examples is still a small (≤ 3 km^2), shallow apophysis above a deeper, main chamber. The 37.6-Ma pluton in the northern Carlin trend conceivably underlies and is represented by the northern part of the large, aeromagnetic anomaly C. This northern edge is about in the middle of the dike distribution. Alternatively, a deep and/or relatively nonmagnetic pluton could be disguised beneath the associated low-susceptibility area (aeromagnetic low D) north of anomaly C.

Three other distinct plutons must underlie the 38.6 Ma Welches Canyon intrusions, the 38.1-37.4 Ma Emigrant Pass volcanic field, and the 36.2-Ma pl-bi-hbl-qtz±sa rhyolite dikes of the Emigrant Pass field (Fig. 3-10). The spatial separation and different ages of the Welches Canyon intrusions and the Emigrant Pass volcanic field require separate bodies. The pluton for the Emigrant Pass volcanic field, which was active from ~38.1 to 37.4 Ma, could be either long-lived or composite. The distribution of subvolcanic intrusions and lava vents and the association with part of magnetic anomaly C (Fig. 3-10) indicate an underlying pluton at least 20 km across. The 36.2 Ma rhyolite dikes in the Emigrant Pass field mark the youngest pluton of the Carlin trend. Their separation by ~1 Ma from the rest of the field with no intervening activity indicates that they did not arise from a single, long-lived chamber that fed both systems. Their similarity to the 37.6-Ma dikes demonstrates the need for precise dating to distinguish events in areas of complex magmatism.

The Welches Canyon and Emigrant Pass rocks fall within the areas of the aeromagnetic anomaly of Hildenbrand and Kucks (1988) and of the similar, upward

continued magnetic anomaly C of Figure 3-10. The amplitude of anomaly C and the steep gradients at its margins indicate a shallow pluton (Grauch, 1996). These aspects and the separate highs C1 and C2 within the anomaly support the interpretation of shallow, composite plutons that fed the Welches Canyon intrusions, the Emigrant Pass volcanic field, and the 36.2 Ma dike swarms. Anomaly C1 is centered on the Welches Canyon intrusions, which are often cited as "the Eocene pluton" of the northern Carlin trend (Chakurian et al., 2003; Emsbo et al., 2003; Hofstra et al., 2003). However, as shown here, the exposed Welches Canyon intrusions are shallow, porphyritic rocks, most likely minor apophyses from a larger and only moderately deeper body shown by the magnetic data. Moreover, the Welches Canyon intrusions are distinctly younger than the dikes of the Betze-Post area and cannot have been the source of the latter. Anomaly C2 coincides with several vents of the Emigrant Pass field and with the 36.2-Ma dikes.

Both geologic and magnetic data are consistent with the plutons underlying the Welches Canyon and Emigrant Pass areas being emplaced at shallow depths, whereas the pluton(s) beneath the northern Carlin trend were probably emplaced at greater depth. The relatively large, subvolcanic intrusions in Welches Canyon, Boulder Valley, and throughout the Emigrant Pass volcanic field; the presence and abundance of lavas in the Emigrant Pass field; and the amplitude and sharp boundary of the associated aeromagnetic anomaly are consistent with shallower-source magma chambers. The fact that only dikes are present in the north and the lesser amplitude of anomaly B support a deeper body.

The Rain deposits of the southern Carlin trend lie ~8 km north of an ~10-km-diameter aeromagnetic anomaly, upward continued to 2000 m, that lies southwest of the 37.4-Ma Bullion stock (Fig. 3-11). Hildenbrand and Kucks (1988) and Grauch (1996) interpret this anomaly to mark another major, underlying pluton. Aeromagnetic data that

are not upward continued show a v-shaped pattern, with highs coinciding with the stock and the northwest-trending rhyolite dike swarm west of the stock. We interpret the 37.5 Ma porphyritic rhyolite dike at the Emigrant deposit, which lies ~8 km north of the magnetic anomaly, to be an apophysis from the pluton represented by the anomaly. Thus plutons were also present to provide heat to generate the CTDs at Rain.

The significance for underlying plutons of the 37.8-Ma basaltic andesite at Dee or the 38.2-Ma basaltic andesite at Rain is less certain, because mafic magmas do not require crustal magma chambers. Mafic rocks are scarce in Eocene igneous centers, found elsewhere only in the Jerritt Canyon CTDs (Fig. 3-2; Phinisey et al., 1996). Their scarcity may reflect the difficulty mafic magmas have propagating through low density, silicic magma chambers (Hildreth, 1981). Mafic magmas can appear after silicic magmatism has ended in an area or on the flanks of silicic centers, such as in the modern Cascades. However, these mafic rocks are important because they are the best indicators of the character of mafic magmas parental to the more silicic rocks.

The distribution of dikes and magnetic anomalies in the northern and central Carlin trend (Fig. 3-10) suggests that an Eocene plutonic complex underlies an area about 50 km north-south and between 12 and 23 km across, or possibly 1000 km^2. The thickness of the complex or of individual plutons is unknown, but magnetotelluric data suggest thicknesses of 10 km or more (Rodriguez, 1998). Thus, possibly 10,000 km^3 or more of Eocene magma were emplaced beneath the northern and central Carlin trend between about 40 and 36 Ma.

Implications of Fission-track Data for Plutons

Fission-track data also support shallow depth of the southern plutons and greater depths of the northern plutons. Apatite fission-track ages are reset to zero at temperatures above ~110-135°C (Green et al., 1989). Chakurian et al. (2003) and Tosdal et al. (2003)

determined apatite fission-track ages of samples in and around the Carlin trend. Three samples from within the area of the large, magnetic anomaly C were reset to 37-38 Ma, and one to 28 Ma (Chakurian et al., 2003); for example, a sample from the Cretaceous Richmond stock gave 37.8 Ma. Only one of these samples is close to a known CTD. In contrast, only two of nineteen apatite samples from the northern Carlin trend outside the anomaly were reset to similar ages. One of three samples from the Carlin deposit gave 40.9 Ma (one was 18.6 Ma), and one of two samples from the Betze-Post deposit gave 35.5 Ma. All other samples, most of which were from CTDs, gave ages ranging from 56.1 to 129 Ma.

Although Chakurian et al. (2003) interpret the fission-track data to indicate the time of Au mineralization, and we agree with an Eocene age for mineralization, they strictly indicate only the time of heating to 110-135°C for sufficient time to reset the fission-track clock. The distribution of ages shows that igneous heating around the shallow, Eocene plutons of the Welches Canyon – Emigrant Pass area reset the fission-track ages to the time of intrusion. In contrast, heating by the hydrothermal systems alone was insufficient to reset ages. Although maximum hydrothermal temperatures in the northern Carlin trend are estimated to have been ~240°C (Hofstra and Cline, 2000), hydrothermal heating apparently was too short in time to reset the apatite fission-track ages, even within major deposits. Similarly, the deep Eocene plutons indicated by our work were too deep to heat country rock around the deposits hot enough or long enough to reset the fission-track ages.

Depth of Pluton Emplacement

Although the southern plutons beneath Welches Canyon and the Emigrant Pass volcanic field were certainly emplaced at shallower depths than were the northern plutons, their absolute depths are less certain. Based on the steep gradients at the margins

of magnetic anomaly C (Grauch, 1996), resetting of apatite fission-track ages
(Chakurian et al., 2003), and the degree of alteration around the Welches Canyon stocks,
we infer that the southern plutons are no more than about 3 km below the present surface.

Several features may place limits on the depth of the postulated plutons beneath the
northern Carlin trend. Quantitative modeling of the fission-track data of Chakurian et al.
(2003) to estimate a combined maximum size, depth, and temperature of such a pluton is
probably possible but beyond the scope of this report. The presence of abundant rhyolite
dikes above the plutons probably precludes their being much deeper than about 8-10 km,
which is the maximum lateral distance that similar rhyolite dikes extend from related
plutons in northeastern Nevada (Ressel et al., 2000a). Although silicic dikes need not
extend identical lateral and vertical distances from a source pluton, this distance is a
probable indicator. Finally, the association of aeromagnetic anomalies with all inferred
plutons suggests they cannot be extremely deep.

Of course, some plutons might have no surface magnetic expression. The 36-Ma
Harrison Pass pluton in the Ruby Mountains has a very low magnetite content (Barnes et
al., 2001) and shows no magnetic anomaly (Hildenbrand and Kucks, 1988). The Harrison
Pass pluton, which is composite and estimated to have been emplaced at ~12 km (Barnes
et al., 2001), is otherwise a good analog to our postulated deep plutons.

Jurassic and Cretaceous Plutons

The same arguments for deeper seated, Eocene plutons apply to the Jurassic and
Cretaceous rocks. The centering of Jurassic dikes around the Goldstrike laccolith
suggests a pluton beneath the laccolith. This interpretation is supported by magnetic
anomaly A, which suggests a feeder beneath the southwestern end of the Goldstrike
laccolith (Fig. 3-10). The Jurassic rocks exhibit two significant differences from the
Eocene rocks. Jurassic magmatism was relatively more mafic, dominated by the

Goldstrike diorite and lamprophyre dikes, although rhyolite dikes are also present. Also, Jurassic magmatism may have been temporally restricted, both in the Carlin trend and more regionally (Mortensen et al., 2000; this study). All Jurassic intrusions in the Carlin trend may have emanated from a single magma body that was centered beneath the Goldstrike laccolith.

From magnetic and other data (see section "Cretaceous Richmond Granite") we infer that a Cretaceous pluton underlies an area in the northeastern part of anomaly C (Fig. 3-10). Distinguishing the magnetic contribution of Eocene and Cretaceous rocks in this area is difficult.

Timing of Eocene Plutons and Carlin-type Deposits

Absolute constraints on the age of ore formation are few. Arehart et al. (2003) determined a Rb-Sr age of 39.8±0.6 Ma on galkhaite, a late ore-stage sulfosalt mineral, from the Rodeo deposit north of Betze-Post. Galkhaite from the Getchell mine, a CTD west of the Carlin trend (Fig. 3-1), gave 39.0±2.1 Ma (Tretbar et al., 2000). Heitt et al. (2003) interpret mineralization at Deep Star to be bracketed at ~39.1 Ma by two closely spaced stages of intrusion of aphyric rhyolite. Mineralization postdates 40.1 to 39.0 Ma dikes at Betze-Post, a 39.5 Ma dike at Griffin (Meikle), a 37.8 Ma dike at Dee, and a 37.6 Ma dike at Beast. We consider it most likely that these data indicate multiple episodes of mineralization in the northern Carlin trend, but that is not proven. Nevertheless, a key point is that the combination of data demonstrates that mineralization was contemporaneous with the intense pulse of Eocene intrusion. Although many factors probably had to converge to generate CTDs and the Carlin trend, magmatic heat was abundant at the appropriate time to generate the deposits.

Depth of Formation of Carlin-type Deposits

In Henry and Ressel (2000a), we used a structural argument that tops of deposits of

the northern Carlin trend probably formed at paleodepths no greater than about 1 km. The present-day elevation of the Eocene-Paleozoic unconformity in the Emigrant Pass volcanic field marks the Eocene paleosurface. Extrapolating the paleosurface northward into the northern Carlin trend requires allowance for relative displacements on intervening structures. The only major post-Eocene structure along this northward projection is the northeast-striking normal fault between Welches Canyon and the Cretaceous granite outcrop (Fig. 3-2). This fault has a maximum displacement of ~2 km at its northeast end (Evans, 1974a, b), but displacement diminishes to the southwest, on a line between the northern Carlin trend and Emigrant Pass. This extrapolation suggests the Eocene paleosurface was not much higher than the present-day surface in the northern Carlin trend. Allowing for uncertainty in this structural reconstruction, most major ore bodies (not the deepest recognized mineralization) probably formed no deeper than about 1 km. Hickey et al. (2003) and Haynes et al. (2003) used apatite fission-track and U-Th/He data to estimate that the present-day surface in the northern Carlin trend lies 500 to 1500 m below the ~42 Ma paleosurface. Given the vertical range of mineralization, CTDs formed between 500 and 2200 m below the surface. However, all significant deposits lie no deeper than 700 m at present-day depths.

Zanetti at UNLV for guidance. Newmont Mining Company allowed the use of aeromagnetic data, and discussions with Mark Goldie greatly helped to explain the significance of these data. Reviews of an early draft by Stephen Castor, Jonathan Price, and Tommy Thompson greatly improved the content and clarity of this report.

References

Anders, E., and Grevesse, N., 1989, Abundances of the elements: Meteoritic and solar: Geochimica et Cosmochimica Acta, v. 53, p. 197-214.

Arehart, G.B., 1996, Characteristics and origin of sediment-hosted gold deposits: A review: Ore Geology Reviews, v. 11, p. 383-403.

Arehart, G.B., Foland, K.A., Naeser, C.W., and Kesler, S.E., 1993, $^{40}Ar/^{39}Ar$, K-Ar, and fission-track geochronology of sediment-hosted disseminated gold deposits at Post/Betze, Carlin Trend, northeastern Nevada: Economic Geology, v. 88, p. 622-646.

Arehart, G.B., Chakurian, A.M., Tretbar, D.R., Christensen, J.N., McInnes, B.A., and Donelick, R.A., 2003, Evaluation of radioisotope dating of Carlin-type deposits in the Great Basin, western North America, and implications for deposit genesis: Economic Geology, v. 98, p. 225-248.

Armstrong, R.L., 1970, Geochronology of Tertiary igneous rocks, eastern Basin and Range province, western Utah, eastern Nevada, and vicinity, U.S.A.: Geochimica et Cosmochimica Acta, v. 34, p. 203-232.

Bakken, B.M., 1990, Gold mineralization, wall-rock alteration, and the geochemical evolution of the hydrothermal system in the main orebody, Carlin Mine, Nevada: Ph.D. thesis, Stanford University, California, 283 p.

Barker, F., 1981, Introduction to special issue on granites and rhyolites: A commentary for the nonspecialist: Journal of Geophysical Research, v. 86, p. 10131-10135.

Barmes. C.G., Burton, B.R., Burling, T.C., Wright, J.E., and Karlsson, H.R., 2001, Petrology and geochemistry of the late Eocene Harrison Pass pluton, Ruby Mountains core complex, Northeastern Nevada: Journal of Petrology, v. 42, p. 901-929.

Bartlett, M.W., Enders, M.S., and Hruska, D.C., 1991, Geology of the Hollister gold deposit, Ivanhoe district, Elko County, Nevada, *in* Raines, G.L., Lisle, R.E., Schafer, R.W., and Wilkinson, W.H., eds., Geology and Ore Deposits of the Great Basin: Geological Society of Nevada Symposium, Reno 1991, Proceedings, p. 957-978.

Barton, M.D., 1996, Granitic magmatism and metallogeny of southwestern North America, *in* Brown, M., Candela, P.A., Peck, D.L., Stephens, W.E., Walker, R.J., and Zen, E-An, eds., Origin of Granites and Related Rocks: Geological Society of America Special Paper 315, p. 261-280.

Bawden, T.M., 2002, Supergene enrichment of copper at the Mike gold deposit, Carlin trend, Nevada: M.S. thesis, Stanford University, California, 167 p.

Bettles, K., 2002, Exploration and geology, 1962-2002, at the Goldstrike property, *in* Gold Deposits of the Carlin Trend, Thompson, T.B., Teal, L., and Meeuwig, R.O., eds.: Nevada Bureau of Mines and Geology Bulletin 111, p. 54-75.

Branham, A., and Arkell, B., 1995, The Mike gold-copper deposit, Carlin trend, Nevada, in Process mineralogy XIII: Applications to beneficiation problems, pyrometallurical products, advanced mineralogical techniques, precious metals, environmental concerns, ceramic material, hydrometallurgy and minerals exploration, proceedings, Hagni, R.D., ed.: The Minerals, Metals, and Materials Society, p. 204-211.

Brooks, W.E., Thorman, W.E., and Snee, L.W., 1995a, The $^{40}Ar/^{39}Ar$ ages and tectonic setting of the middle Eocene northeast Nevada volcanic field: Journal of Geophysical Research, v. 100, p. 10,403-10,416.

Brooks, W.E., Thorman, W.E., Snee, L.W., Nutt, C.W., Potter, C.J., and Dubiel, R.F., 1995b, Summary of chemical analyses and ^{40}Ar/^{39}Ar-spectra data for Eocene volcanic rocks from the central part of the northeast Nevada volcanic field: U.S. Geological Survey Bulletin 1988-K, p. K1-K33.

Castor, S.B., Boden, D.R., Henry, C.D., Cline, J.S., Hofstra, A.H., McIntosh, W.C., Tosdal, R.M., Wooden, J.P., 2003, Geology of the Eocene Tuscarora volcanic-hosted, epithermal precious metal district, Elko County, Nevada: Economic Geology, v. 98, p. 339-366.

Cathles, L.M., Erendi, A.H.J., and Barrie, T., 1997, How long can a hydrothermal system be sustained by a single intrusive event? Economic Geology, v. 92, p. 766–771.

Chakurian, A.M., Arehart, G.B., Donelick, R.A., Zhang, X., and Reiners, P.W., 2003, Timing constraints of gold mineralization along the Carlin trend utilizing apatite fission-track, 40Ar/39Ar, and apatite (U-Th)/He methods: Economic Geology, v. 98, p. 1159-1171.

Christiansen, R.L., and Yeats, R.S., 1992, Post-Laramide geology of the U. S. Cordilleran region, *in* Burchfiel, B.C., Lipman, P.W., and Zoback, M.L., eds., The Geology of North America, The Cordilleran Region: Geological Society of America Decade in North American Geology Series, v. G-3, p. 261-406.

Cline, J.S., Shields, D., Riciputi, L., Fayek, M., Copp, T.L., Muntean, J., and Hofstrat, A.H., 2003, Trace element and isotope microanalyses support a deep ore fluid source at the Getchell Carlin-type gold deposit, northern Nevada: Geological Society of America Abstracts with Programs, v. 35, no. 6, p. 358.

DePaolo, D.J., and Farmer, G.L., 1984, Isotopic data bearing on the origin of Mesozoic and Tertiary granitic rocks in the Western United States: Philosophical Transactions of the Royal Society of London, Series A, v. 310, p. 743-753.

DiVincenzo, G., Viti, C., and Rocchi, S.,2003, The effect of chlorite interlayering on ^{40}Ar-^{39}Ar biotite dating: an ^{40}Ar-^{39}Ar laser-probe and TEM investigations of variably chloritised biotites: Contributions To Mineralogy and Petrology, v. 145, p. 643-658.

Dobak, P.J., Arbonies, D., Hipsely, R., and Visher, M., 2002, Geology of the Storm gold deposits, *in* Gold Deposits of the Carlin Trend, Thompson, T.B., Teal, L., and Meeuwig, R.O., eds.: Nevada Bureau of Mines and Geology Bulletin 111, p. 46-53.

Drews-Armitage, S.P., Romberger, S.B., and Whitney, C.G., 1996, Clay alteration and gold deposition in the Genesis and Blue Start deposits, Eureka County, Nevada: Economic Geology, vo. 91, p. 1383-1393.

Dunbar, W., 2001, A structural model of mineralization at Deep Star, Carlin trend, Nevada, Geological Society of Nevada Special Publication No. 33, p. 243-261.

Emmons, D.L., and Eng, T.L., 1995, Geologic map of the McCoy mining district, Lander county, Nevada: Nevada Bureau of Mines and Geology Map 103, scale 1:12,000, p. 1-12.

Emsbo, P., Hofstra, A., Park, D., Zimmerman, J.M., and Snee, L., 1996, A mid-Tertiary age constraint on alteration and mineralization in igneous dikes on the Goldstrike property, Carlin trend, Nevada: Geological Society of America Abstracts with Programs, v. 28, no. 7, p. A-476.

Emsbo, P., Hofstra, A.H., and Lauha, E.A., 2000, Jurassic auriferous polymetallic mineralization at the Goldstrike mine, Carlin trend, Nevada: Geology and Ore Deposits 2000, Great Basin and Beyond Symposium, Geological Society of Nevada, Reno-Sparks, Nevada, May 2000, p. 46.

Emsbo, P., Hofstra, A.H., Lauha, E.A., Griffin, G.L., and Hutchinson, R.W., 2003, Origin of high-grade gold ore, source of ore fluid components, and genesis of the Meikle and neighboring Carlin-type deposits, northern Carlin trend, Nevada: Economic Geology, v. 98, p. 1069-1105.

Emsbo, P., Hutchinson, R.W., Hofstra, A.H., Volk, J.A., Bettles, K.H., Baschuk, G.J., and Johnson, C.A., 1999, Syngenetic Au on the Carlin trend: Implications for Carlin-type deposits: Geology, v. 27, p. 59-62.

Erickson, R.L., Silberman, M.L., and Marsh, S.P., 1978, Age and composition of igneous rocks, Edna Mountain Quadrangle, Humboldt County, Nevada: U.S. Geological Survey Journal of Research, v. 6, p. 727-743.

Evans, J.G., 1974a, Geologic map of the Welches Canyon quadrangle, Eureka County, Nevada: U.S. Geological Survey Geologic Quadrangle Map GQ-1117, scale 1:24,000.

Evans, J.G., 1974b, Geologic map of the Rodeo Creek Northeast quadrangle, Eureka County, Nevada: U.S. Geological Survey Geological Quadrangle Map GQ-1116, scale 1:24,000.

Evans, J. G., 1980, Geology of the Rodeo Creek NE and Welches Canyon quadrangles, Eureka County, Nevada: U.S. Geological Survey Bulletin 1473, 81 p.

Evans, J.G., and Ketner, K.B., 1971, Geologic map of the Swales Mountain Quadrangle and part of the Adobe Summit Quadrangle, Elko County, Nevada: U.S. Geological Survey Miscellaneous Investigations Map I-667, 1:24,000.

Evans, J.G., and Mullens, T.E., 1976, Bootstrap Window, Elko and Eureka Counties, Nevada: Journal of Research of the U. S. Geological Survey, v .4, p. 119-125.

Farmer, M., 1996, An intrusive study of the Bluestar subdistrict: Internal report, Newmont Gold Company, 33 p.

Ferdock, G.C., Castor, S.B., Leonardson, R.W., and Collins, T., 1997, Mineralogy and paragenesis of ore stage mineralization in the Betze gold deposit, Goldstrike mine, Eureka County, Nevada, *in* Vikre, P., Thompson, T.B., Bettles, K., Christensen, O., and Parratt, R., eds., Carlin-type gold deposits field conference: Society of Economic Geologists Guidebook Series, v. 28, p. 75-86.

Gillerman, V. S., 1982, Tungsten and copper skarns of the Railroad mining district, Nevada: Ph.D. dissertation, University of California, Berkeley, 195 p.

Grauch, V.J.S., 1996, Magnetically interpreted, granitoid plutonic bodies in Nevada, *in* Singer, D.A., ed., An analysis of Nevada's metal-bearing mineral resources: Nevada Bureau of Mines and Geology Open-file Report 96-2, p. 7-1 7-16.

Green, P.F., Duddy, I.R., Laslett, G.M., Hegarty, K.A., Gleadow, A.J.W., and Lovering, J.F., 1989, Thermal annealing of fission tracks in apatite: 4. Quantitative modeling techniques and extension to geological time scales: Chemical Geology, v. 79, p. 155-182.

Groff, J.A., Heizler, M.T., McIntosh, W.C., and Norman, D.I., 1997, ^{40}Ar/^{39}Ar dating and mineral paragenesis for Carlin-type gold deposits along the Getchell trend, Nevada: Evidence for Cretaceous and Tertiary gold mineralization: Economic Geology, v. 92, p. 601-622.

Hall, C.M., Simon, G., and Kesler, S.E., 1997, Age of mineralization at the Twin Creeks SHMG Deposit, Nevada, *in* Vikre, P., Thompson, T.B., Bettles, K., Christensen, O., and Parratt, R., eds., Carlin-type Gold Deposits Field Conference: Society of Economic Geologists Guidebook Series, v. 28, p. 151-154.

Hall, C.M., Kesler, S.E., Simon, G., and Fortuna, J., 2000, Overlapping Cretaceous and Eocene alteration, Twin Creeks Carlin-type deposit: Economic Geology, v. 95, p. 1739-1752.

Hausen, D.M., and Kerr, P.E., 1968, Fine gold occurrence at Carlin, Nevada, *in* Ridge, J.D., ed., Ore deposits of the United States, 1933-1967 (Graton-Sales Volume): American Institute of Mining and Metallurgial Engineers, v. 1, p. 908-940.

Hausen, D.M., Ekburg, C., and Kula, F., 1983, Geochemical and XRD-computer logging method for lithologic ore type classification of Carlin-type gold ores, in Hagni, R.D., ed., Process mineralogy II. Applications in metallurgy, ceramics, and geology: American Institute of Mining Engineers, p. 421-450.

Haynes, S.R., Hickey, K.A., Mortensen, J.K., and Tosdal, R.M., 2002, Onset of extension in the Basin and Range: Basin analysis of the Eocene Elko Formation, NE Nevada: Geological society of American Abstracts with Programs, v. 34, no. 6, p. 83.

Haynes, S.R., Hickey, K.A., and Tosdal, R.M., 2003, Golden highs and soggy bottoms: The link between Eocene paleogeography and gold deposition, northern Carlin trend, Nevada: Geological society of American Abstracts with Programs, v. 35, no. 6, p. 235-236.

Heitt, D.G., Dunbar, W.G., Thompson, T.B., and Jackson, R.G., 2003, Geology and geochemistry of the Deep Star gold deposit, Carlin trend, Nevada: Economic Geology, v. 98, p. 1107-1135.

Henry, C. D., and Boden, D. R., 1998a, Geologic map of the Mount Blitzen quadrangle, Elko County, northeastern Nevada: Nevada Bureau of Mines and Geology Map 110, scale 1:24,000.

Henry, C.D., and Boden, D.R., 1998b, Eocene magmatism: The heat source for Carlin-type gold deposits of northern Nevada: Geology, v. 26, p. 1067-1070.

Henry, C.D., and Faulds, J.E., 1999, Geologic map of the Emigrant Pass Quadrangle, Nevada: Nevada Bureau of Mines and Geology, Open-File Report 99-9, scale: 1:24,000.

Henry, C.D., Faulds, J.E., Boden, D.R., and Ressel, M.W., 2001, Timing and styles of Cenozoic extension near the Carlin trend, northeastern Nevada: Implications for the formation of Carlin-type gold deposits: Geological Society of Nevada Special Publication No. 33, p. 115-128.

Henry, C.D., and Ressel, M.W., 2000a, Eocene magmatism of northeastern Nevada: The smoking gun for Carlin-type gold deposits, *in* Cluer, J.K., Price, J.G., Struhsacker, E.M., Hardyman, R.F., and Morris, C.L., eds., Geology and Ore Deposits 2000: The Great Basin and Beyond: Geological Society of Nevada Symposium Proceedings, May 15-18 2000, p. 365-388.

Henry, C.D., and Ressel, M.W., 2000b, Eocene magmatism and its role in generating sediment-hosted gold deposits of the Carlin trend: Geological Society of Nevada Symposium 2000 Field Trip Guidebook No. 4, 223 p.

Hickey, K.A., Donelick, R.A., Tosdal, R.M., and McInnes, B.I.A., 2003, Restoration of the Eocene landscape in the Carlin-Jerritt Canyon mining district: Constraining depth of mineralization for Carlin-type Au-deposits using low-temperature apatite thermochronology: Geological society of American Abstracts with Programs, v. 35, no. 6, p. 358.

Hildenbrand, T.G., and Kucks, R.P., 1988, Total intensity magnetic anomaly map of Nevada: Nevada Bureau of Mines and Geology Map 93A, scale: 1:750,000.

Hildreth, W., 1981, Gradients in silicic magma chambers; implications for lithospheric magmatism: Journal of Geophysical Research, v. 86, p. 10153-10192.

Hofstra, A.H., 1994, Geology and genesis of the Carlin-type gold deposits in the Jerritt Canyon district, Nevada: unpublished Ph.D. dissertation, University of Colorado, Boulder, 719 p.

Hofstra, A.H., and Cline, J.S., 2000, Characteristics and models for Carlin-type gold deposits: SEG Reviews, v. 13, p. 163-220.

Hofstra, A.H., Snee, L.W., Rye, R.O., Folger, H.W., Phinisey, J.D., Loranger, R.J., Dahl, A.R., Naeser, C.W., Stein, H.J., and Lewchuk, M., 1999, Age constraints on Jerritt Canyon and other Carlin-type gold deposits in the western United States – relationship to mid-Tertiary extension and magmatism: Economic Geology, v. 94, p. 769-802.

Hofstra, A.H., John, D.A., and Theodore, T.G., 2003, A special issue devoted to gold deposits in northern Nevada: Part 2. Carlin-type deposits, Preface: Economic Geology, v. 98, p. 1063-1067.

Howard, K.A., 2000, Geologic map of the Lamoille Quadrangle, Elko County, Nevada: Nevada Bureau of Mines and Geology Geologic Map 125, 1:24,000.

Howard, K.A., Kistler, R.W., Snoke, A.W., and Willden, R., 1979, Geologic map of the Ruby Mountains, Nevada: U.S. Geological Survey Map I-1136, scale 1:125,000.

Ilchik, R.P., and Barton, M.D., 1997, An amagmatic origin of Carlin-type gold deposits: Economic Geology, v. 92, p. 269-288.

John, D.A., 2001, Miocene and early Pliocene epithermal gold-silver deposits in the northern Great Basin, western United States: Characteristics, distribution, and relationship to magmatism: Economic Geology, v. 96, p. 1827-1853.

John, D.A., Hofstra, A.H., Fleck, R.J., Brummer, J.E., and Saderholm, E.C., 2003, Geologic setting and genesis of the Mule Canyon low-sulfidation epithermal gold-silver deposit, north-central Nevada: Economic Geology, v. 98, p. 425-463.

John, D.A., and Wallace, A.R., 2000, Epithermal gold-silver deposits related to the northern Nevada rift, *in* Cluer, J.K., Price, J.G., Struhsacker, E.M., Hardyman, R.F., and Morris, C.L., eds., Geology and Ore Deposits 2000: The Great Basin and Beyond: Geological Society of Nevada Symposium Proceedings, May 15-18 2000, p. 155-175.

John, D.A., Wallace, A.R., Ponce, D.A., Fleck, R.B., and Conrad, J.E., 2000, New perspectives on the geology and origin of the northern Nevada rift, *in* Cluer, J.K., Price, J.G., Struhsacker, E.M., Hardyman, R.F., and Morris, C.L., eds., Geology and Ore Deposits 2000: The Great Basin and Beyond: Geological Society of Nevada Symposium Proceedings, May 15-18 2000, p. 127-154.

Johnston, M.K., 2000, Hypogene alteration and ore characteristics at the Cove gold-silver deposit, Lander County, Nevada, *in* Cluer, J.K., Price, J.G., Struhsacker, E.M., Hardyman, R.F., and Morris, C.L., eds., Geology and Ore Deposits 2000: The Great Basin and Beyond: Geological Society of Nevada Symposium Proceedings, May 15-18 2000, p. 621-641.

Johnston, M.K., 2003, Geology of the Cove Mine, Lander County, Nevada, and a genetic model for the McCoy-Cove magmatic-hydrothermal system: Ph.D. dissertation, University of Nevada, Reno, 353 p.

Johnston, M.K., and Ressel, M.W., 2004, Carlin-type and distal-disseminated Au-Ag deposits: Related distal expressions of Eocene intrusive centers in north-central Nevada: Society of Economic Geologists Newsletter, no. 59, p. 12-14.

Justet, L. and Spell, T.L., 2001, Effusive eruptions from a large shallow magma chamber: The Bearhead Rhyolite, Jemez Volcanic Field, New Mexico: Journal of Volcanology and Geothermal Research, v. 107, p. 241-264.

Kesler, S.E., Fortuna, J., Ye, Z., Alt, J.C., Core, D.P., Zohar, P., Borhauer, J., and Chryssoulis, S.L., 2003, Evaluation of the role of sulfidation in deposition of gold, Screamer section of the Betze-Post Carlin-type deposit, Nevada: Economic Geology, v. 98, p. 1137-1157.

Ketner, K.B., 1998, Geologic map of the southern Independence Mountains, Elko County, Nevada: U.S. Geological Survey Geologic Investigations I-2629, scale 1:24,000.

Ketner, K.B., and Smith, J.F., Jr., 1963, Geology of the Railroad mining district, Elko County, Nevada: U.S. Geological Survey Bulletin 1162-B, p. B1-B27.

Kistler, R.W., Ghent, E.D., and O'Neil, J.R., 1981, Petrogenesis of two-mica granites in the Ruby Mountains, Nevada: Journal of Geophysical Research, v. 86, p. 10591-10606.

Kuehn, C.A., and Rose, A.W., 1992, Geology and geochemistry of wall-rock alteration at the Carlin gold deposit, Nevada: Economic Geology, v. 87, p. 1697-1721.

Lauha, E.A., and Bettles, K.H., 1993, A geologic comparison of the Post/Betze and Purple Vein deposits of the Goldstrike and Meikle mines, Nevada: Society for Mining, Metallurgy, and Exploration, Inc., Pre-print 93-170, 20 p.

Le Bas, M. J., Le Maitre, R. W., Streckeisen, A., and Zanettin, B., 1986, A chemical classification of volcanic rocks based on the total alkali-silica diagram: Journal of Petrology, v. 27, p. 745-750.

Leonardson, R. W., and Rahn, J. E., 1996, Geology of the Betze-Post gold deposits, Eureka County, Nevada, *in* Coyner, A. R., and Fahey, P. L., eds., Geology and ore deposits of the American Cordillera: Geological Society of Nevada, Reno, Nevada, p. 61-94.

Longo, A.A., Thompson, T.B., and Harlan, J.B., 2002, Geologic overview of the Rain subdistrict, *in* Gold Deposits of the Carlin Trend, Thompson, T.B., Teal, L., and Meeuwig, R.O., eds.: Nevada Bureau of Mines and Geology Bulletin 111, p. 168-189.

Mathewson, D., 2001, Tectono-stratigraphic setting for the Rain district gold deposits, Carlin trend, Nevada: Geological Society of Nevada Special Publication No. 33, p. 90-109.

McGrew, A.J., and Snee, L.W., 1994, $^{40}Ar/^{39}Ar$ thermochronologic constraints on the tectonothermal evolution of the northern East Humboldt Range metamorphic core complex, Nevada: Tectonophysics, v. 238, p. 425-450.

McIntosh, W.C., and Chamberlin, R.M., 1994, 40Ar/39Ar geochronology of Middle to Late Cenozoic ignimbrites, mafic lavas, and volcaniclastic rocks in the Quemado Region, New Mexico: New Mexico Geological Society Guidebook, v. 45, p. 165-185.

McKee, E.H., Moring, B.C., and Huber, D.R., 1995, Cenozoic volcanic rocks and Cenozoic mineral deposits of Nevada: U.S. Geological Survey Open-file Report 95-248.

Mohling, J., 2002, Geology and gold mineralization of the Turf deposit, *in* Gold Deposits of the Carlin Trend, Thompson, T.B., Teal, L., and Meeuwig, R.O., eds.: Nevada Bureau of Mines and Geology Bulletin 111, p. 91-105.

Moore, S., 2002, Geology of the northern Carlin trend, *in* Gold Deposits of the Carlin Trend, Thompson, T.B., Teal, L., and Meeuwig, R.O., eds.: Nevada Bureau of Mines and Geology Bulletin 111, scale 1:24,000.

Mortensen, J.K., Thompson, J.F.H., and Tosdal, R.M., 2000, U-Pb age constraints on magmatism and mineralization in the northern Great Basin, Nevada, *in* Cluer, J.K., Price, J.G., Struhsacker, E.M., Hardyman, R.F., and Morris, C.L., eds., Geology and Ore Deposits 2000: The Great Basin and Beyond: Geological Society of Nevada Symposium Proceedings, May 15-18, 2000, p. 419-438.

Morton, J.L., Silberman, M.L., Bonham, H.F., Jr., Garside, L.J., and Noble, D.C., 1977, K-Ar Ages Of Volcanic Rocks, Plutonic Rocks, and Ore Deposits In Nevada and Eastern California--Determinations Run Under The USGS-NBMG Cooperative Program: Isochron/West, no. 20, p. 19-29.

Norby, J.W., 2002, Geology of the Maggie Creek district, Carlin trend, Eureka County, Nevada, *in* Gold Deposits of the Carlin Trend, Thompson, T.B., Teal, L., and Meeuwig, R.O., eds.: Nevada Bureau of Mines and Geology Bulletin 111, scale 1:18,000.

Norby, J.W., and Orobona, M.J.T., 2002, Geology and mineral systems of the Mike deposit, *in* Gold Deposits of the Carlin Trend, Thompson, T.B., Teal, L., and Meeuwig, R.O., eds.: Nevada Bureau of Mines and Geology Bulletin 111, p. 143-167.

Orobona, M.J.T., 1996, Structural setting of the Bluestar subdistrict: Implications for the origin of the Carlin trend, Eureka County, Nevada: unpublished M.S. thesis, Queens University, Kingston, Ontario, Canada, 207 p.

Peccerillo, A., and Taylor, S.R., 1976, Geochemistry of Eocene calc-alkaline volcanic rocks from the Kastamonu area, northern Turkey: Contributions to Mineralogy and Petrology, v. 58, p. 63-81.

Peters, S.G., 2003, Geologic map of the Bobs Flat Quadrangle, Eureka County, Nevada: Nevada Bureau of Mines and Geology Map 138, scale 1:24,000.

Phinisey, J. D., Hofstra, A. H., Snee, L. W., Roberts, T. T., Dahl, A. R., and Loranger, R. J., 1996, Evidence for multiple episodes of igneous and hydrothermal activity and constraints on the timing of gold mineralization, Jerritt Canyon district, Elko County, Nevada, *in* Coyner, A. R., and Fahey, P. L., eds., Geology and ore deposits of the American Cordillera: Geological Society of Nevada, Reno, Nevada, p. 15-39.

Radtke, A.S., 1985, Geology of the Carlin gold deposit, Nevada: U. S. Geological Survey Professional Paper 1267, 124 p.

Radtke, A.S., Rye, R.O., and Dickson, F.W., 1980, Geology and stable isotopes of the Carlin gold deposit, Nevada: Economic Geology, v. 75, p. 641-672.

Rayias, A.C., 1999, Stratigraphy, structural geology, alteration, and geochemistry of the northeastern Railroad district, Elko County, Nevada: M.S. thesis, University of Nevada, Reno, 180 p.

Renne, P.R., Swisher, C.C., Deino, A.L., Karner, D.B., Owens, T.L., and DePaolo, D.J., 1998, Intercalibration of standards, absolute ages and uncertainties in $^{40}Ar/^{39}Ar$ dating: Chemical Geology, v. 145, p. 117-152.

Ressel, M.W., Noble, D.C., Henry, C.D., and Trudel, W.S., 2000a, Dike-hosted ores of the Beast deposit and the importance of Eocene magmatism in gold mineralization of the Carlin trend, Nevada: Economic Geology, v. 95, p. 1417-1444.

Ressel, M.W., Noble, D.C., Henry, C.D., and Trudel, W.S., 2001, Dike-hosted ores of the Beast deposit and the importance of Eocene magmatism in gold mineralization of the Carlin trend, Nevada – A reply: Economic Geology, v. 96, p. 666-668.

Ressel, M.W., Noble, D.C., Volk, J.A., Lamb, J.B., Park, D.E., Conrad, J.E., Heizler, M.T., and Mortensen, J.K., 2000b, Precious-metal mineralization in Eocene dikes at Griffin and Meikle: Bearing on the age and origin of gold deposits of the Carlin trend, Nevada, *in* Cluer, J.K., Price, J.G., Struhsacker, E.M., Hardyman, R.F., and Morris, C.L., eds., Geology and Ore Deposits 2000: The Great Basin and Beyond: Geological Society of Nevada Symposium 2000 Proceedings, p. 79-101.

Roberts, R.J., 1964, Stratigraphy and structure of the Antler Peak quadrangle, Humboldt and Lander Counties, Nevada: U.S. Geological Survey Professional Paper 459-A, 93 p.

Rodriguez, B.D., 1998, Regional crustal structure beneath the Carlin trend, Nevada based on deep electrical geophysical measurements, *in* Tosdal, R.M., ed., Contributions to the Au metallogeny of northern Nevada: U.S. Geological Survey Open-file report 98-338, p. 15-19.

Seedorff, E., 1991, Magmatism, extension, and ore deposits of Eocene to Holocene age in the Great Basin – mutual effects and preliminary proposed genetic relationships, *in* Raines, G.L., Lisle, R.E., Schafer, R.W., and Wilkinson, W.H., eds., Geology and Ore Deposits of the Great Basin: Geologic Society of Nevada Symposium Proceedings, p. 133-178.

Seedorff, E., and Barton, M.D., 2004, Enigmatic origin of Carlin-type deposits: an amagmatic solution? Society of Economic Geologists Newsletter, no. 59, p. 14-18.

Shallow, L.J., 1999, Refractory ores at the Rain mine, Nevada: Structural controls, wallrock alteration, petrography, and geochemistry: M.S. thesis, University of Nevada, Reno, 150 p.

Sillitoe, R.H., and Bonham, H.F., Jr., 1990, Sediment-hosted gold deposits: Distal products of magmatic-hydrothermal systems: Geology, v. 18, p. 157-161.

Sloan, J., Henry, C.D., Hopkins, M., and Ludington, S., 2003, Revision of National Geochronological Database: U.S. Geological Survey Open-File Report 03-236, http://wrgis.wr.usgs.gov/open-file/of03-236/.

Smith, J.F., Jr., and Ketner, K.B., 1976, Stratigraphy of post-Paleozoic rocks and summary of resources in the Carlin-Piñon Range area, Nevada: U.S. Geological Survey Professional Paper 867-B, 48 p.

Smith, J.F., Jr., and Ketner, K.B., 1978, Geologic map of the Carlin-Piñon Range area, Elko and Eureka Counties, Nevada: U.S. Geological Survey Miscellaneous Investigations Map I-1028.

Snoke, A.W., Howard, K.A., McGrew, A.J., Burton, B.R., Barnes, C.G., Peters, M.T., and Wright, J.E., 1997, The grand tour of the Ruby-East Humboldt metamorphic core complex, northeastern Nevada: Brigham Young University Geological Studies, v. 42, p. 1, p. 225-269.

Steiger, R.H., and Jäger, E., 1977, Subcommission on geochronology: Convention on the use of decay constants in geo- and cosmochronology: Earth and Planetary Science Letters, v. 36, p. 359-362.

Stewart, J.H., and Carlson, J. E., 1976, Geologic map of north-central Nevada: Nevada Bureau of Mines and Geology Map 50, scale 1:250,000.

Stewart, J.H., and Carlson, J.E., 1978, Geologic map of Nevada: U.S. Geological Survey in collaboration with Nevada Bureau of Mines and Geology, scale: 1:500,000.

Teal, L., and Jackson, M., 1997, Geologic overview of the Carlin trend gold deposits and descriptions of recent deep discoveries: SEG Newsletter, no. 31, p. 1, 13-25.

Theodore, T.G., 2000, Geology of pluton-related gold mineralization at Battle Mountain, Nevada: Center for Mineral Resources, Tucson, Arizona, Monographs in Mineral Resource Science No. 2, 271 p.

Theodore, T.G., Silberman, M.L., and Blake, D.W., 1973, Geochemistry and Potassium-Argon ages of plutonic rocks in the Battle Mountain Mining District, Lander County, Nevada: U.S. Geological Survey Professional Paper 798-A, 24 p

Thorman, C.H., Brooks, W.E., Snee, L.W., Hofstra, A.H., Christensen, O.D., and Wilton, D.T., 1995, Eocene-Oligocene model for Carlin-type deposits in northern Nevada, *in* Coyner, A.R., and Fahey, P.L., eds., Geology and ore deposits of the American Cordillera, Symposium Proceedings: Geological Society of Nevada, Reno, p. 75.

Tosdal, R.M., Cline, J.S., Fanning, C.M., and Wooden, J.L., 2003, Lead in the Getchell-Turquoise Ridge Carlin-type gold deposits from the perspective of potential igneous and sedimentary rock sources in northern Nevada: implications for fluid and metal sources: Economic Geology, v. 98, p. 1189-1211.

Tosdal, R.M., Wooden, J.L., and Kistler, R.W., 2000, Geometry of the Neoproterozoic continental breakup, and implications for location of Nevadan mineral belts, *in* Cluer, J.K., Price, J.G., Struhsacker, E.M., Hardyman, R.F., and Morris, C.L., eds., Geology and Ore Deposits 2000, The Great Basin and Beyond, Symposium Proceedings, Geological Society of Nevada, Reno, p. 451-466.

Tosdal, R.M., Hickey, K.A., Donelick, R.A., Arehart, G.A., and Chakurian, A.M., 2003, Distinguishing hydrothermal events using apatite fission-track thermochronology; implications for Au-mineralisation in the Carlin – Jerritt Canyon region, northern Nevada: Geological Society of America Abstracts with Programs, v. 35, no. 6 p. 402.

Tretbar, D.R., Arehart, G.B., and Christensen, J.N., 2000, Dating gold deposition in a Carlin-type gold deposit using Rb/Sr methods on the mineral galkhaite: Geology, v. 28, p. 947-950.

Wallace, A.R., 1993, Geologic map of the Snowstorm Mountains and vicinity, Elko and Humboldt Counties, Nevada: U.S. Geological Survey Miscellaneous Investigation Series Map I-2394, scale 1:50,000.

Wallace, A.R., 2003a, Geologic map of the Willow Creek Reservoir SE Quadrangle, Elko, Eureka, and Lander Counties, Nevada: Nevada Bureau of Mines and Geology Map 136, 1:24,000, 15 p.

Wallace, A.R., 2003b, Geology of the Ivanhoe Hg-Au district, northern Nevada: influence of Miocene volcanism, lakes, and active faulting on epithermal mineralization: Economic Geology, v.98 p. 409-424.

Williams, C.L., Thompson, T.B., Powell, J.L., and Dunbar, W., 2000, Gold-bearing breccias of the Rain Mine, Carlin trend, Nevada: Economic Geology, v. 95, p. 391-404.

Wooden, J.L., Kistler, R.W., and Tosdal, R.M., 1998, Pb isotopic mapping of crustal structure in the northern Great Basin and relationships to Au deposit trends, *in* Tosdal, R.M., ed., Contributions to the Au metallogeny of northern Nevada: U.S. Geological Survey Open-file report 98-338, p. 20-33.

Zoback, M.L., McKee, E.H., Blakely, R.J., and Thompson, G.A., 1994, The northern Nevada rift: Regional tectonomagmatic relations and middle Miocene stress direction: Geological Society of America Bulletin, v. 106, p. 371-382.
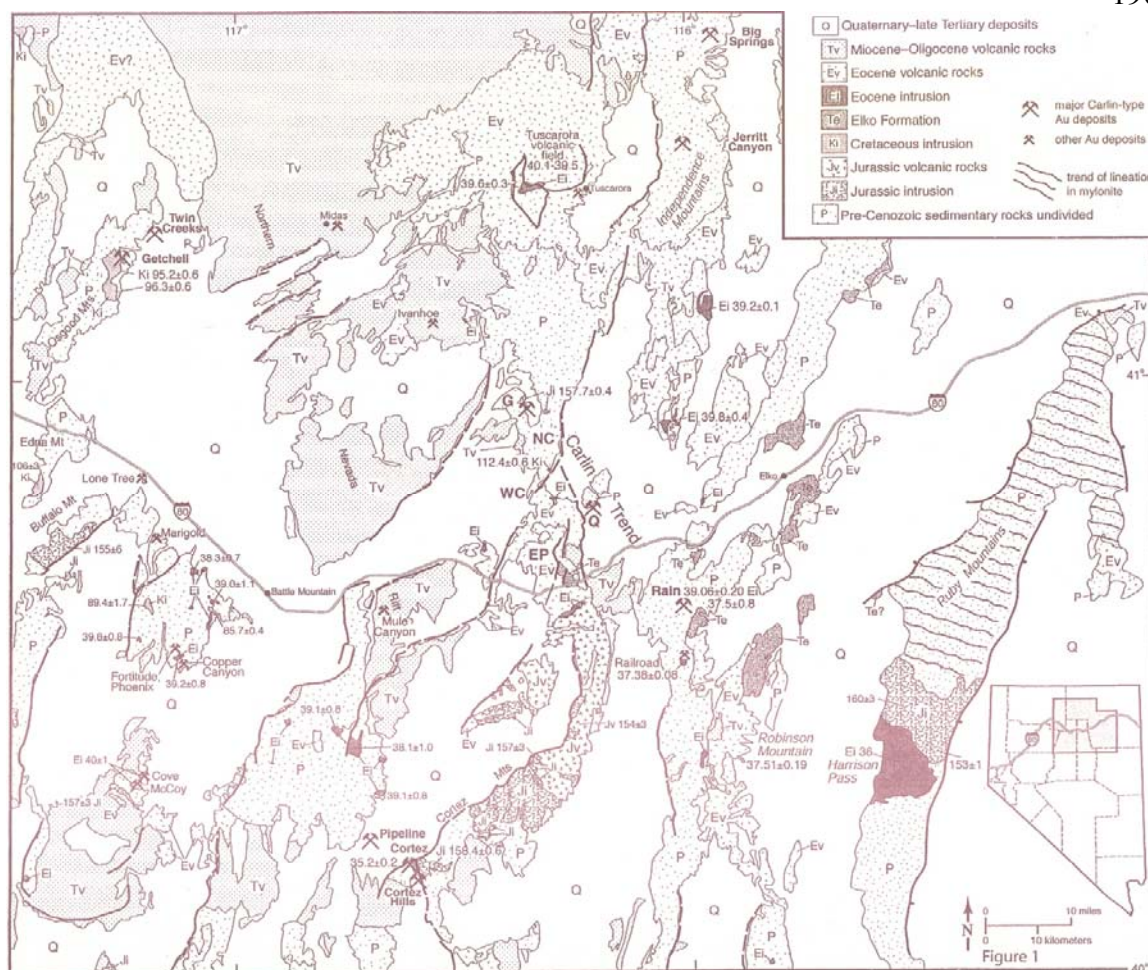
Fig. 3-1. Geologic map of northeastern Nevada (modified from Stewart and Carlson, 1976, 1978), showing Carlin trend, major Carlin-type and other Au deposits, and ages of major Jurassic, Cretaceous, and Eocene intrusions and volcanic rocks. U-Pb and $^{40}Ar/^{39}Ar$ ages are in larger type; K-Ar ages, most of which are on biotite, are in smaller type. Jurassic intrusions in this and adjacent areas cluster tightly at ~158 Ma. Cretaceous intrusions show a wider range between 112 and 86 Ma. Sources: Armstrong, 1970; Erickson et al., 1978; Kistler et al., 1981; Emmons and Eng, 1995; Mortensen et al., 2000; Theodore, 2000; Castor et al., 2003; Sloan et al., 2003; this study. NC = northern Carlin trend, G = Goldstrike mine, Q = Gold Quarry mine, WC = Welches Canyon, EP = Emigrant Pass volcanic field.
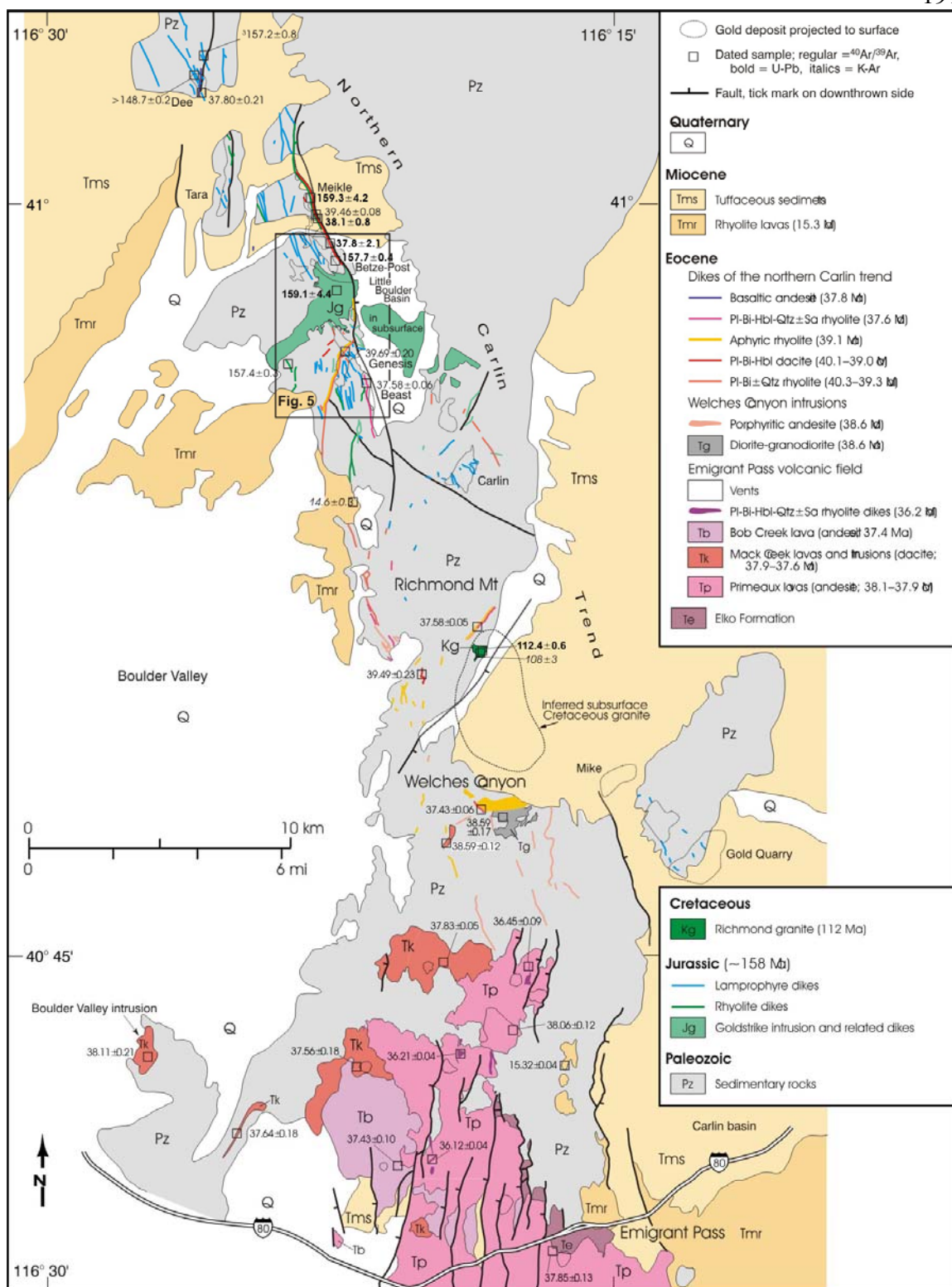
Figure 2

Fig. 3-2. Geologic map of the northern and central Carlin trend emphasizing Jurassic, Cretaceous, Eocene, and Miocene igneous rocks. Jurassic and Eocene dikes and shallow intrusions are abundant throughout this area. Eocene magmatism occurred between ~40 and 36 Ma, contemporaneous with formation of Carlin-type deposits. Box shows area of more detailed map of Figure 3-3. Geology from Evans (1974a, b), Stewart and Carlson (1976), Henry and Faulds (1999), Moore (2002), Norby (2002), Peters (2003), and this study.
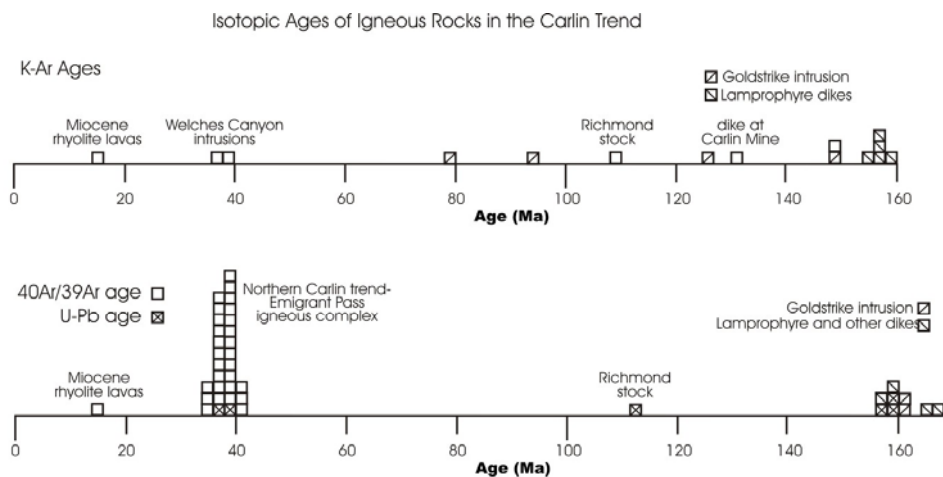
Fig. 3-3. Histogram of isotopic ages of igneous rocks of the Carlin trend. Early K-Ar dating suggested a wide range of activity in the Mesozoic. More precise ^{40}Ar/^{39}Ar and U-Pb dating demonstrate that igneous activity was concentrated in four distinct episodes at ~158 Ma, 112 Ma, 40-36 Ma, and 15 Ma. Data from Table 3-1 and Evans, 1980; Hauser et al., 1983; Theodore et al., 1998; and Mortensen et al., 2000).

194
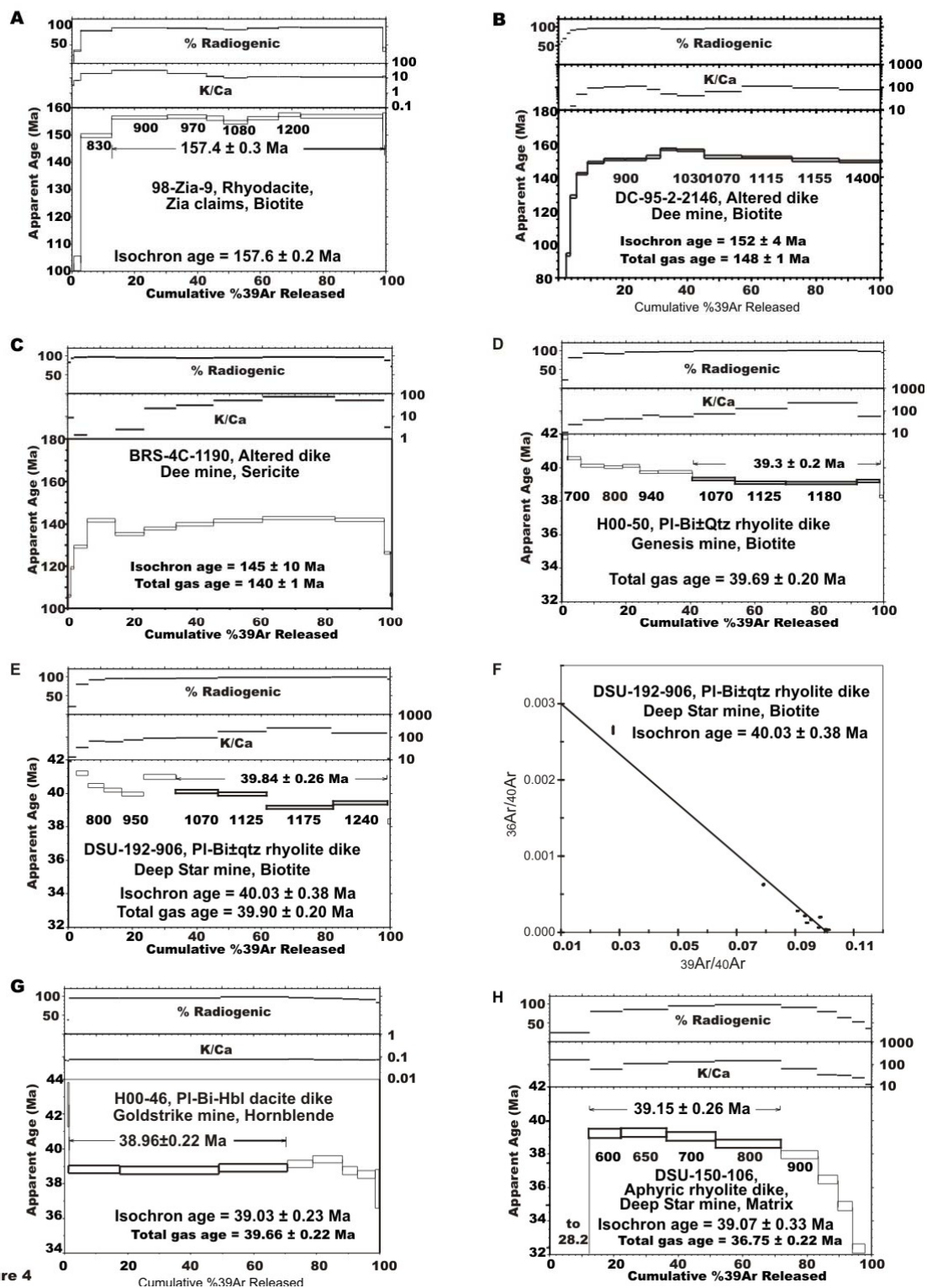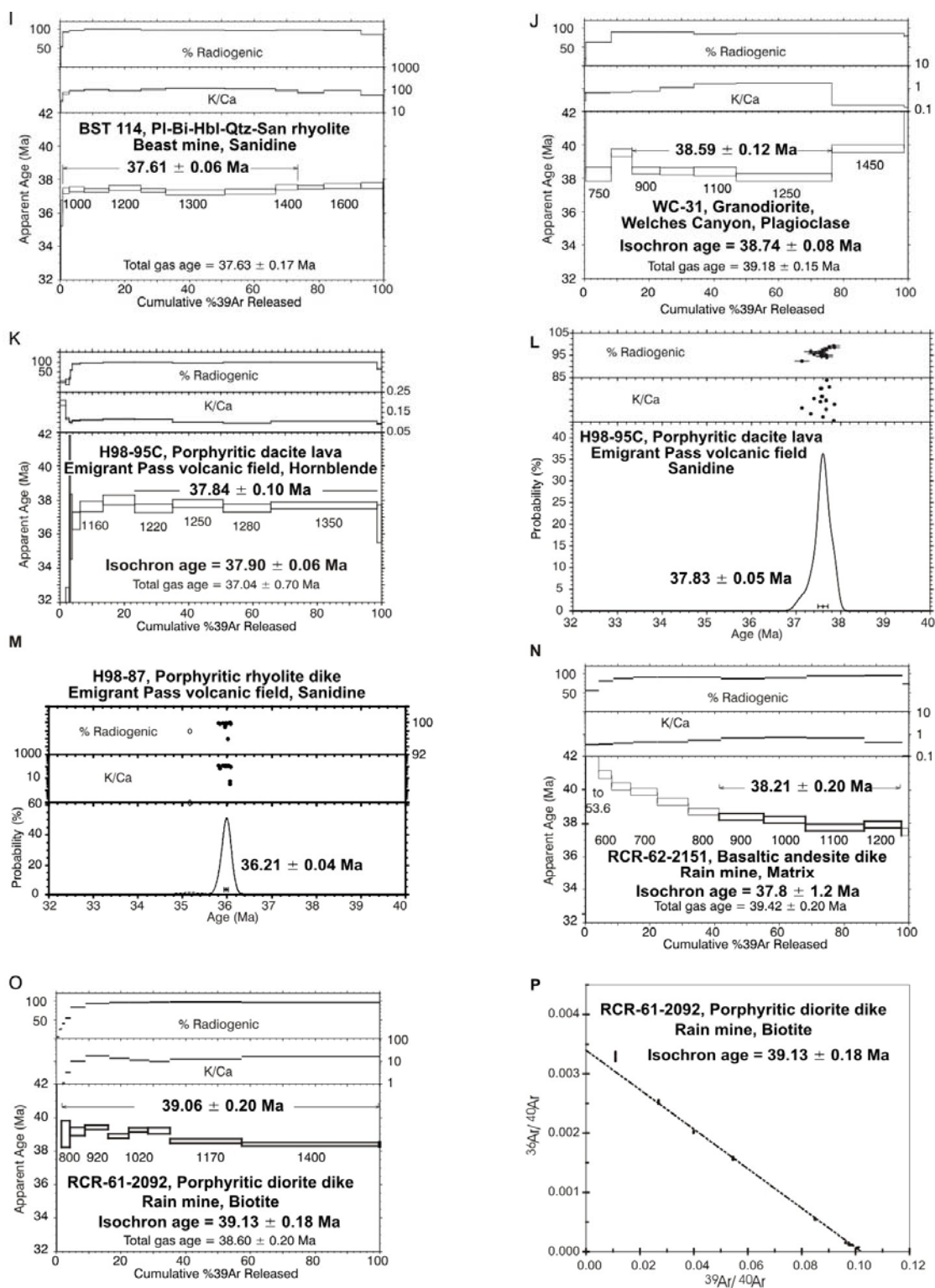
Figure 4

Figure 4 continued

Fig. 3-4. Representative ^{40}Ar/^{39}Ar age spectra, isochrons, and single crystal analyses. Additional spectra are presented in Ressel et al. (2000a, b). **A**. 98-Zia-9, biotite, rhyodacite dike, Zia claims. The mostly flat spectrum gives a plateau age of 157.4±0.3 Ma. Low apparent ages from low-temperature steps suggest minor reheating and Ar loss. **B**. DC-95-2-2146, biotite, altered dike, Dee mine. Best age estimate from this slightly disturbed spectrum, which did not plateau, is about 157 Ma, the ages of the two oldest steps. Low ages at low temperature probably reflect Ar loss from reheating. **C**. BRS-4C-1190, sericite, altered dike, Dee mine. Relatively disturbed spectrum indicates a probable alteration age greater than 143 Ma, the age of the highest temperature steps, and significant Ar loss. **D**. H00-50, biotite, rhyolite dike, Genesis mine. Dropping spectrum suggests ^{39}Ar loss from recoil, probably related to minor chloritization of the biotite. Total gas age of ~39.7 Ma is probably best estimate of emplacement. **E**. DSU-192-906, biotite, rhyolite dike, Deep Star mine. Irregular spectrum probably indicates ^{39}Ar loss from recoil, probably related to minor chloritization. Best age estimate is 40.0 Ma from isochron (Fig. 3-5F), which is consistent with a total gas age of 39.9 Ma. **F**. DSU-192-906, biotite from rhyolite dike, Deep Star mine. Inverse isochron indicates an age of ~40.0 Ma. **G.** H00-46, hornblende, dacite dike, Goldstrike mine. Flat spectrum gives a plateau age of 38.95±0.22 Ma, which is consistent with the isochron age of 39.03±0.23 Ma. **H.** DSU-150-106, whole rock, aphyric rhyolite, Deep Star mine. Disturbed spectrum probably reflects poor Ar retention and ^{39}Ar recoil from the fine matrix of potassium feldspar and quartz. Although somewhat arbitrary, best age estimate is 39.15±0.26 Ma, a weighted mean of the four steps in bold. This is supported by an indistinguishable isochron age of 39.07±0.33 Ma. **I.** BST 114, sanidine, rhyolite dike, Beast mine. Well

behaved, flat spectrum gives age of 37.61±0.11 Ma, which is consistent with ages of 37.58±0.06 from single crystal analysis of same sample and 37.55±0.07 Ma from step heating of biotite (Ressel et al., 2000a). **J.** WC-31, plagioclase, granodiorite, Welches Canyon. Slightly disturbed spectrum gives a plateau age of 38.59±0.17 Ma, which is consistent with isochron age of 38.74±0.08 Ma. Isochron data suggest minor excess Ar. **K** . H98-95C, hornblende, dacite lava, Emigrant Pass volcanic field. Plateau age of 37.84±0.10 Ma agrees well with single crystal sanidine age of 37.83±0.05 Ma from same sample (Fig. 3-5L). **L**. H98-95C, sanidine, dacite lava, Emigrant Pass volcanic field. Analyses of 15 single grains of sanidine give a weighted mean age of 37.83±0.05 Ma. **M**. H98-87, sanidine, rhyolite dike, Emigrant Pass volcanic field. Analyses of 14 single grains of sanidine give a weighted mean age of 36.21±0.04 Ma. One age of ~35.2 Ma on a plagioclase grain, indicated by low K/Ca, was discarded. **N**. RCR-62-2151, matrix, basaltic andesite dike, Rain mine. Slightly disturbed, dropping spectrum probably indicates ^{39}Ar loss from the fine matrix. Best age estimates are ~38.2 Ma, a weighted mean of four steps from relatively flat part of spectrum, and ~37.8 Ma from isochron. **O**. RCR-61-2092, biotite, diorite dike, Rain mine. Slightly irregular spectrum gives a weighted mean age of 39.06±0.20 Ma, in good agreement with isochron age of 39.13±0.18 Ma (Fig. 3-5P). **P**. RCR-61-2092, biotite, diorite dike, Rain mine. Isochron indicates age of 39.1 Ma.

Q

116°23'

Pzu

Tms

37.8±2.1
158.9±0.2

40°59'

Pzl

Q

Post fault

157.7±0.4

Tms

Betze-Post

Pzu

40.13±0.21

Pzl

38.95±0.22

Pzl

39.32±0.11
39.5±0.4

Jg
160.2±1.7
160.8±2.1

159.1±4.4

Mine dump

Mine dump

Jg

Deep Star

Tms

38.98±0.05
39.15±0.26
39.90±0.20

Pzu

Jg

Pzu

Pzl

39.69±0.20

Genesis

Pzu

Mine dump

157.4±0.3

Q

Gen fault

40.3±0.2

Pzl

37.55±0.07
37.58±0.06

N

Jg

Mine dump

Pzu

Pzl

Beast

Tmr

Pzu

40°56'

40°56'

116°23'

Pzu

116°21'

Tms

Legend

⬭ Gold deposit projected to surface

□ Dated sample; regular = $^{40}Ar/^{39}Ar$, bold = U-Pb

Mine dump

Quaternary
Q

Miocene
Tms Tuffaceous sediments
Tmr Rhyolite lavas

Eocene
Pl-Bi-Hbl-Qtz±Sa rhyolite dikes
Aphyric rhyolite dikes
Pl-Bi-Hbl dacite dikes
Pl-Bi±Qtz rhyolite dikes

Jurassic
Lamprophyre dikes
Rhyolite dikes
Jg Goldstrike intrusion and related dikes

Paleozoic
Pzu Upper plate, Roberts Mtn allochton
Pzl Lower plate, Roberts Mtn allochton

0   1 mi
1 km

Figure 5

Fig. 3-5. Geologic map of the Betze-Post to Beast mines part of the northern Carlin trend (from Evans, 1974b; Moore, 2002; and this study.
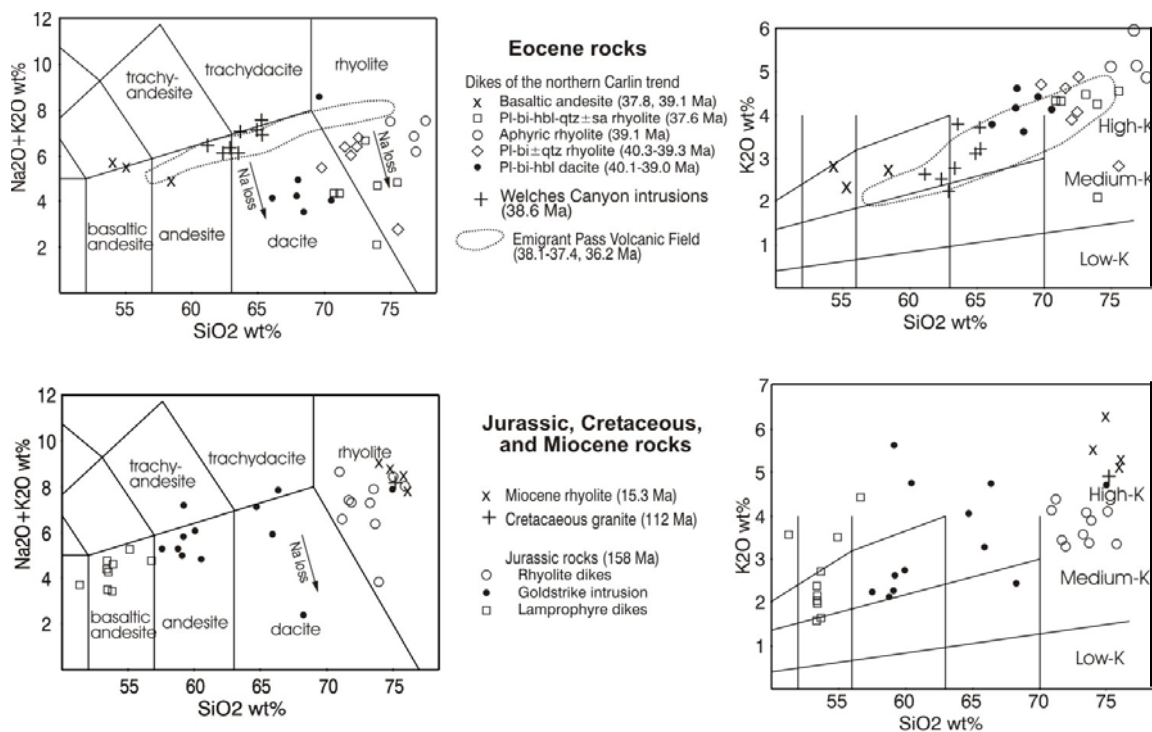
Fig. 3-6. Total alkalis ($Na_2O + K_2O$) versus SiO_2 and K_2O versus SiO_2 diagrams illustrating the range of compositions of the four igneous suites of the Carlin trend. Low total alkalis in many rocks reflect Na loss from alteration. The field of compositions of Emigrant Pass rocks is probably the best indication of pre-alteration compositions of Eocene dikes of the northern Carlin trend. Rock classifications from LeBas et al. (1986) and Peccerillo and Taylor (1976). Data: Table 3-3 and M.W. Ressel and C.D. Henry, unpublished

E

F

bi

hbl

G

glassy

devitrified

H

sa

bi

I

ol

px

pl

J
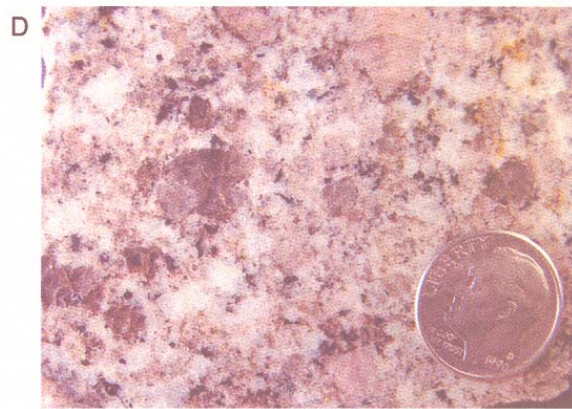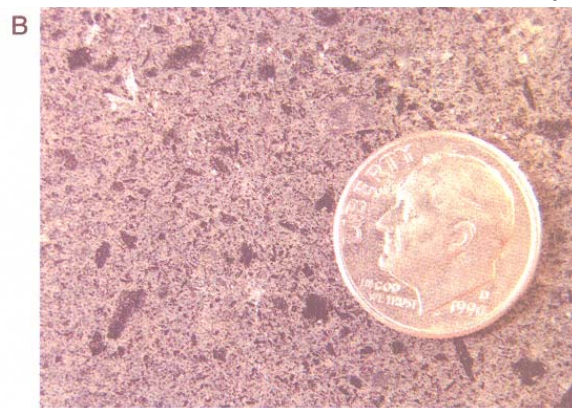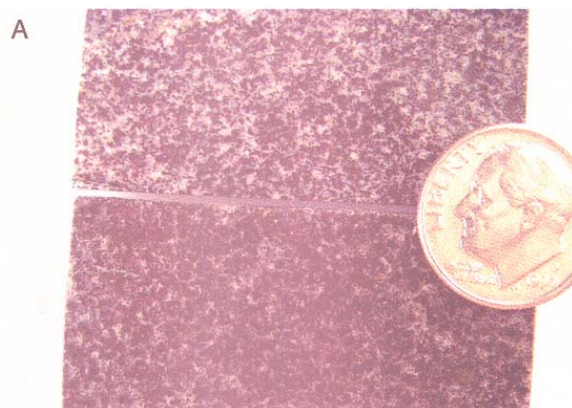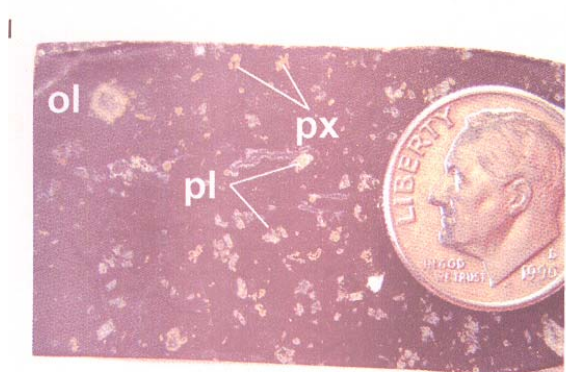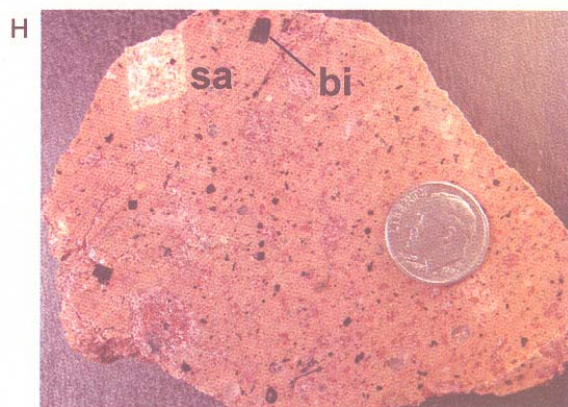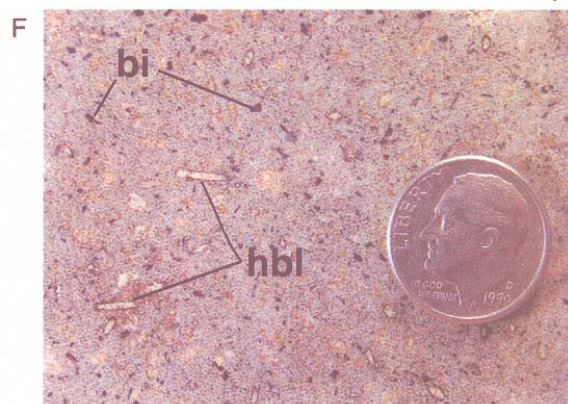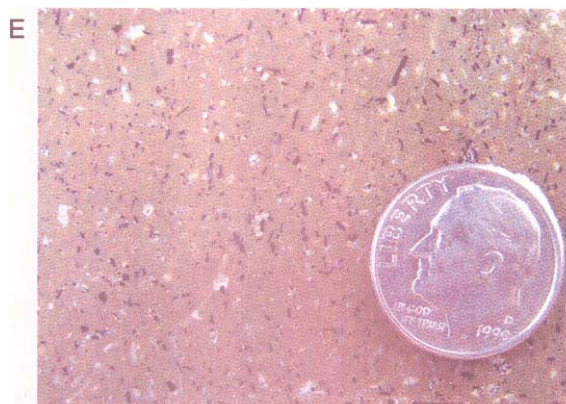
Fig. 3-7. Images of representative igneous rocks. The coin is approximately 18 mm wide. **A**. Equigranular intermediate rocks of the Goldstrike laccolith (158 Ma). Upper sample is plagioclase-hornblende-biotite-quartz granodiorite from the southern, upper part of the laccolith at the North Star mine. Lower sample is plagioclase-hornblende-clinopyroxene-biotite diorite from the central part of the laccolith at the Goldstrike mine. **B**. Phlogopite-phyric lamprophyre (158 Ma) from dike at the Goldstrike mine. Large dark minerals are clinopyroxene and hornblende(?) altered to a mixture of chlorite and carbonate minerals. Groundmass consists of potassium feldspar, phlogopite and lesser quartz. **C**. Quartz-sericite altered finely porphyritic rhyolite (158 Ma) from a dike at the Meikle mine. White minerals are plagioclase phenocrysts altered to sericite. Other phenocrysts not resolvable in image are biotite altered to sericite and rare quartz. **D**. Coarse grained granite (112 Ma) from the Richmond stock, which contains large phenocrysts of perthite (pink) and quartz (gray), with smaller grains of plagioclase (white) and sparse biotite (black). **E**. Finely porphyritic (plagioclase-biotite±quartz) rhyolite (40.3–39.3 Ma) with brown glassy matrix from a dike at the Goldstrike mine. **F**. Weakly clay altered porphyritic (plagioclase-biotite-hornblende) dacite (40.1–39.0 Ma) from a dike at the Goldstrike mine. Conspicuous hornblende phenocrysts (hb) are altered to montmorillonite and calcite, whereas biotite (bi) is unaltered. **G**. Aphyric rhyolite (39.1 Ma) from a dike at the Deep Star mine. Left sample consists of flow-banded, hydrated red glass that characterizes margins of dikes; right sample is of devitrified core of a dike, which consists mainly of spherulitic potassium feldspar and quartz intergrowths. **H**. Argillically-altered porphyritic (plagioclase-biotite-hornblende-quartz±sanidine) rhyolite (37.6 Ma) from a thick dike at the Beast mine. Large sanidine (sa) phenocryst is altered to kaolinite and barite; biotite (bi) phenocrysts are fresh. **I**. Basaltic andesite (37.8 Ma) from the Dee mine. Phenocrysts consist of plagioclase (pl),

clinopyroxene (px), and altered olivine (ol) in a holocrystalline matrix. **J**. Flow-banded rhyolite (~15 Ma) from a lava flow west of the Carlin mine. Sparse phenocrysts consist of sanidine, quartz, and fayalitic olivine.

Figure 8

I. Welches Canyon Intrusions

J. Primeaux Lavas — Emigrant Pass volcanic field

K. Mack Creek Lavas — Emigrant Pass volcanic field

L. Bob Creek Lava — Emigrant Pass volcanic field

M. Porphyritic Rhyolite-Dacite Dikes — Emigrant Pass volcanic field
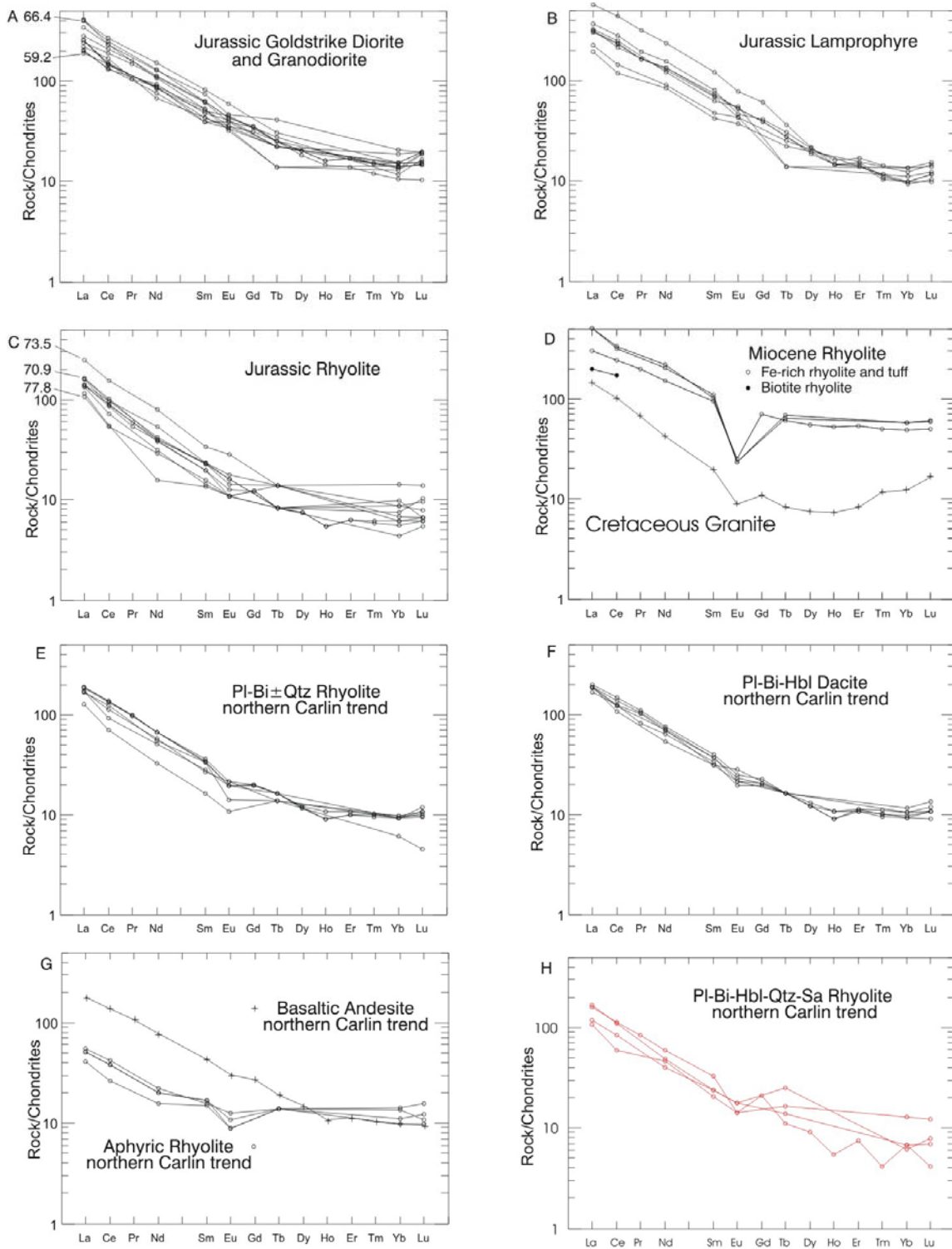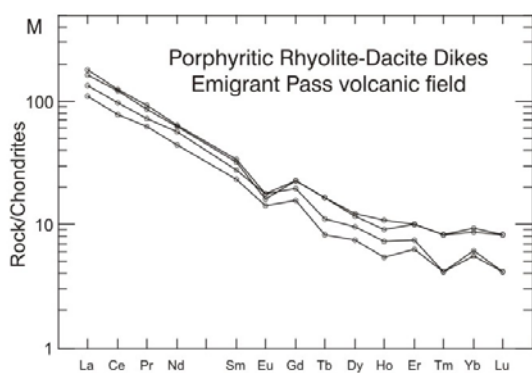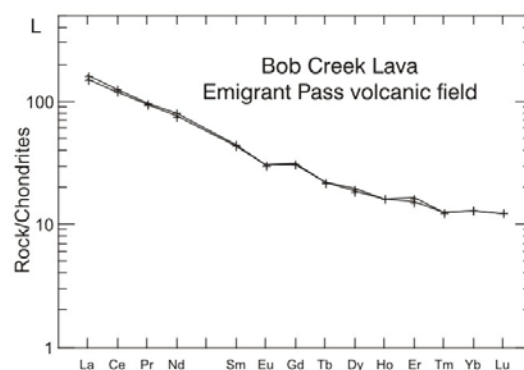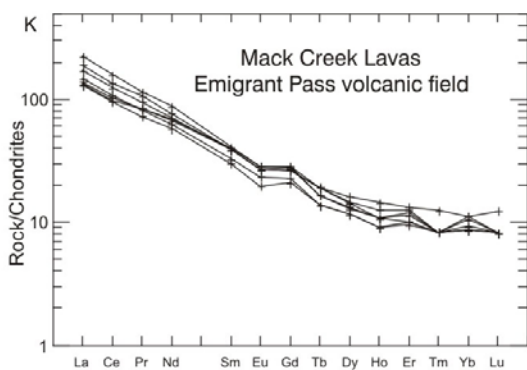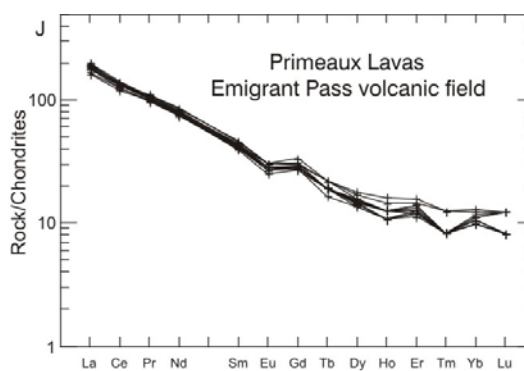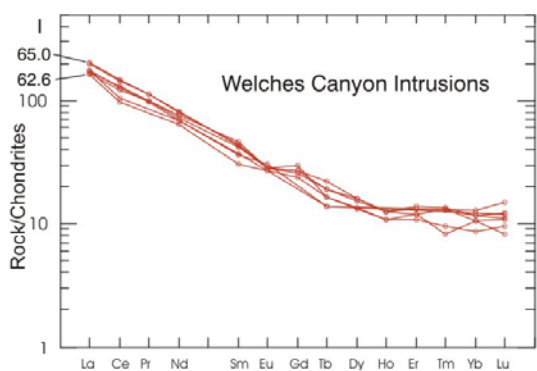
Fig. 3-8. Chondrite-normalized rare earth element patterns for rocks of the Carlin trend (normalization values from Anders and Grevesse, 1989). A-C. Jurassic rocks. LREE concentrations generally increase with increasing SiO_2 in the Goldstrike diorite and related rocks. Numbers at left are weight percent SiO_2. Lamprophyres have the highest REE concentrations of any Jurassic rocks. LREE generally decrease with increasing SiO_2 in rhyolites, with one anomalous sample. D. Miocene rhyolite and Cretaceous granite. Biotite rhyolite was analyzed by XRF only, and only La and Ce were determined. E-M. Eocene rocks. Zig-zag pattern in HREE results because the low concentrations of odd atomic number elements (Tb, Ho, Tm, and Lu) were near detection limits. A trend through the even-numbered elements (Gd, Dy, Er, and Yb) is probably more representative of the patterns.
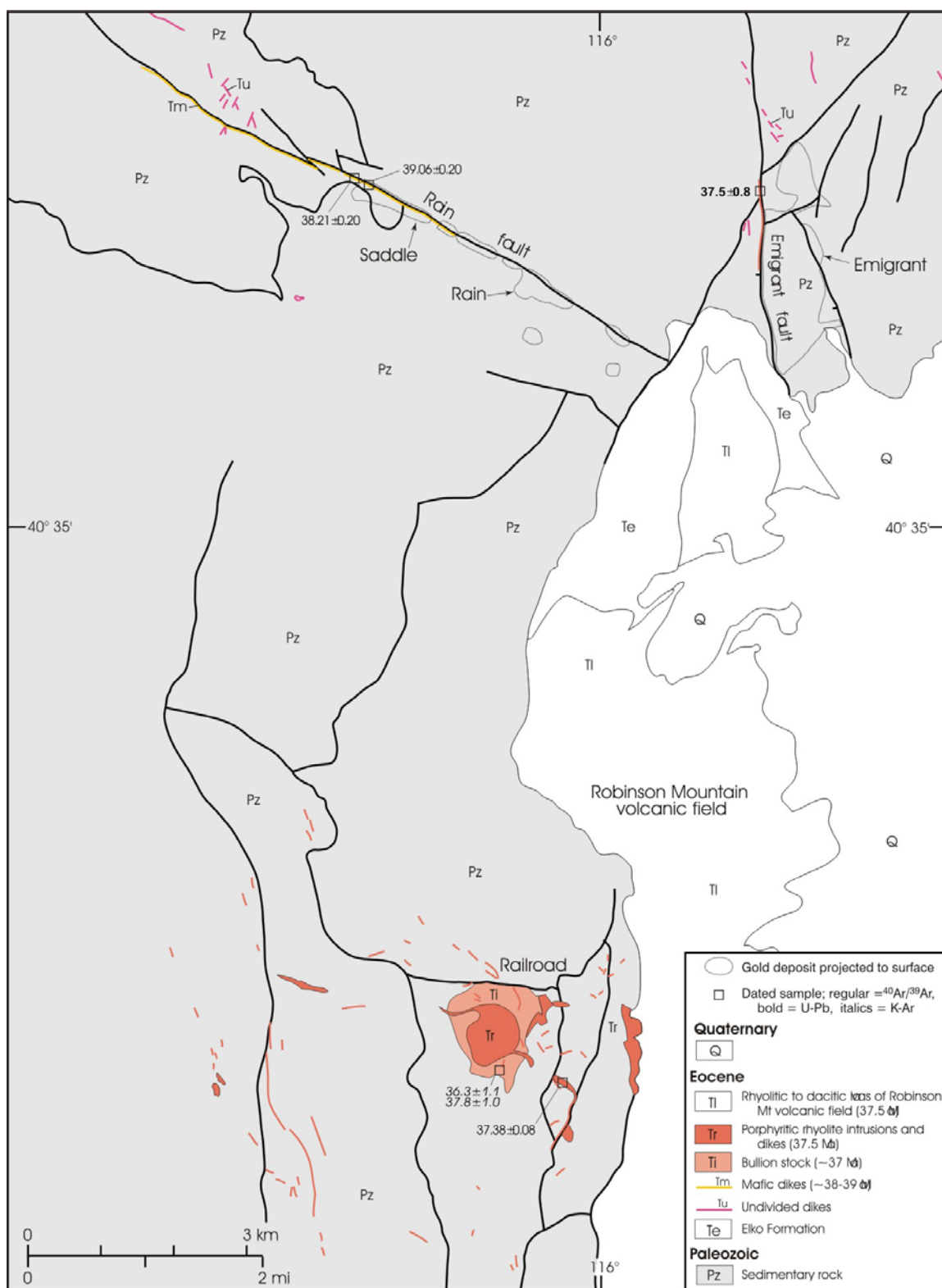
Figure 9

Fig. 3-9. Simplified geologic map of the Rain mine, Emigrant deposit, and Railroad mining district of the southern Carlin trend (modified from Ketner and Smith, 1963; Smith and Ketner, 1978; Mathewson, 2001; Longo et al., 2002; and unpublished geologic maps by Newmont Mining Corporation). K-Ar dates in the Railroad district are from Smith and Ketner (1976), and the U-Pb date in the Emigrant area is from S. Garwin (in Longo et al., 2001).
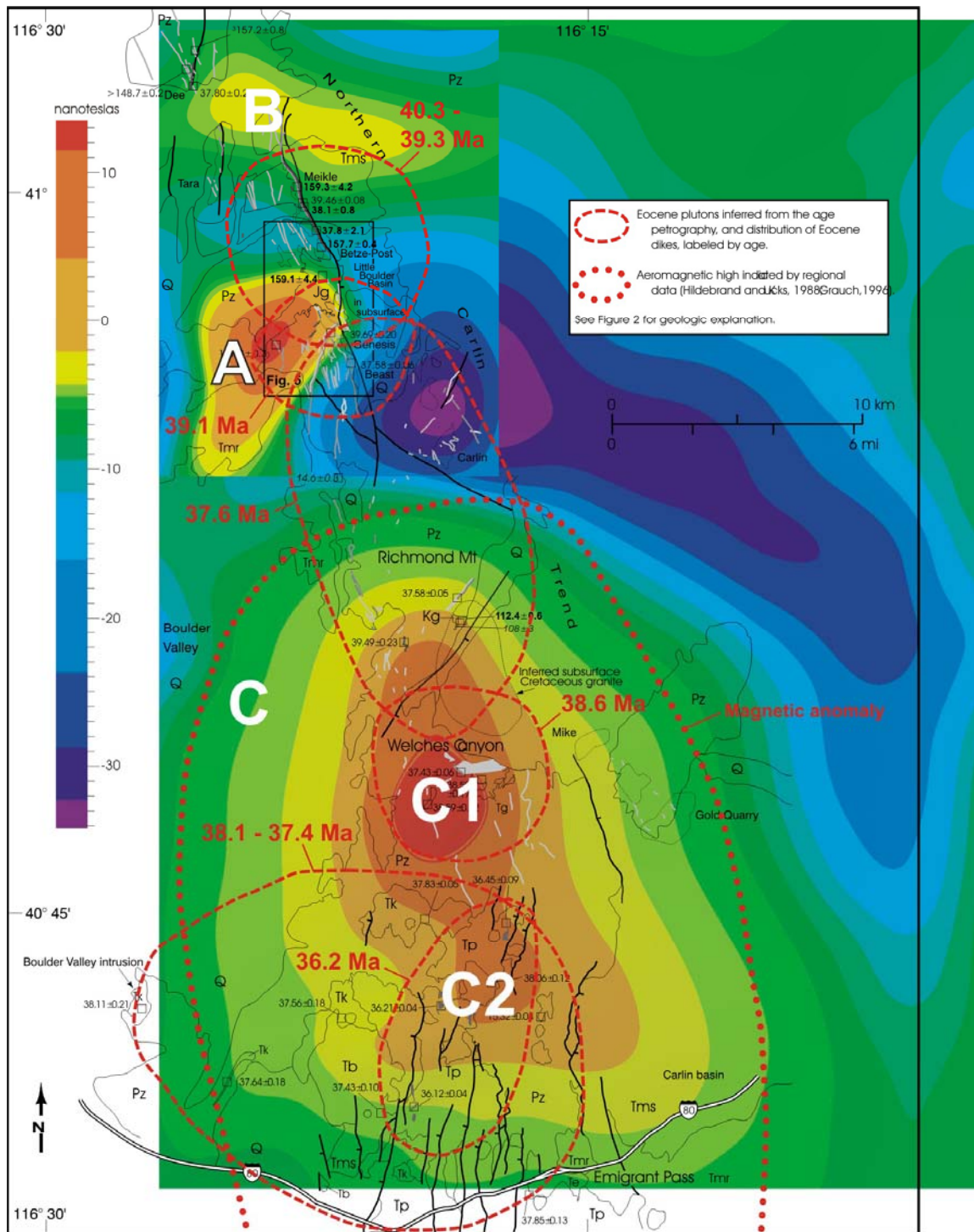
Figure 10

Fig. 3-10. Geologic map of the northern and central Carlin trend from Figure 3-2, showing aeromagnetic data upward continued to 2000 m (M.A. Goldie, written communication, 2004) and Eocene plutons inferred from the age, petrography, and distribution of Eocene dikes (dashed lines labeled by age). The age, petrography, and distribution data alone require at least five plutons (a sixth shown here allows for the possibility of a separate pluton for the 39.1 Ma aphyric rhyolites; see text for detailed discussion).
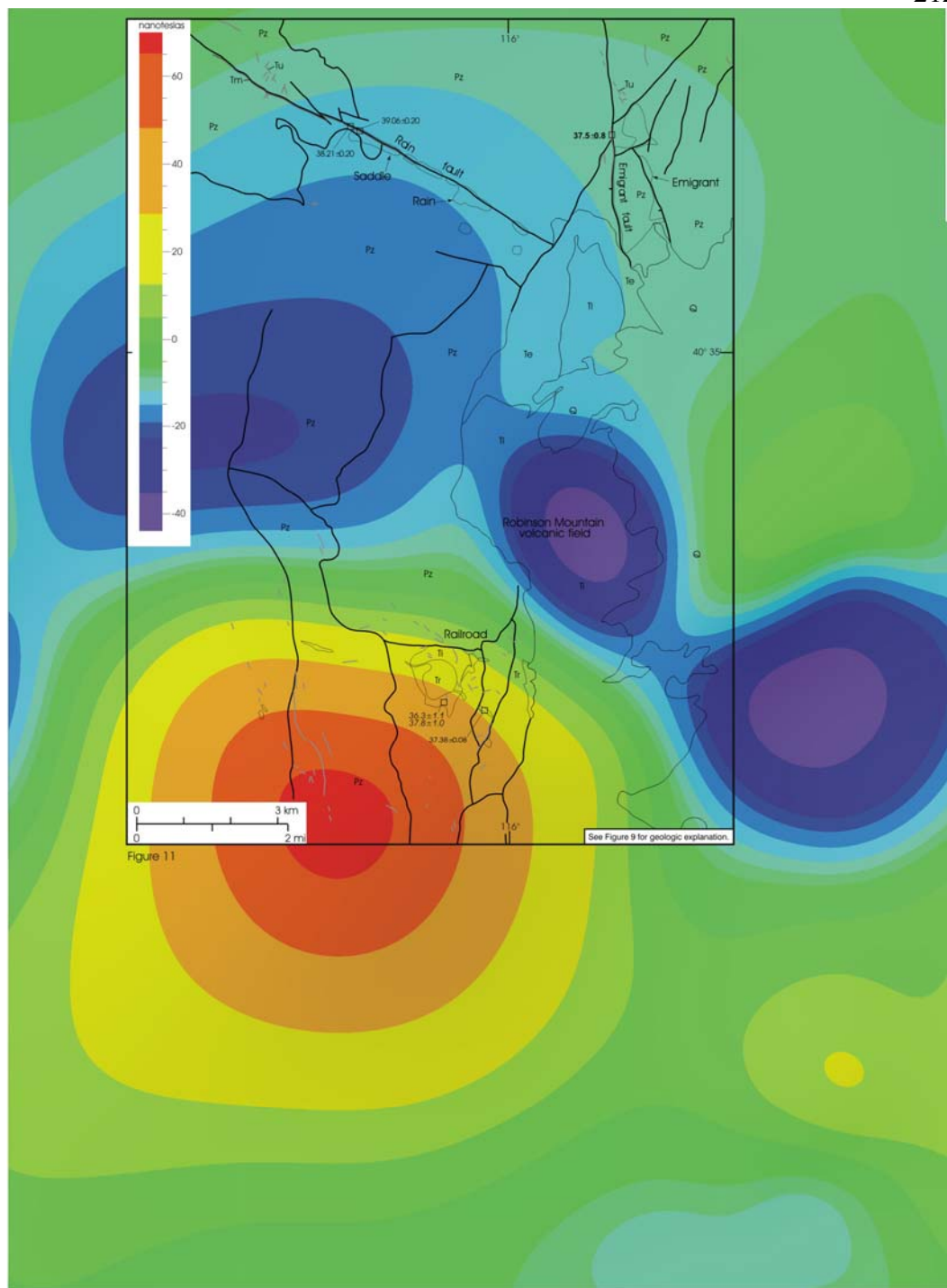
Figure 11

Fig. 3-11. Geologic map of the Rain mine area of the southern Carlin trend from Figure 3-5, with aeromagnetic data upward continued to 2000 m (M. Goldie, written communication, 2004). The dike distributions and magnetic data indicate a large (~10 km diameter) intrusion centered southwest of the Railroad district. The Bullion stock and porphyritic rhyolite dikes are interpreted to be apophyses from this larger intrusion.

Table 3-1. ^{40}Ar/^{39}Ar and U-Pb Age Data, Igneous Rocks of the Carlin Trend.

Sample[1]	Ref.[2]	Rock type, location	W. Long.	N. Lat.	Mineral	Age Method		n/%^{39}Ar[3]	Age[4] (Ma)	±1	isochron	±1	40/36	±1	total gas	±1
JURASSIC ROCKS																
Goldstrike and related intrusions																
96-M-207	5	Goldstrike diorite			titanite	U-Pb, range ^{206}Pb/^{238}U ages			**159.1**	4.4						
96-M-209	5	monzonite sill			zircon	U-Pb, lower intercept			**157.7**	0.4						
EX-24C	5	rhyolite dike, Meikle			zircon	U-Pb, average ^{207}Pb/^{206}Pb ages			**159.3**	4.2						
GSS-1	2	Goldstrike diorite	116°21.8'	40°58.3'	biotite	step heating	wtd mean	96	**159.9**	1.7	NA				158.6	
"	2	"	"	"	hornblende	step heating	wtd mean	72	**160.8**	2.1	NA				162.4	
GSS-2	2	Goldstrike diorite	116°21.8'	40°58.3'	biotite	step heating	wtd mean	94	**160.2**	1.7	NA				157.7	
97-Zia-7	1	microdiorite, Zia claims	116°21.4'	40°56.5'	matrix	step heating	disturbed		~159		NM				139.8	0.80
98-Zia-9	1	rhyolite, Zia claims	116°23.2'	40°56.7'	biotite	step heating	plateau	86.9	**157.4**	0.3	**158**	0.2	286	3		
Lan-34L	1	rhyolite dike, Lantern mine	116°21.7'	40°55.35'	sericite/albite	step heating	disturbed		≥111		NM					
Lamprophyre dikes																
186804	Snee	phlogopite lamprophyre, Goldstrike mine	116°19.25'	40°47.4'	hornblende	step heating	plateau	47.3	**158.9**	0.2	NA					
I-5	3	phlogopite lamprophyre, Genesis mine	116°22.0'	40°57.2'	phlogopite	step heating	plateau	93.0	**164.6**	1.1	166	10.3	160	7		
B5-95-11	6	hornblende lamprophyre, Deep Star mine	116°21.75'	40°57.7'	hornblende	step heating	disturbed	31.0	167.4	2.4	NM				210.0	3.3
Intrusions of the Dee mine area																
94B50/49/DD58	8	phlogopite lamprophyre dike	116°25.6	41°02.35'	biotite	step heating	disturbed		>148.7		NA					
DC-95-2-2146	1	altered Jurassic dike	116°25.6'	41°02.25'	biotite	step heating	disturbed		≥157.2		152	4	376	480	148	1
BRS-4C-1190	1	altered dike	116°25.55'	41°02.5'	sericite	step heating	disturbed		≥143		145	10	208	425	140	1
BRS-4C-1410	1	altered basaltic dike	116°25.55'	41°02.5'	wr (illite)	step heating	disturbed		≥106		NM					
CRETACEOUS ROCKS																
RS-1 (H97-23)	5	Richmond granite	116°18.5'	40°51.06'	zircon	U-Pb, average two ^{206}Pb/^{238}U ages			**112.4**	0.6						
EOCENE ROCKS																
Northern Carlin Trend																
Plagioclase-biotite±quartz rhyolite																
BP-2	1	Goldstrike pit	116° 21.9'	40° 58.6'	biotite	step heating	plateau	98.5	**39.32**	0.11	**39.3**	0.05	308	1	**39.34**	0.20
"	1	"	"	"	plagioclase	step heating	disturbed	55.1	38.35	0.19	38.7	0.08	313	1	43.98	7.70
"	1	"	"	"	matrix	step heating	no plateau		excess Ar		NM					

Sample[1]	Ref.[2]	Rock type, location	W. Long.	N. Lat.	Mineral	Age Method		n/%^{39}Ar[3]	Age[4] (Ma)	±1 σ	isochron	±1σ	40/36	±1 σ	total gas	±1 σ
DSU-192-906	1	Deep Star	116°21.7'	40°57.5'	biotite	step heating	disturbed	65.8	39.84	0.26	**40.03**	0.38	300	50	**39.90**	0.20
H00-50	1	Genesis pit	116°21.7'	40°57.2'	biotite	step heating	disturbed	58.2	39.3	0.2	38.8	0.29	683	240	**39.69**	0.20
I-13	3	Genesis pit	116°22.1'	40°56.8'	biotite	step heating	plateau	100	**40.3**	0.2	40.2	2.0	310	21		
Plagioclase-biotite-hornblende dacite (Betze dacite)																
96-M-208	5	Post-Betze pit			zircon	U-Pb, lower intercept			**37.8**	2.1						
G11-12-1	5	dacite dike, Griffin			zircon	U-Pb, range ^{206}Pb/^{238}U ages			**38.1**	0.8						
G11-005-4-492	1	Griffin deposit	116°22.4'	40°59.8'	biotite	step heating	plateau	76.9	**39.46**	0.08	**39.6**	0.05	270	2	**39.54**	0.11
H00-46	1	Post-Betze pit	116°21.9'	40°58.7'	hornblende	step heating	plateau	69.5	**38.95**	0.22	**39**	0.23	300	13	39.66	0.22
H00-49	1	Post-Betze pit	116°22.0'	40°58.75'	biotite	step heating	wtd mean	66.5	**40.13**	0.21	39.8	1.2	384	190	40.12	0.21
POD-1	2	Post-Betze pit	116°22.0'	40°58.7'	biotite	step heating	wtd mean	95	**39.5**	0.4	NA				39.3	
Aphyric rhyolite (Deep Star rhyolite)																
DSU-150-106	1	Deep Star, core	116°21.7'	40°57.8'	matrix	step heating	wtd mean	59.6	**39.15**	0.26	**39.07**	0.33		8.0	36.75	0.22
DS-13	1	Deep Star	116°21.7'	40°57.8'	matrix	step heating	disturbed				**38.98**	0.05	282	1		
DS-150-105	1, 9	Deep Star, core	116°21.7'	40°57.8'	matrix	step heating	disturbed		~38		38.3	0.05	176	2	36.94	0.70
Basaltic andesite																
98 Dee-8	1	dike, Dee mine	116°25.6'	41°02.0'	matrix	step heating	plateau	61.4	**37.80**	0.21	**37.7**	0.17	295	3.8	40.13	0.21
Plagioclase-biotite-hornblende-quartz±sanidine rhyolite (Beast type)																
BST 114	1	Beast pit	116°21.3'	40°56.4'	sanidine	single crystal	wtd mean	14	**37.58**	0.06						
"	1	"	"	"	sanidine	step heating	plateau	72.6	**37.61**	0.06					37.63	0.17
BST-30	1	Beast pit	116°21.3'	40°56.5'	biotite	step heating	plateau	60.5	**37.55**	0.07	37.8	0.05	300	2	37.66	0.20
Rich-10	1	Richmond Mtn	116°18.2'	40°51.8'	sanidine	single crystal	wtd mean	15	**37.58**	0.05						
H97-22b	1	Welches Canyon	116°18.4'	40°48.0'	sanidine	single crystal	wtd mean	14	**37.43**	0.06						
Welches Canyon - Richmond Mountain area																
H97-21	1	plagioclase-biotite-hornblende dacite	116°19.2'	40°47.4'	hornblende	step heating	plateau	88.3	**38.59**	0.17	**38.8**	0.11	300	3	38.45	0.70
WC-31	1	granodiorite	116°17.9'	40°47.7'	plagioclase	step heating	plateau	61.7	**38.59**	0.12	**38.7**	0.08	308	2	39.18	0.15
WC-106	1	plag-biot-hbl-qtz dacite	116°19.55'	40°50.6'	biotite	step heating	disturbed				43.1	2.1	278	100	**39.49**	0.23
Emigrant Pass Volcanic Field																
Porphyritic (plagioclase-biotite-hornblende-quartz±sanidine) rhyolite dikes																
H98-102	1	porphyritic dacite	116°17.1'	40°44.7'	plagioclase	single crystal	wtd mean	33	**36.45**	0.09						
H98-87	1	porphyritic rhyolite	116°19.1'	40°43.0	sanidine	single crystal	wtd mean	14	**36.21**	0.04						
H98-61	1	porphyritic rhyolite	116°19.8'	40°40.8'	sanidine	single crystal	wtd mean	15	**36.12**	0.04						
Bob Creek lava (hornblende basaltic andesite)																
H98-21C	1	rhyolite inclusion	116°21.0'	40'40.7'	sanidine	single crystal	wtd mean	15	**37.06**	0.04						
H98-20	1	porphyritic andesite	116°20.7'	40°40.8'	hornblende	step heating	plateau	90.6	**37.43**	0.10	37.6	0.10	286	5	37.44	0.49
Mack Creek lavas (plagioclase-hornblende dacite-andesite)																
H98-78	1	porphyritic dacite	116°21.8'	40°42.7'	hornblende	step heating	plateau	50.3	**37.56**	0.18	**37.9**	0.09	269	3	33.79	0.25
"	1	"	"	"	plagioclase	single crystal	wtd mean	34	**37.31**	0.12						

Sample[1]	Ref.[2]	Rock type, location	W. Long.	N. Lat.	Mineral	Age Method		$n/\%^{39}Ar$ [3]	Age[4] (Ma)	±1 σ	isochron	±1 σ	40/36	±1 σ	total gas	±1 σ
H98-95C	1	porphyritic dacite	116°19.6'	40°44.9'	sanidine	single crystal	wtd mean	15	**37.83**	0.05						
"			"	"	hornblende	step heating	plateau	76.6	**37.84**	0.10	**37.90**	0.06	290	2	37.04	0.70
Mack Creek intrusions (plagioclase-hornblende dacite-andesite), Bobs Flat Quadrangle																
H98-1	1	porphyritic dacite	116°24.8'	40°41.6'	hornblende	step heating	plateau	95.1	**37.64**	0.18	**37.7**	0.15	291	5	37.65	0.46
EM-N2	1	porphyritic dacite	116°27.2'	40°42.7'	hornblende	step heating	plateau	62.8	**38.11**	0.21	**37.9**	0.31	302	20	38.50	0.21
Primeaux lavas (plagioclase-hornblende-pyroxene andesite-dacite)																
H98-27	1	coarse hornblende andesite hornblende andesite	116°16.5'	40°39.0'	hornblende	step heating	plateau	92.4	**37.85**	0.13	**38.2**	0.08	255	4	36.26	0.23
H98-109	1	intrusion	116°17.5'	40°43.5'	hornblende	step heating	plateau	93.1	**38.06**	0.12	**38.1**	0.09	280	5	37.14	1.10
Rain-Railroad Area (southern Carlin trend)																
RCR-9-676	4	monzonite porphyry dike, Emigrant Springs			zircon	U-Pb SHRIMP		11	**37.5**	0.8						
RCR-62-2151	1	basaltic andesite dike	116°2.4'	40°38.4'	matrix	step heating	wtd mean	56.3	**38.21**	0.20	**37.8**	1.2	378	73	39.42	0.20
RCR-61-2092	1	porphyritic diorite dike biotite quartz-feldspar	116°2.4'	40°38.4'	biotite	step heating	wtd mean	97.5	**39.06**	0.20	**39.1**	0.18	294	13	38.60	0.20
NEP-44	1	intrusion	116°0.5'	40°30.5'	sanidine	single crystal	wtd mean	14	**37.38**	0.08						
99-DJ-31	1	rhyolite intrusion	115°53.3'	40°23.5'	sanidine	single crystal	wtd mean	9	**37.51**	0.19						
99-DJ-40	1	rhyolite ash-flow tuff	115°53.9'	40°27.8'	sanidine	single crystal	wtd mean	9	**37.70**	0.19						
MIOCENE ROCKS																
99-468	1	rhyolite lava, Marys Mountain	116°16.1'	40°42.7'	sanidine	single crystal	wtd mean	12	**15.32**	0.04						

1 data from this study: samples in regular type were analyzed at the New Mexico Geochronological Research Laboratory (methodology in McIntosh and Chamberlin, 1994);

samples in italics were analyzed at the Nevada lsotope Geochronology Laboratory (Justet and Spell, 2001)

2 Source of data: 1=this study; 2=Arehart et al. (1993); 3=Farmer (1996); 4=Longo et al. (2002); 5 Mortensen et al. (2000); 6=Orobona (1996); 8=Theodore et al. (1998); 9=Thompson (2000)

3 n = number of single grains analyzed; $\%^{39}Ar$ = percent ^{39}Ar used in plateau

4 ages in bold are best estimates of emplacement age; ages in regular type are alternative age calculations not necessarily considered to indicate emplacement age

NA = not available; NM = not meaningful

$^{40}Ar/^{39}Ar$ ages for all samples, including those from other studies, were calculated or recalculated with a monitor age of 28.02 Ma for Fish Canyon sanidine (Renne et al., 1998)

Decay constants and isotopic abundances after Steiger and Jäger (1977); $\lambda_\beta = 4.963 \times 10^{-10}$ yr^{-1}; $\lambda\varepsilon_+\varepsilon = 0.581 \times 10^{-10}$ yr^{-1}; $^{40}K/K = 1.167 \times 10^{-4}$

Table 3-2. Characteristics of Jurassic, Cretaceous, and Miocene Igneous Rocks of the Carlin Trend.

Unit	Rock type	Texture	Phenocrysts or phaneritic mineralogy	Age (Ma)	Distinguishing features	Extent; volume
Miocene						
Sparsely porphyritic sa-qtz-ol-px rhyolite lava and associated porous, glassy tuff	high-Si rhyolite	porphyritic, aphanitic, flow-banded, locally glassy	qtz: 0-2%, 1-4mm sa: 2-3%, 1-3mm ol (fayalite); ≤1%, 2-4mm px (orthopyroxene); ≤1, 2-4 mm	14.6 (KAr)	Sparsely porphyritic, ol-phyric lava and non-welded fall/surge tuff; commonly glassy, flow-band, locally lithophysal	Widespread in Northern Carlin trend along eastern flank of Boulder Valley
Sparsely porphyritic sa-qtz±bi±px rhyolite lava and associated tuff	rhyolite to high-Si rhyolite	sparsely porphyritic, aphanitic, flow-banded, locally glassy	qtz: <0-2%, <3 mm sa:1-2%, <3 mm bi: <1%, <2 mm px: <15, <2 mm	15.3	Sparsely porphyritic, commonly flow-banded lava and fall/surge tuff	Widespread in Southern Carlin trend, west, east, and south of Gold Quarry mine
Cretaceous						
Coarse grained granite	granite	coarsely phaneritic, with Ksp phenocrysts	pl: 45-55%, 0.4-1 cm qtz: 20-30%, 0.2-0.8 cm Ksp: 20-30%, 0.4-2 cm bi: <7%, 0.03-0.6 cm	112	Coarse grained, with large Ksp phenocrysts; locally dikes and small pods of aplite-pegmatite	Small stock at Richmond Mountain, 0.4 km^2 outcrop; possibly ~20 km^2 subsurface
Jurassic						
Goldstrike dioritic laccolith and satellite intrusions	diorite, lesser gabbro near base, granodiorite, tonalite common at top	main phase: equigranular, medium grained phaneritic; locally pl-hbl porphyritic and fine grained	pl: 45-65%, 4-10mm Kf: 0-15%, 4-10 mm hbl: 10-20%, 5-10 mm bi: 0-10%, 2-8 mm px: 0-10%, 2-10 mm qtz: 1-15%, 2-10 mm	~158	Medium grained, compositionally zoned, equigranular granitoid; intermediate compositions predominate	Laccoliths and other sill-like intrusions at Goldstrike, Little Boulder Basin, and Vivian areas; ~7 km^2 total
Qtz-bi-hbl diorite dikes and sills	porphyritic quartz diorite	moderately to coarsely porphyritic	bi: 0-25%, 1-8 mm hbl: 0-20%, 1-8 mm qtz: <2%, with reaction rims	~158	Strongly porphyritic bi- or hbl-phyric dikes with distinctive quartz xenocrysts(?)	1-10 m wide, NW-striking dikes/sills centered on Goldstrike and satellite intrusions
Lamprophyre dikes	lamprophyre	finely to coarsely porphyritic, aphanitic	phl: 0-40%, 1-8 mm hbl: 0-40%, 1-8 mm qtz: <2%, 1-4 mm, with reaction rims ol: <1%, 2-4 mm px: <1%, 2-4 mm	~158	Sparsely porphyritic; lack of pl phenocrysts; commonly glassy; "K-type" dikes of mines	NW-striking dike swarm centered on Goldstrike and satellite intrusions
Finely porphyritic rhyolite dikes	rhyolite	finely porphyritic, aphanitic	pl: 5-8%, 1-3 mm bi: 1-3%, 1-3 mm qtz: 0-1%, 1-3 mm	~158	Finely porphyritic, aphanitic; distinctive sodic alteration assemblage	1-15 m wide dikes within ±5 km radius of Goldstrike intrusion

pl = plagioclase, qtz = quartz, sa = sanidine, Kf = potassium feldspar, bi = biotite, phl = phlogopite, hbl = hornblende, px = pyroxene, ol = olivine

Table 3-3. Representative Chemical Analyses of Miocene, Eocene, Cretaceous, and Jurassic Igneous Rocks In and Adjacent to the Carlin Trend, Northeastern Nevada

Age	Miocene	Miocene	Miocene	Eocene	Eocene	Eocene	Eocene
	Rhyolite lavas and tuffs			Dikes of the northern Carlin trend			
Rock Type[1]	Rhyolite	Rhyolite	Rhyolite	Bas andesite	Bas andesite	Dacite	Rhyolite
Sample No.	LAN-65	H98-112	H98-14	CD96 10C-145	98-DEE-8	PNC 213-1787	GEN-2
Sample Type	outcrop	outcrop	outcrop	core	pit	core	pit
Location	Sheep Ck	Boulder Valley	Marys Mt		Dee	Betze-Post	Genesis
Latitude	40° 54.42'	40° 39.8'	40° 39.8'	40° 59.5'	41 02'06"	40° 58.0'	40° 56.85'
Longitude	116° 22.15'	116° 21.4'	116° 15.6'	116° 24.9'	116° 25'35"	116° 22.0'	116° 22.05'
Occurrence	lava	tuff	lava	dike	dike	dike	dike
Alteration	hydrated glass	hydrated glass	hydrated glass		mod clay	moderate clay	mild clay
Isotopic Age (Ma)	14.60				37.57+/-0.34	38.9+/-	40.1+/-0.4
Analyses[2]	U, N	W, C	W	U, C	U	U, A	U, A
Analytical Method	XRF/INAA	XRF/ICP-MS	XRF	XRF/ICP-MS	XRF	ICP/ICP-MS	XRF/ICP-MS
SiO_2	74.27	76.03	74.94	55.24	54.64	66.06	71.59
TiO_2	0.26	0.30	0.28	1.28	1.55	0.39	0.32
Al_2O_3	12.45	12.05	13.35	16.83	18.50	16.34	15.82
FeO[3]	2.95	2.34	1.41	6.71	4.71	2.97	2.11
MnO	0.06	0.06	0.03	0.07	0.15	0.11	0.07
MgO	0.11	0.52	0.05	4.85	1.74	1.61	1.42
CaO	0.86	0.92	1.07	9.12	12.50	8.13	2.12
Na_2O	3.51	2.53	2.49	3.01	2.82	0.39	1.82
K_2O	5.50	5.22	6.27	2.39	2.82	3.79	4.60
P_2O_5	0.02	0.04	0.11	0.5	0.56	0.21	0.13
LOI	0.05			1.98	11.46	4.76	3.99
	100.05	100.00	100.00	101.98	111.46	104.76	103.99
Recalc Total					100.00	100.00	
Total[4]	99.53	96.59	98.80		99.84	99.06	100.17
Sc	1	1	6				
V	8	8	13	185		40	8
Cr		<1	1			29	13
Co	3	7.8		27		4.1	2.9
Ni	5	0.7	9	87		<10	<10
Cu	7.0	36.5	4	26		<10	<10
Zn	145	108	53	525		56	43
Ga	20	24	16	19		19	19
As	3.6	4.4		209		51	<5
Rb	180	158	279	62		139	154
Sr	13	61	127	641		107	145
Y	84.0	86	42	21		19.0	18
Zr	577	528	213	173		186	158
Nb	44	46.5	29.3	15		16	19
Mo	15.0	4.64		1.7		2.1	1.7
Ag		0.1		-0.5		-0.5	-0.5
Sb	0.2	0.62		11		7.8	0.5
Cs	3	4.68		3		18	16
Ba	140	1006	826	1076	1227	931	1085
La	120	71.3	47	42		44.0	43
Ce	200	146.5	103	83		75.0	81
Pr		17.5		9.6		9.0	8.7
Nd	99	67.8		35		31.0	30
Sm	15.0	14		6.4		5.4	5.1
Eu	1.3	1.4		1.7		1.2	1.14
Gd		14		5.3		4.0	3.8
Tb	2.3	2.2		0.7		0.6	0.6
Dy		13.3		3.6		3.0	2.8
Ho		2.9		0.6		0.5	0.5
Er		8.5		1.8		1.7	1.6
Tm		1.2		0.25		0.25	0.24
Yb	9.5	7.9		1.6		1.5	1.5
Lu	1.43	1.2		0.23		0.22	0.23

Table 3-3. Representative Chemical Analyses of Miocene, Eocene, Cretaceous, and Jurassic Igneous Rocks In and Adjacent to the Carlin Trend, Northeastern Nevada

Rock Type[1]	Rhyolite	Rhyolite	Rhyolite	Bas andesite	Bas andesite	Dacite	Rhyolite
Sample No.	LAN-65	H98-112	H98-14	CD96 10C-145	98-DEE-8	PNC 213-1787	GEN-2
Hf	19.0	16.7		4.6		4.8	4.6
Ta		3.25		0.9		1.2	1.65
W	6.0			1		1.3	1.6
Au							
Hg							
Tl		1.16		0.6		6.0	0.9
Pb	32.0	25	24	26		21.0	18
Bi		0.77		0.4		1.9	0.6
Th	19.0	18	19	9.3		10.0	12
U	5.8	5.7		1.9		3.6	4

[1] Pl=plagioclase, bi=biotite, hbl=hornblende, qtz=quartz, sa=sanidine, px=pyroxene, phl=phlogopite

[2] Analytical methods: U = XRF at University of Nevada, Reno; W = XRF at Washington State University; C = ICP/MS and ICP/AES at ALS Chemex (Vancouver, Canada)

A = ICP/MS at Actlabs (Ontario, Canada); N = INAA at Activation Laboratories (Ontario, Canada).

[3] Total Fe reported as FeO.

Table 3-3. Representative Chemical Analyses of Miocene, Eocene, Cretaceous, and Jurassic Igneous Rocks In and Adjacent to the Carlin Trend, Northeastern Nevada

Age	Eocene	Eocene	Eocene	Eocene	Eocene	Eocene	Eocene
Rock Type[1]	Rhyolite	Rhyolite	Rhyolite	Rhyolite	Rhyolite	Rhyolite	Rhyolite
Sample No.	BP-2	BST-130	RICH-10	WC-2	H97-22A	DSU-143-30	DS-1
Sample Type	pit	pit	outcrop	outcrop	outcrop	core	underground
Location	Betze-Post	Beast	Richmond Mtn	Welches Canyon	Welches Canyon	Deep Star	Deep Star
Latitude	40° 58.6'	40° 56.37'	40° 51.8'	40° 48'00"	40° 47.9'	40° 57.7'	40° 57.7'
Longitude	116° 21.9'	116° 21.40'	116° 18.2'	116° 19'15"	116° 18.4'	116° 21.7'	116° 21.7'
Occurrence	dike	dike	dike	dike	dike	dike	dike
Alteration	hyd. glass	mild clay	mild clay	mild clay	fresh	devitrified	hydrated glass
Isotopic Age (Ma)	39.07+/-0.21	37.37+/-0.1	37.34+/-0.05	37.19+/-0.11	37.19+/-0.11	38.9	38.9
Analyses[2]	U, A	U, N	U, N	U, N	W, C	U, N	U, N
Analytical Method	ICP/ICP-MS	XRF/INAA	XRF/INAA	XRF/INAA	XRF WSU	XRF/INAA	XRF/INAA
SiO_2	72.01	71.21	77.33	73.06	72.59	76.98	75.09
TiO_2	0.29	0.31	0.21	0.30	0.30	0.07	0.05
Al_2O_3	15.81	15.19	14.72	14.47	14.66	14.09	14.64
FeO^3	2.17	2.05	1.58	2.53	1.88	0.88	0.86
MnO	0.06	1.37	0.06	0.07	0.04	0.09	0.09
MgO	0.74	3.10	0.55	1.23	0.84	0.68	0.06
CaO	2.73	2.25	0.52	2.16	2.99	0.99	1.57
Na_2O	2.18	0.10	0.46	1.59	2.20	1.07	2.39
K_2O	3.88	4.32	4.45	4.46	4.38	5.12	5.18
P_2O_5	0.13	0.11	0.11	0.12	0.13	0.04	0.05
LOI	3.08	7.13	3.40	5.92		4.97	8.14
	103.08	107.13	103.40	105.92	100.00	104.97	108.14
Recalc Total	100.00	100.00		100.00		100.00	100.00
Total[4]	100.44	100.09	99.33	98.82	97.33	99.38	
Sc		5	2	3	6	2	2
V	<5	46	20		22	2	8
Cr	24				2		
Co	2.4		2	3.0	11.1	<1	
Ni	<10	9	5	<20	1.1	2	2
Cu	<10	5	<2	<1	3.9	2	1
Zn	50	52	25	72	45	28	44
Ga	18		23		18	29	13
As	39	12.8		2.3	1.3	17.0	32.0
Rb	99	149	289	140	139	150	299
Sr	592	58	55		328	91	862
Y	18.0	10.0	16		14	20.0	50.0
Zr	146		69		133	72	72
Nb	19		13		17.2		29
Mo	2.0	<2	4	5.0	0.62	3.0	6.0
Ag	-0.5				0.11		-5.0
Sb	44.0	7.6	3.9	0.5	0.91	1.8	6.5
Cs	260			2	1.57	5	260
Ba	1395	1100	723	910	1406	640	1300
La	44.0	27.6	25	39.0	36.9	12.0	12.0
Ce	83.0	51.0	36	66.0	67.8	23.0	23.0
Pr	8.8				7.4		
Nd	30.0	18.0	21	22.0	26.6	9.0	9.0
Sm	4.9	3.5	3	3.5	4.8	2.5	2.5
Eu	1.1	1.0	0.8	1.0	0.8	0.6	0.5
Gd	3.9				4.1		
Tb	0.6	<0.5	0.6	0.9	0.4	<0.5	<0.5
Dy	2.9				2.2		
Ho	0.5				0.3		
Er	1.6				1.2		
Tm	0.23				0.1		
Yb	1.5	1.1	2.1	1.0	1.1	1.8	2.2
Lu	0.25	0.17	0.2	0.19	0.1	0.30	0.26

Table 3-3. Representative Chemical Analyses of Miocene, Eocene, Cretaceous, and Jurassic Igneous Rocks In and Adjacent to the Carlin Trend, Northeastern Nevada

Rock Type[1]	Rhyolite	Rhyolite	Rhyolite	Rhyolite	Rhyolite	Rhyolite	Rhyolite
Sample No.	BP-2	BST-130	RICH-10	WC-2	H97-22A	DSU-143-30	DS-1
Hf	4.3		1	6.0	2.1	2.0	2.0
Ta	1.7	1.0	0	1.6	1.34	2.3	2.4
W	1.3	3.0					
Au							
Hg							
Tl	2.0				0.7		
Pb	30.0	30.0	27	<1	30	28.0	21.0
Bi	1.7				0.27		
Th	12.0	13.8	11	12.0	13	4.9	4.9
U	5.2	5.7	10	5.1	5.4	6.3	6.4

Table 3-3. Representative Chemical Analyses of Miocene, Eocene, Cretaceous, and Jurassic Igneous Rocks In and Adjacent to the Carlin Trend, Northeastern Nevada

Age	Eocene	Eocene	Eocene	Eocene	Eocene	Eocene	Eocene
	Welches Cyn					Emigrant Pass volcanic field	
						Bob Creek lava	Primeaux lavas
Rock Type[1]	Diorite	Andesite	Dacite	And–Dac		Andesite	And–Dac
Sample No.	WC-31	WC-9	WC-106	H97-21	WC-3	H98-20	H98-27
Sample Type	outcrop	outcrop	outcrop	outcrop	outcrop	outcrop	outcrop
Location	Welches Canyo	Welches Canyo	Welches Canyo	Welches Canyo	Welches Canyon	Emigrant Pass Quadrangle	
Latitude	40° 47.73'	40° 47'25"	40° 50.6'	40° 47.4'	40° 47.75'	40° 40.8'	40° 39.0'
Longitude	116° 17.92'	116° 19'10"	116° 19.55'	116° 19.1'	116° 18.08'	116° 20.7'	116° 16.5'
Occurrence	intrusion	dike	dike	dike	dike	lava	lava
Alteration	fresh	fresh	sl. clay	fresh	fresh	fresh	fresh
Isotopic Age (Ma)	38.59+/-0.23		39.24	38.59		Tb	Tph2
Analyses[2]	U	U, A	U, N	W, C	U, A	W, C	W, C
Analytical Method	XRF	XRF/ICP-MS	XRF/INAA	XRF WSU	XRF/ICP-MS	XRF WSU	XRF WSU
SiO_2	61.28	62.15	63.63	62.64	64.96	57.89	60.30
TiO_2	0.83	0.79	0.84	0.74	0.59	1.20	0.94
Al_2O_3	17.34	17.21	17.07	17.14	17.48	16.10	17.26
FeO^3	5.79	5.74	4.98	5.34	3.71	7.79	6.15
MnO	0.13	0.12	0.10	0.13	0.08	0.13	0.11
MgO	2.33	2.45	2.22	2.41	1.13	3.37	2.65
CaO	5.47	5.09	3.85	5.08	4.27	7.72	6.01
Na_2O	3.88	3.62	3.29	3.66	4.35	2.98	4.12
K_2O	2.62	2.49	3.77	2.54	3.20	2.37	2.15
P_2O_5	0.32	0.34	0.25	0.33	0.22	0.43	0.32
LOI	0.48	0.94	3.41		0.23		
	100.48	100.94	103.41	100.00	100.23	100.00	100.00
Recalc Total	100.00				100.00		
Total[4]	98.93	100.27	97.68	98.09	98.83	99.16	99.32
Sc			9	14		24	19
V		95	111	93	47	202	148
Cr		40		1	63	94	7
Co		11		18.7	7.5	26.2	20.7
Ni		<10	1	1.6	35	30.4	3.9
Cu		<10	7	9.9	35	9.7	6.2
Zn		92	57	105	40	83	85
Ga		19	15	20.5	20	20.6	21
As		<5		<0.2	<5	3.7	2.9
Rb		61	94	61	93	38	56
Sr		660	587	725	673	839	892
Y		19	31	18	23.0	25	19
Zr		139	184	158	199	174	203
Nb		8	19	13.3	15	13.5	12.4
Mo		1.4		0.91	2.6	0.43	1.49
Ag		-0.5		0.1	-0.5	0.04	0.1
Sb		0.2		0.08	0.4	0.48	0.55
Cs		1		0.63	3	0.28	2.31
Ba	1180	1097	1354	1261	1070	981	1217
La		41	41	39.1	48.0	37.8	43.3
Ce		77	63	73.5	90.0	75.3	78.6
Pr		8.7	0	8.8	10.1	8.6	9.2
Nd		31	31	34.5	37.0	36.4	35.4
Sm		5.5	5.3	6.8	6.4	6.5	6
Eu		1.5	1.7	1.6	1.6	1.7	1.6
Gd		4.7	0	5.8	5.0	6.1	5.5
Tb		0.6	0.5	0.6	0.7	0.8	0.7
Dy		3.2	0	3.3	3.7	4.7	3.6
Ho		0.6	0	0.6	0.7	0.9	0.7
Er		1.7	0	1.9	2.2	2.6	1.9
Tm		0.23	0	0.2	0.33	0.3	0.2
Yb		1.4	2.1	1.7	1.9	2.1	1.6
Lu		0.23	0.36	0.2	0.30	0.3	0.2

Table 3-3. Representative Chemical Analyses of Miocene, Eocene, Cretaceous, and Jurassic Igneous Rocks In and Adjacent to the Carlin Trend, Northeastern Nevada

Rock Type[1]	Diorite	Andesite	Dacite		And–Dac			Andesite	And–Dac
Sample No.	WC-31	WC-9	WC-106		H97-21	WC-3		H98-20	H98-27
Hf			4		1.9	5.6		4.7	5.6
Ta			0.8		1.12	1.2		0.85	0.93
W			0.7			1.0			
Au			0						
Hg			0						
Tl			0.2		0.14	0.4		0.12	0.28
Pb			16	20	19	16.0		6	12
Bi			0		<0.01	0.3		0.02	0.03
Th			11	12	9	13.0		7	10
U			2.8		2.1	3.6		1.5	2

**Table 3-3. Representative Chemical Analyses of Miocene, Eocene, Cretaceous, and Jurassic Igneous Rocks
In and Adjacent to the Carlin Trend, Northeastern Nevada**

Age	Eocene	Eocene	Eocene	Eocene	Eocene	Eocene	Eocene
			Mack Creek lavas			Late porphyritic dikes	
Rock Type[1]			And–Dac			Rhyolite–Dacite	
Sample No.	H98-68	H98-101	H98-97	H98-1	H98-96	H98-56	H98-102
Sample Type	outcrop	outcrop	outcrop	outcrop	outcrop	outcrop	outcrop
Location							
Latitude	40° 41.6'	40° 45.1'	40° 44.5'	40° 41.6'	40° 44.7'	40° 42.2'	40° 44.7'
Longitude	116° 20.0'	116° 17.1'	116° 20.0'	116° 24.8'	116° 20.7'	116° 18.1'	116° 17.1'
Occurrence	lava	lava	lava	intrusion	lava	dike	dike
Alteration	fresh	fresh	fresh	fresh	fresh	fresh	fresh
Isotopic Age (Ma)	Tphb	Tppc	Tkd2	Tkdi	Tkd2	Tid	Tir
Analyses[2]	W, C	W, C	W, C	W, C	W, C	W, C	W, C
Analytical Method	XRF WSU	XRF WSU	XRF WSU	XRF WSU	XRF WSU	XRF WSU	XRF WSU
SiO_2	63.61	65.88	59.76	65.11	67.10	68.53	71.45
TiO_2	0.78	0.64	0.98	0.73	0.62	0.46	0.41
Al_2O_3	16.67	16.75	16.83	15.98	15.20	16.07	14.53
FeO^3	5.03	4.14	6.86	4.55	3.73	2.70	2.09
MnO	0.12	0.09	0.10	0.11	0.09	0.04	0.05
MgO	2.08	1.05	2.84	2.29	1.87	1.18	1.15
CaO	4.88	3.99	6.46	4.68	3.99	2.96	3.23
Na_2O	3.75	3.92	3.36	2.97	3.20	3.77	3.51
K_2O	2.80	3.28	2.52	3.32	4.00	4.09	3.40
P_2O_5	0.28	0.25	0.31	0.27	0.20	0.21	0.16
LOI							
	100.00	100.00	100.00	100.00	100.00	100.00	100.00
Recalc Total							
Total[4]	98.63	99.77	98.77	97.68	98.80	99.22	99.60
Sc	13	12	17	8	12	4	3
V	106	67	156	97	89	49	52
Cr	4	2	41	19	20	6	10
Co	21.1	13.3	21.7	19.9	23.9	15.5	23.1
Ni	3.3	2	24.5	6.8	10.3	9.2	5.6
Cu	7.9	5.3	19.2	23	12.5	6.3	4.8
Zn	82	67	92	89	68	88	48
Ga	21.8	21.8	23.3	20.2	20.4	21.6	18.95
As	0.6	2.2	1	7.2	4.5	2.9	3.3
Rb	71	94	64	86	113	111	133
Sr	699	668	740	565	528	536	516
Y	21	21	22	20	18	14	11
Zr	196	191	149	181	152	143	115
Nb	14.7	20.6	13.9	14.8	17.0	14.8	12.8
Mo	0.96	1.1	1.15	1.32	2.76	1.27	0.7
Ag	0.1	0.09	0.1	0.17	0.1	0.09	0.05
Sb	0.11	0.13	0.2	1.12	0.46	0.55	0.49
Cs	1.6	2.59	1.62	1.83	6.61	2.86	6.18
Ba	1326	1134	1122	1424	1084	1713	1007
La	44.5	42.3	31	40.1	30.6	31.4	25.7
Ce	82.8	77.9	58	74.2	57.1	58.8	46.4
Pr	9.4	9	7.5	8.5	6.5	6.5	5.5
Nd	34.5	34	31.4	31.8	25.9	25.3	19.9
Sm	6.2	5.8	5.9	5.7	4.4	4.1	3.4
Eu	1.6	1.4	1.6	1.5	1.1	1	0.8
Gd	5.6	5.3	5.5	5.2	4.1	3.8	3.1
Tb	0.7	0.7	0.7	0.7	0.5	0.4	0.3
Dy	3.7	3.5	3.9	3.4	2.8	2.3	1.8
Ho	0.7	0.6	0.8	0.6	0.5	0.4	0.3
Er	2.1	2	2.1	1.9	1.6	1.2	1
Tm	0.2	0.2	0.3	0.2	0.2	0.1	0.1
Yb	1.8	1.7	1.8	1.7	1.5	1	0.9
Lu	0.3	0.2	0.2	0.2	0.2	0.1	0.1

Table 3-3. Representative Chemical Analyses of Miocene, Eocene, Cretaceous, and Jurassic Igneous Rocks In and Adjacent to the Carlin Trend, Northeastern Nevada

Rock Type[1]		And–Dac				Rhyolite–Dacite	
Sample No.	H98-68	H98-101	H98-97	H98-1	H98-96	H98-56	H98-102
Hf		2.8	5.1	3.4	2.2	4	3.1	2.2
Ta		1.44	1.47	0.86	1.86	2.11	1.56	1.91
W								
Au								
Hg								
Tl		0.38	0.39	0.2	0.46	0.71	0.58	0.57
Pb		16	17	16	18	24	22	20
Bi		0.01	0.08	0.02	0.05	0.2	0.12	0.09
Th		12	11	7	12	12	9	7
U		2.2	3.8	2.2	3.7	6.7	4.6	3.1

Table 3-3. Representative Chemical Analyses of Miocene, Eocene, Cretaceous, and Jurassic Igneous Rocks In and Adjacent to the Carlin Trend, Northeastern Nevada

Age	Eocene	Cretaceous	Jurassic	Jurassic	Jurassic	Jurassic	Jurassic
		Richmond intrusion	Lamprophyre dikes				Goldstrike com
Rock Type[1]		Granite	Phl lamprophyr	Hb lamprophyre			Diorite
Sample No.	H98-61	RICH-1	GEN-3	DS-40	CE52-1538	LAN-17	TURF-11
Sample Type	outcrop	outcrop	pit	underground	core	outcrop	outcrop
Location		Richmond District	Genesis	Deep Star	Lantern	Lantern	Vivian sill
Latitude	40° 40.8'	40° 51'05"	40° 57'00"	40° 51.67'	40° 55'45"	40° 55'15"	40° 56.97'
Longitude	116° 19.8'	116° 18'25"	116° 21'40"	116° 21.75'	116° 22'10"	116° 21'33"	116° 18.95'
Occurrence	dike	intrusion	dike	dike	dike	dike	intrusion
Alteration	fresh	fresh	chloritic	chloritic	propylitic	propylitic	propylitic
Isotopic Age (Ma)	Tir	112	158	158			
Analyses[2]	W, C	U, A	U, A	U, N	U, N	U, N	U, N
Analytical Method	XRF WSU	XRF/ICP-MS	XRF/ICP-MS	XRF/INAA	XRF/INAA	XRF/INAA	XRF/INAA
SiO_2	74.78	75.04	52.69	53.85	53.84	53.86	53.47
TiO_2	0.23	0.17	1.04	1.08	1.08	1.06	1.05
Al_2O_3	13.49	13.73	12.27	13.85	13.85	14.06	13.17
FeO^3	1.47	1.32	7.93	7.69	7.69	7.88	8.76
MnO	0.03	0.03	0.09	0.13	0.13	0.14	0.12
MgO	0.28	0.41	11.42	9.98	9.98	10.27	11.12
CaO	1.61	1.16	9.29	8.25	8.25	7.97	7.71
Na_2O	3.54	3.21	2.69	2.76	2.76	2.30	1.92
K_2O	4.46	4.86	2.03	2.04	2.04	2.15	2.36
P_2O_5	0.10	0.08	0.54	0.38	0.38	0.32	0.32
LOI		0.62	8.28		3.19		0.10
	100.00	100.62	108.28	100.00	103.19	100.00	100.10
Recalc Total		100.00	100.00	100.00			
Total[4]	99.52	100.69	99.40	98.96	98.55	99.42	96.73
Sc	4			21	24	25	19
V	9	7	185	181			146
Cr	1						
Co	18.2	1.6	43	35	34	32	24
Ni	1.1	37	211	327	280	<21	88
Cu	2.9	280	144	36			16
Zn	44	14	58	66	105	97	81
Ga	18.1	16	16	12			17
As	1.6	<5	9.0	4.6	2.8	3.9	2.5
Rb	154	285	68	54	45	51	59
Sr	316	202	1398	1200	<500	<500	771
Y	19	16.0	27.0	21.0			23
Zr	175	112	182	234			203
Nb	18.3	29	9	14			22
Mo	1.93	1.0	0.8	4.0	5	<1	<1
Ag	0.06	-0.5					
Sb	0.33	0.2	1.6	0.4	1.7	1.2	0.4
Cs	4.47	9	16	-1	2	2	2
Ba	1146	482	1390	1242	1200	1100	960
La	42.2	34.0	133.0	76.0	53	45	52
Ce	75.1	62.0	265.0	150.0	86	72	100
Pr	8.3	6.0	28.3				
Nd	29.1	19.0	107.0	55.0	41	38	30
Sm	4.9	2.9	18.0	9.2	7	6.2	6.4
Eu	1	0.5	4.3	3.1	2.4	2.1	2
Gd	4.4	2.1	12.0				
Tb	0.6	0.3	1.3	<0.5	0.5	0.8	0.8
Dy	2.8	1.8	5.2				
Ho	0.5	0.4	0.8				
Er	1.6	1.3	2.4				
Tm	0.2	0.28	0.26				
Yb	1.4	2.0	1.6	1.8	2.2	2	2.4
Lu	0.2	0.40	0.24	0.30	0.34	0.35	0.38

Table 3-3. Representative Chemical Analyses of Miocene, Eocene, Cretaceous, and Jurassic Igneous Rocks In and Adjacent to the Carlin Trend, Northeastern Nevada

Rock Type[1]		Granite	Phl lamprophyre	Hb lamprophyre			Diorite
Sample No.	H98-61	RICH-1	GEN-3	DS-40	CE52-1538	LAN-17	TURF-11
Hf	3.5	3.7	5.0	6.0	5	5	7
Ta	2.46	3.4	0.7	1.4	<5	<5	1
W		23	0.9	<1	<1	<1	<1
Au				4.0	-2	7	-2
Hg				-1.0	-1	-1	-1
Tl	0.87	1.6	0.3				
Pb	21	15.0	8.0	19.0	<1	<1	12
Bi	0.01	45.0	1.1				
Th	16	41	32	13	10	9	12
U	4.7	14.0	5.2	3.0	3.1	1.9	3.5

Table 3-3. Representative Chemical Analyses of Miocene, Eocene, Cretaceous, and Jurassic Igneous Rocks In and Adjacent to the Carlin Trend, Northeastern Nevada

Age	Jurassic	Jurassic	Jurassic	Jurassic	Jurassic
	ιple›				Rhyolite dike
Rock Type[1]	Diorite	Diorite	Diorite	Granodiorite	Rhyolite
Sample No.	NS-1	SJ 489C-1071	98-ZIA-7	GEN-2-1534	98-Zia-9
Sample Type	pit	core	outcrop	core	outcrop
Location	North Star	Screamer	West of Genesi	Genesis	Zia Claims
Latitude	40° 57.42'	40° 59'	40° 56.47'	40° 57.5'	40° 56.18'
Longitude	116° 21.47'	116° 23'	116° 21.40'	116° 22.0'	116° 23.22'
Occurrence	intrusion	dike	intrusion	dike	dike
Alteration	fresh	fresh	fresh	fresh	fresh
Isotopic Age (Ma)	158	158	~158	158	157.4+/-0.4
Analyses[2]	U, A	U, A	U, N	U, N	U, N
Analytical Method	XRF/ICP-MS	XRF/ICP-MS	XRF/INAA	XRF/INAA	XRF/INAA
SiO_2	58.01	59.77	60.43	66.44	73.57
TiO_2	0.94	1.02	0.99	0.80	0.21
Al_2O_3	15.95	13.42	18.02	15.38	15.23
FeO^3	6.26	5.97	5.94	3.88	1.02
MnO	0.11	0.10	0.11	0.05	0.03
MgO	6.40	5.84	2.47	2.04	0.36
CaO	6.77	5.90	5.70	3.42	1.67
Na_2O	3.07	2.12	3.32	3.08	3.76
K_2O	2.22	5.27	2.74	4.72	4.06
P_2O_5	0.27	0.60	0.29	0.19	0.09
LOI	0.70	4.61	0.04	2.15	0.72
	100.70	104.61	100.04	102.15	100.72
Recalc Total	100.00	100.00		100.00	100.00
Total[4]	98.51	100.56	99.05		97.56
Sc			11	9	4
V	164	128	127	82	24
Cr					
Co	21	22	10	9.0	1.0
Ni	31	49	2	30	26
Cu	<10	36	9	24	11
Zn	67	42	68	44	157
Ga	19	16	20	18	12
As	<5	<5	1.7	8.1	3.9
Rb	72	191	93	167	99
Sr	1012	627	844	501	507
Y	28.0	25.0	32.0	31.0	30.0
Zr	191	341	270	340	151
Nb	15	22	25	26	25
Mo	1.4	2.0	8.0	4.0	8.0
Ag	-0.5	-0.5	-5.0	-5.0	-5.0
Sb	0.5	0.9	0.1	1.8	0.8
Cs	2	6	2	5	-1
Ba	826	1255	938	666	2062
La	56.0	65.0	60.0	94.0	58.0
Ce	113.0	126.0	89.0	140.0	93.0
Pr	13.3	14.0			
Nd	50.0	51.0	39.0	49.0	36.0
Sm	8.9	9.2	6.4	7.7	4.9
Eu	2.2	2.4	1.9	1.8	1.6
Gd	6.7	7.0			
Tb	0.9	0.9	0.8	<0.5	<0.5
Dy	4.9	4.4			
Ho	0.9	0.8			
Er	2.7	2.2			
Tm	0.37	0.29			
Yb	2.3	1.7	2.5	2.1	2.3
Lu	0.35	0.25	0.47	0.45	0.34

**Table 3-3. Representative Chemical Analyses of Miocene, Eocene, Cretaceous, and Jurassic Igneous Rocks
In and Adjacent to the Carlin Trend, Northeastern Nevada**

Rock Type[1]	Diorite	Diorite	Diorite	Granodiorite	Rhyolite
Sample No.	NS-1	SJ 489C-1071	98-ZIA-7	GEN-2-1534	98-Zia-9
Hf	5.4	10.0	7.0	13.0	6.0
Ta	1.1	1.5	1.5	2.2	1.8
W	1.0	2.1	<1	<1	<1
Au			-2.0	4.0	3.0
Hg			-1.0	-1.0	-1.0
Tl	0.3	0.4			
Pb	16.0	15.0	18.0	18.0	44.0
Bi	0.5	1.7			
Th	12	19	11	29	13
U	2.3	5.8	3.6	8.7	4.3

Table 3-4. Characteristics of Eocene Igneous Rocks of the Carlin Trend, Northeastern Nevada

Unit	Rock type	Texture	Phenocrysts	Age	Distinguishing features	Extent; volume
Northern Carlin trend						
Porphyritic (pl-bi-hbl-qtz±sa) rhyolite dikes	low-Si rhyolite to high-Si dacite	coarsely porphyritic, aphanitic	pl: 5-15%, 1-6mm qtz: 1-2%, 1-4mm sa: 0-2%, 1-15mm bi: 1-3%, 1-4mm hbl: 1-4, 1-2mm	37.6 Ma	ore host at Beast; identical to late porphyritic dikes of Emigrant Pass; "Beast-type" dikes of mines	3-km-long dike at Beast mine; several dikes to south
Basaltic andesite dikes	basalt to basaltic andesite	sparsely porphyritic, aphanitic	pl: <0-1%, <5 mm px:1-2%, <3 mm ol: 3%, <3 mm	37.8 Ma	Dense mafic dikes; altered, weakly mineralized at Dee	several dikes near Dee and Goldstrike deposits
Aphyric rhyolite dikes	high-Si rhyolite	aphyric	sparse microlites of feldspar, Fe-rich pyroxene, and zircon	~39.1 Ma	commonly glassy; locally altered ± mineralized; "Deep Star-type" dikes of mines	several dikes; total 8 km long
Porphyritic (pl-bi-hbl) dacite dikes	dacite	finely to coarsely porphyritic, aphanitic	pl: 15%, 1-6mm bi: 2%, 1-5 mm- hbl: 3-5%, 2-10 mm qtz: 0-1%, <3mm	40.1-39.0 Ma	hbl ghosts altered to bi and smectite; host ore at Griffin and Meikle; altered at Betze-Post; "BFP-type" dikes of mines	≥5-km-long swarm from Betze-Post to Meikle
Finely porphyritc (pl-bi±qtz) rhyolite dikes	rhyolite	finely porphyritic, aphanitic	pl: 5-7%; 1-2 mm bi: 2-4%; 1-3 mm qtz: 0-1%; 1-2 mm	40.3-39.3 Ma	Sparsely porphyritic; commonly glassy; "K-type" dikes of mines	Abundant dikes along Post fault system
Welches Canyon						
Aphyric rhyolite dome and dikes	rhyolite	aphyric		Post 38.6 Ma, pre 37.4 Ma	flow-banded, partly glassy but clay-altered	Small volcanic dome and abundant dikes
Porphyritic andesite to dacite	andesite to dacite	strongly porphyritic, aphanitic	pl: 5-15%, 1-6mm qtz: 1-2%, 1-4mm sa: 0-4%, 1-15mm bi: 1-3%, 1-4mm hbl: 1-4, 1-2mm	38.6 Ma	Aphanitic, locally glassy, mostly coarsely porphyritic; includes "Beast-and K-type" dikes of mines	abundant N and NE dikes
Microdiorite (Tg)	diorite	fine grained, equigranular, phaneritic	pl: 55-60% px: 15-20% altered hbl: 10% qtz: 10%	38.6 Ma	Fine grained, equigranular, intermediate intrusion; propylitized	1 km2 stock; south side of Welches Canyon
Emigrant Pass volcanic field						
Porphyritic (pl-bi-hbl-qtz±sa) rhyolite-dacite dikes	rhyolite to high-Si dacite	coarsely porphyritic	pl: 5-15%, 1-6mm qtz: 1-2%, 1-4mm sa: 0-2%, 1-15mm bi: 1-3%, 1-4mm hbl: 1-4, 1-2mm	36.2 Ma	coarsely porphyritic	~10-km-long belt
Bob Creek lava (Tb)	andesite (57% SiO2)	porphyritic	hbl: 12%, 1-8mm px: 3-5%; 1mm pl: trace; ≤1cm	37.4 Ma	hbl>>pl	30km^2; 3 km^3
Mack Creek lavas and intrusions (Tk)	dacite	coarsely porphyritic	pl: 15-30%, 1-5mm hbl: 6-10%, 1-7mm bi: 3%, ≤3mm qtz: 0-3%, 1-3mm px: 1-3%, 1mm	37.9-37.6 Ma	abundantly to moderately and coarsely porphyritic domes	~12km^2; ~5 km^3

Primeaux lavas: (Tp)	andesite	finely, abundantly porphyritic	pl: 16-30%, ≤2mm hbl: 4-10%, 1-8mm px: 1-4%, ≤1mm bi: 0-2%, ≤3mm	38.1-37.9 Ma	finely porphyritic andesite, but coarse hbl	75 km^2; ~30 km^3
Rain-Railroad						
Diorite and basaltic andesite dikes	andesite to basaltic andesite	porphyritic, aphanitic	pl: 5-10%; 1-3 mm px: 1-3%; 1 mm ol: <1 %; 2 mm altered hbl: <2%; 2 mm	39.1, 38.2 Ma	Mafic porphyritic dikes; mostly highly altered along Rain fault	several dikes; several km long at and NW of Rain
Porphyritic (pl-bi-hbl-qtz±sa) rhyolite stock and dikes	Rhyolite to dacite	coarsely porphyritic	pl: 5-15%, 1-6mm qtz: 1-2%, 1-4mm sa: 0-2%, 1-15mm bi: 1-3%, 1-4mm hbl: 1-4, 1-2mm	37.5-37.4Ma	Nearly identical to coarsely porphyritic rhyolite dikes of Carlin trend	1 km^2 porphyry stock at Railroad and radial dikes; also dikes at Emigrant Springs

pl = plagioclase, qtz = quartz, sa = sanidine, bi = biotite, hbl = hornblende, px = pyroxene, ol = olivine

Appendix 3-1. Explanation of Analytical Methods

Laboratories:
Actlabs = Activation Laboratories, Ltd., Ancaster, Ontario, Canada; Acme = Acme
Analytical Laboratories, Ltd, Vancouver, British Columbia, Canada; Chemex = ALS
Chemex USA, Inc., Sparks, Nevada, USA; USML = U.S. Mineral Laboratories, Inc.,
Auburn, California, USA; UNR = Nevada Bureau of Mines and Geology, University of
Nevada, Reno, Reno, Nevada, USA

Methods:
INAA = Instrumental neutron activation analyses; Actlabs analytical package 1H or 1D
ICP/ICP-MS = Inductively coupled plasma spectrometry, including atomic emission and
    mass spectrometry; Actlabs analytical package 4B
ICP – 4 acid = Inductively coupled plasma atomic emission spectrometry using 4-acid
    digestion; Actlabs analytical package 1F
ICP = Inductively coupled plasma atomic emission spectrometry; USML analytical
    package GXPL10 using "Magic" 3-acid dissolution or Acme analytical package 1E,
    using 4-acid dissolution
XRF-FD = X-ray fluorescence analyses for major elements on Li-metaborate fused disks
    using a Phillips 1404 wave-dispersive spectrometer; variance was generally ≤3% from
    published values for USGS standards AGV-1, RGM-1, and BIR-1 (Taggart, J.E.,
    Lindsay, J.R., Scott, B.A., Vivit, D.V., Bartel, A.J., and Stewart, K.C., 1987, Analysis
    of geologic materials by wavelength-dispersive x-ray fluorescence spectrometry, in
    P.A. Baedecker, ed., Methods for Geochemical Analysis: U.S. Geological Survey
    Bulletin 1770, p. E1-E19).
XRF-P = X-ray fluorescence analyses for trace elements on pressed rock powders using
    cellulose as a binder. USGS standards AGV -1, RGM-1, and BIR-1 were routinely
    used to monitor accuracy and reproducibility and values were generally within 2-10%
    for most trace elements.
AuFA = Fire assay gold analyses with ICP finish; Acme package 6

Appendix 3-1: Table of Geochemical Data for Carlin Trend Igneous Rocks

Sample Name	Sample Type	Location	Latitude	Longitude	Occurrence	Rock Type
Miocene Rocks						
LAN-65	outcrop	Lantern, south	40 54.42'	116 22.15'	lava flow	rhyolite
LAN-65	outcrop	Lantern, south	40 54.42'	116 22.15'	lava flow	rhyolite
LAN-65	outcrop	Lantern, south	40 54.42'	116 22.15'	lava flow	rhyolite
LAN-65	outcrop	Lantern, south	40 54.42'	116 22.15'	lava flow	rhyolite
98-Zia-6	outcrop	Zia Claims	40 56.08'	116 23.73'	lava, devitrified	rhyolite of Zia
98-Zia-6	outcrop	Zia Claims	40 56.08'	116 23.73'	lava, devitrified	rhyolite of Zia
98-Zia-6	outcrop	Zia Claims	40 56.08'	116 23.73'	lava, devitrified	rhyolite of Zia
MM-1	outcrop	Marys Mtn.	40 42' 09"	116 16' 13"	lava, glassy	rhyolite of Marys Mtn
Eocene Rocks						
BST-30	open pit	Beast	40 56'25"	116 21'20"	dike	rhyolite of Beast deposit
BST-30	open pit	Beast	40 56'25"	116 21'20"	dike	rhyolite of Beast deposit
BST-30	open pit	Beast	40 56'25"	116 21'20"	dike	rhyolite of Beast deposit
BST-20	open pit	Beast	40 56'23"	116 21'20"	dike breccia	rhyolite of Beast deposit
BST-20	open pit	Beast	40 56'23"	116 21'20"	dike breccia	rhyolite of Beast deposit
BST-20	open pit	Beast	40 56'23"	116 21'20"	dike breccia	rhyolite of Beast deposit
BST-20	open pit	Beast	40 56'23"	116 21'20"	dike breccia	rhyolite of Beast deposit
BST-103	open pit	Beast	40 56'15"	116 21'20"	dike breccia	rhyolite of Beast deposit
BST-103	open pit	Beast	40 56'15"	116 21'20"	dike breccia	rhyolite of Beast deposit
BST-103	open pit	Beast	40 56'15"	116 21'20"	dike breccia	rhyolite of Beast deposit
BST-103	open pit	Beast	40 56'15"	116 21'20"	dike breccia	rhyolite of Beast deposit
BST-101	open pit	Beast	40 56'20"	116 21'20"	heterolithic breccia	heterolithic breccia
BST-104	open pit	Beast	40 56'19"	116 21'20"	dike breccia	rhyolite of Beast deposit
BST-105	open pit	Beast	40 56'17"	116 21'20"	dike breccia	rhyolite of Beast deposit
BST-105	open pit	Beast	40 56'17"	116 21'20"	dike breccia	rhyolite of Beast deposit
BST-130	open pit	Beast	40 56'22"	116 21'24"	dike	rhyolite of Beast deposit
BST-130	open pit	Beast	40 56'22"	116 21'24"	dike	rhyolite of Beast deposit
BST-130	open pit	Beast	40 56'22"	116 21'24"	dike	rhyolite of Beast deposit
BST-144	open pit	Beast	40 56'30"	116 21'24"	heterolithic breccia	heterolithic breccia
BST-144	open pit	Beast	40 56'30"	116 21'24"	heterolithic breccia	heterolithic breccia
BST-143	open pit	Beast	40 56'30"	11621'24"	heterolithic breccia	heterolithic breccia
BP-27a	open pit	Betze-Post	40 58.6'	116 21.9'	dike	rhyolite of Post
BP-27b	open pit	Betze-Post	40 58.6'	116 21.9'	dike	rhyolite of Post
BP-2-2	open pit	Betze-Post	40 58.6'	116 21.9'	dike	rhyolite of Post
BP-2-2	open pit	Betze-Post	40 58.6'	116 21.9'	dike	rhyolite of Post
PNC 213-1787	core	Betze-Post	40 58.6'	116 21.9'	dike	dacite of Betze-Post
PNC 213-1787	core	Betze-Post	40 58.6'	116 21.9'	dike	dacite of Betze-Post
CN-3	core	Betze-Post	40 58.6'	116 21.9'	dike	dacite of Betze-Post
CN-3	core	Betze-Post	40 58.6'	116 21.9'	dike	dacite of Betze-Post
BP-2	open pit	Betze-Post	40 58.6'	116 21.9'	dike	rhyolite of Post
BP-2	open pit	Betze-Post	40 58.6'	116 21.9'	dike	rhyolite of Post
BP-27	open pit	Betze-Post	40 58.6'	116 21.9'	dike	rhyolite of Post
BP-27	open pit	Betze-Post	40 58.6'	116 21.9'	dike	rhyolite of Post
BP-2(vug)	open pit	Betze-Post	40 58.6'	116 21.9'	dike	rhyolite of Post
BP-27	open pit	Betze-Post	40 58.6'	116 21.9'	dike	rhyolite of Post
BP-27	open pit	Betze-Post	40 58.6'	116 21.9'	dike	rhyolite of Post
BP-27wr	open pit	Betze-Post	40 58.6'	116 21.9'	dike	rhyolite of Post
BP-27a	open pit	Betze-Post	40 58.6'	116 21.9'	dike	rhyolite of Post
BP-2A-VUG	open pit	Betze-Post	40 58.6'	116 21.9'	dike	rhyolite of Post
96M-208	open pit	Betze-Post	40 58.6'	116 21.9'	dike	dacite of Betze-Post
BP-23	open pit	Betze-Post	40 59.0'	116 22.1'	dike	dacite of Betze-Post
BP-23	open pit	Betze-Post	40 59.0'	116 22.1'	dike	dacite of Betze-Post
BP-23	open pit	Betze-Post	40 59.0'	116 22.1'	dike	dacite of Betze-Post
BP-26A	open pit	Betze-Post	40 58.7'	116 21.9'	dike	rhyolite of Post
BP-26A	open pit	Betze-Post	40 58.7'	116 21.9'	dike	rhyolite of Post
BP-26A	open pit	Betze-Post	40 58.7'	116 21.9'	dike	rhyolite of Post
BP-4460	open pit	Betze-Post	40 58.7'	116 21.9'	dike	rhyolite of Post
BP-4460	open pit	Betze-Post	40 58.7'	116 21.9'	dike	rhyolite of Post
BP-4460	open pit	Betze-Post	40 58.7'	116 21.9'	dike	rhyolite of Post
BP-2-1-clvug	open pit	Betze-Post	40 58.6'	116 21.9'	dike	rhyolite of Post
BP-2-1-clvug	open pit	Betze-Post	40 58.6'	116 21.9'	dike	rhyolite of Post
BP-2-2-clvug	open pit	Betze-Post	40 58.6'	116 21.9'	dike	rhyolite of Post

Appendix 3-1: Table of Geochemical Data for Carlin Trend Igneous Rocks 234

Sample Name	Sample Type	Location	Latitude	Longitude	Occurrence	Rock Type
BP-2-altfeld	open pit	Betze-Post	40 58.6'	116 21.9'	dike	rhyolite of Post
BP-2-altfeld	open pit	Betze-Post	40 58.6'	116 21.9'	dike	rhyolite of Post
GB 720C-1744	core	Betze-Post	40 59' 27"	116 22' 29"	dike	dacite of Betze-Post
GB 720C-1744	core	Betze-Post	40 59' 27"	116 22' 29"	dike	dacite of Betze-Post
VG-1	open pit	Betze-Post	40 58.6'	116 21.9'	dike	rhyolite of Post
VG-1	open pit	Betze-Post	40 58.6'	116 21.9'	dike	rhyolite of Post
BP-2glass	open pit	Betze-Post	40 58.6'	116 21.9'	dike	rhyolite of Post
BP-27wr	open pit	Betze-Post	40 58.6'	116 21.9'	dike	rhyolite of Post
BP-2glass	open pit	Betze-Post	40 58.6'	116 21.9'	dike	rhyolite of Post
DS-1	underground mine	Deep Star	40 57.7'	116 21.7'	dike	rhyolite of Deep Star
DS-1	underground mine	Deep Star	40 57.7'	116 21.7'	dike	rhyolite of Deep Star
DS-1	underground mine	Deep Star	40 57.7'	116 21.7'	dike	rhyolite of Deep Star
DS-1	underground mine	Deep Star	40 57.7'	116 21.7'	dike	rhyolite of Deep Star
DSU-143-30	core	Deep Star	40 57.7'	116 21.7'	dike	rhyolite of Deep Star
DSU-143-30	core	Deep Star	40 57.7'	116 21.7'	dike	rhyolite of Deep Star
DSU-143-182	core	Deep Star	40 57.8'	116 21.7	dike	rhyolite of Deep Star
DS-13	underground mine	Deep Star	40 57.8'	116 21.7	dike	rhyolite of Deep Star
DS-42	underground mine	Deep Star	40 57.8'	116 21.7	dike	rhyolite of Deep Star
DS-42	underground mine	Deep Star	40 57.8'	116 21.7	dike	rhyolite of Deep Star
DS-42A	underground mine	Deep Star	40 57.8'	116 21.7	dike	rhyolite of Deep Star
DS-42A	underground mine	Deep Star	40 57.8'	116 21.7	dike	rhyolite of Deep Star
DS-42A	underground mine	Deep Star	40 57.8'	116 21.7	dike	rhyolite of Deep Star
EMP-2	outcrop	Emigrant Pass	40 41 ' 05"	116 27' 16.5	dike	rhyolite
RM97C-7-1336	core	Betze-Post	40 57.8'	116 21.7	dike	rhyolite of Post
RM97C-7-1336			40 57.8'	116 21.7		
RM97C-7-1342	core	Betze-Post	40 57.8'	116 21.7	dike	rhyolite of Post
RM97C-7-1342			40 57.8'	116 21.7		
RM97C-7-1359	core	Betze-Post	40 57.8'	116 21.7	dike	rhyolite of Post
RM97C-7-1359			40 57.8'	116 21.7		
BS1004-504	core	Genesis	40 57.8'	116 21.7	dike	rhyolite
BS1004-504			40 57.8'	116 21.7		
BS1004-522	core	Genesis	40 57.8'	116 21.7	dike	rhyolite
BS1004-522			40 57.8'	116 21.7		
BS1004-523	core	Genesis	40 57.8'	116 21.7	dike	rhyolite
BS1004-523			40 57.8'	116 21.7		
98-GEN-23	open pit	Genesis	40 57.77'	116 21.75'	dike	rhyolite?
GEN-2	open pit	Genesis	40 56.85'	116 22.05'	dike	rhyolite of Genesis
GEN-2	open pit	Genesis	40 56.85'	116 22.05'	dike	rhyolite of Genesis
GEN-2	open pit	Genesis	40 56.85'	116 22.05'	dike	rhyolite of Genesis
98Gen-11	open pit	Genesis	40 57.0'	116 22.05'	dike	rhyolite of Genesis
98Gen-11	open pit	Genesis	40 57.0'	116 22.05'	dike	rhyolite of Genesis
98-GEN-1	open pit	Genesis	40 56.9'	116 22.05'	dike	rhyolite of Genesis
98-GEN-1	open pit	Genesis	40 56.9'	116 22.05'	dike	rhyolite of Genesis
BSTR-3	open pit	Genesis	40 56.6'	116 22.05'	dike	rhyolite of Genesis
M8-0317-4-482	core	Griffin	41 00' 01"	116 22' 45"	dike	dacite of Betze-Post
M8-0317-4-482	core	Griffin	41 00' 01"	116 22' 45"	dike	dacite of Betze-Post
IV-1	subcrop	Ivanhoe-Hatter	41 06' 34.1'	116 31' 08.7	intrusion	dacite
IV-1	subcrop	Ivanhoe-Hatter	41 06' 34.1'	116 31' 08.7	intrusion	dacite
LAN-70	outcrop	Lantern	40 55.95'	116 22.45'	dike	rhyolite of Genesis
RICH-12	outcrop	Richmond Mt	40 51'47"	116 18'17"	dike	dacite
RICH-12	outcrop	Richmond Mt	40 51'47"	116 18'17"	dike	dacite
RICH-10	outcrop	Richmond Mt	40 51'49"	116 18'10"	dike	rhyolite
RICH-10	outcrop	Richmond Mt	40 51'49"	116 18'10"	dike	rhyolite
RICH-10	outcrop	Richmond Mt	40 51'49"	116 18'10"	dike	rhyolite
RICH-10	outcrop	Richmond Mt	40 51'49"	116 18'10"	dike	rhyolite
RICH-10	outcrop	Richmond Mt	40 51'49"	116 18'10"	dike	rhyolite
WC-4	outcrop	Welches Canyon	40 47'42"	116 17'58"	intrusion	granodiorite
WC-4	outcrop	Welches Canyon	40 47'42"	116 17'58"	intrusion	granodiorite
WC-5	outcrop	Welches Canyon	40 47'43"	116 17'56"	intrusion	diorite
WC-5	outcrop	Welches Canyon	40 47'43"	116 17'56"	intrusion	diorite
WC-9	outcrop	Welches Canyon	40 47'25"	116 19'10"	dike	dacite
WC-9	outcrop	Welches Canyon	40 47'25"	116 19'10"	dike	dacite
WC-3	outcrop	Welches Canyon	40 47'45"	116 18'05"	dike	andesite

Appendix 3-1: Table of Geochemical Data for Carlin Trend Igneous Rocks

Sample Name	Sample Type	Location	Latitude	Longitude	Occurrence	Rock Type
WC-3	outcrop	Welches Canyon	40 47'45"	116 18'05"	dike	andesite
WC-3	outcrop	Welches Canyon	40 47'45"	116 18'05"	dike	andesite
WC-3	outcrop	Welches Canyon	40 47'45"	116 18'05"	dike	andesite
WC-2	outcrop	Welches Canyon	40 48'00"	116 19'15"	dike intruding dome?	rhyolite
WC-2	outcrop	Welches Canyon	40 48'00"	116 19'15"	dike intruding dome?	rhyolite
WC-31	outcrop	Welches Canyon	40 47'44"	116 17'55"	intrusion	microdiorite
WC-56	outcrop	Welches Canyon	40 47'38"	116 19'00"	dike	andesite
WC-56	outcrop	Welches Canyon	40 47'38"	116 19'00"	dike	andesite
WC-105	outcrop	Richmond Mt	40 51'05"	116 20'48"	dike	dacite
WC-105	outcrop	Richmond Mt	40 51'05"	116 20'48"	dike	dacite
WC-106	outcrop	Richmond Mt	40 50'43"	116 19'58"	dike	andesite porphyry
WC-106	outcrop	Richmond Mt	40 50'43"	116 19'58"	dike	andesite porphyry
WC-104	outcrop	Richmond Mt	40 50'00"	116 20'10"	dike	rhyolite
WC-104	outcrop	Richmond Mt	40 50'00"	116 20'10"	dike	rhyolite
WC-102	outcrop	east of IB claims	40 49'00"	116 19'50"	dike	rhyolite
WC-103	outcrop	east of IB claims	40 49'00"	116 19'50"	dike	rhyolite
WC-103	outcrop	east of IB claims	40 49'00"	116 19'50"	dike	rhyolite
98-WC-3	outcrop	Welches Canyon	40 48'02"	116 18'00"	dome	rhyolite
98-WC-3	outcrop	Welches Canyon	40 48'02"	116 18'00"	dome	rhyolite
98-GEN-24	outcrop	Genesis	40 57.77'	116 21.75'	dike	rhyolite
98-GEN-24	outcrop	Genesis	40 57.77'	116 21.75'	dike	rhyolite
LAN-80	outcrop	Lantern	40 55.8'	116 22.47'	dike	rhyolite
LAN-80	outcrop	Lantern	40 55.8'	116 22.47'	dike	rhyolite
98-DEE-7	open pit	Dee	41 02'06"	116 25'35"	dike	basalt
98-DEE-8	open pit	Dee	41 02'06"	116 25'35"	dike	basalt
98-DEE-8	open pit	Dee	41 02'06"	116 25'35"	dike	basalt
LAN-57	outcrop	Lantern	40 55'47"	116 22'30"	dike	rhyolite of Deep Star
LAN-57	outcrop	Lantern	40 55'47"	116 22'30"	dike	rhyolite of Deep Star
CD 96 10C-1455	core	Clydesdale claims	40 59.5'	116 24.3'	dike	basalt
Cretaceous Rocks						
RICH-1	outcrop	Richmond Mt	40 51'05"	116 18'25"	intrusion	granite of Richmond stock
RICH-1	outcrop	Richmond Mt	40 51'05"	116 18'25"	intrusion	granite of Richmond stock
Jurassic Rocks						
BC-2	outcrop	Bell Creek/Ren	41 00.6'	116 23.2'	dike	monzonite
BC-2	outcrop	Bell Creek/Ren	41 00.6'	116 23.2'	dike	monzonite
RM97c-2-443	core	Betze-Post	40 58' 37"	116 21' 57"	intrusion	diorite of Goldstrike stock
RM97C-2-443	core	Betze-Post	40 58' 37"	116 21' 57"	intrusion	diorite of Goldstrike stock
RM97C-2-443	core	Betze-Post	40 58' 37"	116 21' 57"	intrusion	diorite of Goldstrike stock
BP-41A	open pit	Betze-Post	40 58.9'	116 22.15'	dike	diorite of Goldstrike stock
BP-41A	open pit	Betze-Post	40 58.9'	116 22.15'	dike	monzonite
BP-41A	open pit	Betze-Post	40 58.9'	116 22.15'	dike	monzonite
96M-206a	open pit	Betze-Post	40 58.8'	116 22.37'	dike	lamprophyre
96M-206b	open pit	Betze-Post	40 58.8'	116 22.37'	dike	lamprophyre
96M-207	open pit	Betze-Post	40 58.8'	116 22.37'	intrusion	diorite of Goldstrike stock
96M-209	open pit	Betze-Post	40 58.8'	116 22.37'	dike	monzonite
BP-22	open pit	Betze-Post	40 58.8'	116 22.37'	dike	lamprophyre, phlogopitic
BP-22	open pit	Betze-Post	40 58.8'	116 22.37'	dike	lamprophyre, phlogopitic
BP-31	open pit	Betze-Post	40 58.8'	116 22.45'	dike	lamprophyre, phlogopitic
BP-31	open pit	Betze-Post	40 58.8'	116 22.45'	dike	lamprophyre, phlogopitic
BP-120	open pit	Betze-Post	40 58'20"	116 22'30"	dike	microdiorite
BP-120	open pit	Betze-Post	40 58'20"	116 22'30"	dike	microdiorite
BAZ-2	open pit	West Bazza	40 58'45"	116 23'01"	dike	porphyritic diorite
BAZ-2	open pit	West Bazza	40 58'45"	116 23'01"	dike	porphyritic diorite
DS-40	underground mine	Deep Star	~40 51' 40"	~116 21'45"	dike	lamprophyre, hbl
DS-40	underground mine	Deep Star	~40 51' 40"	~116 21'45"	dike	lamprophyre, hbl
DS-40	underground mine	Deep Star	~40 51' 40"	~116 21'45"	dike	lamprophyre, hbl
DS-40	underground mine	Deep Star	~40 51' 40"	~116 21'45"	dike	lamprophyre, hbl
DS-41	underground mine	Deep Star	~40 51' 40"	~116 21'45"	dike	lamprophyre, hbl
DS-41	underground mine	Deep Star	~40 51' 40"	~116 21'45"	dike	lamprophyre, hbl
GEN-2-1534	core	Genesis	40 57' 42	116 21' 15"	dike	granodiorite of Goldstrike
GEN-2-1534	core	Genesis	40 57' 42	116 21' 15"	dike	granodiorite of Goldstrike
GEN-3	open pit	Genesis	40 57'00"	116 21'40"	dike	lamprophyre, phlogopitic

Appendix 3-1: Table of Geochemical Data for Carlin Trend Igneous Rocks

Sample Name	Sample Type	Location	Latitude	Longitude	Occurrence	Rock Type
GEN-3	open pit	Genesis	40 57'00"	116 21'40"	dike	lamprophyre, phlogopitic
GA-13	outcrop	Golden April claim	40 59'50"	116 24'05"	dike	felsic dike
GA-13	outcrop	Golden April claim	40 59'50"	116 24'05"	dike	felsic dike
GA-10	outcrop	Golden April claim	40 59'40"	116 24'05"	dike	lamprophyre? dike
GA-10	outcrop	Golden April claim	40 59'40"	116 24'05"	dike	lamprophyre? dike
GA-12	outcrop	Golden April claim	40 59'55"	116 23'58"	dike	lamprophyre
GA-12	outcrop	Golden April claim	40 59'55"	116 23'58"	dike	lamprophyre
GA19C-1636	core	Golden April claim	40 59' 25"	116 24' 10"	dike	diorite
GA19C-1636	core	Golden April claim	40 59' 25"	116 24' 10"	dike	diorite
CE52-1538	core	Lantern-Exodus	~40 55'45"	~116 22'10"	dike	lamprophyre, coarse hbl
CE52-1538	core	Lantern-Exodus	~40 55'45"	~116 22'10"	dike	lamprophyre, coarse hbl
LAN-10	outcrop	Lantern	40 55'42"	116 21'41"	dike	lamprophyre, bio-hbl
LAN-10	outcrop	Lantern	40 55'42"	116 21'41"	dike	lamprophyre
LAN-17	outcrop	Lantern	40 55'15"	116 21'33"	dike	lamprophyre, hbl
LAN-17	outcrop	Lantern	40 55'15"	116 21'33"	dike	lamprophyre, hbl
96M-211	underground mine	Meikle		925 level	dike	lamprophyre
96M-212	underground mine	Meikle		925 level	dike	monzonite porphyry
PAL-1	outcrop	Palisades, north	40 37' 50"	116 14' 23"	intrusion	granodiorite
PAL-1	outcrop	Palisades, north	40 37' 50"	116 14' 23"	intrusion	granodiorite
NS-1	open pit	North Star	40 57'25"	116 21'28"	intrusion	diorite of Goldstrike stock
NS-1	open pit	North Star	40 57'25"	116 21'28"	intrusion	diorite of Goldstrike stock
98-Zia-9	outcrop	Zia Claims	40 56'11"	116 23'13"	dike	granophyre
98-Zia-9	outcrop	Zia Claims	40 56'11"	116 23'13"	dike	granophyre
GB718C-1829	core	Rodeo	40 59' 40"	116 22' 57"	dike	lamprophyre
GB718C-1829	core	Rodeo	40 59' 40"	116 22' 57"	dike	lamprophyre
SJ-526C-1022	core	Screamer	40 58' 56"	116 23' 17"	dike	porphyritic diorite
SJ 489C-1071	core	Screamer	40 58' 56"	116 23' 17"	dike	porphyritic diorite
SJ 489C-1071	core	Screamer	40 58' 56"	116 23' 17"	dike	porphyritic diorite
NB-3	outcrop	SE of SOB Hill	41 00'00"	116 23'35"	dike	lamprophyre
NB-3	outcrop	SE of SOB Hill	41 00'00"	116 23'35"	dike	lamprophyre
NB-3	outcrop	SE of SOB Hill	41 00'00"	116 23'35"	dike	lamprophyre
SC-3	outcrop	Simon Creek	40 54'52"	116 18'00"	dike	diorite porphyry
SC-3	outcrop	Simon Creek	40 54'52"	116 18'00"	dike	diorite porphyry
TURF-11	outcrop	Turf	40 56'58"	116 18'57"	intrusion	diorite, pyroxene
TURF-11	outcrop	Turf	40 56'58"	116 18'57"	intrusion	diorite, pyroxene
TURF-11	outcrop	Turf	40 56'58"	116 18'57"	intrusion	diorite, pyroxene
98-Zia-7	outcrop	Zia Claims	40 56'28"	116 23'18"	intrusion	microdiorite
98-Zia-7	outcrop	Zia Claims	40 56'28"	116 23'18"	intrusion	microdiorite
RO-108-1270	core	Zia Claims	40 56' 36	116 23' 20"	intrusion	microdiorite
RO-108-1270	core	Zia Claims	40 56' 36	116 23' 20"	intrusion	microdiorite
98-Zia-1	outcrop	Zia Claims	40 56'20"	116 23'12"	intrusion	microdiorite
98-DEE-1	open pit	Dee	41 02'02"	116 25'50"	dike	lamprophyre
98-DEE-2	open pit	Dee	41 02'10"	116 25'45"	dike	lamprophyre
98-DEE-11	open pit	Dee	41 02'11"	116 25'35"	dike	basalt
98-REN-8	open pit	Ren, north	41 01'05"	116 23'10"	dike	lamprophyre
LANC-197-1137.3	core	Lantern	40 55' 24"	116 21' 27"	dike	rhyolite of Lantern
LANC-197-1143.5	core	Lantern	40 55' 24"	116 21' 27"	dike	rhyolite of Lantern
LTN-OC-1	outcrop	Lantern	40 55.4'	116 21.8'	dike	rhyolite of Lantern
LTN-OC-1	outcrop	Lantern	40 55.4'	116 21.8'	dike	rhyolite of Lantern
BST-110	open pit	Beast	40 56'17"	116 21'24"	dike	rhyodacite of Lantern
BST-110	outcrop	Beast	40 56'17"	116 21'24"	dike	rhyolite of Lantern
BST-110	outcrop	Beast	40 56'17"	116 21'24"	dike	rhyolite of Lantern
LANC-197-1116.6	core	Lantern	40 55' 24"	116 21' 27"	dike	rhyolite of Lantern
LANC-197-1120.8	core	Lantern	40 55' 24"	116 21' 27"	dike	rhyolite of Lantern
LANC-197-1125.2	core	Lantern	40 55' 24"	116 21' 27"	dike	rhyolite of Lantern
LANC-197-1131.3	core	Lantern	40 55' 24"	116 21' 27"	dike	rhyolite of Lantern
LANC-197-1137.3	core	Lantern	40 55' 24"	116 21' 27"	dike	rhyolite of Lantern
LANC-197-1143.5	core	Lantern	40 55' 24"	116 21' 27"	dike	rhyolite of Lantern
LANC-197-1146.8	core	Lantern	40 55' 24"	116 21' 27"	dike	rhyolite of Lantern
LANC-197-1149.5	core	Lantern	40 55' 24"	116 21' 27"	dike	rhyolite of Lantern
LANC-197-1150.7	core	Lantern	40 55' 24"	116 21' 27"	dike	rhyolite of Lantern
LANC-197-1151.5	core	Lantern	40 55' 24"	116 21' 27"	dike	rhyolite of Lantern
CE64-1315	core	Lantern-Exodus	40 55' 52"	116 22' 13	dike	rhyolite of Lantern

Appendix 3-1: Table of Geochemical Data for Carlin Trend Igneous Rocks

Sample Name	Sample Type	Location	Latitude	Longitude	Occurrence	Rock Type
CE64-1315	core	Lantern-Exodus	40 55' 52"	116 22' 13	dike	rhyolite of Lantern
LAN-64	outcrop	Lantern	40 54.7'	116 21.8'	dike	dacite of Lantern
LAN-64	outcrop	Lantern	40 54.7'	116 21.8'	dike	dacite of Lantern
Meikle925-3650	underground mine	Meikle	925 level; 3650 stope		dike	rhyodacite of Meikle
Meikle925-3650	underground mine	Meikle	925 level; 3650 stope		dike	rhyodacite of Meikle
REN-3	open pit	Ren	41 01.08'	116 23.2'	dike	rhyodacite of Meikle
REN-3	open pit	Ren	41 01.08'	116 23.2'	dike	rhyodacite of Meikle
Paleozoic Rocks and Rocks of Uncertain Age						
SC-2A	outcrop	Simon Creek	40 54'50"	116 17'58"	basalt flow?	basalt
SC-2A	outcrop	Simon Creek	40 54'50"	116 17'58"	basalt flow?	basalt
WC-101	outcrop	east of IB claims	40 48'57"	116 19'55"	basalt flow?	basalt
WC-101	outcrop	east of IB claims	40 48'57"	116 19'55"	basalt flow?	basalt
WC-10	outcrop	IB claims	40 49'02"	116 20'10"	dike or sill	basalt, alkalic
WC-10	outcrop	IB claims	40 49'02"	116 20'10"	dike or sill	basalt, alkalic
SL-1	outcrop	Simon Creek	40 54'55"	116 17'55"	dike	diabase
SL-1	outcrop	Simon Creek	40 54'55"	116 17'55"	dike	diabase
SL-1	outcrop	Simon Creek	40 54'55"	116 17'55"	dike	diabase
IB-1	outcrop	IB claims	40 49'42"	116 20'12"	intrusion?	basalt
IB-1	outcrop	IB claims	40 49'42"	116 20'12"	intrusion?	basalt
IB-1	outcrop	IB claims	40 49'42"	116 20'12"	intrusion?	basalt
IB-2	outcrop	IB claims	40 49'02"	116 20'14"	tectonite	
IB-2	outcrop	IB claims	40 49'02"	116 20'14"	tectonite	
WC-20	outcrop	IB claims	40 49'40"	116 20'08"	intrusion?	basalt clast in breccia
WC-20	outcrop	IB claims	40 49'40"	116 20'08"	intrusion?	basalt clast in breccia
WC-20	outcrop	IB claims	40 49'40"	116 20'08"	intrusion?	basalt clast in breccia
WC-20	outcrop	IB claims	40 49'40"	116 20'08"	intrusion?	basalt clast in breccia
WC-20	outcrop	IB claims	40 49'40"	116 20'08"	intrusion?	basalt clast in breccia
LAN-60	outcrop	Lantern	40 55'43"	116 22'29"	silicified limestone	limestone
CRZY8-TUFF	outcrop	Lantern	40 55'47"	116 22'29"	altered limestone?	limestone
RN-6	outcrop	Rain, northwest	40 37' 28	116 02' 07"	dike	mafic? dike
RN-6	outcrop	Rain, northwest	40 37' 28	116 02' 07"	dike	mafic? dike
RN-6	outcrop	Rain, northwest	40 37' 28	116 02' 07"	dike	mafic? dike
RN-5	outcrop	Rain, northwest	40 37' 28	116 02' 07"	dike	mafic? dike
RN-5	outcrop	Rain, northwest	40 37' 28	116 02' 07"	dike	mafic? dike
RN-5	outcrop	Rain, northwest	40 37' 28	116 02' 07"	dike	mafic? dike
RN-10	outcrop	Emigrant	40 36' 44"	115 59' 13"	dike	mafic? dike
RN-10	outcrop	Emigrant	40 36' 44"	115 59' 13"	dike	mafic? dike
RN-10	outcrop	Emigrant	40 36' 44"	115 59' 13"	dike	mafic? dike
98-Zia-11	outcrop	Zia Claims	40 56'45"	116 23'21"		biotite hornfels
98-Zia-11	outcrop	Zia Claims	40 56'45"	116 23'21"		biotite hornfels
TURF-12	outcrop	Turf	40 57'06"	116 19'14"	dike	mafic? dike
TURF12	outcrop	Turf	40 57'06"	116 19'14"	dike	mafic? dike
TURF-12	outcrop	Turf	40 57'06"	116 19'14"	dike	mafic? dike

Appendix 3-1: Table of Geochemical Data for Carlin Trend Igneous Rocks

Sample Name	Alteration	Laboratory	Method	Prep Method	SiO$_2$	TiO$_2$	Al$_2$O$_3$
Miocene Rocks							
LAN-65	fresh, non-hydrated, glassy	Actlabs	INAA				
LAN-65	fresh, non-hydrated, glassy	Actlabs	ICP-4 acid				
LAN-65	fresh, non-hydrated, glassy	UNR	XRF-FD	Li-borate fusion	74.03	0.26	12.40
LAN-65	fresh, non-hydrated, glassy	UNR	XRF-P	pressed pellet			
98-Zia-6	slight oxidation	Actlabs	INAA				
98-Zia-6	slight oxidation	Actlabs	ICP-4 acid				
98-Zia-6	slight oxidation	UNR	XRF-FD	Li-borate fusion	75.90	0.23	11.79
MM-1	fresh, slightly hydrated, glassy	UNR	XRF-FD	Li-borate fusion	74.88	0.27	12.95
Eocene Rocks							
BST-30	clay-hematite; biotite fresh	Actlabs	INAA				
BST-30	clay-hematite; biotite fresh	Actlabs	ICP-4 acid				
BST-30	clay-hematite; biotite fresh	UNR	XRF-FD	Li-borate fusion	74.05	0.47	16.55
BST-20	silicified, pyritic	USML	ICP/AuFA	2-acid; partial			
BST-20	silicified, pyritic	UNR	XRF-FD	Li-borate fusion	87.16	0.27	10.11
BST-20	silicified, pyritic	Actlabs	INAA	2-acid; partial			
BST-20	silicified, pyritic	Actlabs	ICP-4 acid				
BST-103	silicified, pyritic	Actlabs	INAA	2-acid; partial			
BST-103	silicified, pyritic	USML	ICP/AuFA	2-acid; partial			
BST-103	silicified, pyritic	ACME	ICP	4-acid digestion			
BST-103	silicified, pyritic	UNR	XRF-FD	Li-borate fusion	88.21	0.36	6.26
BST-101	silicified, pyritic	Actlabs	INAA				
BST-104	silicified, pyritic	Actlabs	INAA				
BST-105	silicified, oxidized	Actlabs	ICP-4 acid	2-acid; partial			
BST-105	silicified, oxidized	USML	ICP	4-acid digestion			
BST-130	mild clay	UNR	XRF-FD	Li-borate fusion	71.04	0.30	15.16
BST-130	mild clay	Actlabs	INAA				
BST-130	mild clay	Actlabs	ICP-4 acid	4-acid digestion		(.21%Ti)	(6.87%A
BST-144	silicified, pyritic	USML	ICP	Li-borate fusion			
BST-144	silicified, pyritic	UNR	XRF-FD	Li-borate fusion	93.70	0.19	4.15
BST-143	silicified, pyritic	UNR	XRF-FD	Li-borate fusion	92.70	0.18	3.35
BP-27a	mild clay	USML	ICP	2-acid; partial			
BP-27b	quartz-sericite-pyrite	USML	ICP	2-acid; partial			
BP-2-2	fresh, glassy	Actlabs	XRF-P	pressed pellet			
BP-2-2	fresh, glassy	Actlabs	ICP-4 acid				
PNC 213-1787	moderate clay	UNR	XRF-FD	Li-borate fusion	66.06	0.39	16.34
PNC 213-1787	moderate clay	Actlabs	ICP/ICP-MS				
CN-3	mild clay	UNR	XRF-FD	Li-borate fusion	67.99	0.53	17.07
CN-3	mild clay	Actlabs	ICP/ICP-MS				
BP-2	fresh, glassy	UNR	XRF-FD	Li-borate fusion	72.01	0.29	15.81
BP-2	fresh, glassy	Actlabs	ICP/ICP-MS				
BP-27	fresh, glassy	UNR	XRF-FD	Li-borate fusion	72.41	0.26	15.08
BP-27	fresh, glassy	Actlabs	ICP/ICP-MS				
BP-2(vug)	vapor cavity	Actlabs	INAA				
BP-27	fresh, glassy	Actlabs	ICP	2-acid; partial			
BP-27	fresh, glassy	Acme	AuFA	Fire assay			
BP-27wr	fresh, glassy	Acme	ICP	2-acid; partial			
BP-27a	moderate clay	Actlabs	INAA				
BP-2A-VUG	fresh, glassy	Actlabs	INAA				
96M-208	moderate clay	Actlabs	ICP/ICP-MS		76.52	0.28	14.81
BP-23	mild clay	UNR	XRF-FD	Li-borate fusion	70.50	0.50	17.91
BP-23	mild clay	Actlabs	INAA				
BP-23	mild clay	UNR	XRF-P	pressed pellet			
BP-26A	moderate clay	UNR	XRF-FD	Li-borate fusion	76.40	0.28	16.15
BP-26A	moderate clay	Actlabs	INAA				
BP-26A	moderate clay	UNR	XRF-P	pressed pellet			
BP-4460	moderate clay	UNR	XRF-FD	Li-borate fusion	74.91	0.31	15.57
BP-4460	moderate clay	Actlabs	INAA				
BP-4460	moderate clay	UNR	XRF-P	pressed pellet			
BP-2-1-clvug	vapor cavity	UNR	XRF-FD	Li-borate fusion	72.59	0.26	15.24
BP-2-1-clvug	vapor cavity	Actlabs	INAA				
BP-2-2-clvug	vapor cavity	Actlabs	INAA				

Appendix 3-1: Table of Geochemical Data for Carlin Trend Igneous Rocks

Sample Name	Alteration	Laboratory	Method	Prep Method	SiO_2	TiO_2	Al_2O_3
BP-2-altfeld	moderate clay next to cavity	UNR	XRF-FD	Li-borate fusion	72.87	0.27	15.38
BP-2-altfeld	moderate clay next to cavity	ActLabs	INAA				
GB 720C-1744	moderate clay	UNR	XRF-FD	Li-borate fusion	67.84	0.46	17.39
GB 720C-1744	moderate clay	Actlabs	ICP/ICP-MS				
VG-1	vapor cavity	Actlabs	INAA	4-acid digestion			
VG-1	vapor cavity	UNR	XRF-P	pressed pellet			
BP-2glass	fresh, glassy	Acme	ICP	2-acid; partial			
BP-27wr	fresh, glassy	Acme	ICP	4-acid digestion			
BP-2glass	fresh, glassy	Acme	ICP	4-acid digestion			
DS-1	fresh, hydrated glass	UNR	XRF-FD	Li-borate fusion	75.09	0.05	14.64
DS-1	fresh, hydrated glass	UNR	XRF-FD	Li-borate fusion	75.64	0.06	14.22
DS-1	fresh, hydrated glass	Actlabs	INAA				
DS-1	fresh, hydrated glass	UNR	XRF-P	pressed pellet			
DSU-143-30	fresh, quenched crystallized	UNR	XRF-FD	Li-borate fusion	76.98	0.07	14.09
DSU-143-30	fresh, quenched crystallized	Actlabs	INAA				
DSU-143-182	fresh, quenched crystallized	UNR	XRF-FD	Li-borate fusion	76.80	0.06	13.94
DS-13	fresh, quenched crystallized	Actlabs	INAA				
DS-42	fresh, hydrated glass	Actlabs	ICP				
DS-42	fresh, hydrated glass	UNR	XRF-FD	Li-borate fusion	75.00	0.07	14.42
DS-42A	fresh, hydrated glass	Actlabs	INAA				
DS-42A	fresh, hydrated glass	Actlabs	ICP	4-acid digestion		(0.04%T	(6.28%A
DS-42A	fresh, hydrated glass	Actlabs	ICP	4-acid digestion		(.04%Ti)	(6.21%A
EMP-2	fresh, glassy	Actlabs	INAA				
RM97C-7-1336	moderate clay	UNR	XRF-FD	Li-borate fusion	69.32	0.48	25.07
RM97C-7-1336		Actlabs	INAA				
RM97C-7-1342	severe clay	UNR	XRF-FD	Li-borate fusion	76.56	0.36	18.59
RM97C-7-1342		Actlabs	INAA				
RM97C-7-1359	severe clay	UNR	XRF-FD	Li-borate fusion	71.90	0.98	14.92
RM97C-7-1359		Actlabs	INAA				
BS1004-504	mild clay	UNR	XRF-FD	Li-borate fusion	69.77	0.43	16.48
BS1004-504		Actlabs	INAA				
BS1004-522	mod. silicification	UNR	XRF-FD	Li-borate fusion	81.68	0.30	15.62
BS1004-522		Actlabs	INAA				
BS1004-523	severe clay	UNR	XRF-FD	Li-borate fusion	80.25	0.32	16.96
BS1004-523		Actlabs	INAA				
98-GEN-23	severe clay	Actlabs	INAA				
GEN-2	mild clay	UNR	XRF-FD	Li-borate fusion	71.59	0.32	15.82
GEN-2	mild clay	UNR	XRF-FD	Li-borate fusion	71.98	0.30	15.22
GEN-2	mild clay	Actlabs	INAA				
98Gen-11	fresh, quenched crystallized	Actlabs	INAA				
98Gen-11	fresh, quenched crystallized	UNR	XRF-FD	Li-borate fusion	72.57	0.25	14.96
98-GEN-1	mild clay	UNR	XRF-FD	Li-borate fusion	75.54	0.28	15.29
98-GEN-1	mild clay	Actlabs	INAA				
BSTR-3	strong oxidation	Actlabs	INAA				
M8-0317-4-482	moderate clay	Actlabs	INAA				
M8-0317-4-482	moderate clay	UNR	XRF-FD	Li-borate fusion	68.46	0.50	17.68
IV-1	propylitized	UNR	XRF-FD	Li-borate fusion	65.01	0.78	16.34
IV-1	propylitized	Actlabs	ICP/ICP-MS				
LAN-70	mild clay	Actlabs	INAA				
RICH-12	propylitized	Actlabs	INAA				
RICH-12	propylitized	UNR	XRF-FD	Li-borate fusion	69.55	0.44	15.58
RICH-10	mild clay-carbonate	Actlabs	ICP	4-acid digestion			
RICH-10	mild clay-carbonate	UNR	XRF-FD	4-acid digestion	77.20	0.21	14.70
RICH-10	mild clay-carbonate	USML	ICP	2 acid partial			
RICH-10	mild clay-carbonate	UNR	XRF-FD	Li-borate fusion	77.02	0.20	14.80
RICH-10	mild clay-carbonate	Actlabs	INAA				
WC-4	propylitized	UNR	XRF-FD	Li-borate fusion	64.71	0.63	17.39
WC-4	propylitized	Actlabs	ICP/ICP-MS				
WC-5	fresh; mild oxidation	UNR	XRF-FD	Li-borate fusion	63.06	0.88	16.76
WC-5	fresh; mild oxidation	Actlabs	ICP/ICP-MS				
WC-9	fresh; some sulfide	UNR	XRF-FD	Li-borate fusion	62.15	0.79	17.21
WC-9	fresh; some sulfide	Actlabs	INAA				
WC-3	fresh, quenched crystallized	UNR	XRF-FD	Li-borate fusion	64.96	0.59	17.48

Appendix 3-1: Table of Geochemical Data for Carlin Trend Igneous Rocks

Sample Name	Alteration	Laboratory	Method	Prep Method	SiO_2	TiO_2	Al_2O_3
WC-3	fresh, quenched crystallized	Actlabs	ICP	4-acid digestion			
WC-3	fresh, quenched crystallized	Actlabs	ICP/ICP-MS	Fire Assay			
WC-3	fresh, quenched crystallized	Actlabs	INAA				
WC-2	mild clay	UNR	XRF-FD	Li-borate fusion	73.06	0.30	14.47
WC-2	mild clay	Actlabs	INAA				
WC-31	fresh	UNR	XRF-FD	Li-borate fusion	60.89	0.83	17.23
WC-56	fresh, quenched glassy?	Actlabs	INAA				
WC-56	fresh, quenched glassy?	UNR	XRF-FD	Li-borate fusion	62.62	0.74	17.02
WC-105	propylitized	Actlabs	INAA				
WC-105	propylitized	UNR	XRF-FD	Lit-borate fusion	73.75	0.27	14.46
WC-106	fresh; mild oxidation	Actlabs	INAA				
WC-106	fresh; mild oxidation	UNR	XRF-FD	Li-borate fusion	63.28	0.84	16.98
WC-104	fresh, mild oxidation/carbonate	Actlabs	INAA				
WC-104	fresh, mild oxidation/carbonate	UNR	XRF-FD	Li-borate fusion	77.77	0.13	13.28
WC-102	fresh, mild oxidation/carbonate	UNR	XRF-FD	Li-borate fusion	75.06	0.16	14.62
WC-103	fresh, mild oxidation/carbonate	Actlabs	INAA				
WC-103	fresh, mild oxidation/carbonate	UNR	XRF-FD	Li-borate fusion	75.79	0.15	14.53
98-WC-3	oxidized	Actlabs	INAA				
98-WC-3	oxidized	Actlabs	ICP	4-acid digestion		(.1%Ti)	(6.48%A
98-GEN-24	oxidized; silicified	Actlabs	INAA				
98-GEN-24	oxidized, silicified	Actlabs	ICP	4-acid digestion		(.15%Ti)	(6.78%A
LAN-80	oxidized, silicified	Actlabs	INAA				
LAN-80	oxidized, silicified	Actlabs	ICP	4-acid digestion		(.04%Ti)	(6.16%A
98-DEE-7	severe clay	UNR	XRF-FD	Li-borate fusion	58.45	1.37	16.35
98-DEE-8	mod. serpent/carb?	UNR		Li-borate fusion			
98-DEE-8	mod. serpent/carb?	UNR	XRF-FD	Li-borate fusion	54.36	1.54	18.40
LAN-57	silicified	UNR	XRF-FD	Li-borate fusion	84.70	0.08	14.22
LAN-57	silicified	Actlabs	INAA				
CD 96 10C-1455	mild serpent/carbonate	Actlabs	ICP/ICP-MS		55.24	1.28	16.83
Cretaceous Rocks							
RICH-1	slight oxidation	UNR	XRF-FD	Li-borate fusion	75.04	0.17	13.73
RICH-1	slight oxidation	Actlabs	INAA				
Jurassic Rocks							
BC-2	quartz-sericite	UNR	XRF-FD	Li-borate fusion	73.29	0.35	16.53
BC-2	quartz-sericite	Actlabs	INAA				
RM97c-2-443	fresh, mild chloritization	Actlabs	INAA				
RM97C-2-443	fresh, mild chloritization	UNR	XRF-FD	Li-borate fusion	60.51	1.35	15.42
RM97C-2-443	fresh, mild chloritization	Actlabs	INAA				
BP-41A	quartz-sericite-pyrite	UNR	XRF-FD	Li-borate fusion	70.01	0.87	18.09
BP-41A	quartz-sericite-pyrite	UNR	XRF-FD	Li-borate fusion	69.89	0.91	18.50
BP-41A	quartz-sericite-pyrite	Actlabs	INAA				
96M-206a	moderate clay	Actlabs	ICP/ICP-MS				
96M-206b	moderate clay	Actlabs	ICP/ICP-MS		53.74	1.18	14.49
96M-207	fresh, mild chloritization	Actlabs	ICP/ICP-MS		59.21	1.15	17.42
96M-209	quartz-sericite-pyrite	Actlabs	ICP/ICP-MS		70.20	0.86	17.84
BP-22	moderate clay	UNR	XRF-FD	Li-borate fusion	63.29	1.26	15.08
BP-22	moderate clay	UNR	XRF-P	pressed pellet			
BP-31	moderate clay; sulfidic	UNR	XRF-FD	Li-borate fusion	68.73	2.39	17.86
BP-31	moderate clay; sulfidic	Actlabs	INAA				
BP-120	fresh, quenched crystallized	Actlabs	INAA				
BP-120	fresh, quenched crystallized	UNR	XRF-FD	Li-borate fusion	59.15	1.13	16.34
BAZ-2	severe clay	UNR	XRF-FD	Li-borate fusion	68.24	1.53	19.64
BAZ-2	severe clay	Actlabs	INAA				
DS-40	fresh, mild epidotization	UNR	XRF-P	pressed pellet			
DS-40	fresh, mild epidotization	UNR	XRF-FD	Li-borate fusion	53.39	1.07	13.73
DS-40	fresh, mild epidotization	UNR	XRF-P	pressed pellet			
DS-40	fresh, mild epidotization	Actlabs	INAA				
DS-41	fresh, calcite veined	UNR	XRF-P	pressed pellet			
DS-41	fresh, calcite veined	UNR	XRF-FD	Li-borate fusion	51.32	1.10	13.89
GEN-2-1534	fresh	Actlabs	INAA				
GEN-2-1534	fresh	UNR	XRF-FD	Li-borate fusion	66.44	0.80	15.38
GEN-3	fresh; some chlorite/carbonate	Actlabs	INAA				

Appendix 3-1: Table of Geochemical Data for Carlin Trend Igneous Rocks

Sample Name	Alteration	Laboratory	Method	Prep Method	SiO$_2$	TiO$_2$	Al$_2$O$_3$
GEN-3	fresh; some chlorite/carbonate	UNR	XRF-FD	Li-borate fusion	52.69	1.04	12.27
GA-13	quartz-sericite-carbonate	Actlabs	INAA				
GA-13	quartz-sericite-carbonate	UNR	XRF-FD	Li-borate fusion	74.19	0.54	17.20
GA-10	chloritized, oxidized	Actlabs	INAA				
GA-10	chloritized, oxidized	UNR	XRF-FD	Li-borate fusion	64.74	0.92	15.76
GA-12	strong oxidation	Actlabs	INAA				
GA-12	strong oxidation	UNR	XRF-FD	Li-borate fusion	72.47	1.45	17.25
GA19C-1636	quartz-sericite-pyrite	Actlabs	INAA				
GA19C-1636	quartz-sericite-pyrite	UNR	XRF-FD	Li-borate fusion	76.34	0.55	17.12
CE52-1538	fresh; some chlorite/carbonate	Actlabs	INAA				
CE52-1538	fresh; some chlorite/carbonate	UNR	XRF-FD	Li-borate fusion	53.39	1.05	13.94
LAN-10	fresh, mild chloritization	Actlabs	INAA				
LAN-10	fresh, mild chloritization	UNR	XRF-FD	Li-borate fusion	53.76	1.10	13.86
LAN-17	fresh, mild chloritization	UNR	XRF-FD	Li-borate fusion	53.48	1.05	13.17
LAN-17	fresh, mild chloritization	Actlabs	INAA				
96M-211	moderate clay	Actlabs	ICP/ICP-MS		59.48	1.44	17.86
96M-212	quartz-sericite-pyrite	Actlabs	ICP/ICP-MS		79.03	0.28	15.34
PAL-1	mild chloritization/oxidation	Actlabs	INAA				
PAL-1	mild chloritization/oxidation	UNR	XRF-FD	Li-borate fusion	68.03	0.57	15.34
NS-1	fresh	UNR	XRF-FD	Li-borate fusion	58.84	1.17	15.61
NS-1	fresh	Actlabs	ICP/ICP-MS				
98-Zia-9	fresh, slight oxidation	Actlabs	INAA				
98-Zia-9	fresh, slight oxidation	UNR	XRF-FD	Li-borate fusion	73.49	0.21	15.22
GB718C-1829	moderate clay	UNR	XRF-P	pressed pellet			
GB718C-1829	moderate clay	UNR	XRF-FD	Li-borate fusion	55.04	1.09	13.99
SJ-526C-1022	fresh; some chlorite/carbonate	UNR	XRF-FD-P	Li-borate fusion; p	59.22	1.11	14.27
SJ 489C-1071	fresh; some chlorite/carbonate	Actlabs	ICP/ICP-MS				
SJ 489C-1071	fresh; some chlorite/carbonate	UNR	XRF-FD	Li-borate fusion	59.77	1.02	13.42
NB-3	severe oxidation of sulfidic rock	Actlabs	INAA				
NB-3	severe oxidation of sulfidic rock	UNR	XRF-P	pressed pellet			
NB-3	severe oxidation of sulfidic rock	UNR	XRF-FD	Li-borate fusion	34.22	1.38	11.47
SC-3	propylitized	Actlabs	INAA				
SC-3	propylitized	UNR	XRF-FD	Li-borate fusion	65.88	0.75	16.08
TURF-11	fresh	UNR	XRF-P	pressed pellet			
TURF-11	fresh	UNR	XRF-FD	Li-borate fusion	57.61	0.94	15.84
TURF-11	fresh	Actlabs	INAA				
98-Zia-7	fresh, quenched crystallized	Actlabs	INAA				
98-Zia-7	fresh, quenched crystallized	UNR	XRF-FD	Li-borate fusion	60.03	0.98	17.90
RO-108-1270	fresh, quenched crystallized	Actlabs	INAA				
RO-108-1270	fresh, quenched crystallized	Actlabs	INAA				
98-Zia-1	fresh, quenched crystallized	Actlabs	INAA				
98-DEE-1	severe clay	UNR	XRF-FD	Li-borate fusion	66.70	1.13	17.17
98-DEE-2	moderate clay	UNR	XRF-FD	Li-borate fusion	56.75	1.81	17.16
98-DEE-11	moderate clay	UNR	XRF-FD	Li-borate fusion	57.11	1.35	16.96
98-REN-8	severe clay	UNR	XRF-FD	Li-borate fusion	63.24	1.29	16.04
LANC-197-1137.3	quartz-sericite-carbonate	Actlabs	INAA				
LANC-197-1143.5	quartz-sericite-carbonate	Actlabs	INAA				
LTN-OC-1	quartz-sericite-carbonate	Actlabs	ICP/ICP-MS				
LTN-OC-1	quartz-sericite-carbonate	UNR	XRF-FD	Li-borate fusion	73.73	0.29	15.69
BST-110	quartz-sericite-carbonate	UNR	XRF-FD	Li-borate fusion	71.13	0.31	15.12
BST-110	quartz-sericite-carbonate	Actlabs	INAA				
BST-110	quartz-sericite-carbonate	Actlabs	ICP	2-acid partial		(.12%Ti)	(6.88%A
LANC-197-1116.6	quartz-sericite-carbonate	Chemex	ICP/ICP-MS	4-acid digestion	73.32	0.30	15.21
LANC-197-1120.8	quartz-sericite-carbonate	Chemex	ICP/ICP-MS	4-acid digestion	72.27	0.29	14.69
LANC-197-1125.2	quartz-sericite-carbonate	Chemex	ICP/ICP-MS	4-acid digestion	71.60	0.30	15.05
LANC-197-1131.3	quartz-sericite-carbonate	Chemex	ICP/ICP-MS	4-acid digestion	71.89	0.29	14.87
LANC-197-1137.3	quartz-sericite-carbonate	Chemex	ICP/ICP-MS	4-acid digestion	71.68	0.30	15.07
LANC-197-1143.5	quartz-sericite-carbonate	Chemex	ICP/ICP-MS	4-acid digestion	71.90	0.30	14.88
LANC-197-1146.8	quartz-sericite-carbonate	Chemex	ICP/ICP-MS	4-acid digestion	71.95	0.30	15.32
LANC-197-1149.5	quartz-sericite-carbonate	Chemex	ICP/ICP-MS	4-acid digestion	71.74	0.30	15.19
LANC-197-1150.7	quartz-sericite-carbonate	Chemex	ICP/ICP-MS	4-acid digestion	71.52	0.29	15.18
LANC-197-1151.5	quartz-sericite-carbonate	Chemex	ICP/ICP-MS	4-acid digestion	71.82	0.29	15.21
CE64-1315	quartz-sericite-carbonate	UNR	XRF-P	pressed pellet			

Appendix 3-1: Table of Geochemical Data for Carlin Trend Igneous Rocks

Sample Name	Alteration	Laboratory	Method	Prep Method	SiO_2	TiO_2	Al_2O_3
CE64-1315	quartz-sericite-carbonate	UNR	XRF-FD	Li-borate fusion	73.81	0.27	15.47
LAN-64	propylitized	Actlabs	INAA				
LAN-64	propylitized	UNR	XRF-FD	Li-borate fusion	70.92	0.31	15.31
Meikle925-3650	quartz-sericite	UNR	XRF-FD	Li-borate fusion	78.27	0.28	15.31
Meikle925-3650	quartz-sericite	Actlabs	INAA				
REN-3	quartz-sericite; oxidization	Actlabs	INAA				
REN-3	quartz-sericite; oxidization	UNR	XRF-FD	Li-borate fusion	77.76	0.31	17.42
Paleozoic Rocks an							
SC-2A	moderate clay-carbonate-oxide	Actlabs	INAA				
SC-2A	moderate clay-carbonate-oxide	UNR	XRF-FD	Li-borate fusion	50.81	3.54	18.98
WC-101	biotitization/carbonate	Actlabs	INAA				
WC-101	biotitization/carbonate	UNR	XRF-FD	Li-borate fusion	56.32	3.62	14.43
WC-10	carbonate	UNR	XRF-FD	Li-borate fusion	53.49	3.40	17.13
WC-10	carbonate	Actlabs	ICP/ICP-MS				
SL-1	fresh; some chlorite/carbonate	Actlabs	INAA				
SL-1	fresh; some chlorite/carbonate	UNR	XRF-FD	Li-borate fusion	47.06	3.50	14.63
SL-1	fresh; some chlorite/carbonate	Actlabs	ICP				
IB-1	biotitization/carbonate	UNR	XRF-FD	Li-borate fusion	54.59		18.9
IB-1	biotitization/carbonate	Actlabs	ICP				
IB-1	biotitization/carbonate	Actlabs	ICP	2-acid; partial			
IB-2	clay/sulfide	UNR	XRF-FD	Li-borate fusion	56.54	0.29	11.15
IB-2	clay/sulfide	Actlabs	ICP				
WC-20	biotitization/carbonate	Actlabs	ICP				
WC-20	biotitization/carbonate	UNR	XRF-FD	Li-borate fusion	50.95	3.29	19.70
WC-20	biotitization/carbonate	UNR	XRF-FD	Li-borate fusion	49.76	4.53	19.92
WC-20	biotitization/carbonate	Actlabs	ICP				
WC-20	biotitization/carbonate	Actlabs	ICP	2-acid; partial			
LAN-60	strong silicification	Actlabs	INAA				
CRZY8-TUFF	severe clay	Actlabs	INAA				
RN-6	severe clay	UNR	XRF-P	pressed pellet			
RN-6	severe clay	UNR	XRF-FD	Li-borate fusion	72.83	6.10	13.61
RN-6	severe clay	Actlabs	INAA				
RN-5	severe clay	UNR	XRF-P	pressed pellet			
RN-5	severe clay	UNR	XRF-FD	Li-borate fusion	70.79	1.17	18.24
RN-5	severe clay	Actlabs	INAA				
RN-10	severe clay	UNR	XRF-P	pressed pellet			
RN-10	severe clay	UNR	XRF-FD	Li-borate fusion	84.63	2.57	10.53
RN-10	severe clay	Actlabs	INAA				
98-Zia-11	biotitization	UNR	XRF-P	pressed pellet			
98-Zia-11	biotitization	UNR	XRF-FD	Li-borate fusion	72.88	0.57	13.54
TURF-12	propylitized?	UNR	XRF-P	pressed pellet			
TURF12	propylitized?	UNR	XRF-FD	Li-borate fusion	62.12	0.47	9.48
TURF-12	propylitized?	Actlabs	INAA				

Sample Name	FeO*	Fe$_2$O$_3$*	MnO	MgO	CaO	Na$_2$O	K$_2$O	P$_2$O$_5$	LOI	Total	Cr	Ni	Co
Miocene Rocks													
LAN-65											480		-1.0
LAN-65												5	
LAN-65	2.94	3.27	0.06	0.11	0.85	3.50	5.49	0.02	0.05	99.54			
LAN-65												10	3.0
98-Zia-6											290		-1.0
98-Zia-6												1	
98-Zia-6	2.65	2.94	0.05	0.10	0.52	3.30	5.12	0.03	1.11	98.44			
MM-1	0.00	1.90	0.03	0.18	1.01	2.41	6.32	0.07	2.90	100.28			
Eocene Rocks													
BST-30											120		5.0
BST-30												9	
BST-30	3.14	3.49	0.05	0.98	2.17	0.00	2.09	0.14	6.66	100.35			
BST-20													
BST-20	0.00	2.19	0.00	0.03	0.09	-0.15	0.09	0.07	5.13	98.87			
BST-20											220		9.0
BST-20												17	
BST-103											240	-25	23.0
BST-103													
BST-103											173	56	28.0
BST-103	3.27	3.63	0.00	0.11	0.09	-0.16	1.42	0.07	4.48	99.99			
BST-101											230	410	79.0
BST-104											110	60	6.0
BST-105													
BST-105										a	64	6	-2.0
BST-130		2.27	1.37	3.09	2.25	0.10	4.31	0.11	7.13	za			
BST-130					(4%Ca)	(.35%Na)				x		-20	
BST-130	l)		(495ppm	(.67%Mg	(2.88%Ca)		(3.08%K	(.057%P)				9	
BST-144											65		5.0
BST-144	0.00	1.42	0.00	0.10	0.09	-0.03	0.29	0.06	2.61	99.28			
BST-143	0.00	2.60	0.00	0.20	0.14	-0.14	0.78	0.05	5.14	100.23			
BP-27a													
BP-27b													
BP-2-2											71		4.0
BP-2-2												3	
PNC 213-1787	2.97	3.30	0.11	1.61	8.13	0.39	3.79	0.21	4.76	99.06			
PNC 213-1787											29		4.1
CN-3	3.13	3.48	0.09	1.67	4.30	0.38	4.60	0.24	3.72	97.08			
CN-3											-10	-10	3.7
BP-2	2.17	2.41	0.06	0.74	2.73	2.18	3.88	0.13	3.08	100.44			
BP-2											24	-10	2.4
BP-27	2.09	2.32	0.05	0.68	2.85	2.39	4.05	0.13	5.06	100.29			
BP-27											49	-10	2.2
BP-2(vug)											57		2.0
BP-27													
BP-27													
BP-27wr											15	1	5.0
BP-27a											32	-20	2.0
BP-2A-VUG											-5	-20	4.0
96M-208	1.69	1.88	0.02	0.93	0.47	0.29	4.89	0.12	5.02	99.56			
BP-23	3.93	4.37	0.07	1.87	0.85	0.00	4.11	0.26	3.71	99.95			
BP-23											16		9.0
BP-23												34	
BP-26A	1.65	1.83	0.00	0.91	0.54	0.00	3.95	0.12	3.55	99.57			
BP-26A											108		2.0
BP-26A												1	
BP-4460	2.46	2.73	0.07	0.97	3.72	0.00	1.87	0.12	6.59	97.95			
BP-4460											56		5.0
BP-4460												1	
BP-2-1-clvug	2.41	2.68	0.05	0.64	2.37	2.12	4.18	0.12	4.55	99.40			
BP-2-1-clvug											130	-20	2.0
BP-2-2-clvug											110	-20	3.0

Sample Name	FeO*	Fe$_2$O$_3$*	MnO	MgO	CaO	Na$_2$O	K$_2$O	P$_2$O$_5$	LOI	Total	Cr	Ni	Co
BP-2-altfeld	2.43	2.70	0.07	0.77	1.39	1.24	5.45	0.13	5.20	99.48			
BP-2-altfeld											150	-20	2.0
GB 720C-1744	4.28	4.76	0.08	3.95	1.42	0.12	4.17	0.29	3.11	97.71			
GB 720C-1744											11	57	4.8
VG-1											4		3.2
VG-1												2	
BP-2glass											53	4	2.0
BP-27wr											22	3	5.0
BP-2glass											72	6	2.0
DS-1	0.86	0.95	0.09	0.06	1.57	2.39	5.18	0.05	8.14				
DS-1	0.83	0.92	0.08	0.04	1.59	2.34	5.14	0.05	7.57	101.78			
DS-1											91		-1.0
DS-1												2	
DSU-143-30	0.88	0.97	0.09	0.68	0.99	1.07	5.12	0.04	4.97	99.38			
DSU-143-30												2	-1.0
DSU-143-182	0.71	0.79	0.04	0.95	0.61	0.78	6.08	0.03	4.86	99.74			
DS-13	0.63	0.70				1.13					150	-20	-1.0
DS-42												-7	3.0
DS-42	0.84	0.93	0.12	0.19	1.05	3.07	5.09	0.06	7.86	99.17			
DS-42A	(0.76%Fe)				(-1%)	(2.64%Na)					-5	-84	-1.0
DS-42A	l)		(811ppm	(0.06%M	(.77%Ca)		(3.85%K	(0.017%P)				2	
DS-42A	l)		(757ppm	(.06%Mg	(.76%Ca)		(3.78%K	(.016%P)				2	
EMP-2											7	-20	2.0
RM97C-7-1336	2.10	2.33	0.01	1.14	0.85	0.00	0.85	0.17	8.31	99.70			
RM97C-7-1336											15	11	3.0
RM97C-7-1342	1.50	1.67	0.06	1.20	2.33	0.00	-0.76	0.15	7.25	97.91			
RM97C-7-1342											34	5	2.0
RM97C-7-1359	5.93	6.59	0.06	1.02	2.11	0.00	2.64	0.43	7.50	100.30			
RM97C-7-1359											361	37	14.0
BS1004-504	3.25	3.62	0.09	1.47	2.85	0.77	4.69	0.19	4.47	99.31			
BS1004-504											62	4	5.0
BS1004-522	0.91	1.01	0.02	0.20	0.30	0.00	0.86	0.11	4.53	99.39			
BS1004-522											68	6	
BS1004-523	1.59	1.77	0.02	0.00	0.15	0.00	0.62	0.08	5.39	98.70			
BS1004-523											55	7	1.0
98-GEN-23											-5	-20	-1.0
GEN-2	2.11	2.35	0.07	1.42	2.12	1.82	4.60	0.13	3.99	100.17			
GEN-2	2.38	2.64	0.06	1.43	2.16	1.75	4.58	0.13	5.34	99.19			
GEN-2											13	-10	2.9
98Gen-11											110	-6	2.0
98Gen-11	1.73	1.92	0.05	1.24	2.08	1.94	4.88	0.11	4.95	99.42			
98-GEN-1	2.13	2.37	0.03	1.13	2.74	-0.02	2.80	0.09	6.16	99.42			
98-GEN-1											270	7	3.0
BSTR-3											270	-20	-1.0
M8-0317-4-482											90	5	4.0
M8-0317-4-482	3.64	4.05	0.09	1.69	3.67	-0.09	3.62	0.25	8.00	100.66			
IV-1	4.39	4.88	0.09	2.20	3.98	3.23	3.70	0.29	1.92	101.13			
IV-1											58	15	10.0
LAN-70	2.48	2.76				1.62					100	-20	4.0
RICH-12											84	-20	4.0
RICH-12	2.23	2.48	0.05	1.37	1.69	4.23	4.43	0.17	3.61	99.18			
RICH-10											25	5	-2.0
RICH-10	1.58	1.75	0.06	0.55	0.52	0.46	4.44	0.11	3.40	99.62			
RICH-10													
RICH-10	1.69	1.88	0.05	0.50	0.50	0.30	4.65	0.10	3.07	97.98			
RICH-10										3.07	98.00	62	3	2.0
WC-4	4.10	4.56	0.11	1.26	4.47	4.03	3.08	0.22	0.37	99.40			
WC-4											58	20	6.4
WC-5	5.67	6.31	0.16	2.11	4.94	3.34	2.75	0.30	0.79	98.49			
WC-5											63	-10	11.0
WC-9	5.74	6.38	0.12	2.45	5.09	3.62	2.49	0.34	0.94	100.27			
WC-9											40	-10	11.0
WC-3	3.71	4.13	0.08	1.13	4.27	4.35	3.20	0.22	0.23	98.83			

Sample Name	FeO*	Fe$_2$O$_3$*	MnO	MgO	CaO	Na$_2$O	K$_2$O	P$_2$O$_5$	LOI	Total	Cr	Ni	Co
WC-3													
WC-3											63	35	7.5
WC-3											120	-20	4.0
WC-2	2.53	2.81	0.07	1.23	2.16	1.59	4.46	0.12	5.92	98.82			
WC-2											130	-20	3.0
WC-31		6.40	0.13	2.31	5.43	3.86	2.60	0.31	0.48	98.93			
WC-56											89	16	9.0
WC-56	4.94	5.49	0.11	2.26	5.16	4.10	2.23	0.27	3.33	97.21			
WC-105											91	8	3.0
WC-105	1.80	2.00	0.03	0.76	1.84	5.30	1.49	0.10	2.31	99.32			
WC-106											110	1	9.0
WC-106	4.95	5.50	0.10	2.20	3.83	3.27	3.75	0.25	3.41	97.68			
WC-104											110	-20	1.0
WC-104	0.45	0.50	0.02	0.37	0.33	2.70	4.85	0.05	2.18	97.89			
WC-102	0.94	1.05	0.01	0.31	0.29	4.38	4.08	0.05	0.84	98.81			
WC-103											110	-20	2.0
WC-103	0.76	0.85	0.01	0.32	0.32	4.65	3.32	0.06	0.96	97.73			
98-WC-3	(.64%Fe)				(-1%Ca)	(2.21%Na)					116	-20	-1.0
98-WC-3	l)		(128ppm	(.22%Mg	(.17%Ca)		(3.59%K	(.16%P)				3	
98-GEN-24	(.51%Fe)					(0.02%Na)					110	-20	-1.0
98-GEN-24	l)		(60ppmM	(.04%Mg	(.05%Ca)		(.28%K)	(.01%P)				3	
LAN-80	(.38%Fe)				(-1%Ca)	(.05%Na)					129	-20	-1.0
LAN-80	l)		(108ppm	(.08%Mg	(.07%Ca)		(.48%K)	(.002%P)				7	
98-DEE-7	0.00	3.34	0.20	2.21	12.68	2.15	2.70	0.55	13.70	98.91			
98-DEE-8													
98-DEE-8	0.00	5.21	0.15	1.73	12.43	2.81	2.81	0.56	11.46	99.84			
LAN-57	0.34	0.38	0.02	0.02	0.14	-0.02	0.46	0.04	4.71	97.76			
LAN-57											110	4	-1.0
CD 96 10C-1455	6.71	7.46	0.07	4.85	9.12	3.01	2.39	0.50	1.98	96.96	189	87	27.0
Cretaceous Rocks													
RICH-1	1.32	1.47	0.03	0.41	1.16	3.21	4.86	0.08	0.62	100.69			
RICH-1											62	37	1.6
Jurassic Rocks													
BC-2	1.85	2.06	0.02	0.21	0.40	3.68	3.55	0.13	1.32	101.06			
BC-2											136	5	2.0
RM97c-2-443											420	91	30.0
RM97C-2-443	5.20	5.78	0.09	5.99	5.97	0.09	4.73	0.65	7.07	99.41			
RM97C-2-443											467	41	26.0
BP-41A	5.24	5.82	0.01	0.99	0.40	0.02	4.15	0.22	5.89	99.07			
BP-41A	4.74	5.27	0.00	0.95	0.45	0.00	4.35	0.21	5.63	101.81			
BP-41A											114	19	5.0
96M-206a									7.46				
96M-206b	8.11	9.01	0.15	9.19	9.31	1.82	1.63	0.37	7.96	98.50			
96M-207	6.40	7.12	0.12	3.24	6.47	3.19	2.57	0.23	0.79	99.15			
96M-209	4.39	4.88	0.01	0.97	0.34	0.13	5.03	0.22	4.96	99.56			
BP-22	6.65	7.39	0.02	7.74	0.85	0.00	4.79	0.32	4.53	101.21			
BP-22											1868	168	33.0
BP-31	3.36	3.73	0.01	0.63	2.57	0.00	2.73	1.74	6.09	100.50			
BP-31											598	95	26.0
BP-120											120	-21	16.0
BP-120	6.77	7.53	0.11	3.66	6.83	2.74	2.26	0.25	0.36	98.10			
BAZ-2	7.06	7.85	0.00	0.28	0.40	0.00	2.41	0.43	5.86	99.78			
BAZ-2											521	45	14.0
DS-40											327		35.0
DS-40	7.63	8.48	0.13	9.90	8.18	2.74	2.02	0.38	4.33	98.96			
DS-40											287		33.0
DS-40											660	150	34.0
DS-41											416		34.0
DS-41	8.73	9.70	0.09	9.14	10.33	0.16	3.55	0.72	11.91	98.65			
GEN-2-1534											200	30	9.0
GEN-2-1534	3.88	4.31	0.05	2.04	3.42	3.08	4.72	0.19	2.15		253	15	8.0
GEN-3											705	211	43.0

Appendix 3-1: Table of Geochemical Data for Carlin Trend Igneous Rocks

Sample Name	FeO*	Fe$_2$O$_3$*	MnO	MgO	CaO	Na$_2$O	K$_2$O	P$_2$O$_5$	LOI	Total	Cr	Ni	Co
GEN-3	7.93	8.82	0.09	11.42	9.29	2.69	2.03	0.54	8.28	99.40			
GA-13											53	6	-1.0
GA-13	0.77	0.85	0.00	0.29	0.40	3.33	2.98	0.22	2.52	99.28			
GA-10											62	1	16.0
GA-10	6.10	6.77	0.09	3.10	1.14	3.07	4.03	0.38		99.38			
GA-12											310	100	25.0
GA-12	5.71	6.35	0.15	0.13	1.23	-0.08	0.10	0.87	7.02	98.54			
GA19C-1636											62	2	5.0
GA19C-1636	2.16	2.40	0.00	0.21	0.32	-0.11	2.86	0.19	4.58	99.28			
CE52-1538											730	280	34.0
CE52-1538	7.81	8.68	0.14	10.18	7.90	2.28	2.13	0.32	3.19	98.55			
LAN-10											661	77	28.0
LAN-10	7.73	8.59	0.13	9.61	8.72	1.92	2.72	0.46	9.16	97.08			
LAN-17	8.76	9.73	0.12	11.12	7.71	1.92	2.36	0.32	4.71	99.48			
LAN-17											800	-21	32.0
96M-211	10.37	11.52	0.06	2.21	3.13	0.43	4.57	0.45	10.74	98.55			
96M-212	0.53	0.59	0.01	0.29	0.16	0.02	4.26	0.09	2.50	99.92			
PAL-1											120	10	9.0
PAL-1	3.38	3.75	0.04	1.89	2.55	3.15	4.48	0.19	2.57	99.80			
NS-1	6.58	7.31	0.10	4.88	7.27	3.16	2.11	0.30	0.70	98.51			
NS-1											141	31	21.0
98-Zia-9											380	26	1.0
98-Zia-9	1.02	1.13	0.03	0.36	1.67	3.75	4.05	0.09	0.72	97.56			
GB718C-1829											645	119	30.0
GB718C-1829	8.03	8.93	0.11	8.61	7.17	2.10	3.46	0.39	5.23	97.20			
SJ-526C-1022	5.83	6.48	0.09	5.57	6.11	1.55	5.60	0.66	4.56	101.45	417	30	18.0
SJ 489C-1071											277	49	22.0
SJ 489C-1071	5.97	6.63	0.10	5.84	5.90	2.12	5.27	0.60	4.61	100.56			
NB-3										95.10	380	390	27.0
NB-3												709	54.0
NB-3	41.47	46.09	0.06	1.45	0.51	0.13	2.82	1.86	8.04	95.10			
SC-3											210	86	16.0
SC-3	4.44	4.93	0.05	3.47	2.72	2.68	3.24	0.21	4.92	97.71			
TURF-11												102	20.0
TURF-11	6.22	6.91	0.11	6.35	6.72	3.05	2.21	0.27	0.10	96.73			
TURF-11											380	88	24.0
98-Zia-7											260	2	10.0
98-Zia-7	5.90	6.56	0.11	2.45	5.66	3.29	2.72	0.29	0.04	99.05			
RO-108-1270	6.98	7.76				3.40					280	-23	20.0
RO-108-1270											280	-24	21.0
98-Zia-1	6.82	7.58				2.91					300	-20	18.0
98-DEE-1	0.00	5.68	0.02	3.32	2.11	-0.03	3.15	0.75	10.90	102.32			
98-DEE-2	0.00	9.61	0.04	3.92	3.57	0.39	4.39	2.35	7.02	98.56			
98-DEE-11	0.00	3.93	0.19	2.32	12.53	2.52	2.61	0.49	13.58	100.65			
98-REN-8	0.00	9.33	0.13	4.69	1.86	0.12	2.83	0.48	11.12	98.12			
LANC-197-1137.3										100.90	240	-20	4.0
LANC-197-1143.5											210	-20	4.0
LTN-OC-1											38	10	1.4
LTN-OC-1	1.88	2.09	0.02	0.32	1.98	2.72	3.36	0.01	3.88	99.62			
BST-110		2.39	0.04	1.25	3.08	2.23	4.32	0.11	5.12	99.57			
BST-110	(1.73%Fe)				(2%Ca)	(1.48%Na)					102	-20	5.0
BST-110	l)		(242ppm	(.68%Mg	(2.09%Ca)		(3.28%K	(.42%P)				16	
LANC-197-1116.6	1.74	1.94	0.03	1.53	3.34	0.15	4.29	0.09	6.82	99.22	68	6	2.0
LANC-197-1120.8	1.78	1.98	0.02	0.83	2.80	3.34	3.89	0.10	4.77	99.07	122	4	3.0
LANC-197-1125.2	1.80	2.00	0.02	0.79	2.66	3.38	4.29	0.10	4.50	98.84	85	3	3.0
LANC-197-1131.3	1.85	2.06	0.02	0.91	2.81	3.93	3.32	0.10	4.74	98.94	103	3	3.0
LANC-197-1137.3	1.87	2.08	0.02	0.97	2.68	3.88	3.43	0.10	4.68	99.41	95	4	2.0
LANC-197-1143.5	1.88	2.09	0.02	0.96	2.73	3.94	3.29	0.10	4.82	98.63	87	4	2.0
LANC-197-1146.8	1.52	1.69	0.02	0.84	2.85	3.47	3.64	0.08	4.73	98.97	89	3	3.0
LANC-197-1149.5	1.61	1.79	0.02	0.81	2.79	3.50	3.96	0.08	4.60	98.94	82	5	2.0
LANC-197-1150.7	1.78	1.98	0.02	0.88	2.36	3.02	4.86	0.09	4.27	98.16	90	3	3.0
LANC-197-1151.5	1.77	1.97	0.02	1.03	2.65	2.64	4.47	0.09	5.02	98.49	117	144	32.0
CE64-1315												8	5.0

Appendix 3-1: Table of Geochemical Data for Carlin Trend Igneous Rocks

Sample Name	FeO*	Fe$_2$O$_3$*	MnO	MgO	CaO	Na$_2$O	K$_2$O	P$_2$O$_5$	LOI	Total	Cr	Ni	Co
CE64-1315	1.72	1.91	0.08	0.82	3.65	-0.09	3.90	0.09	5.15	97.99			
LAN-64											440	-20	6.0
LAN-64	2.13	2.37	0.04	1.07	1.30	4.49	4.09	0.10	0.44	98.44			
Meikle925-3650	1.84	2.04	0.00	0.14	0.13	0.00	3.93	0.09	2.97	99.34			
Meikle925-3650											98	5	2.0
REN-3											250	5	-1.0
REN-3	0.64	0.71	0.00	0.30	0.10	-0.09	3.29	0.10	5.19	99.30			
Paleozoic Rocks an													
SC-2A											100	98	18.0
SC-2A	12.93	14.37	0.01	3.54	1.36	6.02	0.50	0.87	4.43	98.16			
WC-101											49	-20	23.0
WC-101	10.24	11.38	0.05	2.02	3.58	0.29	7.73	0.58	2.43	100.32			
WC-10	10.34	11.49	0.11	2.32	4.94	6.91	0.23	1.12	2.46	98.76			
WC-10											-10	37	18.0
SL-1											115	25	44.0
SL-1	13.78	15.31	0.17	5.80	9.88	3.43	1.07	0.67	2.92	100.50			
SL-1											89	-23	36.0
IB-1	9.35	10.39	0.02	2.26	0.66	0.19	8.82	0.45	2.40	99.87			
IB-1											35	26	30.0
IB-1													
IB-2	13.95	15.50	-0.01	0.26	0.11	0.32	6.88	0.26	11.10	99.98			
IB-2											25	7	3.0
WC-20											84	12	10.0
WC-20	10.32	11.47	0.12	5.28	1.91	1.81	6.18	0.44	5.92	99.50			
WC-20	7.21	8.01	0.15	5.10	1.43	0.10	6.38	1.03	4.00	99.20			
WC-20											792	84	35.0
WC-20													
LAN-60	0.39	0.43				0.01					360	-20	-1.0
CRZY8-TUFF	0.69	0.77				0.05					260	-20	-1.0
RN-6												20	2.0
RN-6	4.92	5.47	0.00	0.23	0.30	-0.06	0.56	0.89	8.91	98.98			
RN-6										98.91	52	-73	4.0
RN-5												5	2.0
RN-5	2.55	2.84	0.00	0.30	0.13	0.12	5.64	0.77	7.26	101.12			
RN-5											21	60	-1.0
RN-10												2	4.0
RN-10	0.59	0.66	0.00	0.20	0.28	-0.09	0.95	0.19	7.86	98.49			
RN-10											830	-20	2.0
98-Zia-11											430	34	7.0
98-Zia-11	3.41	3.79	0.02	2.92	0.43	0.29	5.48	0.08	0.76	98.44			
TURF-12												21	9.0
TURF12	4.86	5.40	0.39	8.71	8.61	1.55	3.17	0.08	3.30	99.26			
TURF-12											85	35	4.0

Sample Name	Sc	V	Cu	Pb	Zn	Bi	Cd	In	Sn	W	Mo	S
Miocene Rocks												
LAN-65	1.1								-100.0	6.0		
LAN-65		-10	7.0	32.0	145.0	-5.0	-0.5				15.0	
LAN-65												
LAN-65		8	4.0	40.0	150.0							
98-Zia-6	1.2								-100.0	-1.0		
98-Zia-6		14	5.0	36.0	115.0	-5.0					16.0	
98-Zia-6												
MM-1												
Eocene Rocks												
BST-30	4.5						-0.5	-0.02	-100.0	-1.0		
BST-30		48	5.0	24.0	60.0	7.0					3.0	
BST-30												
BST-20			5.7	11.4	11.2		37.2				1.5	
BST-20												
BST-20	2.3								-400.0	42.0		
BST-20		45			14.0	-5.0	36.0				2.0	
BST-103	3.4	105	19.0	33.0	11.0	-5.0	-0.5		-200.0	12.0	-1.0	
BST-103			21.1	5.3	3.2	-0.2	-0.1		-1.0		4.4	
BST-103	3.0	100	25.0	14.0	10.0	-5.0	-0.4		-2.0	13.0	6.0	
BST-103												
BST-101	3.0				1270.0				-1000.0	-4.0	60.0	
BST-104	3.8				146.0				-200.0	8.0	78.0	
BST-105			2.5	14.5	4.8	-0.2	0.1				3.0	
BST-105	3.0	62	2.0	33.0	11.0	-5.0	0.6		-2.0	12.0	3.0	
BST-130												
BST-130	5.2				-50.0				-100.0	3.0		
BST-130		46	5.0	30.0	52.0	-5.0	1.0				-2.0	100
BST-144											-1.0	
BST-144												
BST-143												
BP-27a			1.1	6.2	34.3		0.1				0.3	
BP-27b			2.0	33.6	84.5		0.2				0.9	
BP-2-2	3.5								-200.0	-1.0		
BP-2-2		15	2.0	20.0	43.0	-5.0	-0.5				-2.0	
PNC 213-1787												
PNC 213-1787		40	-10.0	21.0	56.0	1.9		-0.02	6.0	1.3	2.1	
CN-3												
CN-3		27	-10.0	23.0	49.0	0.7		-0.02	2.0	1.0	1.8	
BP-2												
BP-2		-5	-10.0	30.0	50.0	1.7		0.00	3.0	1.3	2.0	
BP-27												
BP-27	4.0	17	-10.0	23.0	66.0	0.7		-0.20	3.0	1.3	1.9	200
BP-2(vug)	2.8				57.0						-2.0	
BP-27			1.5	8.6	32.7		-0.1				1.4	
BP-27												
BP-27wr		12	-1.0	9.0	23.0	-2.0	0.8			-10.0	1.0	
BP-27a	4.4				67.0				-200.0	-1.0	6.0	
BP-2A-VUG	2.6				-50.0					2.0	-1.0	
96M-208	-1.0	12	36.0	20.8	201.0							
BP-23												
BP-23	3.8											
BP-23		45	6.0	12.0	303.0						4.0	
BP-26A												
BP-26A	2.8										3.0	
BP-26A		25	1.0	18.0	44.0						6.0	
BP-4460												
BP-4460	2.7										2.0	
BP-4460		23	1.0	17.0	38.0						3.0	
BP-2-1-clvug												
BP-2-1-clvug	3.2				55.0				-200.0	-1.0	8.0	240
BP-2-2-clvug	3.3				59.0				-200.0	-1.0	7.0	240

Appendix 3-1: Table of Geochemical Data for Carlin Trend Igneous Rocks

Sample Name	Sc	V	Cu	Pb	Zn	Bi	Cd	In	Sn	W	Mo	S
BP-2-altfeld												
BP-2-altfeld	3.3				-50.0				-200.0	-1.0	7.0	210
GB 720C-1744												
GB 720C-1744		30	-10.0	22.0	70.0	0.0		-0.02	17.0	1.1	1.9	
VG-1	2.8					-5.0	1.3		3.0	2.0		
VG-1		30	6.0	45.0	45.0						2.0	
BP-2glass		3	2.0	7.0	11.0	-2.0	-0.5			-10.0	2.0	
BP-27wr		17	-1.0	39.0	39.0	-2.0	0.7			-10.0	2.0	
BP-2glass		5	2.0	40.0	29.0	-2.0	-0.5			-10.0	3.0	
DS-1												
DS-1												
DS-1	2.3								-100.0	-1.0		-100
DS-1		8	1.0	21.0	44.0						6.0	
DSU-143-30												
DSU-143-30	2.2	2	2.0	28.0	28.0	-5.0	-0.5		-100.0	-1.0	3.0	
DSU-143-182												
DS-13	1.9				-50.0				-100.0	-1.0	-1.0	
DS-42		3	-5.0	81.0	42.0							
DS-42												
DS-42A	3.3				-50.0				-400.0	-1.0	18.0	
DS-42A		2	7.0	29.0	49.0	-5.0	0.9				2.0	100
DS-42A		2	4.0	31.0	49.0	-5.0	0.9				2.0	100
EMP-2	4.0				85.0				-100.0	-1.0	-1.0	
RM97C-7-1336												
RM97C-7-1336	4.5	34	2.0	33.0	12.0					18.0		
RM97C-7-1342												
RM97C-7-1342	3.4	35	2.0	19.0	41.0					3.0		
RM97C-7-1359												
RM97C-7-1359	15.0	182	25.0	17.0	89.0					39.0		
BS1004-504												
BS1004-504	4.0	43	5.0	14.0	63.0					1.0		
BS1004-522												
BS1004-522	2.5	26		14.0	26.0					27.0		
BS1004-523												
BS1004-523	3.0	26	1.0	26.0	40.0					12.0	6.0	
98-GEN-23	4.2				-50.0				-100.0	-1.0	-1.0	
GEN-2												
GEN-2												
GEN-2		8	-10.0	18.0	43.0	0.6		-0.02	29.0	1.6	1.7	
98Gen-11	2.9	27	-3.0	63.0	32.0				-100.0	1.0	3.0	
98Gen-11												
98-GEN-1												
98-GEN-1	3.4	18	8.0	11.0	17.0	-5.0	0.8		-100.0	1.0	6.0	
BSTR-3	2.9				82.0				-100.0	5.0	10.0	
M8-0317-4-482	4.2	54	3.0	19.0	53.0				-100.0	-1.0	3.0	
M8-0317-4-482												
IV-1												
IV-1		84	-10.0	21.0	61.0	0.7		-0.02	2.0	1.3	1.3	
LAN-70	4.1				67.0				-100.0	-1.0	2.0	
RICH-12	4.9	76	7.0	32.0	263.0				-100.0	2.0	5.0	
RICH-12												
RICH-10	2.0	20	-2.0	27.0	25.0	-5.0	-0.4		4.0	-4.0	-2.0	-100
RICH-10												
RICH-10			0.5	17.7	22.4	0.4					0.5	
RICH-10												
RICH-10	3.7	24	-5.0	53.0	27.0				-100.0	5.0	4.0	
WC-4												
WC-4		63	11.0	27.0	166.0	0.0		-0.02	2.0	1.0	1.8	
WC-5												
WC-5		122	-10.0	47.0	94.0	0.3		-0.02	1.0	1.2	1.7	
WC-9												
WC-9		95	-10.0	16.0	92.0	0.0		-0.02	2.0	0.7	1.4	
WC-3												

Appendix 3-1: Table of Geochemical Data for Carlin Trend Igneous Rocks

Sample Name	Sc	V	Cu	Pb	Zn	Bi	Cd	In	Sn	W	Mo	S
WC-3			2.3	3.6	59.0		-0.1				1.6	300
WC-3		47	35.0	16.0	40.0	0.3		0.30	1.0	1.0	2.6	300
WC-3	5.8				75.0				-100.0	-1.0	3.0	
WC-2												
WC-2	3.1				72.0				-100.0	-1.0	5.0	
WC-31												
WC-56	8.1	114	11.0	19.0	89.0				-100.0	-1.0	3.0	
WC-56												
WC-105	3.4	26	6.0	55.0	22.0				-100.0	3.0	-1.0	
WC-105												
WC-106	9.0	111	7.0	20.0	57.0				-100.0	-1.0	7.0	
WC-106												
WC-104	2.6				-50.0				-100.0	3.0	7.0	
WC-104												
WC-102												
WC-103	2.5	22	2.0	32.0	27.0				-100.0	-1.0	5.0	
WC-103												
98-WC-3	3.2				-50.0				-100.0	-1.0	5.0	
98-WC-3		7	4.0	12.0	9.0	-5.0	0.8				4.0	600
98-GEN-24	2.7				-50.0				-100.0	5.0	6.0	
98-GEN-24		25	18.0	23.0	14.0	-5.0	0.9				5.0	200
LAN-80	3.0				68.0				-100.0	4.0	5.0	
LAN-80		17	2.0	8.0	59.0	-5.0	0.7				4.0	100
98-DEE-7												
98-DEE-8												
98-DEE-8												
LAN-57												
LAN-57	3.5	3	3.0	24.0	11.0	-5.0	0.5		-100.0	7.0	3.0	
CD 96 10C-1455		185	26.0	26.0	525.0	0.4		-0.02	2.0	1.0	1.7	
Cretaceous Rocks												
RICH-1												
RICH-1		7	280.0	15.0	14.0	45.0		-0.02	2.0	23.0	1.0	
Jurassic Rocks												
BC-2												
BC-2	3.0	31	1.0	23.0	35.0							
RM97c-2-443	23.0	158	50.0	8.0	73.0	-5.0	0.5		-200.0	68.0	-2.0	
RM97C-2-443												
RM97C-2-443	20.0	187	37.0	7.0	70.0					77.0	3.0	
BP-41A												
BP-41A												
BP-41A	11.0	110	8.0	5.0	162.0					3.0		
96M-206a	27.0	146	105.0	11.4	111.0							
96M-206b	17.0	150	116.0	13.0	117.0							
96M-207	20.0	179	29.0	14.9	106.0							
96M-209	13.0	117	22.0	8.6	92.0							
BP-22												
BP-22		182	74.0	2.0	470.0							
BP-31												
BP-31	22.0	393	52.0	55.0	298.0					29.0	6.0	
BP-120	22.0				102.0				-100.0	-1.0	7.0	
BP-120												
BAZ-2												
BAZ-2	26.0	247	51.0	16.0	122.0						16.0	
DS-40		181	36.0	19.0	66.0							
DS-40												
DS-40		171	30.0	14.0	66.0							
DS-40	21.0				76.0				-100.0	-1.0	4.0	
DS-41		241	55.0	15.0	63.0							
DS-41												
GEN-2-1534	9.0	82	24.0	18.0	44.0	-5.0	-0.5		-100.0	-1.0	4.0	
GEN-2-1534		90	20.0	17.0	36.0							
GEN-3		185	144.0	8.0	58.0	1.1	1.1	-0.02	2.0	0.9	0.8	

Appendix 3-1: Table of Geochemical Data for Carlin Trend Igneous Rocks

Sample Name	Sc	V	Cu	Pb	Zn	Bi	Cd	In	Sn	W	Mo	S
GEN-3												
GA-13	3.7	63	-2.0	24.0	25.0				-100.0	-1.0	2.0	
GA-13												
GA-10	14.0	210	11.0	28.0	83.0				-100.0	-1.0	3.0	
GA-10												
GA-12	19.0				643.0				-100.0	12.0	10.0	
GA-12												
GA19C-1636	5.0	61	5.0	39.0	58.0				-200.0	-1.0	-1.0	
GA19C-1636												
CE52-1538	24.0				105.0				-100.0	-1.0	5.0	
CE52-1538												
LAN-10	19.0	169	51.0	11.0	74.0							
LAN-10												
LAN-17												
LAN-17	25.0				97.0				-100.0	-1.0	-1.0	
96M-211	17.0	196	85.0	-1.0	131.0							
96M-212	-1.0	36	28.0	7.0	65.0							
PAL-1	8.3	74	6.0	18.0	18.0				-100.0	-1.0	5.0	
PAL-1												
NS-1												
NS-1		164	-10.0	16.0	67.0	0.5		-0.02	2.0	1.0	1.4	
98-Zia-9	3.7	24	11.0	44.0	157.0				-100.0	-1.0	8.0	
98-Zia-9												
GB718C-1829		174	41.0	11.0	64.0							
GB718C-1829												
SJ-526C-1022		134	45.0	19.0	57.0							
SJ 489C-1071		128	36.0	15.0	42.0	1.7		-0.02	4.0	2.1	2.0	
SJ 489C-1071												
NB-3	18.0				695.0				-100.0	-1.0	16.0	
NB-3		280	64.0	15.0	793.0							
NB-3												
SC-3	12.0	118	16.0	26.0	60.0				-200.0	-1.0	4.0	
SC-3												
TURF-11		146	16.0	12.0	60.0							
TURF-11												
TURF-11	19.0				81.0				-100.0	-1.0	-1.0	
98-Zia-7	11.0	127	9.0	18.0	68.0				-100.0	-1.0	8.0	
98-Zia-7												
RO-108-1270	18.0				89.0				-100.0	-1.0	7.0	
RO-108-1270	19.0				117.0				-100.0	-1.0	8.0	
98-Zia-1	19.0				77.0				-100.0	-1.0	5.0	
98-DEE-1												
98-DEE-2												
98-DEE-11												
98-REN-8												
LANC-197-1137.3	4.3				-50.0				-100.0	-1.0	7.0	420
LANC-197-1143.5	4.5				-50.0				-200.0	-1.0	7.0	
LTN-OC-1		15	-10.0	15.0	52.0	0.0		-0.02	3.0	1.1	2.5	
LTN-OC-1												
BST-110												
BST-110	4.7				-50.0				-100.0	-1.0	-1.0	4600
BST-110		26	13.0	19.0	38.0	-5.0	0.6				2.0	
LANC-197-1116.6	1.0	-10	16.0	46.0	-10.0	-2.0	4.5			4.0	1.0	354
LANC-197-1120.8	2.0	-10	-1.0	10.0	-10.0	-2.0	-0.5			7.0	2.0	24
LANC-197-1125.2	2.0	-10	-1.0	12.0	-10.0	-2.0	-0.5			6.0	1.0	24
LANC-197-1131.3	2.0	-10	-1.0	16.0	-10.0	-2.0	-0.5			7.0	1.0	26
LANC-197-1137.3	2.0	-10	-1.0	14.0	-10.0	-2.0	-0.5			6.0	-1.0	24
LANC-197-1143.5	2.0	-10	-1.0	14.0	-10.0	-2.0	-0.5			6.0	2.0	30
LANC-197-1146.8	2.0	-10	-1.0	14.0	-10.0	-2.0	-0.5			4.0	2.0	28
LANC-197-1149.5	1.0	-10	-1.0	16.0	-10.0	-2.0	-0.5			4.0	2.0	30
LANC-197-1150.7	1.0	-10	3.0	10.0	-10.0	-2.0	-0.5			3.0	1.0	34
LANC-197-1151.5	2.0	-10	60.0	12.0	-10.0	-2.0	-0.5			4.0	1.0	116
CE64-1315		31	-5.0	56.0	31.0							

Appendix 3-1: Table of Geochemical Data for Carlin Trend Igneous Rocks

Sample Name	Sc	V	Cu	Pb	Zn	Bi	Cd	In	Sn	W	Mo	S
CE64-1315												
LAN-64	1.2	42	19.0	28.0	33.0				-100.0	-1.0	16.0	
LAN-64												
Meikle925-3650												
Meikle925-3650	2.9	46	2.0	1.0	16.0					5.0		
REN-3	4.2	33	15.0	127.0	11.0				-100.0	-1.0	4.0	
REN-3												
Paleozoic Rocks an												
SC-2A	13.0	402	6.0	-4.0	144.0				-100.0	-1.0	-1.0	
SC-2A												
WC-101	16.0				82.0				-100.0	-1.0	-1.0	
WC-101												
WC-10												
WC-10		152	-10.0	-5.0	74.0	0.0		-0.02	3.0	0.9	1.5	
SL-1		334	40.0	8.0	97.0							
SL-1												
SL-1	28.0				110.0				-100.0	-1.0	-1.0	
IB-1												
IB-1	14.0	159	5.0	6.0	49.0	-5.0	-0.4		2.0	-4.0	-2.0	500
IB-1			3.8	0.4	40.3	0.2	0.0				0.2	
IB-2												
IB-2	1.0	56	26.0	11.0	14.0	-5.0	-0.4		3.0	-4.0	-2.0	22540
WC-20		336	24.0	2.0	100.0					0.0		
WC-20												
WC-20												
WC-20	39.0	405	39.0	5.0	112.0	-5.0	0.8		3.0	-4.0	-2.0	400
WC-20			40.9	3.7	90.7	0.4	0.7				0.9	
LAN-60	0.9				-50.0				-100.0	-1.0	11.0	
CRZY8-TUFF	3.1				-50.0				-100.0	4.0	13.0	
RN-6		660	12.0	10.0	35.0							
RN-6												
RN-6	280.0				-50.0				-500.0	21.0	-5.0	
RN-5		171	13.0	26.0	27.0							
RN-5												
RN-5	9.6				-50.0				-100.0	-1.0	7.0	
RN-10		330	4.0	164.0	9.0							
RN-10												
RN-10	21.0				-50.0				-100.0	20.0	5.0	
98-Zia-11	12.0	96	14.0	9.0	27.0				-100.0	2.0	7.0	
98-Zia-11												
TURF-12		84	11.0	16.0	81.0							
TURF12												
TURF-12	6.7				81.0				-100.0	-1.0	2.0	

Sample Name	As	Sb	Ag	Au	Hg	Rb	Cs	Ba	Sr	Tl	Ga	Ta	Nb
Miocene Rocks													
LAN-65	3.6	0.2	-5.0	-2.0	-1.0	180	3	140			20	-0.5	44
LAN-65			-0.4						13				
LAN-65								140					
LAN-65						193		179	12		23		44
98-Zia-6	6.3	0.4	-5.0	-2.0	-1.0	170	2	600			19	3.0	52
98-Zia-6			-0.4						20				
98-Zia-6								600					
MM-1								1524					
Eocene Rocks													
BST-30	17.0	3.8	-5.0	-2.0	-1.0	80	18	360					1.0
BST-30			-0.4						25				
BST-30													
BST-20	5432.0	63.5	0.1	348.0	1.2					3.4	1		
BST-20								266					
BST-20	11000.0	120.0	-5.0	477.0	-1.0	-15	-1	540				4.3	
BST-20			-0.4						55				
BST-103	3200.0	120.0	-5.0	5900.0	11.0	30	3	580	47		10	-0.5	13
BST-103	2900.0	67.7	1.0	3800.0	10.0					5.7	0		
BST-103	1582.0	113.0	2.3	5000.0	-1.0			487	50				7
BST-103													
BST-101	1000.0	4600.0	-5.0	2480.0	-4.0	-15	-1	-200	-500			-0.5	
BST-104	800.0	340.0	-5.0	85.0	-1.0	-15	1	200	-500			-0.5	
BST-105	765.0	80.1	0.3	1.9	9.2					0.6	1		
BST-105	798.0	101.0	1.1	-4000.0				752	39				8
BST-130								1842					
BST-130	12.8	7.6	-5.0	-2.0		149		1100	-500			1.0	
BST-130			-0.4						58				
BST-144					4.0		27	143					
BST-144								143					
BST-143								106					
BP-27a	4.2	5.7	0.1	0.5	-0.1					2.1	2		
BP-27b	378.0	4.7	0.1	-0.5	0.5					2.7	1		
BP-2-2	34.0	62.0	-5.0	-2.0	-1.0	83	360	1700				-0.5	
BP-2-2									627				
PNC 213-1787													
PNC 213-1787	51.0	7.8	-0.5			139	18	931	107	6.0	19	1.2	16
CN-3													
CN-3	10.0	1.5	-0.5			140	11	1279	136	0.9	19	1.3	15
BP-2													
BP-2	39.0	44.0	-0.5			99	260	1395	592	2.0	18	1.7	19
BP-27													
BP-27	24.0	19.0	-0.5			107	358	1796	677	2.6	19	1.7	21
BP-2(vug)	23.0	45.0	-0.5	13.0		74	280	1300				1.1	
BP-27	6.6	4.1	0.1	-0.5	-0.1					2.2	3		
BP-27				1.0									
BP-27wr	6.0	3.0	0.4					295	40	-10.0	-10		
BP-27a	11.0	11.0	-5.0	-2.0	-1.0	210	25	1400	-500		0	1.4	0
BP-2A-VUG	7.7	31.0	-5.0	10.0		89	180	810	-500			4.2	
96M-208						167		1829	48		17		22
BP-23													
BP-23	21.0	2.3		5.0		152	22	910			15		18
BP-23									69				
BP-26A													
BP-26A	1500.0	23.0		6.0		96	13	1300			11	1.2	25
BP-26A									61				
BP-4460													
BP-4460	24.0	5.1				67	4	340	92		7	1.3	28
BP-4460													
BP-2-1-clvug													
BP-2-1-clvug	17.0	47.0	-5.0	-2.0	-1.0	93	300	1300	900			1.5	
BP-2-2-clvug	21.0	49.0	-5.0	7.0	-1.0	90	310	1200	800			1.2	

Appendix 3-1: Table of Geochemical Data for Carlin Trend Igneous Rocks

Sample Name	As	Sb	Ag	Au	Hg	Rb	Cs	Ba	Sr	Tl	Ga	Ta	Nb
BP-2-altfeld													
BP-2-altfeld	7.2	19.0	-5.0	5.0	-1.0	140	150	1100	-500		0	1.6	0
GB 720C-1744													
GB 720C-1744	-5.0	1.3	-0.5			113	14	1148	96	0.8	19	1.4	15
VG-1	6.0	27.9	0.4	9.0	-1.0	81	166	938	200			21.9	
VG-1													
BP-2glass	6.0	3.0	0.3					148	35	-10.0	-10		
BP-27wr	19.0	4.0	-0.3					170	104	-10.0	10		
BP-2glass	18.0	15.0	0.4		30.0			221	159	-10.0	-10		
DS-1													
DS-1													
DS-1	32.0	6.5	-5.0	3.0	-1.0	299	260	1300	862		13	2.4	29
DS-1													
DSU-143-30													
DSU-143-30	17.0	1.8	-5.0	-2.0	-1.0	150	5	640	91			2.3	
DSU-143-182													
DS-13	18.0	0.3	-5.0	-2.0	-1.0	130	3	730	-500			2.1	
DS-42						333		858	314		13		25
DS-42								858					
DS-42A	12.8	4.4	-5.0	-2.0	-1.0	500	258	970	-500			1.0	
DS-42A			-0.4						430				
DS-42A			-0.4						432				
EMP-2	2.1	0.5	-5.0	-2.0	-1.0	170	8	1400	-500			1.6	
RM97C-7-1336													
RM97C-7-1336	12.0	30.0		17.0		37	15	357	50		29	2.5	35
RM97C-7-1342													
RM97C-7-1342	8.0	9.5		6.0		49	4	240	30		19	1.4	23
RM97C-7-1359													
RM97C-7-1359	3500.0	52.0		5060.0		86	6	850	50		14	1.4	23
BS1004-504													
BS1004-504	2.7	1.9				174	28	995	111		18	2.1	20
BS1004-522													
BS1004-522	220.0	13.0		0.0	2.0	46	7	200	23		14	1.1	20
BS1004-523													
BS1004-523	470.0	18.0		35.0	2.0	44	8	350	21		20	1.3	27
98-GEN-23	2.2	61.0	-5.0	3.0	-1.0	120	2	350	-500			2.5	
GEN-2													
GEN-2													
GEN-2	-5.0	0.5	-0.5			154	16	1085	145	0.9	19	1.6	19
98Gen-11	3.8	0.6	-5.0	-2.0	-1.0	120	5	900	156		12	1.5	24
98Gen-11								900					
98-GEN-1													
98-GEN-1	11.0	3.8	-5.0	-2.0	-1.0	120	6	380	64			1.7	
BSTR-3	190.0	7.4	-5.0	2.0	-1.0	32	3	5000	-500			1.7	
M8-0317-4-482	10.0	6.3	-5.0	6.0	-1.0	110	11	380	113		16	1.4	21
M8-0317-4-482								380					
IV-1													
IV-1	-5.0	0.9	-0.5			98	6	1403	639	0.8	20	1.2	10
LAN-70	4.5	1.5	-5.0	-2.0	-1.0	110	3	780	-500			1.7	
RICH-12	6.0	10.0	-5.0	4.0	-1.0	160	3	1419	492		15	1.6	19
RICH-12								1419					
RICH-10	-5.0	-5.0	-0.5	-400.0		289	-5	723	55		23		13
RICH-10								723					
RICH-10	2.0	2.8		0.4						1.1	3		
RICH-10													
RICH-10	3.5	3.9	-5.0	-2.0	-1.0	280	13	703	49		17	4.6	32
WC-4													
WC-4	-5.0	0.4	-0.5			92	3	1104	667	0.3	22	1.1	15
WC-5													
WC-5	-5.0	0.8	-0.5			69	1	979	571	0.2	19	0.8	8
WC-9													
WC-9	-5.0	0.2	-0.5			61	1	1097	660	0.2	19	0.8	8
WC-3													

Appendix 3-1: Table of Geochemical Data for Carlin Trend Igneous Rocks

Sample Name	As	Sb	Ag	Au	Hg	Rb	Cs	Ba	Sr	Tl	Ga	Ta	Nb
WC-3	-1.0	0.3	0.1	0.7	-0.5					2.5	6		
WC-3	-5.0	0.4	-0.5			93	3	1070	673	0.4	20	1.2	15
WC-3	1.5	0.6	-5.0	-2.0	-1.0	87	2	1000	1000		0	0.3	0
WC-2													
WC-2	2.3	0.5	-5.0	-2.0	-1.0	140	2	910	-500			1.6	
WC-31								1180					
WC-56	3.6	0.5	-5.0	-2.0	-1.0	70	5	1200	716		14	1.5	17
WC-56								1200					
WC-105	3.4	0.6	-5.0	2.0	-1.0	52	1	764	448		8	1.8	11
WC-105								764					
WC-106	2.4	0.5	-5.0	-2.0	-1.0	94	10	1354	587		15	2.2	19
WC-106								1354					
WC-104	6.5	1.2	-5.0	2.0	-1.0	180	8	573	-500			2.5	
WC-104								573					
WC-102								1332					
WC-103	5.0	2.6	-5.0	-2.0	-1.0	100	3	1701	103		13	1.9	16
WC-103								1701					
98-WC-3	6.6	1.6	-5.0	-2.0	-1.0	157	1	1500	-500			1.9	
98-WC-3			-0.4						264				
98-GEN-24	137.0	23.2	-5.0	-2.0	1.0	20	4	180	-500			1.4	
98-GEN-24			-0.4						13				
LAN-80	24.3	8.1	-5.0	-2.0	-1.0	52	4	180	-500			1.6	
LAN-80			0.4						22				
98-DEE-7								1169					
98-DEE-8								1227					
98-DEE-8								1227					
LAN-57													
LAN-57	45.0	8.5	-5.0	-2.0	-1.0	23	2	140	24			2.1	
CD 96 10C-1455	209.0	11.0	-0.5			62	3	1076	641	0.6	19	0.9	15
Cretaceous Rocks													
RICH-1													
RICH-1	-5.0	0.2	-0.5			285	9	482	202	1.6	16	3.4	29
Jurassic Rocks													
BC-2													
BC-2	10.0	0.6		9.0		122	4	960	267		10	0.0	19
RM97c-2-443	610.0	12.0	-5.0	5.0	-1.0	92	3	1700	632			1.9	
RM97C-2-443													
RM97C-2-443	550.0	10.0				95	3	1300	622		10		27
BP-41A													
BP-41A													
BP-41A	50.0	3.9		12.0		147	5	930	27		20	1.2	19
96M-206a						40		3067	1126		14		15
96M-206b						46		3798	1197		14		16
96M-207						83		1158	759		20		15
96M-209						175		1011	21		21		20
BP-22													
BP-22	0.0					176		958	283		6		7
BP-31													
BP-31	6900.0	35.0		22.0		107	5	560	290		18	0.9	25
BP-120	7.7	0.7	-5.0	5.0	-1.0	72	2	1007	1200			-0.5	
BP-120								1007					
BAZ-2													
BAZ-2	910.0	19.0				88	5	390	243		14	1.9	30
DS-40						58		1242	941		11		22
DS-40								1242					
DS-40						53			919		12		14
DS-40	4.6	0.4	-5.0	4.0	-1.0	54	-1	1000	1200			1.4	
DS-41						130			267		9		20
DS-41													
GEN-2-1534	8.1	1.8	-5.0	4.0	-1.0	200	5	1000	501			2.2	
GEN-2-1534	0.0					167		666	525		18		26
GEN-3	9.0	1.6	-0.5			68	16	1390	1398	0.3	16	0.7	9

Appendix 3-1: Table of Geochemical Data for Carlin Trend Igneous Rocks

Sample Name	As	Sb	Ag	Au	Hg	Rb	Cs	Ba	Sr	Tl	Ga	Ta	Nb
GEN-3								1390					
GA-13	3.4	0.7	-5.0	3.0	-1.0	83	4	460	128		15	2.3	32
GA-13								460					
GA-10	6.9	0.3	-5.0	4.0	-1.0	79	2	5612	1373		18	0.5	14
GA-10								5612					
GA-12	130.0	2.5	-5.0	-2.0	-1.0	-15	-1	430	-500			2.0	
GA-12								430					
GA19C-1636	2400.0	32.0	-5.0	312.0	-1.0	95	4	450	26		17	2.2	30
GA19C-1636								450					
CE52-1538	2.8	1.7	-5.0	-2.0	-1.0	45	2	1200	-500			-0.5	
CE52-1538								1200					
LAN-10	4.7	0.7				54	2	2000	1302		10		25
LAN-10													
LAN-17													
LAN-17	3.9	1.2	-5.0	7.0	-1.0	51	2	1100	-500			-0.5	
96M-211						226		583	76		20		23
96M-212						156		458	30		18		15
PAL-1	2.1	0.3	-5.0	2.0	3.0	130	5	1300	474		14	2.0	21
PAL-1								1300					
NS-1													
NS-1	-5.0	0.5	-0.5			72	2	826	1012	0.3	19	1.1	15
98-Zia-9	3.9	0.8	-5.0	3.0	-1.0	99	-1	2062	507		12	1.8	25
98-Zia-9								2062					
GB718C-1829	0.0					68		2132	1298		16		23
GB718C-1829													
SJ-526C-1022	0.0	0.0				213	0	701	920		10		27
SJ 489C-1071	-5.0	0.9	-0.5			191	6	1255	627	0.4	16	1.5	22
SJ 489C-1071													
NB-3	27.0	3.0	-5.0	2.0	-1.0	120	6	1900	-500			2.2	
NB-3						111			162		20		35
NB-3													
SC-3	14.0	1.6	-5.0	-2.0	-1.0	84	2	2000	260		14	2.6	20
SC-3								2000					
TURF-11						76		960	771		17		22
TURF-11								960					
TURF-11	2.5	0.4	-5.0	-2.0	-1.0	59	2	960	-500			1.0	
98-Zia-7	1.7	0.1	-5.0	-2.0	-1.0	93	2	730 (93	844		20	1.5	25
98-Zia-7								938					
RO-108-1270	2.9	0.4	-5.0	-2.0	-1.0	51	2	590	1200			1.4	
RO-108-1270	2.3	-0.1	-5.0	9.0	-1.0	72	2	810	1200			-0.5	
98-Zia-1	-0.5	0.2	-5.0	-2.0	-1.0	45	1	690	1100			1.0	
98-DEE-1								898					
98-DEE-2								1625					
98-DEE-11								1090					
98-REN-8													
LANC-197-1137.3	22.0	1.9	-5.0	6.0	-1.0	150	7	1700	-500		0	1.5	0
LANC-197-1143.5	26.0	3.2	-5.0	-2.0	-1.0	140	6	1400	-500		0	1.6	0
LTN-OC-1	51.0	4.6	-0.5			128	4	1379	70	2.3	17	1.6	13
LTN-OC-1													
BST-110								1889					
BST-110	212.0	2.7	-5.0	6.0	-1.0	134	5	1600	-500			-0.5	
BST-110			-0.4						249				
LANC-197-1116.6	260.0	12.0	-0.2	35.0	1.0	73		2250	83				14
LANC-197-1120.8	8.0	-2.0	-0.2	-0.5	1.0	44		1860	305				18
LANC-197-1125.2	12.0	-2.0	-0.2	-0.5	-1.0	59		1580	273				16
LANC-197-1131.3	14.0	-2.0	-0.2	-0.5	-1.0	28		1410	332				18
LANC-197-1137.3	8.0	-2.0	-0.2	-0.5	-1.0	28		1390	272				17
LANC-197-1143.5	8.0	-2.0	-0.2	-0.5	-1.0	20		1090	273				16
LANC-197-1146.8	12.0	2.0	-0.2	-0.5	-1.0	35		1350	264				17
LANC-197-1149.5	18.0	2.0	-0.2	-0.5	-1.0	45		1500	289				16
LANC-197-1150.7	32.0	-2.0	-0.2	-0.5	-1.0	61		2370	262				18
LANC-197-1151.5	270.0	2.0	-0.2	-0.5	-1.0	67		1940	215				14
CE64-1315						147			141		11		17

Appendix 3-1: Table of Geochemical Data for Carlin Trend Igneous Rocks

Sample Name	As	Sb	Ag	Au	Hg	Rb	Cs	Ba	Sr	Tl	Ga	Ta	Nb
CE64-1315													
LAN-64	19.0	0.4	-5.0	-2.0	-1.0	170	3	2200	265		12	1.9	15
LAN-64								2200					
Meikle925-3650													
Meikle925-3650	420.0	11.0		75.0		127	4	698	23		15	0.8	17
REN-3	27.0	1.2	-5.0	-2.0	-1.0	87	3	730	33		14	1.4	18
REN-3								730					
Paleozoic Rocks an													
SC-2A	4.7	0.5	-5.0	5.0	-1.0	12	6	800	105		22	4.3	77
SC-2A								800					
WC-101	2.7	0.2	-5.0	-2.0	-1.0	90	3	1798	-500			3.3	
WC-101								1798					
WC-10													
WC-10	-5.0	0.5	-0.5			5		394	184	-0.1	25	5.4	90
SL-1	0.0					22	0	623	379		11		33
SL-1													
SL-1	2.4	-0.1	-5.0	3.0	-1.0	39	2	910	-500			1.5	
IB-1													
IB-1	-5.0	-5.0	0.6	-400.0		256	-5	2117	76		27		26
IB-1	0.8	0.6	0.0	0.2	0.0					0.8	6		
IB-2													
IB-2	792.0	20.0	0.8	500.0		222	-5	3548	77		34		80
WC-20						167		524	172		19		57
WC-20													
WC-20													
WC-20	-5.0	-5.0	-0.5	-400.0		241	-5	576	41		35		79
WC-20	1.7	0.6	0.1		0.0					1.3	6		
LAN-60	17.0	200.0	-5.0	15.0	-1.0	18	1	170	-500			-0.5	
CRZY8-TUFF	100.0	36.0	-5.0	120.0	-1.0	50	3	580	-500			-0.5	
RN-6						21			168		14		50
RN-6													
RN-6	80.0	10.0	-5.0	-5.0	-1.0	-15	-1	3100	-500			3.1	
RN-5						130			350		19		29
RN-5													
RN-5	25.0	1.4	-5.0	4.0	-1.0	110	4	5200	-500			1.5	
RN-10						34			166		12		41
RN-10													
RN-10	70.0	13.0	-5.0	8.0	4.0	47	4	840	-500				
98-Zia-11	2.0	0.7	-5.0	4.0	-1.0	140	4	980	67		11	-0.5	15
98-Zia-11								980					
TURF-12						93			192		9		15
TURF12													
TURF-12	3.1	2.6	-5.0	8.0	-1.0	78	3	800	-500			0.6	

Sample Name	Hf	Zr	Y	Th	U	La	Ce	Pr	Nd	Sm	Eu	Gd	Tb	Dy
Miocene Rocks														
LAN-65	19.0	577		19.0	5.8	120.0	200.0		99.0	15.0	1.3		2.3	
LAN-65			84.0											
LAN-65														
LAN-65		570	85.0											
98-Zia-6	20.0	523		21.0	4.7	120.0	190.0		92.0	16.0	1.3		2.5	
98-Zia-6			66.0											
98-Zia-6														
MM-1														
Eocene Rocks														
BST-30	4.0			11.0	5.4	27.0	45.0		18.0	3.0	0.8		-0.5	
BST-30			11.0											
BST-30														
BST-20														
BST-20														
BST-20	3.0			7.3	6.1	20.0	34.0		-5.0	2.9	-0.2		-0.5	
BST-20			7.0											
BST-103	3.0	106	10.0	6.2	5.9	19.0	30.0		10.0	1.4	-0.2		-0.5	
BST-103														
BST-103		71	9.0	5.0	18.0	20.0								
BST-103														
BST-101	6.0			-0.5	-3.8	17.0	-6.0		-10.0	1.2	-0.2		-0.5	
BST-104	3.0			10.0	5.6	20.0	34.0		11.0	2.6	0.5		-0.5	
BST-105														
BST-105		39	6.0	9.0	18.0	21.0								
BST-130														
BST-130				13.8	5.7	27.6	51.0		18.0	3.5	1.0		-0.5	
BST-130			10.0											
BST-144	4.0													
BST-144														
BST-143														
BP-27a														
BP-27b														
BP-2-2	6.0			12.0	5.2	52.0	82.0		30.0	5.4	1.3		-0.5	
BP-2-2			18.0											
PNC 213-1787														
PNC 213-1787	4.8	186	19.0	10.0	3.6	44.0	75.0	9.0	31.0	5.4	1.2	4.0	0.6	3.0
CN-3														
CN-3	5.4	190	19.0	11.0	3.9	44.0	83.0	9.2	33.0	5.5	1.3	4.0	0.6	3.0
BP-2														
BP-2	4.3	146	18.0	12.0	5.2	44.0	83.0	8.8	30.0	4.9	1.1	3.9	0.6	2.9
BP-27														
BP-27	4.3	147	16.0	11.0	5.0	44.0	82.0	8.6	30.0	5.3	1.2	3.9	0.6	3.0
BP-2(vug)	4.0			10.0	4.5	42.0	60.0		21.0	3.6	1.0		0.5	
BP-27														
BP-27														
BP-27wr				6.0	-5.0	18.0								
BP-27a	6.0	0	0.0	13.0	5.9	53.0	94.0		29.0	5.8	1.4		0.3	
BP-2A-VUG	3.0			7.9	4.2	28.8	46.0		20.0	3.1	0.7		0.3	
96M-208		159	19.8	12.1	6.5	39.0	75.1	7.3	28.7	5.0	1.1	3.8	0.6	3.0
BP-23														
BP-23	6.0	222		9.1	3.4	44.0	65.0		24.0	4.6	1.2		0.6	
BP-23			31.0											
BP-26A														
BP-26A	5.0	149		11.0	4.3	46.0	67.0		25.0	3.9	1.0		0.5	
BP-26A			25.0											
BP-4460														
BP-4460	5.0	147		8.7	3.5	41.0	58.0		24.0	3.9	1.0		0.5	
BP-4460			23.0											
BP-2-1-clvug														
BP-2-1-clvug	5.0			12.0	4.4	46.0	76.0		24.0	4.5	1.2		0.3	
BP-2-2-clvug	5.0			11.0	4.4	45.0	71.0		23.0	4.3	1.2		0.8	

Sample Name	Hf	Zr	Y	Th	U	La	Ce	Pr	Nd	Sm	Eu	Gd	Tb	Dy
BP-2-altfeld														
BP-2-altfeld	5.0	0	0.0	12.0	4.5	45.0	78.0		26.0	4.6	1.1		0.3	
GB 720C-1744														
GB 720C-1744	5.6	191	19.0	12.0	4.2	46.0	89.0	9.7	34.0	5.9	1.4	4.4	0.6	3.2
VG-1	2.8			8.0	3.0	31.0	53.0		19.0	3.0	0.7		0.4	
VG-1														
BP-2glass				7.0	-5.0	20.0								
BP-27wr				-2.0	23.0	-5.0								
BP-2glass				-2.0	24.0	-5.0								
DS-1														
DS-1														
DS-1	2.0	72		4.9	6.4	12.0	23.0		9.0	2.5	0.5		0.5	
DS-1			50.0											
DSU-143-30														
DSU-143-30	2.0		20.0	4.9	6.3	12.0	23.0		9.0	2.5	0.6		-0.5	
DSU-143-182														
DS-13	3.0			4.8	6.5	13.0	25.0		10.0	2.3	0.7		-0.5	
DS-42		55	56.0											
DS-42														
DS-42A				6.8	11.2	15.4	33.0		16.0	3.8	1.3		-0.5	
DS-42A			20.0											
DS-42A			20.0											
EMP-2	8.0			17.0	6.7	49.0	91.0		26.0	4.6	1.4		0.7	
RM97C-7-1336														
RM97C-7-1336	9.0	255	23.0	16.0	7.1	71.0	119.0		43.0	6.6	1.8		0.3	
RM97C-7-1342														
RM97C-7-1342	5.0	178	21.0	11.0	4.0	50.0	73.0		29.0	4.9	1.3		0.6	
RM97C-7-1359														
RM97C-7-1359	7.0	227	29.0	13.0	4.9	77.0	140.0		52.0	8.0	2.7		0.9	
BS1004-504														
BS1004-504	5.0	152	33.0	9.3	2.8	40.0	56.0		23.0	4.2	1.1		0.6	
BS1004-522														
BS1004-522	5.0	146	21.0	11.0	4.1	48.0	76.0		30.0	4.4	1.1		0.6	
BS1004-523														
BS1004-523	5.0	168	20.0	12.0	4.0	49.0	77.0		30.0	4.7	0.9		0.6	
98-GEN-23	3.0			5.8	6.5	15.0	32.0		12.0	3.1	0.8		0.6	
GEN-2														
GEN-2														
GEN-2	4.6	158	18.0	12.0	4.0	43.0	81.0	8.7	30.0	5.1	1.1	3.8	0.6	2.8
98Gen-11	5.0	132	29.0	9.5	3.5	40.0	68.0		26.0	4.0	1.2		-0.5	
98Gen-11														
98-GEN-1														
98-GEN-1	4.0		10.0	11.0	3.3	30.0	42.0		15.0	2.4	0.6		-0.5	
BSTR-3	5.0			11.0	4.2	45.0	64.0		31.0	4.4	1.3		0.7	
M8-0317-4-482	7.0	200	29.0	9.1	4.3	43.0	73.0		32.0	4.6	1.6		0.6	
M8-0317-4-482														
IV-1														
IV-1	5.0	176	17.0	14.0	4.4	43.0	80.0	8.7	30.0	5.3	1.3	3.9	0.6	2.8
LAN-70	6.0			9.1	3.5	42.0	69.0		29.0	4.3	1.5		-0.5	
RICH-12	5.0	154	29.0	12.0	4.8	37.0	52.0		22.0	3.6	0.9		-0.5	
RICH-12														
RICH-10	1.0	69	16.0	11.0	10.0	23.0	39.0							
RICH-10														
RICH-10														
RICH-10														
RICH-10	3.0	73	41.0	13.0	5.9	25.0	36.0		21.0	3.0	0.8		0.6	
WC-4														
WC-4	5.3	192	24.0	13.0	3.6	46.0	87.0	10.1	36.0	6.5	1.6	5.3	0.8	3.9
WC-5														
WC-5	4.6	159	22.0	11.0	2.7	40.0	78.0	8.9	33.0	6.2	1.6	5.3	0.7	3.9
WC-9														
WC-9	4.0	139	19.0	11.0	2.8	41.0	77.0	8.7	31.0	5.5	1.5	4.7	0.6	3.2
WC-3														

Appendix 3-1: Table of Geochemical Data for Carlin Trend Igneous Rocks

Sample Name	Hf	Zr	Y	Th	U	La	Ce	Pr	Nd	Sm	Eu	Gd	Tb	Dy
WC-3														
WC-3	5.6	199	23.0	13.0	3.6	48.0	90.0	10.1	37.0	6.4	1.6	5.0	0.7	3.7
WC-3	6.0	0	0.0	11.0	2.7	46.0	74.0		31.0	5.3	1.6		0.7	
WC-2														
WC-2	6.0			12.0	5.1	39.0	66.0		22.0	3.5	1.0		0.9	
WC-31														
WC-56	5.0	203	24.0	9.5	4.0	38.0	58.0		29.0	4.5	1.5		-0.5	
WC-56														
WC-105	4.0	140	13.0	12.0	4.6	28.0	37.0		9.0	2.3	0.7		-0.5	
WC-105														
WC-106	6.0	184	31.0	12.0	4.5	41.0	63.0		31.0	5.3	1.7		-0.5	
WC-106														
WC-104	4.0			19.0	12.0	9.6	16.0		7.0	2.2	0.5		-0.5	
WC-104														
WC-102														
WC-103	3.0	98	21.0	11.0	3.8	25.0	32.0		13.0	2.3	0.6		-0.5	
WC-103														
98-WC-3	4.0			14.1	3.7	53.3	96.0		33.0	5.2	1.2		0.6	
98-WC-3			13.0											
98-GEN-24	4.0			11.6	4.5	39.1	74.0		25.0	5.0	0.8		-0.5	
98-GEN-24			13.0											
LAN-80	2.0			5.4	5.6	15.0	32.0		15.0	3.5	1.0		0.5	
LAN-80			20.0											
98-DEE-7														
98-DEE-8														
98-DEE-8														
LAN-57														
LAN-57	2.0		53.0	5.2	4.7	16.0	31.0		12.0	3.5	1.5		1.0	
CD 96 10C-1455	4.6	173	21.0	9.3	1.9	42.0	83.0	9.6	35.0	6.4	1.7	5.3	0.7	3.6
Cretaceous Rocks														
RICH-1														
RICH-1	3.7	112	16.0	41.0	14.0	34.0	62.0	6.0	19.0	2.9	0.5	2.1	0.3	1.8
Jurassic Rocks														
BC-2														
BC-2	4.0	156	26.0	8.5	2.0	27.0	33.0		7.0	2.0	0.6		0.3	
RM97c-2-443	7.0		30.0	15.0	4.0	95.0	160.0		68.0	12.0	3.3		1.1	
RM97C-2-443														
RM97C-2-443	6.0	286	31.0	14.0	4.0	74.0	130.0		63.0	11.0	2.8		1.2	
BP-41A														
BP-41A														
BP-41A	7.0	261	36.0	14.0	9.8	59.0	87.0		32.0	5.8	1.6		0.9	
96M-206a		228	22.6	18.3	2.2	71.5	140.2	14.4	61.0	10.4	2.9	7.6	1.0	4.5
96M-206b		240	24.1	18.9	1.9	72.2	141.9	14.6	61.2	10.8	2.9	7.7	1.0	4.7
96M-207		231	27.3	16.0	3.9	43.9	89.4	9.3	39.8	7.7	2.0	6.1	0.9	4.8
96M-209		271	31.4	18.2	19.1	53.0	103.5	10.2	41.3	7.4	1.5	5.6	0.9	4.6
BP-22														
BP-22		255	43.0											
BP-31														
BP-31	26.0	864	32.0	16.0	4.7	84.0	140.0		55.0	12.0	3.2		1.0	
BP-120	5.0			8.9	2.7	48.0	79.0		42.0	7.0	2.3		0.8	
BP-120														
BAZ-2														
BAZ-2	14.0	538	35.0	19.0	16.0	80.0	140.0		58.0	11.0	2.6		1.5	
DS-40		232	20.0											
DS-40														
DS-40		234	21.0											
DS-40	6.0			13.0	3.0	76.0	150.0		55.0	9.2	3.1		-0.5	
DS-41		192	37.0											
DS-41														
GEN-2-1534	13.0		31.0	29.0	8.7	94.0	140.0		49.0	7.7	1.8		-0.5	
GEN-2-1534	0.0	340	36.0											
GEN-3	5.0	182	27.0	32.0	5.2	133.0	265.0	28.3	107.0	18.0	4.3	12.0	1.3	5.2

Appendix 3-1: Table of Geochemical Data for Carlin Trend Igneous Rocks

Sample Name	Hf	Zr	Y	Th	U	La	Ce	Pr	Nd	Sm	Eu	Gd	Tb	Dy
GEN-3														
GA-13	7.0	248	29.0	16.0	4.1	71.0	98.0		40.0	5.3	1.6		-0.5	
GA-13														
GA-10	8.0	318	30.0	18.0	4.7	93.0	150.0		59.0	9.1	2.4		1.0	
GA-10														
GA-12	13.0			18.0	6.3	69.0	110.0		53.0	1.8	3.1		-0.5	
GA-12														
GA19C-1636	7.0	234	28.0	15.0	4.9	69.0	100.0		35.0	5.9	1.6		-0.5	
GA19C-1636														
CE52-1538	5.0			10.0	3.1	53.0	86.0		41.0	7.0	2.4		0.5	
CE52-1538														
LAN-10	4.0	262	24.0	13.0	2.6	75.0	130.0		58.0	10.0	2.4		0.9	
LAN-10														
LAN-17														
LAN-17	5.0			9.4	1.9	45.0	72.0		38.0	6.2	2.1		0.8	
96M-211		271	30.3	16.5	10.0	85.7	168.4	17.2	70.9	11.7	2.6	8.1	1.1	5.1
96M-212		155	14.2	11.2	6.0	32.7	51.1	4.8	17.8	2.9	0.6	2.4	0.3	1.8
PAL-1	8.0	232	35.0	17.0	4.1	69.0	110.0		47.0	7.0	2.1		-0.5	
PAL-1														
NS-1														
NS-1	5.4	191	28.0	12.0	2.3	56.0	113.0	13.3	50.0	8.9	2.2	6.7	0.9	4.9
98-Zia-9	6.0	151	30.0	13.0	4.3	58.0	93.0		36.0	4.9	1.6		-0.5	
98-Zia-9														
GB718C-1829		246	26.0											
GB718C-1829														
SJ-526C-1022		438	40.0											
SJ 489C-1071	10.0	341	25.0	19.0	5.8	65.0	126.0	14.0	51.0	9.2	2.4	7.0	0.9	4.4
SJ 489C-1071														
NB-3	9.0			21.0	7.1	55.0	96.0		51.0	7.5	2.3		-0.5	
NB-3		340	34.0											
NB-3														
SC-3	7.0	204	27.0	20.0	6.2	60.0	87.0		40.0	5.8	1.9		-0.5	
SC-3														
TURF-11		203	23.0											
TURF-11														
TURF-11	7.0			12.0	3.5	52.0	100.0		30.0	6.4	2.0		0.8	
98-Zia-7	7.0	270	32.0	11.0	3.6	60.0	89.0		39.0	6.4	1.9		0.8	
98-Zia-7														
RO-108-1270	6.0			8.7	2.6	47.0	80.0		34.0	5.8	2.2		0.8	
RO-108-1270	6.0			9.3	2.5	50.0	83.0		34.0	6.2	2.0		0.8	
98-Zia-1	5.0			7.0	1.8	60.0	92.0		38.0	7.4	2.5		0.9	
98-DEE-1														
98-DEE-2														
98-DEE-11														
98-REN-8														
LANC-197-1137.3	5.0	0	0.0	15.0	4.1	37.0	53.0		18.0	3.3	0.9		0.3	
LANC-197-1143.5	6.0	0	0.0	15.0	6.3	38.0	62.0		18.0	3.4	0.9		0.3	
LTN-OC-1	3.9	145	12.0	13.0	4.1	32.0	54.0	5.3	17.0	2.9	0.7	2.4	0.3	1.8
LTN-OC-1														
BST-110														
BST-110	4.0			12.8	4.8	33.1	59.0		19.0	3.3	0.8		-0.5	
BST-110			10.0											
LANC-197-1116.6		148	11.0			10.0								
LANC-197-1120.8		153	10.0			20.0								
LANC-197-1125.2		154	12.0			20.0								
LANC-197-1131.3		153	10.0			20.0								
LANC-197-1137.3		154	10.0			20.0								
LANC-197-1143.5		154	9.0			20.0								
LANC-197-1146.8		159	11.0			20.0								
LANC-197-1149.5		154	9.0			20.0								
LANC-197-1150.7		152	9.0			10.0								
LANC-197-1151.5		151	8.0			20.0								
CE64-1315		124	26.0											

Appendix 3-1: Table of Geochemical Data for Carlin Trend Igneous Rocks

Sample Name	Hf	Zr	Y	Th	U	La	Ce	Pr	Nd	Sm	Eu	Gd	Tb	Dy
CE64-1315														
LAN-64	7.0	158	27.0	14.0	3.6	38.0	58.0		24.0	3.4	1.0		-0.5	
LAN-64														
Meikle925-3650														
Meikle925-3650	4.0	135	27.0	9.8	7.0	31.0	43.0		14.0	2.1	0.6		0.3	
REN-3	6.0	129	15.0	9.9	4.2	21.0	30.0		12.0	1.2	0.5		-0.5	
REN-3														
Paleozoic Rocks an														
SC-2A	9.0	362	27.0	6.0	1.9	58.0	100.0		40.0	7.9	2.5		1.3	
SC-2A														
WC-101	7.0			5.9	1.8	35.0	59.0		31.0	5.3	2.4		1.0	
WC-101														
WC-10														
WC-10	9.1	340	40.0	11.0	1.6	80.0	163.0	18.1	68.0	13.0	3.6	11.0	1.5	8.2
SL-1		188	21.0											
SL-1														
SL-1	4.0			2.0	1.5	25.0	53.0		21.0	5.0	2.0		0.7	
IB-1														
IB-1	5.0	184	26.0	2.0	12.0	41.0	74.0							
IB-1														
IB-2														
IB-2	1.0	631	60.0	5.0	29.0	77.0	185.0							
WC-20		240	38.0											
WC-20														
WC-20														
WC-20	3.0	351	40.0	5.0	30.0	72.0	152.0							
WC-20														
LAN-60	2.0			2.0	0.9	8.6	12.0		-5.0	0.6	0.0		-0.5	
CRZY8-TUFF	11.0			5.8	5.0	27.0	43.0		15.0	2.3	0.8		-0.5	
RN-6		264	18.0											
RN-6														
RN-6	9.0			3.4	4.2	35.0	62.0		23.0	5.2	2.6		-0.5	
RN-5		356	40.0											
RN-5														
RN-5	12.0			18.0	5.8	100.0	190.0		63.0	10.0	3.3		1.1	
RN-10		412	24.0											
RN-10														
RN-10	15.0			20.0	6.5	150.0	270.0		94.0	15.0	5.6		1.4	
98-Zia-11	8.0	233	34.0	10.0	1.8	27.0	43.0		20.0	2.6	0.8		-0.5	
98-Zia-11														
TURF-12		218	30.0											
TURF12														
TURF-12	8.0			7.2	2.7	22.0	44.0		16.0	3.7	1.0		0.6	

Appendix 3-1: Table of Geochemical Data for Carlin Trend Igneous Rocks

Sample Name	Ho	Er	Tm	Yb	Lu	Br	Cl	Be	Li	Se	Te
Miocene Rocks											
LAN-65				9.5	1.43	-0.5					
LAN-65								2.00			
LAN-65											
LAN-65											
98-Zia-6				9.3	1.49	1.3					
98-Zia-6								2.00			
98-Zia-6											
MM-1											
Eocene Rocks											
BST-30				0.9	0.16						
BST-30								2.00			
BST-30											
BST-20											
BST-20											
BST-20				1.7	0.30						
BST-20								2.00			
BST-103				1.3	0.21	-0.5					
BST-103										2.71	-0.50
BST-103								-1.00			
BST-103											
BST-101				-0.8	-0.12	-1.4					
BST-104				0.9	0.18	-0.5					
BST-105										1.09	-0.50
BST-105								-1.00			
BST-130											
BST-130				1.1	0.17	-0.5				-3.00	
BST-130								2.00			
BST-144											
BST-144											
BST-143											
BP-27a											
BP-27b											
BP-2-2				1.6	0.44						
BP-2-2								-2.00			
PNC 213-1787											
PNC 213-1787	0.5	1.7	0.25	1.5	0.22						
CN-3											
CN-3	0.5	1.8	0.24	1.6	0.26						
BP-2											
BP-2	0.5	1.6	0.23	1.5	0.25						
BP-27											
BP-27	0.6	1.7	0.25	1.6	0.24						
BP-2(vug)				1.2	0.25						
BP-27											
BP-27											
BP-27wr											
BP-27a				2.6	0.30	-0.5					
BP-2A-VUG				1.0	0.16						
96M-208	0.6	1.7	0.23	1.5	0.26						
BP-23											
BP-23				1.7	0.29						
BP-23											
BP-26A											
BP-26A				1.5	0.25						
BP-26A											
BP-4460											
BP-4460				1.5	0.29						
BP-4460											
BP-2-1-clvug											
BP-2-1-clvug				2.0	0.25	-0.5					
BP-2-2-clvug				2.1	0.31	0.5					

Appendix 3-1: Table of Geochemical Data for Carlin Trend Igneous Rocks

Sample Name	Ho	Er	Tm	Yb	Lu	Br	Cl	Be	Li	Se	Te
BP-2-altfeld											
BP-2-altfeld				1.9	0.25	-0.5					
GB 720C-1744											
GB 720C-1744	0.6	1.8	0.27	1.7	0.26						
VG-1				1.1	0.17						
VG-1											
BP-2glass											
BP-27wr											
BP-2glass											
DS-1											
DS-1											
DS-1				2.2	0.26	-0.5					
DS-1											
DSU-143-30											
DSU-143-30				1.8	0.30						
DSU-143-182											
DS-13				1.6	0.24	-0.5					
DS-42											
DS-42											
DS-42A				2.4	0.36	-0.5				-3.00	
DS-42A								3.00			
DS-42A								3.00			
EMP-2				1.8	0.29	1.7					
RM97C-7-1336											
RM97C-7-1336				2.5	0.48						
RM97C-7-1342											
RM97C-7-1342				1.9	0.36						
RM97C-7-1359											
RM97C-7-1359				2.3	0.48						
BS1004-504											
BS1004-504				1.5	0.29						
BS1004-522											
BS1004-522				1.8	0.30						
BS1004-523											
BS1004-523				1.8	0.33						
98-GEN-23				2.2	0.35	-0.5					
GEN-2											
GEN-2											
GEN-2	0.5	1.6	0.24	1.5	0.23						
98Gen-11				1.6	0.26	-0.5					
98Gen-11											
98-GEN-1											
98-GEN-1				1.0	0.11						
BSTR-3				2.0	0.29	-0.5					
M8-0317-4-482				1.9	0.33	-0.5					
M8-0317-4-482											
IV-1											
IV-1	0.5	1.5	0.21	1.3	0.21						
LAN-70				1.6	0.29	-0.5					
RICH-12				1.4	0.20	-0.5					
RICH-12											
RICH-10								4.00	167		
RICH-10											
RICH-10											0.12
RICH-10											
RICH-10				2.1	0.30	-0.5					
WC-4											
WC-4	0.7	2.1	0.31	1.9	0.27						
WC-5											
WC-5	0.7	1.9	0.32	1.7	0.26						
WC-9											
WC-9	0.6	1.7	0.23	1.4	0.23						
WC-3											

Appendix 3-1: Table of Geochemical Data for Carlin Trend Igneous Rocks

Sample Name	Ho	Er	Tm	Yb	Lu	Br	Cl	Be	Li	Se	Te
WC-3											
WC-3	0.7	2.2	0.33	1.9	0.30						
WC-3				2.1	0.31						
WC-2											
WC-2				1.0	0.19	-0.5					
WC-31											
WC-56				2.0	0.29	-0.5					
WC-56											
WC-105				0.9	0.17	-0.5					
WC-105											
WC-106				2.1	0.36	-0.5					
WC-106											
WC-104				2.3	0.38	-0.5					
WC-104											
WC-102											
WC-103				1.0	0.16	-0.5					
WC-103											
98-WC-3				1.7	0.26	-0.5				-3.00	
98-WC-3								2.00			
98-GEN-24				1.5	0.26	-0.5				-3.00	
98-GEN-24											
LAN-80				1.6	0.20	-0.5				-3.00	
LAN-80								2.00			
98-DEE-7											
98-DEE-8											
98-DEE-8											
LAN-57											
LAN-57				3.6	0.52						
CD 96 10C-1455	0.6	1.8	0.25	1.6	0.23						
Cretaceous Rocks											
RICH-1											
RICH-1	0.4	1.3	0.28	2.0	0.40						
Jurassic Rocks											
BC-2											
BC-2				0.7	0.13						
RM97c-2-443				2.5	0.47						
RM97C-2-443											
RM97C-2-443				1.9	0.32						
BP-41A											
BP-41A											
BP-41A				2.4	0.45						
96M-206a	0.8	2.3	0.25	1.6	0.28						
96M-206b	0.8	2.2	0.28	1.6	0.28						
96M-207	0.9	2.7	0.36	2.5	0.37						
96M-209	0.9	2.8	0.39	2.6	0.40						
BP-22											
BP-22											
BP-31											
BP-31				3.0	0.48						
BP-120				3.0	0.47	-0.5					
BP-120											
BAZ-2											
BAZ-2				3.3	0.47						
DS-40											
DS-40											
DS-40											
DS-40				1.8	0.30	-0.5					
DS-41											
DS-41											
GEN-2-1534				2.1	0.45						
GEN-2-1534											
GEN-3	0.8	2.4	0.26	1.6	0.24						

Appendix 3-1: Table of Geochemical Data for Carlin Trend Igneous Rocks

Sample Name	Ho	Er	Tm	Yb	Lu	Br	Cl	Be	Li	Se	Te
GEN-3											
GA-13				2.1	0.39	-0.5					
GA-13											
GA-10				1.9	0.40	-0.5					
GA-10											
GA-12				2.3	0.35	-0.5					
GA-12											
GA19C-1636				2.7	0.41	-0.5					
GA19C-1636											
CE52-1538				2.2	0.34	-0.5					
CE52-1538											
LAN-10				1.5	0.25						
LAN-10											
LAN-17											
LAN-17				2.0	0.35	-0.5					
96M-211	0.9	2.7	0.34	2.2	0.37						
96M-212	0.3	1.0	0.15	1.0	0.15						
PAL-1				3.0	0.48	-0.5					
PAL-1											
NS-1											
NS-1	0.9	2.7	0.37	2.3	0.35						
98-Zia-9				2.3	0.34	2.3					
98-Zia-9											
GB718C-1829											
GB718C-1829											
SJ-526C-1022				0.0	0.00						
SJ 489C-1071	0.8	2.2	0.29	1.7	0.25						
SJ 489C-1071											
NB-3				2.2	0.34	-0.5					
NB-3											
NB-3											
SC-3				2.3	0.35	-0.5					
SC-3											
TURF-11											
TURF-11											
TURF-11				2.4	0.38	-0.5					
98-Zia-7				2.5	0.47	-0.5					
98-Zia-7											
RO-108-1270				2.2	0.36	-0.5					
RO-108-1270				2.6	0.40	-0.5					
98-Zia-1				2.2	0.46	-0.5					
98-DEE-1											
98-DEE-2											
98-DEE-11											
98-REN-8											
LANC-197-1137.3				1.4	0.19	-0.5					
LANC-197-1143.5				1.6	0.16	-0.5					
LTN-OC-1	0.3	1.0	0.14	0.9	0.15						
LTN-OC-1											
BST-110											
BST-110				1.1	0.16	-0.5				-3.00	
BST-110								2.00			
LANC-197-1116.6											
LANC-197-1120.8											
LANC-197-1125.2											
LANC-197-1131.3											
LANC-197-1137.3											
LANC-197-1143.5											
LANC-197-1146.8											
LANC-197-1149.5											
LANC-197-1150.7											
LANC-197-1151.5											
CE64-1315											

Appendix 3-1: Table of Geochemical Data for Carlin Trend Igneous Rocks

Sample Name	Ho	Er	Tm	Yb	Lu	Br	Cl	Be	Li	Se	Te
CE64-1315											
LAN-64				1.4	0.23	2.6					
LAN-64											
Meikle925-3650											
Meikle925-3650				1.2	0.25						
REN-3				0.9	0.18						
REN-3											
Paleozoic Rocks an											
SC-2A				1.8	0.35	-0.5					
SC-2A											
WC-101				2.4	0.37	-0.5					
WC-101											
WC-10											
WC-10	1.5	4.0	0.57	3.3	0.46						
SL-1											
SL-1											
SL-1				2.8	0.42	-0.5					
IB-1											
IB-1								1.00	50		
IB-1										0.04	0.08
IB-2											
IB-2								1.00	14		
WC-20											
WC-20											
WC-20											
WC-20								2.00	54		
WC-20											0.05
LAN-60				0.7	0.14	-0.5					
CRZY8-TUFF				2.5	0.44	-0.5					
RN-6											
RN-6											
RN-6				2.3	0.45	-1.2					
RN-5											
RN-5											
RN-5				3.5	0.55	-0.5					
RN-10											
RN-10											
RN-10				4.0	0.64	-0.5					
98-Zia-11				2.0	0.37	-0.5					
98-Zia-11											
TURF-12											
TURF12											
TURF-12				2.1	0.33	-0.5					

Appendix 3-2. Lead Isotopic Compositions of Igneous Rocks of the Carlin Trend, Nevada[1]

Sample	Unit	Rock Type	Mineral	Location
Ordovician(?)				
WC-10	Vinini Fm.	spilitized basalt	whole-rock; feldspar concentrate	IB claims
WC-101	Vinini Fm.	spilitized basalt	whole-rock; feldspar concentrate	IB claims
Jurassic (~158 Ma)				
LAN-17	lamprophyre dike	hbl-phlg lamprophyre	K-feldspar	Lantern
NST-1	Goldstrike laccolith	equigranular hbl-cpx diorite	plagioclase	Northstar
TURF-11	Vivian sill	equigranular hbl-cpx diorite	plagioclase	Turf
98-ZIA-7	Goldstrike stock	equigranular cpx diorite	plagioclase	Zia claims
CE52-1538	lamprophyre dike	coarse hbl-phlg lamprophyre	whole rock	Lantern
98-ZIA-9	rhyolite dike	plg-bio-qtz rhyolite	plagioclase	Zia claims
WC-103	rhyolite dike	plg-qtz rhyolite	plagioclase	IB claims
LAN-34	rhyolite dike	plag-qtz-bio rhyolite	whole-rock; feldspar concentrate	Lantern
Cretaceous (112 Ma)				
RICH-1	Richmond stock	coarse porphyritic granite	K-feldspar	Richmond Mountain
RICH-16	Richmond stock	coarse porphyritic granite	K-feldspar	Richmond Mountain
Eocene (40-36 Ma)				
BP-2	rhyolite dike	plag-bio rhyolite	plagioclase	Betze-Post
BP-2G	rhyolite dike	plag-bio rhyolite	hydrated glass	Betze-Post
DS-1	rhyolite dike	aphyric, vitrophyre	hydrated glass	Deep Star
DSU-143-30	rhyolite dike	aphyric, vitrophyre	K-feldspar	Deep Star
WC-2	rhyolite dike	plg-bio-san-qtz rhyolite	whole-rock	Welches Cyn
WC-9	dacite dike	plag-hbl-bio-(san) dacite	whole-rock	Welches Cyn
BST-130	rhyolite dike	plag-bio-san-qtz rhyolite	sanidine	Beast
BST-114	rhyolite dike	plag-bio-san-qtz rhyolite	sanidine	Beast
RICH-10	rhyolite dike	plag-bio-san-qtz rhyolite	sanidine	Richmond Mountain
Miocene (15 Ma)				
LAN-65	rhyolite lava	san-fay-opx-qtz vitrophyre	sanidine	Lantern

Mineral abbreviations for rock type: bio-biotite; cpx-clinopyroxene; hbl-hornblende; phlg-phlogopite; plg-plagioclase; qtz-quartz; san-sanidine;

[1] Lead isotopic determinations by J.L. Wooden and R.M. Tosdal at U.S. Geological Survey, Menlo Park, CA, USA

Measured lead isotope compositions were corrected for 0.125% fractionation per AMU, based on replicate analyses of the National Bureau of Standards 981 and 982

Uncertainties for pure and homogeneous minerals±0.8, ±0.1, and ±0.14% (2σ), respectively for 206Pb/204Pb, 207Pb/204Pb, and 208Pb/204Pb

Sample	Latitude	Longitude	Pb (ppm)	$^{206}Pb/^{204}Pb$	$^{207}Pb/^{204}Pb$	$^{208}Pb/^{204}Pb$
Ordovician(?						
WC-10	40° 49'20"	116° 20'20"	<5	20.276	15.723	41.541
WC-101	40° 48'57"	116° 19'55"	5	21.798	15.803	41.966
Jurassic (~15						
LAN-17	40° 55' 26"	-116° 21' 36"		20.394	15.764	40.164
NST-1	40° 57' 43"	-116° 22' 36"		19.824	15.735	39.666
TURF-11	40° 56'58"	116° 18'57"	12	19.940	15.738	39.524
98-ZIA-7	40° 56'28"	116° 21'24"	18	20.035	15.657	39.839
CE52-1538	40° 55'45"	116° 22'10"	10	20.661	15.772	40.411
98-ZIA-9	40° 56'11"	116° 23'13"	44	19.819	15.742	39.231
WC-103	40° 50'00"	116° 20'10"	32	19.946	15.700	39.347
LAN-34	40° 55' 26"	-116° 21' 36"		20.962	15.752	40.742
Cretaceous (1						
RICH-1	40° 51'05"	116° 18'25"	15	19.500	15.721	39.052
RICH-16	40° 51'05"	116° 18'23"		19.525	15.708	39.014
Eocene (40-3						
BP-2	40° 58' 39"	-116° 22' 00"		19.184	15.718	39.184
BP-2G	40° 58' 39"	-116° 22' 00"		19.261	15.707	39.177
DS-1	40° 57' 34"	-116° 21' 49"		19.251	15.716	39.234
DSU-143-30	40° 57' 34"	-116° 21' 49"		19.239	15.709	39.210
WC-2	40° 48'00"	116° 19'15"		19.262	15.693	39.244
WC-9	40° 51'05"	116° 18'25"		19.175	15.682	39.238
BST-130	40° 56'32	116° 22'15"	17			
BST-114	40° 56'35"	116° 21'24"	17	19.156	15.686	39.171
RICH-10	40° 51'49"	116° 18' 10"		19.222	15.702	39.257
Miocene (15						
LAN-65	40° 54'42"	116° 22'15"	32	18.896	15.655	39.045

Appendix 3-3. Strontium Isotopic Compositions of Igneous Rocks of the Carlin Trend, Nevada

Sample	Rock Unit	Age (Ma)	Mineral	Rb (ppm)	2σ	Sr(ppm)	2σ
Miocene							
LAN-65	Miocene rhyolite lava	15	sanidine	75.1	0.002	86.8	0.08
Eocene							
BP-2	Post rhyodacite	39	plagioclase	99	WR	592	
DS-1	Deep Star rhyolite	38	whole-rock	299	WR	862	
BST-114	Beast rhyolite	37	sanidine	161.5	0.02	726	4
RICH-10	Richmond rhyolite	37	sanidine	40.0	0.004	43	0.012
Cretaceous							
RICH-16	Richmond granite	112	orthoclase	439.6	0.016	244	0.03
Jurassic							
98 ZIA-7	Zia microdiorite	~158	plagioclase	93.0	WR	843	
98 ZIA-9	Zia rhyodacite	~158	plagioclase	90.8	0.016	456	0.9
LANC 197-1121	Lantern rhyodacite	~158	whole-rock	150	WR	305	
TURF 11	Vivian pyx diorite	~158	plagioclase	63.8	0.001	1272	0.3
Paleozoic							
WC-10	Paleozoic basalt?	Ord (?)	whole-rock	5.0	WR	184	

Sample	$^{87}Sr/^{86}Srm$	$^{87}Sr/^{86}Sri$	2σ	ЄSr
LAN-65	0.71013	0.70961	0.000014	73
BP-2	0.70754	0.70728	0.000011	39
DS-1	0.70849	0.70795	0.000012	49
BST-114	0.70745	0.70712	0.000015	37
RICH-10	0.70829	0.70689	0.00001	34
RICH-16	0.71387	0.70575	0.000009	18
98 ZIA-7	0.70729	0.70660	0.000009	30
98 ZIA-9	0.70834	0.70708	0.000008	37
LANC 197-1121	0.70879	0.70569	0.000005	17
TURF 11	0.70562	0.70531	0.000010	11
WC-10	0.70899	0.70850	0.000017	57

WR = Rb and Sr analyses from whole rocks

Appendix 3-4. Neodymium Isotopic Compositions of Igneous Rocks of the Carlin Trend, Nevada

Sample	Rock Unit	Sm (ppm)	2σ	Nd (ppm)	2σ	^{143}Nd/^{144}Ndm	2σ	ЄNd
Miocene								
LAN-65	Miocene rhyolite lava	0.109	0.100	1.327	0.002	0.512147	0.000014	-9.58
Eocene								
BP-2	Post rhyodacite	4.9 WR-INAA		30		0.512239	0.000007	-7.78
DS-1	Deep Star rhyolite	2.5 WR-INAA		9		0.512269	0.000011	-7.20
BST-114	Beast rhyolite	0.061	0.001	0.383	0.003	0.512204	0.000025	-8.47
RICH-10	Richmond rhyolite	0.15	0.000	0.8	0.0100	0.512180	0.000011	-8.93
Cretaceous								
RICH-16	Richmond granite	0.091	0.008	0.738	0.020	0.512405	0.000015	-4.55
Jurassic								
98 ZIA-7	Zia microdiorite	7 WR-INAA		38		0.512192	0.000027	-8.70
98 ZIA-9	Zia rhyodacite	3.33	0.040	19.22	0.080	insufficient Nd		NA
LANC 197-1121	Lantern rhyodacite	3.3 WR-INAA		18		0.512281	0.000017	-6.96
TURF 11	Vivian pyx diorite	0.863	0.001	8.37	0.019	0.512285	0.000018	-6.89
Paleozoic								
WC-10	Paleozoic basalt?	13 WR-INAA		68		0.512180	0.000011	-4.04

WR-INAA = Nd and Sm analyses from whole rocks by neutron activation

Appendix 3-5. Stable Isotope Compositions of Igneous Rocks of the Carlin Trend, Nevada

Sample No.	Mineral	Rock Type	$\delta^{13}C$ PDB	$\delta^{18}O$ SMOW	δD SMOW
Eocene					
BP-2	matrix	rhyolite		8.8[4]	-145[1]
BP-2	biotite	rhyolite			-82[1]
BP-2	plagioclase	rhyolite		8.68[4]	
BP-2	matrix carbonate	rhyolite	-1.9[3]	9.8[3]	
98-Gen-1	matrix carbonate	rhyolite	-1.2[3]	11.5[3]	
RICH-10	sanidine	rhyolite		7.22[2]	
BST-30	sanidine	rhyolite		7.6[2]	
WC-31	plagioclase+/-quartz	diorite		5.78[2]	
DS-13	whole-rock	aphyric rhyolite		8.29[2]	
Jurassic					
LAN-197-1137	matrix carbonate	rhyolite	-3.7[3]	15.2[3]	
LAN-197-1137	whole rock	rhyolite		11.6[4]	
NS-1	matrix carbonate	diorite	-4.7[3]	14[3]	
LAN-17	matrix carbonate	lamprophyre	-3.6[3]	18.4[3]	

Sample locations given in Appendix 3-3

[1] δD analyses by R. O. Rye, U.S. Geological Survey, Denver, CO, USA

[2] $\delta^{18}O$ analyses by J. Dilles and A. Grunder, Oregon State University, Corvallis, OR, USA;
Precision and accuracy: ± 0.2 per mil using standard UWG-2 garnet = 5.8

[3] Analyses by K. Winters, Coastal Science Laboratories, Austin, TX, USA' Precision and accuracy relative to PDB±0.2 per mil

[4] Analyses by Geochron Laboratories, Cambridge, MA, USA

Chapter 4. Conclusions and Recommendations

The goals of this study were to further characterize the igneous rocks of the Carlin trend, including their distribution and age, and to provide evidence for the age of mineralization based on cross cutting relationships with igneous rocks. Some of the more important findings of this study include:

- Five pulses of magmatism are recognized on the Carlin trend, only two of which, Jurassic and Eocene, are widespread.

- Jurassic and Eocene intrusions are spatially associated with all ore deposits.

- All pulses were of relatively short duration; Eocene magmatism was longest lived at over 4 Ma.

- Jurassic, Cretaceous, and Eocene rocks are broadly calc-alkaline, "arc-like" and dominated by feldspar and hydrous mafic minerals. Miocene rhyolite is anhydrous, alkaline, olivine-bearing, and consistent with a rift origin.

- Jurassic rocks generally are more mafic, diorite-dominant, with abundant lamprophyre dikes; lamprophyre is silica saturated, phlogopite- or amphibole-phyric, without feldspar phenocrysts and similar geochemically to Goldstrike diorite.

- Eocene intrusions of the northern trend are mostly rhyolite; andesite-dacite lavas and similar intrusions dominate the southern trend.

- Magma sources are enigmatic, but preliminary isotopic analyses, especially of Pb, show large differences between suites that suggest different sources.

- An Eocene age for gold mineralization on the Carlin trend is now well established. The Beast deposit is constrained between 37.3 and 18.6 Ma.

The Meikle-Griffin deposit is approximately coeval with ~39 Ma porphyritic dacite dikes.

- Major gold mineralization on the Carlin trend was contemporaneous with magmatism between ~40 and 36 Ma.

- Deposits formed at relatively shallow depths (≤ 2 km) based on structural relationships between Eocene volcanic rocks and mineralized dikes and on dike textures. Depths are consistent with epithermal mineralization.

- Scale of hydrothermal activity requires a major process. Two competing models invoke either Eocene magmatism or release of deeply circulating (i.e., metamorphic) fluids during crustal extension.

- Large-scale extension is not evident during the Eocene on the Carlin trend based on modest tilts of coeval volcanic rocks, and there are no temporal ties between extension and mineralization.

- Mapping and dating of Eocene dike swarms and aeromagnetic data suggest numerous buried Eocene plutons in the Carlin trend, which are both younger and shallower to the south.

- A spatial and temporal tie between Eocene magmatism and Carlin-type Au mineralization logically leads to a possible genetic relation.

- Eocene plutons generated heat necessary to drive gold -related hydrothermal circulation; fission-track data indicate broad re-setting to >120° C at ~38 Ma in southern Carlin trend where plutons are shallowest and only partial re-setting to the north where plutons are deeper.

- Other models, which invoke deeply derived fluids (i.e., mid-crustal) related to metamorphism and/or extension have not demonstrated any temporal or spatial links to mineralization.

- Eocene extension is modest in the Carlin trend, so models (e.g., Seedorff et al., 1991) that require large-magnitude extension are not valid.

Future work should utilize geochemical and isotopic data on igneous rocks of the Carlin trend in order to constrain the origin of magmas related to each suite. What is the relative importance of a subducted slab? The relationship of magmatic activity to tectonism, either contraction or extension should be analyzed. What can be said about the sources for magmas, and how much did magmas interact with the crust? What proportion of magmatism reflects components derived from the mantle? More specific petrologic and regional work on Paleozoic alkali basalt of the Roberts Mountains allochthon should be undertaken. Similarly, Miocene rhyolite associated to the northern Nevada should be studied in more detail. Notably, Miocene rhyolite of the rift in and near the Carlin trend is highly variable geochemically, including rocks that range from peraluminous to mildly peralkaline. What are the processes that may have contributed to this variation?

The scale of Eocene magmatism should be better evaluated through thermal modeling. A critical question for any modeling is: Do deposits of the Carlin trend represent discrete fossil hydrothermal sytems or was hydrothermal activity broad and pervasive over the entire trend? On-going fission-track studies of ores and other rocks distributed widely around the Carlin trend should help to answer this question. Detailed alteration studies of individual deposits coupled with stable isotope mapping of calcite veins associated with those deposits may help delineate the scale of individual hydrothermal systems. Are interpreted deeply buried intrusions sufficient to have driven hydrothermal circulation? Likewise, was Eocene extension of the Carlin trend alone sufficient to drive large-scale hydrothermal circulation in the highest levels of the crust?